Universidad de Huelva

Departamento de Ciencias Integradas

Caracterización y valorización de residuos inorgánicos procedentes de industrias químicas de Huelva

Memoria para optar al grado de doctora
presentada por:

Silvia María Pérez Moreno

Fecha de lectura: 28 de febrero de 2018

Bajo la dirección de los doctores:

Juan Pedro Bolívar Raya

Manuel Jesús Gázquez González

Huelva, 2018

CARACTERIZACIÓN Y VALORIZACIÓN DE RESIDUOS INORGÁNICOS PROCEDENTES DE INDUSTRIAS QUÍMICAS DE HUELVA

Memoria presentada por:

SILVIA PÉREZ MORENO

para optar al título de DOCTOR

Memoria realizada dentro del marco del Programa de Doctorado en Ciencia y Tecnología Industrial y Ambiental del Departamento de Ciencias Integradas de la Universidad de Huelva

Tesis supervisada por:

Dr. Juan Pedro Bolívar Raya

Dr. Manuel Jesús Gázquez González

JUAN PEDRO BOLÍVAR RAYA, Catedrático de Universidad del Departamento de Ciencias Integradas de la Universidad de Huelva;

MANUEL GÁZQUEZ GONZÁLEZ, Profesor del Departamento de Física de Aplicada de la Universidad de Cádiz;

DECLARAN: que la tesis doctoral denominada **"Caracterización y Valorización de Residuos Inorgánicos procedentes de Industrias Químicas de Huelva",** ha sido realizada por Dña. SILVIA PÉREZ MORENO en el Departamento de Ciencias Integradas de la Universidad de Huelva bajo su dirección, para optar al grado de Doctor por la Universidad de Huelva.

En Huelva, Diciembre de 2017

Fdo. Dr. Juan Pedro Bolívar Raya

Fdo. Dr. Manuel Gázquez González

ABSTRACT

Waste is currently one of the most serious environmental problems arising from the economic and social development of human beings, mainly because of the amount of waste continues to increase year after year. The emergence of materials more resistant to natural degradation processes, which remain longer in the environment, and the increase in their dangerous characteristics, are factors that aggravate the current situation of waste. The high generation of waste that accompanies economic growth without limits, causes not only the lack of space and inadequate treatments to eliminate them, but also a depletion of the resources used in their manufacture. Therefore, it is necessary to find solutions to these environmental problems that allow the sustainable development of our society.

In this sense, the industrial complex located in Huelva is today one of the main industrial centre of Spain. The presence of industrial focus in this city has contributed for more than half a century very positive effects in the creation of employment and wealth generation. But also, it has generate environmental problems. Such problems are identified as waste generation, wastewater release, and gas emissions between others, which suppose source of release pollutant into the water, soil and atmosphere that could adversely affect to the environment and health of human.

The main objective of this doctoral thesis has been to characterise physically and chemically different industrial wastes produced in several factories the industrial complex from Huelva, and also find commercial applications in which they can be used without implying any risk for environment or people. The studied wastes has been: red gypsum and ilmenite mud generated in the TiO_2 production industry; reprocessed slag cleaning furnace flue dust from copper smelting; and phosphogypsum from phosphoric acid production industry. Some of them are considered as NORM (Naturally Occurring Radioactive Material).

For that purpose, a number of instrumental techniques were deployed to characterise the wastes and the new materials designed, such as, laser diffraction particle sizing analysis, X-ray Diffraction (XRD), X-ray Fluorescence (XRF), Inductively Coupled Plasma Optical Emission Spectroscopy (ICP-OES), Inductively Coupled Plasma Mass

Spectrometry (ICP-MS), Scanning Electron Microscopy (SEM), Thermogravimetry (TGA/DTA), alpha-particle spectrometry with PIPS detectors and gamma spectrometry with Ge detectors. In addition, several tests were applied in order to evaluate the environmental and radiological implications of the studied wastes, as well as evaluate the technological properties of new obtained material.

The researches carried out involve the use of red gypsum (RG) and tionite as potential building materials for fire wall insulation or as fire-resistant panels. The study demonstrated that plates manufactured with RG (main components: CaSO4·2H2O) and iron and titanium oxides) and tionite (main components: $FeTiO_3$, TiO_2, $ZrSiO_4$, SiO_2 and $Fe_3Ti_3O_{10}$) perform better than some materials used in construction such as Pladur® against fire. The tested materials also present acceptable mechanical properties that showed no noticeable distortion or breakage during the test. In addition, it has been proven that the plates manufactured are agree with EU radioactivity requirements, since the use of these wastes as building materials not exceeded the radioactive thresholds.

Furthermore, RG was proposed as a source for CO_2 sequestration. The results show that RG could be used as capture agent for carbon dioxide sequestration. It has been demonstrate that a high carbonation efficiency is reached using NaOH as Ca extracting agent, as well as a reduction of the resulted solid. However, the natural radionuclides are concentrated in calcite ($CaCO_3$), the main product of the carbonation process, which implies its consideration as a NORM material, which requires radiological studies in their commercial applications.

On the other hand, flue dust from copper smelting was subjected to an exhaustive characterization as an indispensable preliminary step to choose the best available technology to recover their major metals, principally Zn and Pb, which are in form of zincite (ZnO), carbonate ($PbCO_3$) and sulphate ($PbSO_4$). It has been demonstrated that the wastes are an important secondary resource of Zn and Pb and their reprocessing has both remarkable economic and environmental benefits in contrast with their disposal. Pyrometallurgical and hydrometallurgical process appears to be attractive options for the management of these hazardous wastes.

Finally, the environmental impact due to natural radionuclides contained in the phosphogypsum (PG) stored in Huelva, was evaluated using the BCR sequential extraction method, previously validated for radionuclides. This aspect is essential because the release of the pollutant into the environment depend strongly on their specific chemical forms or ways of binding. It has been demonstrated that the BCR sequential extraction procedure is a useful tool for assessing the speciation of different radionuclides due to reproduces environmental conditions. In this sense, the results shown that U-isotopes contained in PG show highest mobility, being its total mobile fraction around 70%, while ^{210}Po and ^{226}Ra present a total mobility of about 50% and 30%, respectively. And the Th-isotopes have very low mobility (mobile fraction < 5%), being fixed to the crystalline forms of the PG. This behaviour was also found in the water samples taken from the stacks.

CONTENT

CHAPTER 1. INTRODUCTION 1
1.1 BACKGROUND 3
1.1.1 State of the art 3
1.1.2 Waste generation 9
1.1.2.1 Red gypsum and ilmenite mud from TiO_2 production industry 9
1.1.2.2 Reprocessed Slag Cleaning Furnace Flue Dust from Copper Smelting 12
1.1.2.3 Phosphogypsum from phosphoric acid production industry 14
1.2 OBJECTIVES 19
1.3 TESIS STRUCTURE 19
CHAPTER 2. MATERIALS AND METHODS 23
2.1. SAMPLINGS AND PRE-TREATMENTS 25
2.1.1. Samplings waste 25
2.1.2. Sample pre-treatment 26
2.2. MEASURING TECHNIQUES 26
2.2.1. Granulometry 26
2.2.2. XRD 28
2.2.3. XRF 30
2.2.4. ICP-OES 32
2.2.5. ICP-MS 35
2.2.6. Scanning Electron Microscope (SEM) 36
2.2.7. Thermogravimetric Analysis (TGA) and Differential Thermal Analysis (DTA) 39
2.2.8. Alpha spectrometry 43
2.2.8.1. Radiochemical method 43
2.2.8.2. Alpha spectrometric system with passivated implanted planar silicon (PIPS) detectors 48
2.2.8.3. Counting efficiency 49
2.2.8.4. Activity concentration calculation 50
2.2.8.5. Lower limit of detection (LLD) and Minimum Detectable Activity (MDA) 52
2.2.8.6. Quality Control (QC) 53
2.2.9. Gamma spectrometry with Ge detectors 55
2.3. TECHNIQUES FOR ENVIRONMENTAL RISK EVALUATION 57
2.3.1. Leaching test 57
2.3.1.1. TCLP 57
2.3.1.2. UNE-EN 12457/4 60

2.3.1.3. BCR Extraction Procedure 61
2.3.2. Radiological implications in building materials 63
2.4. TECHNIQUES FOR TECHNOLOGICAL PROPERTIES 64
2.4.1. Fire resistance Test 64
CHAPTER 3. RESULTS AND DISCUSSION 67
3.1. THERMAL CHARACTERIZATION OF NEW FIRE-INSULATING MATERIALS FROM INDUSTRIAL INORGANIC TiO_2 WASTES 69
3.1.1. INTRODUCTION 69
3.1.2. MATERIALS AND METHODS 71
3.1.2.1. Materials 71
3.1.2.1.1. Waste 71
3.1.2.1.2. Additives 71
3.1.2.1.3. Blends 72
3.1.2.1.4. Pladur® 72
3.1.2.2. Methods 73
3.1.2.2.1. X-Ray Diffraction (XRD) 73
3.1.2.2.2. X-ray Fluorescence (XRF) 73
3.1.2.2.3. TGA 73
3.1.2.2.4. Fire-resistance tests 73
3.1.3. RESULTS AND DISCUSSION 74
3.1.3.1. Characterization of materials 74
3.1.3.1.1. Mineral composition 74
3.1.3.1.2. Major elements 75
3.1.3.2. Thermogravimetric analysis (TGA) 76
3.1.3.2.1. Tionite 76
3.1.3.2.2. Red gypsum 78
3.1.3.2.3. Vermiculite 82
3.1.3.2.4. PLADUR® 83
3.1.3.2.5. Plate 2 (75% red gypsum, 25% tionite) 84
3.1.3.2.6. Plate 3 (80% red gypsum, 15% mud, 5% vermiculite) 86
3.1.3.3. Fire-resistance tests 89
3.1.4. CONCLUSIONS 92
3.2. CO_2 SEQUESTRATION BY INDIRECT CARBONATION OF ARTIFICIAL GYPSUM GENERATED IN THE MANUFACTURE OF TITANIUM DIOXIDE PIGMENTS 95
3.2.1. INTRODUCTION 95
3.2.2. MATERIALS AND METHODS 97
3.2.2.1. Materials 97
3.2.2.2. Measurement techniques 98

3.2.2.2.1. X-Ray Fluorescence (XRF) 98
3.2.2.2.2. X-Ray Diffraction (XRD) 98
3.2.2.2.3. Scanning Electron Microscopy (SEM) 98
3.2.2.2.4. Inductively coupled plasma–mass spectrometry (ICP-MS) 98
3.2.2.2.5. Thermogravimetric Analysis (TGA) 99
3.2.2.2.6. Alpha-Particle Spectrometry 99
3.2.2.3. Carbonation Method 99
3.2.3. Results and discussion 101
3.2.3.1. Mineral Composition 101
3.2.3.2. Major and Trace Elements 103
3.2.3.3. Morphologic Characterisation 107
3.2.3.4. Radiological Characterisation 110
3.2.3.5. CO2 Sequestration Efficiency 112
3.2.4. CONCLUSIONS 117
3.3. DIAGNOSE FOR VALORISATION OF REPROCESSED SLAG CLEANING FURNACE FLUE DUST FROM COPPER SMELTING 119
3.3.1. INTRODUCTION 119
3.3.2. MATERIALS AND METHODS 121
3.3.2.1. Materials 121
3.3.2.2. Methods for physical and chemical characterisation 121
3.3.2.2.1. Granulometry 121
3.3.2.2.2. Mineralogy 121
3.3.2.2.3. Chemical analysis 122
3.3.2.2.4. Thermogravimetric analysis 122
3.3.2.2.5. Scanning electron microscopy 122
3.3.2.2.6. Leaching test 122
3.3.3. Results and discussion 123
3.3.3.1. Granulometry 123
3.3.3.2. Elemental composition 125
3.3.3.3. Mineralogy 126
3.3.3.4. Thermogravimetric analysis 128
3.3.3.5. Scanning electron microscopy 131
3.3.3.6. Lixiviation Test 135
3.3.4. Diagnose for their valorisation 138
3.3.5. CONCLUSIONS 140
3.4. VALIDATION OF THE BCR SEQUENTIAL EXTRACTION PROCEDURE FOR NATURAL RADIONUCLIDES 141
3.4.1. INTRODUCTION 142

3.4.2. MATERIALS AND METHODS 143
3.4.2.1. Modified BCR Sequential Extraction Procedure 143
3.4.2.2. Materials 145
3.4.2.3. Characterisation Techniques 146
3.4.3. RESULTS AND DISCUSSION 147
3.4.3.1. Chemical Characterisation 147
3.4.3.2. Validation of the BCR Procedure in our laboratory by using BCR-701 150
3.4.3.2.1. Metals 150
3.4.3.2.1.1. Aqueous Phase 150
3.4.3.2.1.2. Solid Phase 154
3.4.3.3. BCR Validation for Natural Radionuclides using he CRM BCR-701 157
3.4.3.3.1. Aqueous Phase 157
3.4.3.3.2. Solid Phase 163
3.4.4. CONCLUSIONS 164
3.5. ASSESMENT OF NATURAL RADIONUCLIDES MOBILITY IN A PHOSPHOGYPSUM DISPOSAL AREA 167
3.5.1. INTRODUCTION 168
3.5.2. MATERIALS AND METHODS 170
3.5.2.1. Samplings 170
3.5.2.2. Physico-Chemical Characterization Techniques 171
3.5.2.3. Optimised BCR Sequential Extraction Procedure 171
3.5.2.4. Alpha Spectrometry 173
3.5.3. RESULTS AND DISCUSSION 173
3.5.3.1. Physical-Chemical parameters 173
3.5.3.2. Characterization of phosphogypsum in depth 175
3.5.3.3. Mobility of Natural Radionuclides in Phosphogypsum 178
3.5.3.4. Waters of Disposal Area 187
3.5.4. CONCLUSIONS 191
CHAPTER 4. GENERAL CONCLUSIONS 193
CHAPTER 5. REFERENCES 197

Chapter 1. Introduction

1.1 BACKGROUND

1.1.1 State of the art

Waste is an unavoidable by-product of most human activity. Economic development and rising living standards have led to increases in the quantity and complexity of generated waste, whilst industrial diversification have added substantial quantities of industrial hazardous waste with potentially severe environmental and human health consequences.

In 2012, EU Member States discarded 2.5 billion tonnes of waste, of which close to 4 % was classified as hazardous. Although rates of overall waste generation in Europe declined between 2006 and 2012 by more than 3 % in absolute terms, the proportion of hazardous waste in total waste is slowly increasing. The amount of hazardous waste generated in the EU increased slightly from previous years to around 100 million tonnes in 2012.The predominant waste types, accounting for more than half the generated amount, were mineral and solidified wastes, whereas one third were chemical and medical wastes (EEA, 2015). In this sense, hazardous waste is of high concern because of the potential risks it poses to humans and the environment. For that reason, hazardous waste is subject to restrictive and extensive regulation, both in Europe and around the world.

The Directive 2008/98/EC of the European Parliament and of the council of 19 November 2008 (Waste Framework Directive), lays down measures to protect the environment and human health by preventing or reducing the adverse impacts of the generation and management of waste and by reducing overall impacts of resource use and improving the efficiency of such use.

For the purposes of the Directive, "waste" and "hazardous waste" are defined as follow:

Waste: any substance or object which the holder discards or intends or is required to discard.

Hazardous waste: waste which displays one or more of the hazardous properties listed in Annex III *(modified by Regulation 1357/2014/CE)*

The Directive establishes the waste hierarchy, which shall apply as a priority order in waste prevention and management legislation and policy:

(a) Prevention, which means measures taken before a substance, material or product has become waste, that reduce:

- The quantity of waste, including through the re-use of products or the extension of the life span of products;
- the adverse impacts of the generated waste on the environment and human health; or
- the content of harmful substances in materials and products

(b) Re-use, which means any operation by which products or components that are not waste are used again for the same purpose for which they were conceived;

(c) Recycling, which means any recovery operation by which waste materials are reprocessed into products, materials or substances whether for the original or other purposes. It includes the reprocessing of organic material but does not include energy recovery and the reprocessing into materials that are to be used as fuels or for backfilling operations;

(d) Recovery or valorisation, which means any operation the principal result of which is waste serving a useful purpose by replacing other materials which would otherwise have been used to fulfil a particular function, or waste being prepared to fulfil that function, in the plant or in the wider economy.

(e) Disposal, which means any operation which is not recovery even where the operation has as a secondary consequence the reclamation of substances or energy.

The Directive approves a list of waste established by Decision 2000/532/EC *(modified by Decision 2014/955/UE, according to Regulation (CE) 1272/2008).* The list of waste includes hazardous waste and shall take into account the origin and composition of the waste and, where necessary, the limit values of concentration of hazardous substances. However, some considerations should be take into account:

1. A Member State may consider waste as hazardous waste where, even though it does not appear as such on the list of waste, it displays one or more of the properties listed in Annex III *(modified by Regulation 1357/2014/CE)*

2. Where a Member State has evidence to show that specific waste that appears on the list as hazardous waste does not display any of the properties listed in Annex III *(modified by Regulation 1357/2014/CE)*, it may consider that waste as non-hazardous waste.

3. The reclassification of hazardous waste as non-hazardous waste may not be achieved by diluting or mixing the waste with the aim of lowering the initial concentrations of hazardous substances to a level below the thresholds for defining waste as hazardous.

In addition, as a novelty the Waste Framework Directive lay down in the article 6 that certain specified waste shall cease to be waste when it has undergone a recovery, including recycling, operation and complies with specific criteria to be developed in accordance with the following conditions:

(a) The substance or object is commonly used for specific purposes;

(b) A market or demand exists for such a substance or object;

(c) The substance or object fulfils the technical requirements for the specific purposes and meets the existing legislation and standards applicable to products; and

(d) The use of the substance or object will not lead to overall adverse environmental or human health impacts.

On the other hand, an important consideration concerning environmental impact is the emission of greenhouse gases (e.g. CO_2) by human activity, mainly due to the burning of fossil fuels, which accelerates the natural greenhouse effect and increases global warming. The Global warming is causing changes in the planet, such as: increase in average global temperature, greater melting of the polar ice-caps, increases in sea level, increase in the frequency of heat waves, increased rainfall in some regions and drastic

decrease in others. Fossil fuel emissions (including cement production) accounted for about 91% of total CO_2 emissions from human sources in 2014. This portion of emissions originates from coal (42%), oil (33%), gas (19%), cement (6%) and gas flaring (1%) (McGee, 2017).

The Figure 1.1 shows monthly mean carbon dioxide measured (Hawaii, Mauna Loa Observatory) of the last four years until the current year. As it can be observed the CO_2 concentration is increasing every year, and this trend does not seem that will change in the coming years.

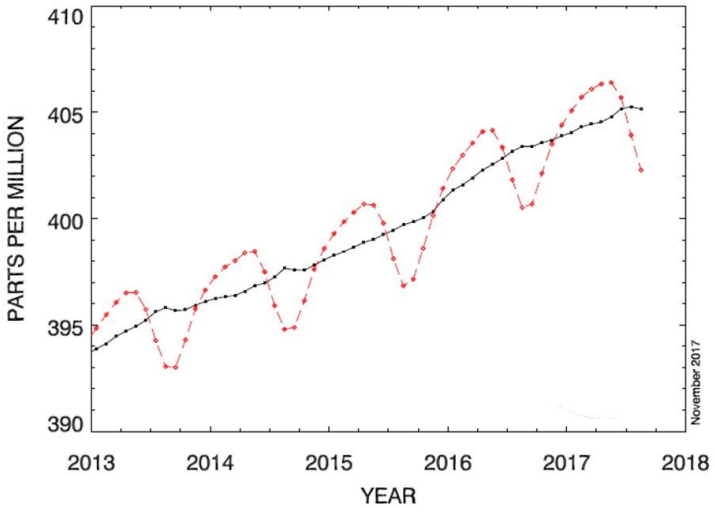

Figure 1.1 *Global monthly mean CO^2 in last years.*[1]

The Sixth Community Environment Action Programme established by Decision No 1600/2002/EC of the European Parliament and of the Council identifies climate change as a priority for action and provides for the establishment of a Community-wide emissions trading scheme by 2005. That Programme recognises that the Community is committed to achieving an 8 % reduction in emissions of greenhouse gases by 2008 to 2012 compared to 1990 levels, and that, in the longer-term, global emissions of greenhouse gases will need to be reduced by approximately 70 % compared to 1990 levels.

[1]The dashed red line with diamond symbols represents the monthly mean values, centred on the middle of each month. The black line with the square symbols represents the same, after correction for the average seasonal cycle (McGee, 2017).

The objective of the United Nations Framework Convention on Climate Change is to achieve stabilisation of greenhouse gas concentrations in the atmosphere at a level which prevents dangerous anthropogenic interference with the climate system.

The Community and its Member States have agreed to fulfil their commitments to reduce anthropogenic greenhouse gas emissions under the Kyoto Protocol jointly, in accordance with Decision 2002/358/EC. This Directive aims to contribute to fulfilling the commitments of the European Community and its Member States more effectively, through an efficient European market in greenhouse gas emission allowances, with the least possible diminution of economic development and employment.

On the other hand, the Directive 2010/75/EU of the European Parliament and the Council on industrial emissions, known as Industrial Emissions Directive (IED), is the main EU instrument regulating pollutant emissions from industrial installations. The IED aims to achieve a high level of protection of human health and the environment taken as a whole by reducing harmful industrial emissions across the EU, in particular through better application of Best Available Techniques (BAT).

In this sense, all these European Regulations that promote the protection of the environment and the human life, without forgetting the continuous economic development, are those that are being applied in the industrial complex located in Huelva. Huelva and its surroundings are today one of the main industrial centre of Spain. It is considered one of the most diversified industrial locations in terms of production sectors that coexist in it: gas and oil refining, metallurgy, power generation (through combined cycles, biomass, cogeneration and other systems) basic and inorganic chemistry and fertilizers. Figure 1.2 shows the location of industries, which conform the Association of Chemical Industries Basic and Energy of Huelva (AIQB). The consolidation of this powerful industrial focus has contributed for more than half a century very positive effects in the creation of employment and wealth generation.

Figure 1.2 *Location map of industries in Huelva*

However, the presence of industrial focus not only generates benefits, but also environmental problems. Such problems are identified as waste generation, wastewater release, and gas emissions between others, which suppose source of release pollutant into the water, soil and atmosphere that could adversely affect to the environment and health of human.

In this sense, this doctoral thesis framed within the general objective of characterize and valorise several inorganic industrials waste such us: red gypsum and ilmenite mud generated in the TiO_2 production industry; reprocessed slag cleaning furnace flue dust from copper smelting; and phosphogypsum from phosphoric acid production industry. Currently, all these waste are disposed in landfill.

The researches carried out involve the use of red gypsum and tionite as potential building materials for fire wall insulation or as fire-resistant panels. In addition, red gypsum was proposed as a source for CO_2 sequestration. On the other hand, flue dust from copper smelting was subjected to an exhaustive characterization as an indispensable preliminary step to choose the best available technology to recover their major metals, principally Zn and Pb. Finally, the environmental impact due to natural radionuclides contained in the phosphogypsum stored in Huelva, was evaluated using the BCR sequential extraction method, previously validated for radionuclides. This aspect is essential because the

release of the pollutant into the environment depend strongly on their specific chemical forms or ways of binding.

1.1.2 Waste generation

1.1.2.1 Red gypsum and ilmenite mud from TiO_2 production industry

Titanium is the ninth most abundant element in the Earth's crust and the fourth most abundant metal of major industrial importance after aluminium, iron and magnesium. Its occurrence in nature is usually in chemical combination with oxygen and iron. More than 90% of titanium mineral production is in the form of ilmenite, a mixed oxide of titanium and iron ($FeTiO_3$ or $FeO{\cdot}TiO_2$ with an equivalent TiO_2 content of 34–69%). In addition rutile (93–96.5% TiO_2) and leucoxene ($Fe_2O_3{\cdot}TiO_2$ with a TiO_2 content of 70–90%) are also considered others titanium sources. All of the titanium minerals are used directly as feedstocks for the production of titanium dioxide pigments and other titanium products.

Titanium minerals contain radionuclides of natural origin in the ^{232}Th and ^{238}U decay series. The radionuclide activity concentrations are moderately elevated above those in normal rocks and soil (around 45 Bq kg^{-1} and 40 Bq kg^{-1} for U- and Th-series radionuclides, respectively) (Unscear, 2000). During processing, the radionuclides may become mobilized and migrate to dusts, scales and other process residues, leading to the possibility of radionuclide activity concentrations higher than those in the relevant feedstock mineral. In some process materials or waste, the activity concentrations of radionuclides in the ^{232}Th decay series (and to a lesser extent the ^{238}U series) are such that these materials can be considered as naturally occurring radioactive material (NORM)[2] (IAEA, 2012).

Titanium dioxide pigments are produced from a variety of ores by two different routes: the sulphate process route and the chloride process route. The sulphate process accounts for about 45% of pigment production and involves the use of sulphuric acid to separate the titanium dioxide from the other components of the mineral concentrate. The chloride process route accounts for the remaining 55% of production and involves the use of gaseous chlorine to produce $TiCl_4$, which is then converted to titanium dioxide by

[2] NORM is considered when the activity concentration of any radionuclide in the uranium or thorium decay chains is greater than 1 Bq/g or the activity concentration of 40K is greater than 10 Bq/g.

oxidation. The choice of process route and of specific processes depends on local conditions such as the market situation, the environmental management situation in terms of its implications for waste disposal, the economic situation (for instance, the costs of power and chemicals) and the availability of technology. In addition, the feedstock, determined by its content of titanium dioxide equivalent is crucial in the choice of process. The majority of chloride process plants require feedstocks of relatively high grade (rutile and leucoxene), while sulphate process plants can be operated with feedstocks of lower grade (ilmenite).

The need for whiteness and brightness of titanium dioxide pigment requires that the product be made to a high degree of purity, whose process generates different by-products and/or wastes. The range of by-products produced is dependent on the feedstock and the process route. The major by-products associated with the sulphate process route are gypsum, iron sulphates, sulphuric acid, digester residue and iron oxide, while those associated with the chloride process route are iron chloride, hydrochloric acid and neutralized iron oxides, hydroxides or carbonates.

Titanium dioxide has excellent properties (high refractivity, reflectivity, opacity), which causes it to be the most widely used white pigment for a variety of applications including paints and coatings, plastics, paper, ceramic glazes, printing inks, food and toothpaste. It is also used as a pigment and thickener in cosmetics (ultraviolet (UV) blockers, make-up and skin care products) and as a tattoo pigment. The annual worldwide production of titanium dioxide pigments is close to 6 million t. Nearly two thirds of the worldwide production of titanium minerals comes from just four countries: Australia, South Africa, Canada and China.

This thesis covers the production of titanium dioxide generated by sulphate route, using ilmenite as raw material. This process is carried out in Tioxide- Europe S.L, the only titanium production industry in Spain, located in Huelva. The sulphate process involves the use of concentrated sulphuric acid to dissolve ilmenite. A simplified, schematic representation of the sulphate process and products associated with the titanium dioxide is given in Fig. 1.3.

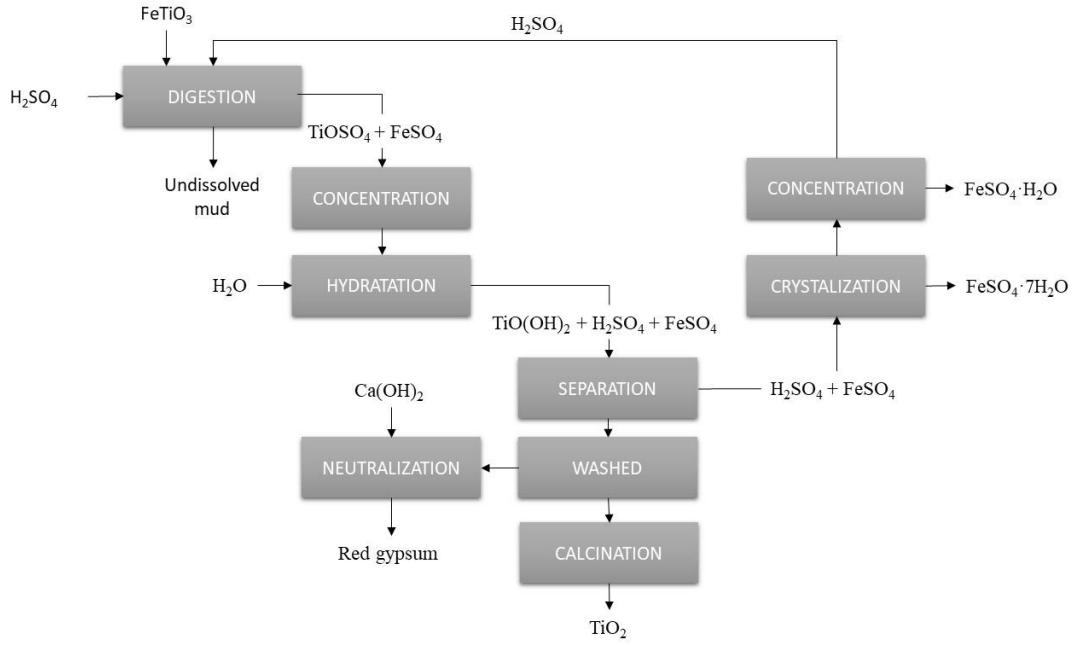

Figure 1.3 *Simplified scheme of the production of TIO_2 via sulphate process.*

The ilmenite (around 142,000 tons), previously ground, is digested with highly concentrated sulphuric acid (160,000 tons) (80–95%) to form titanyl sulphate and ferrous sulphate. A highly exothermic reaction is initiated at a temperature of about 140°C by the addition of measured quantities of steam, water and diluted acid. The basic digestion reaction is:

$$FeTiO_3\,(s) + 2H_2SO_4(aq) \rightarrow TiOSO_4\,(aq) + 2H_2O\,(aq) + FeSO_4\,(aq) \qquad [Eq.1.1]$$

Undissolved feedstock (ilmenite mud or tionite) and other solids suspended in the acid solution are removed by flocculation (decantation) and filtration. The clarified solution is concentrated by evaporation and then hydrolysed with steam in mild steel vessels lined with rubber or brick to produce hydrated titanium dioxide:

$$TiOSO_4\,(aq) + 2H_2O\,(aq) \rightarrow TiO(OH)_2\,(s) + H_2SO_4\,(aq) \qquad [Eq.1.2]$$

The clarified solution is usually pumped to batch cooler crystallizers where the bulk of the iron sulphate is separated as crystalline ferrous sulphate heptahydrate ($FeSO_4 \cdot 7H_2O$), known as copperas. The separation process, involves vacuum crystallization followed by thickening and removal by centrifuge. The resulting liquor is concentrated by evaporation

and sulphate monohydrated ($FeSO_4 \cdot H_2O$) precipitates. The clarified solution, which content high concentration of sulphuric acid (80% and 65%) is returned to the digestion step.

After separation from the mother liquor, the hydrated titanium dioxide is then fed to rotary kilns, where it is calcined to expel water and oxides of sulphur while moving under gravity, counter-currently to the combustion gases. In the so-called 'finishing' step, the resulting solid is cooled, coated, washed, dried, finely ground ('micronized' to 0.2–0.4 μm) and packed.

The resulting solution of hydration of titanyl sulphate contain low concentration of sulphuric acid and ferrous sulphate that is neutralised using calcium hydroxide to above pH 7. In this process "red gypsum", a mix of gypsum and iron hydroxides, is form:

$$3FeSO_4(aq) + 3Ca(OH)_2(s) \rightarrow Fe(OH)_2(s) + CaSO_4\ (s) \qquad \text{[Eq.1.3]}$$

The Tioxide- Europe S.L produces about 7×10^4 tons of red gypsum and 3×10^4 tons of mud per year. Currently these wastes have no commercial value and are disposed of in an authorized and controlled repository area. Red gypsum is included in the Waste Catalogue List (06 11 01: Calcium waste from the production of titanium dioxide) according to the European Legislation, as well as ilmenite mud, but this residue is considered as hazardous materials (06 11 99* Undissolved ilmenite).

1.1.2.2 Reprocessed Slag Cleaning Furnace Flue Dust from Copper Smelting

Copper is one of the oldest metals ever used, and has been one of the most significant materials in the development of many civilizations. Since it is a ductile metal with very high thermal and electrical conductivity, it is mainly used as electrical conductor, and to a lesser extent as a heat conductor (Doebrich, 2009).

Copper occurs in nature predominantly as chalcopyrite ($CuFeS_2$), and is almost always accompanied by the iron sulphides pyrite (FeS_2) and pyrrhotite (FeS). Copper sulphide ores also can contain other metal sulphides such as molybdenite (MoS_2), sphalerite (ZnS) and galena (PbS). Copper is generally found in very low percentages in nature as native

metal (0.5%–2%), but its ore can be ground up and concentrated to around 25% to 30 % using froth flotation.

The pyrometallurgical process for obtaining very pure metal begins by mixing the copper concentrate with a SiO_2 flux and introducing it into the flash furnace, where the fusion process takes place. Most sulphur is converted to SO_2 and sent to the acid plant to be converted to sulphuric acid. The oxidised iron combines with the silica, added initially to the concentrate, to form fayalite slag ($2FeO \cdot SiO_2$). The remaining melt phase (Cu, Fe, and other metals) forms a liquid copper matte containing 50%–70% of Cu (Figure 1.4).

The matte (mainly Cu_2S and FeS) is separated from the slag and fed into the converting furnace, where the copper is separated from the left-over sulphur, iron and other metals. Consequently, SO_2 and slag are produced again. The conversion furnace yields a product called “blister copper”, which has a copper content of approximately 99%. The small amounts of sulphur and iron still remaining in the blister copper are removed by further oxidation in a fire-refining furnace. The fire-refined copper is cast into anodes that go to the electrolytic cell to be refined to 99.99% copper in the cathodes (Seetharaman et al., 2014).

Atlantic Copper, located in Huelva (Spain), is one of the largest producers in Europe, which produce more than 285.000 tons (per year) of cathodic copper as main product. The pyrometallurgical process involved also generate by-products such as iron silicates or slag (~670.000 tons/year) between others, which is widely marketed in civil engineering (Raposeiras et al., 2016; Prasad et al., 2016). The commercial slag is produced in the slag cleaning furnace (SCF), where under high temperature (1250 °C) and reducing atmosphere its remaining copper content (5%, approximately) decrease (below to 1 %), and flue dust, mainly enriched of Zn and Pb among other metals, is formed (Schlesinger et al., 2011). After treatment of the off gases through a scrubbing with water system, about 2500 tons per year of filtered cake is obtained (Scrubbing Water Cake-SWC) (Rios et al., 2012). The Zn and Pb-rich waste, containing about 60% water, is classified as hazardous material (100607* Sludges and filter cakes from gas treatment) according to the Waste European Directive. Currently, the waste is disposal in a controlled landfill, located about 70 km from the factory.

As novelty, a pilot plant has been installed in the factory for reducing the amount of produced waste in this area. The new technology consists of flue-gas desulphurisation in a ceramic sleeve filter using micronized calcium hydroxide. This operation is based on the adsorption of gas pollutants onto fine-grained solid particles of $Ca(OH)_2$, which is introduced in the gas stream and is finally collected onto the filter. The new treatment, which reduce the water consumption, gives lower volume of final dry solid waste (Ceramic Filter Dust -CFD) produced (Figure 1.4).

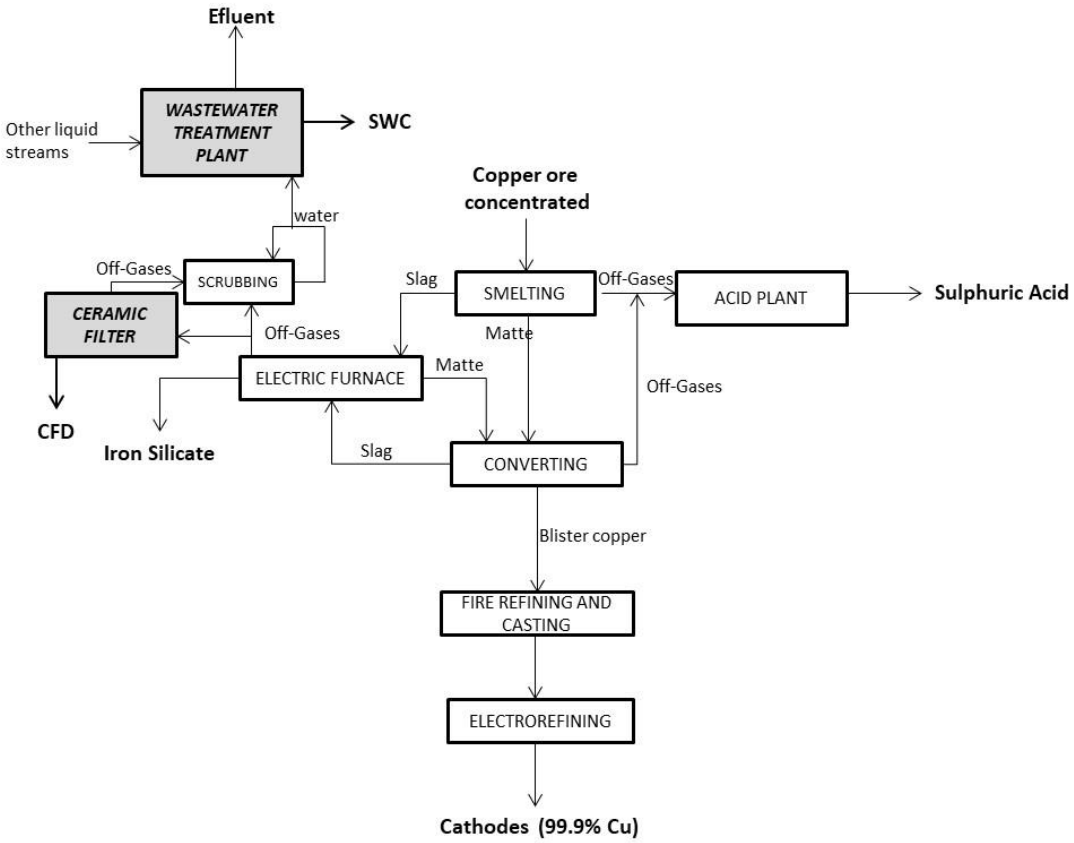

Figure 1.4 *Overview of material flows and processes from smelting copper*

1.1.2.3 Phosphogypsum from phosphoric acid production industry

Phosphorus is an essential component of all living systems, such as nervous tissue, bone and cell protoplasm. Phosphorus is highly reactive and, therefore, is not found as a free element in nature. It occurs principally in rock deposits containing various mineralized forms of calcium phosphate, from which commercial phosphate, a non-substitutable, non-renewable resource, is derived on a large scale. The production of phosphate fertilizers and animal feeds constitutes the major commercial activity in the phosphate industry.

Phosphorus compounds are also used in a wide variety of food, pharmaceutical, industrial and domestic products.

Phosphate deposits contain the naturally occurring radionuclides ^{238}U and ^{232}Th together with their decay progeny. The activity concentrations of radionuclides in the ^{238}U decay series are such that exceed 1 Bq/g. So, phosphoric acid production industry is considered NORM (Naturally Occurring Radioactive Materials) (IAEA, 2013).

Phosphate ores contain one or more phosphate minerals suitable for commercial use, such as calcium fluophosphate. The mineralogy of phosphorus rich rocks is complex and there are more than 200 known phosphate minerals. The main mineral group is the apatite group of calcium phosphates having the general chemical formula $Ca_{10}(PO_4,\pm CO_3,\pm OH)_6(OH,F,Cl)_2$. The exact chemical composition varies with origin. Apatites are found mainly in sedimentary, metamorphic and igneous rocks and include fluorapatite ($Ca_{10}(PO_4)_6F_2$), hydroxyapatite ($Ca_{10}(PO_4)_6(OH)_2$), carbonate-hydroxyapatite ($Ca_{10}(PO_4,CO_3)_6(OH)_2$) and francolite ($Ca_5(PO_4,CO_3)_3F,OH$)).

Phosphate ore is converted into commercial products using the following three main process steps:

(i) After being mined, phosphate ore is beneficiated to produce a concentrate known as phosphate rock (also known as beneficiated phosphate rock or phosphate rock concentrate).

(ii) As much as 85% of the phosphate rock produced in step (i) is converted into intermediate or final products using a process of acid digestion known as the ‘wet process’. A relatively small amount is converted directly into elemental phosphorus by reduction in an electric arc furnace in a process known as the ‘thermal process’. It is estimated that 71% of all phosphate rock produced is processed into phosphoric acid (involving, in most cases, the co-production of large amounts of phosphogypsum), 24% is processed directly into fertilizer and the remaining 5% is converted directly into various other products. The annual production of P_2O_5 in the form of phosphoric acid is more than 30 million t.

(iii) Most of the phosphoric acid produced in step (ii) (estimates vary from 75% to 90%) is subjected to further chemical processing to convert it into fertilizer. The fertilizer products so derived from phosphoric acid thus account for some 55–60% of total phosphate rock production. Of the remaining 10–25% of phosphoric acid produced in step (ii), about half is processed into animal feed supplements and half into a variety of other products.

Digestion of phosphate rock with sulphuric acid is the most common type of wet process used for phosphoric acid production. This process is carried out in Fertiberia S.A, the fertilizer industry, located in Huelva (southwest Spain), which is object of study in this thesis, using fluorapatite as raw material.

The process begin with the digestion of phosphate rock with sulphuric acid in a reactor vessel. The chemical reaction for the digestion of fluorapatite may be expressed as follows:

$$Ca_{10}(PO_4)_6F_2(s) + 10H_2SO_4(aq) + 20H_2O(aq) \rightarrow 10CaSO_4 \cdot 2H_2O(s) + 6H_3PO_4(aq) + 2HF(g) \quad \text{[Eq.1.4]}$$

In this process phosphoric acid, hydrogen fluoride and calcium sulphate, known as phosphogypsum, are produced. Following acid attack, the resulting phosphoric acid is transferred to one or more filtration assemblies in order to separate the acid from the phosphogypsum (PG), Figure 1.5. After separation the wet phosphogypsum is sent to a residue pile (stack) for storage, usually after washing to remove traces of phosphoric acid and fluoride. Hydrogen fluoride is collected and sent into scrubber where is absorbed in water producing a hydrofluoric acid weak effluent. This stream is mixed with phosphogypsum and deposited in the stockpiles, precipitating as hexafluorosilic acid (H_2SiF_6).

Phosphoric acid emerging from the filtration step has a P_2O_5 content in the range 24–36%. However, for most industrial applications, additional concentration step is required. The strength of the phosphoric acid is increased by evaporation to 40–55% P_2O_5. In Figure 1.5 is show the diagram of sulphuric acid digestion process for the production of high purity phosphoric acid.

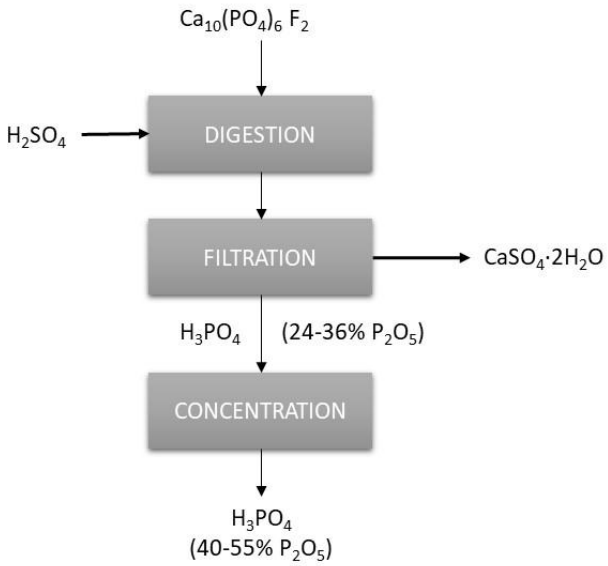

Figure 1.5 *Simplified diagram of sulphuric acid digestion process for the production of high purity phosphoric acid.*

PG is included in the Waste Catalogue List (06 09 04: Calcium waste from the production of phosphoric acid) according to the European Legislation, and it is classified as non-hazardous waste.

The current annual production of phosphogypsum worldwide is about 160 million t. Production is increasing worldwide and could reach 200–250 million t within the next decade or two. Due to the large quantities produced, two main alternative management approaches exist for surplus phosphogypsum:

(i) Stockpiling in large, above ground containment structures known as stacks, allowing the material to be used at a later time;

(ii) Discharging to water bodies, usually large rivers, river estuaries or the sea, thus permanently disposing of the material.

But, progressive changes in environmental regulation, have largely brought the discharge of phosphogypsum to water bodies to an end, causing considerably more phosphogypsum to be stored on land.

In Spain, concretely in Huelva, the production of phosphoric acid, and hence the generation of PG, began in 1965 and remained active for 45 years until 31 December 2010. During this period about 100 Mt of PG were stored in piles that reach up to 30 m in height, covering a surface of approximately 1200 ha. These deposits are located at the confluence of the Tinto and Odiel rivers (Fig 1.6), an estuarine area of salt marshes with a high ecological value, declared as Biosphere Reserve by UNESCO in 1983, which is known as "Ría de Huelva". In 1992, around 30% of the disposal area (zone 1) was restored, covering it with a 30 cm layer of natural soil and vegetation (Mas et al., 2001). Subsequently, another area (zone 4) was restored (20% of the total area) with more complex cover that comprises the following layers (in ascending order): a 1 m layer of building wastes, a 2 m layer of theoretically inert industrial wastes and 30–50 cm layer of topsoil (Directive 96/61/EC). However, nowadays about 50% of the disposal area is openly exposed to the environment weathering (unrestored areas; zones 2 and 3). In addition, the piles have a series of perimeter channels for collecting leachates from the PG weathering, but there are numerous points and diffuse sources of edge outflows that discharge to the estuary (Pérez-López et al., 2016)

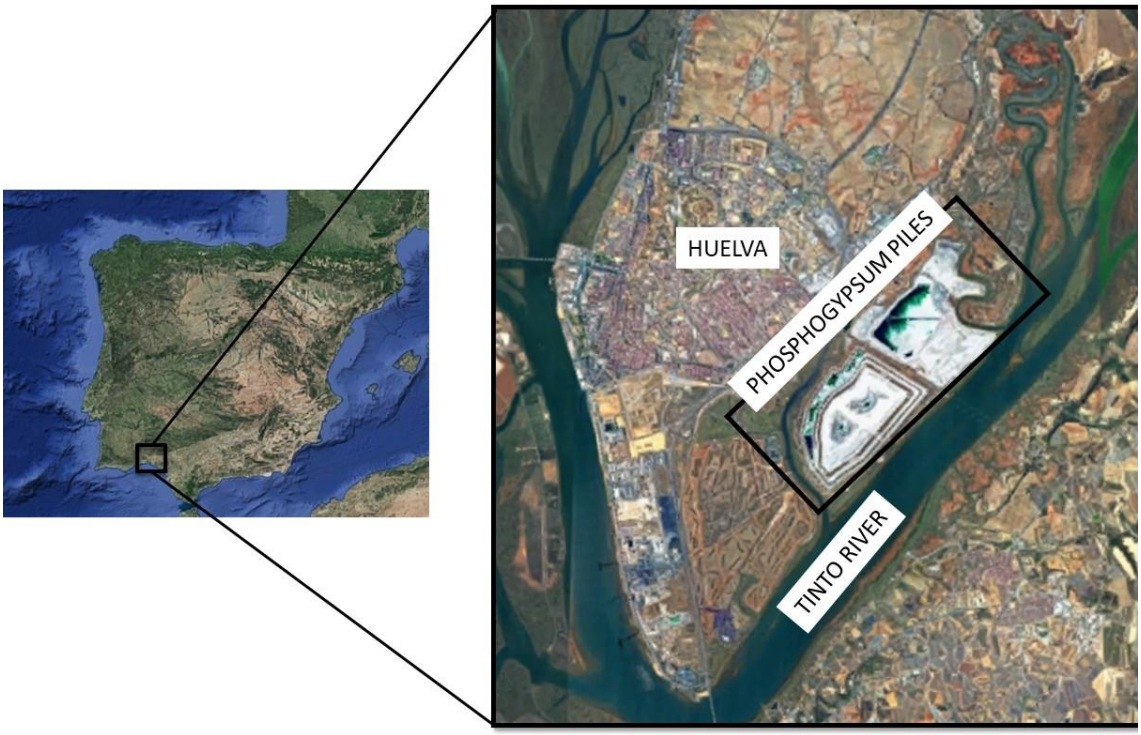

Figure 1.6 *Location of the phosphogypsum piles.*

1.2 OBJECTIVES

The main goal of this thesis has been to characterise physically and chemically the different industrial wastes describe previously, and also find commercial applications in which they can be used without implying any risk for environment or people.

To that aim, the following specific objectives are established:

1. To develop an adequate protocol of action with the objective of carrying out a correct characterisation and subsequent valorisation of the wastes.

2. To characterise physically, chemically, mineralogically and radiologically the waste, in order to know in depth their composition and potential toxicity.

3. To study the process of manufacture and formulation of the new materials, adjusting to the current regulations and the best available technology.

4. To assess the environmental impact of the new materials by carrying out leaching test and the measurement of the relevant radiological parameters, taking into account the regulation in force for the future application in order to ensure a negligible environmental risk.

1.3 TESIS STRUCTURE

This work is structured in 4 chapters. In this chapter 1, the background are presented, where the problems of the worldwide generation waste and the current European regulations are described. An exhaustive study of the different waste generation process studied are also detailed. In addition, the established objectives and the thesis structure are presented.

In chapter 2, materials and methods are deeply explained. Firstly, sampling waste and pre-treatment are described. Then, the measuring techniques used for the characterisation of the waste and new materials have been summarised. Finally, different methods used to evaluate the potential environmental risk and some technological properties for building materials are shown.

Chapter 3 is the core of this thesis where the results are presented and is divided in five parts:

- Section 3.1 reports the possibility of using tionite and red gypsum wastes as potential building materials for fire wall insulation or as fire-resistant panels. In this work have been carried out a depth physicochemical characterisation and TGA thermal analysis of these wastes, as well as a study of the new materials obtained. In addition, a preliminary fire resistance test was carried out with the aim of study their properties under certain conditions. This work has been published in Journal of Thermochimica Acta (Pérez-Moreno et al., 2013).

- Section 3.2 reports the use of red gypsum as a source of calcium for CO_2 sequestration by an indirect carbonation process. The study analyses the advantages and disadvantages of using sodium hydroxide or ammonium as extracting agents, calculating the carbonation factor. This work also evaluate the behaviour of radionuclides as well as the trace and major elements contained in the waste during the capture process. This work has been published in Chemical Engineering Journal (Pérez-Moreno et al., 2015).

- Section 3.3 shows the diagnosis for the choice of the best available techniques for the metal recovery, mainly Zn and Pb, from the two wastes produced in copper smelting, based on their extensive characterization. This work has been sent for publish in Journal of Cleaner Production (current status: under review).

- Section 3.4 reports the validation of the optimized BCR sequential extraction method for determining the mobility of natural radionuclides (^{210}Po, U-isotopes, Th-isotopes, and ^{226}Ra) in different environmental conditions. BCR-701 is proposed in this work as a potential certified reference material for radionuclides. This work has been sent for publish in Chemosphere Journal (current status: under review).

- Section 3.5reports the mobility of natural radionuclides contained in the PG stored in Huelva, ^{210}Po, U-isotopes, Th-isotopes, and ^{226}Ra, applying the optimized BCR sequential extraction procedure. In addition, the potential application of BCR sequential extraction is validated by comparison with the activity concentrations found in pore-waters, edge outflow leachates reaching the Estuary of Huelva and process water of perimeter channel. This work will be sent for publish as soon as possible.

Finally, in the chapter 4 the main conclusions of this thesis are described, as well as proposed research lines for the future.

Chapter 2. Materials and Methods

This chapter aims to show the samplings, pre-treatments, materials, methods, and equipment used in the studies carried out in this doctoral thesis. Different characterisation techniques were used in this work, such as laser diffraction particle sizing analysis, X-ray Diffraction (XRD), X-ray Fluorescence (XRF), Inductively Coupled Plasma Optical Emission Spectroscopy (ICP-OES), Inductively Coupled Plasma Mass Spectrometry (ICP-MS), Scanning Electron Microscopy (SEM), Thermogravimetry (TGA/DTA), alpha-particle spectrometry with PIPS detectors and gamma spectrometry with Ge detectors.

In addition, several tests were applied in order to evaluate the environmental implications of the studied materials. The mobility of pollutants were assessed using the TCLP test (Toxicity Characteristic Leaching Procedure), UNE-EN12457-4 leaching test, and BCR (Bureau Communautaire de Référence) sequential extraction procedure. On the other hand, the radiological implications of the use of final materials were analysed through the radiological index for building material. Furthermore, EN-1363-1 fire resistance test were implemented in order to evaluate the technological properties of new obtained material.

In the next section, the quality control applied in the different measurement techniques and tests will be also described.

2.1. SAMPLINGS AND PRE-TREATMENTS

In this section a description of the samplings and sample pre-treatments will be developed.

2.1.1. Samplings waste

The samplings were carried out by different ways:

(1) Tionite and red gypsum was supplied by TiO_2 pigment industry. The sampling process was taking one sample every 5 days along one month in order to ensure the homogeneity of the wastes used in the research (6 samples of each waste).

(2) Cake from scrubbing with water of slag cleaning furnace flue dust and ceramic filter dust, were provided by copper smelting. Five sampling campaigns were organised over a period of one month (5 samples of each waste).

(3) Phosphogypsum was directly collected from the pile number 3, where two sampling points were selected. From them, several samples were taken in depth, approximately at intervals of 50 cm, being the thickness of each sample around 5 cm.

2.1.2. Sample pre-treatment

After collection, the waste samples were preserved in plastic bags, and then, in the laboratory, they were dried until constant weight and homogenised[3].

The treatment to which the samples have been submitted to carry out the different measuring techniques is exposed in the following section.

2.2. MEASURING TECHNIQUES

This section we will outline the measurements techniques and equipment used in the physico-chemical and radiological characterisation of the collected samples and final materials.

Most of the measured have been performed using the techniques and tests described below. It should be noted that most of them have been carried out in accredited laboratories outside of FRYMA (acronym in Spanish of Física de Radiaciones y Medio Ambiente, Radiation Physics and Environment) research group where this doctoral thesis has been developed. Therefore, the general principles of each techniques and the quality control applied to ensure the quality of the measurements are summarised below.

2.2.1. Granulometry

Laser diffraction spectroscopy measures particle size distributions by determining the angular variation in intensity of light scattered when a laser beam passes through the suspended sample into water or another liquid where the sample is not soluble. The ISO 13320 (“Particle size analysis - Laser Diffraction methods - Part 1: General principles”) establishes Mie theory as the best option to determine the volume distribution of the particle size present in a granulated material.

Laser diffraction analysis, also known as laser diffraction spectroscopy, is a technology that uses diffraction patterns of a laser beam to measure geometrical dimensions of a particle. This process does not depend on volumetric flow rate, the amount of particles that passes through a surface over time. Large particles scatter light at small relative angles to the laser beam, while the smaller particles scatter light at larger angles. The

[3] Samples were homogenised using the cone and quarter technique.

angular scattering intensity is then analysed to calculate the size of the particles responsible for creating the scattering pattern, using the Mie theory of light scattering. The particle size is reported as a volume equivalent sphere diameter, which is defined as the diameter of a sphere having the same volume as the particle.

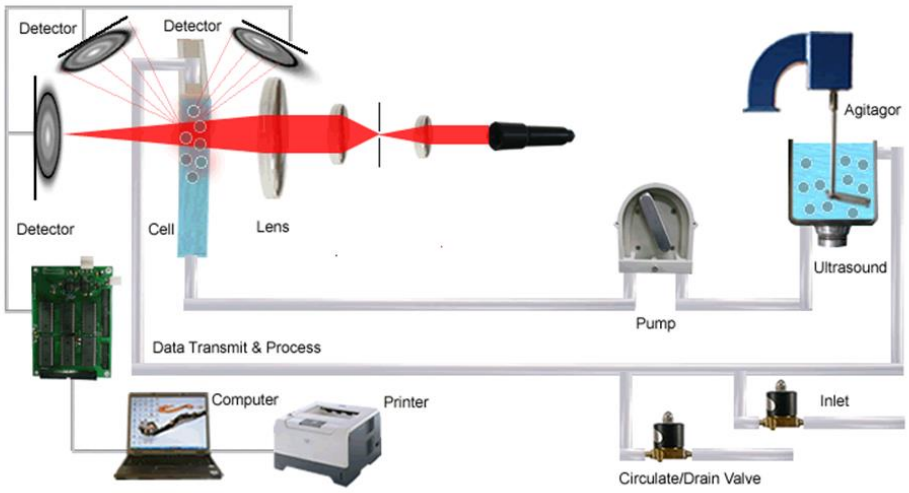

Figure 2.1. *Laser diffraction particle size analysis scheme.*

There are three main steps in the measurement process (Fig. 2.1):

1. The sample must be prepared and dispersed in a non-soluble solution and then delivered to the optical bench. This is the purpose of the sample dispersion units.

2. The capturing of the scattering pattern from the prepared sample - known as "measurement". The detector array within the optical bench is made up of many individual detectors. Each detector collects the light scattering from a particular range of angles.

3. Once the measurement is complete, raw data is analysed by software using the Mie theory. The resulting particle diameter is the geometric mean for each particular range of size particle.

The particle size analysis was performed by laser granulometry in wet suspensions with different dispersants depending of the sample, using a Malvern Mastersizer 2000 particle sizer with 52 detectors, Hydro 2000M accessory and He-Ne as light source, installed in the Central Research Services at the University of Huelva (Spain). The laser analyser provides the primary size information for particles in the 0.02 to 2000 μm range. For this,

weight of about 20-30 g of sample was placed in beakers with 50 cm^3 of dispersant. Subsequently, in order to facilitate the disaggregation of the sample, all the beakers were subjected, for 10 minutes, to an ultrasonic bath at a constant temperature of 35 °C. They were then placed in a flask and mixed using a magnetic stirrer at a constant speed (700 rpm) during 30 min to ensure the homogeneous distribution of the particles. Aliquots were then collected for granulometric analysis. The calibration method was performed with different certified reference materials: LTX3300C Nanosphere Size Standard; 2009A and 2009B Duke Polymer Microspheres Uniform Standards; 4009, 4009A and 4009B Duke Standards Microsphere Size Standards. Before each run, it is verified that the device parameters are in the range of measurement.

The program runs 10 counting on each aliquot (15 s measuring interval each) with 5 seconds delay between measurements. This process assures the sample is dispersed completely without a change in the distribution curve, otherwise the analysis is re-run. In addition, three aliquots are measured and the results and standard deviation given. The accuracy of this method is ± 1 % on the Malvern and the instrument-to-instrument reproducibility is better than 1 % RSD.

2.2.2. XRD

X-ray diffraction (XRD) is an analytical technique primarily used to study the internal structure of solids, in order to identify the crystalline phases of a powdered sample. XRD analysis is based on constructive interference between a monochromatic X-rays beam and a crystalline sample. The interaction of the incident rays with the sample produces a diffracted ray, being the maximum of interference given by the Bragg's Law (Eq. 2.1):

$$n\lambda = 2\mathrm{d}\sin\theta \qquad \text{[Eq. 2.1]}$$

, where λ is the wavelength of the laser ray, θ is the angle between the incident rays and the surface of the crystal, d is the spacing between layers of atoms and n is the order of diffraction integer (integer number). The key component is the angle between the incident and diffracted rays, since each crystalline phase has its own characteristic peaks in a diffractogram.

X-ray diffractometers consist in an X-ray tube where electrons are produced and accelerated onto the target (Fig. 2.2). When electrons have sufficient energy to dislodge electrons of the target material, characteristic X-ray spectra are produced. The specific wavelengths are filtered by a crystal monochrometer to produce monochromatic X-rays.

These X-rays are collimated and directed onto the sample, placed in a sample holder. The refracted X-rays are detected by the counter. In addition, the X-ray tube and X- ray detector are installed in a rotation system around the sample holder.

The characteristic x-ray diffraction pattern generated in a typical XRD analysis provides a unique "fingerprint" of the crystals present in the sample. When properly interpreted, by comparison with standard reference patterns, this fingerprint allows identification of the crystalline forms present in the sample.

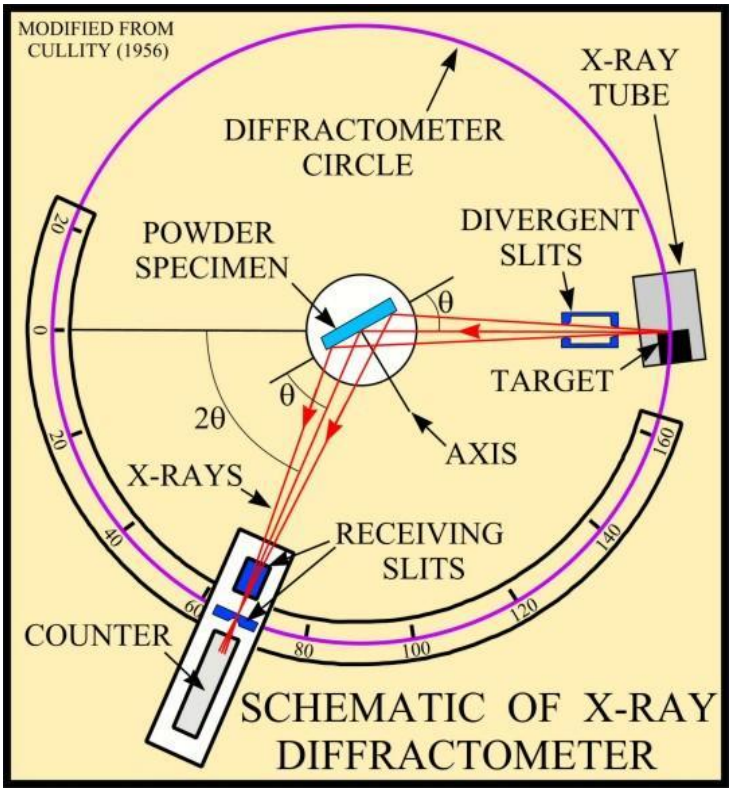

Figure 2.2. *Schematic of X-ray Diffractometer.*

The mineralogical characterisation of the powder samples was performed in the Central Research Services of the University of Seville (Spain) by using a Bruker diffractometer (D8-Advance A25 with $Cu_{K\alpha}$ radiation). Diffractometer settings were 40 kV, 30 mA, a scan range of 3-70° (2θ) with a step size of 0.015º, a rotational speed of 30 rpm and a counting time of 0.1 s per step. Similarly, at the Activation Laboratories Ltd. (Actlabs) a Panalytical X'Pert Pro diffractometer equipped with a Cu X-ray source and an X'celerator detector was used, operating at the following conditions: voltage: 40 kV; current: 40 mA; range: 5-70 deg 2θ step size: 0.017 deg 2θ; time per step: 50.165 sec; divergence slit:

fixed, angle 0.5°. Under these measurement conditions, the detection limit was around 5 % in both cases.

The X-ray diffraction analysis has been performed according to the disoriented powder method. Random mounts are preferred when identification of phases in a specimen is required. In this type of mount, a few tenths of a gram (or more) of the purest material are needed. The sample is grinded to a fine powder, typically less than 10 μm in size is preferred. Then, the sample is placed into a sample holder, smeared uniformly onto a glass slide, assuring a flat upper surface, packed into a sample container and sprinkled on double sticky tape. Care must be taken to create a flat upper surface and to achieve a random distribution of lattice orientations.

The crystalline mineral phases were identified in X'Pert HighScore Plus using the PDF-4 Minerals 2013 ICDD database, according to (ACTLABS, Ontario, Canada), and their quantification were determined using the Rietveld method. The Rietveld method is based on the calculation of the full diffraction pattern from crystal structure information. In this case, the powdered samples were mixed with corundum as an internal standard, to determine the amount of X-ray amorphous material. On the other hand, only the crystalline mineral phases were identified in the obtained spectra from Seville, using software "Match" with COD database.

The quality of the measurements is verified with Standard Reference Materials (SRMs), such as Corindon (SRM 1976a), in which is checked that the measured interatomic distance corresponds to the certified ones. The statistical error of ± 5 % in an intensity-related quantitative analysis should be considered reasonable.

2.2.3. XRF

X-ray fluorescence (XRF) is based on the principle that individual atoms, when excited by an external X-ray energy source, emit X-ray photons of characteristic energies. This characteristic radiation permits to identify and quantify each element in the sample.

A XRF spectrometers consist of an X-ray tube that produces an intense X-ray beam onto the sample. The excited sample emits X-rays along a spectrum of wavelengths/energy characteristic of the atoms present in the sample. The atoms in the sample absorb X-ray energy by ionising, ejecting electrons from the lower (usually K and L) energy levels (Fig. 2.3). Electrons from outer levels replace the ejected electrons, and then energy is

released in the form of emission of characteristic X-rays indicating the type of atom present.

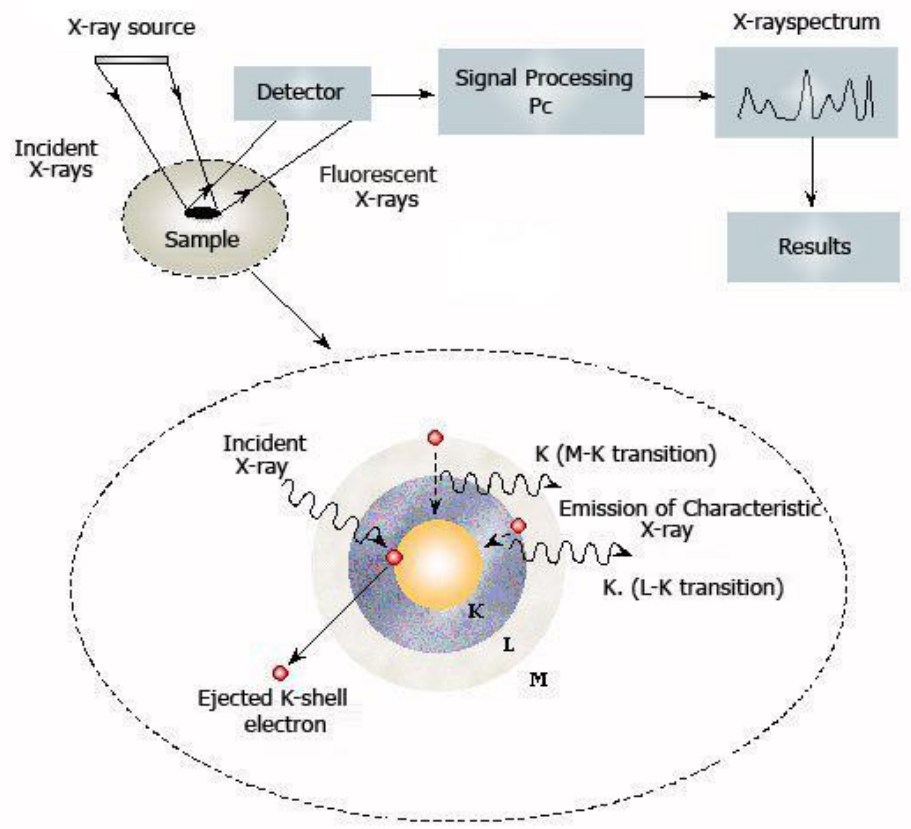

Figure 2.3. *General scheme of X-ray fluorescence analysis.*

The detectors measure the intensity of the X-rays emitted by the sample, and a multichannel analyser assigns to each pulse height an energy value, given its representation the XRF spectrum. The net area of each peak is proportional to the abundance of the corresponding element in the sample. The exact value of this proportionality for each element is derived by comparison to mineral or rock standards whose composition is known.

Major elements were determined by X-ray Fluorescence sequential spectrophotometer Panalytical (model AXIOS) in the Central Research Services of the University of Seville (Spain). The system is equipped with X-ray tube of 4 kW, Rh front window and anode, five analysing crystals (PX1, PE 002, LIF 200, Ge 111, and LIF220) and two X-ray detectors, flow and scintillation. Flow detectors measure elements from C to Cu and

scintillators from Cu to U. In general, elements with a concentration below 50 mg kg-1 (50 ppm) are difficult to detect.

This technique requires the samples under analysis to be as homogeneous as possible. Thus, 1 g of dry grounded sample was mixed with 10 g of lithium tetraborate and 5 drops of 20 % lithium iodide to form a homogenous glass ready for examination (Fig. 2.4).

Figure 2.4. *Sample preparation for XRF analysis.*

The calibration method was performed with a standard containing an adequate number of elements to provide sufficient peaks for calibration. These peaks should be separated from other peaks by at least 3 to 4 keV to avoid confusion in assigning peaks to their corresponding elements. The calibration standard used was the M.A.C.® 80090-20 X-Ray Fluorescence Universal Set 20 elements (Na, Mg, Al, Si, P, S, Cl, Ca, Ti, Cr, Mn, Fe, Ni, Cu, Zn, Nb, Sn, Ba, W, Pb). In general, the detection limits according to the average and standard deviations from 6 blanks ranged from 1 to 100 ppm depending on each particular element. The analysis was performed in duplicate with differences below 5 % between them. The analytical accuracy was checked by the analysis of certified reference materials GBW 07238 (NCS DC 70006), SX18-04 and BIR-1a. The average accuracy of the measurements was smaller than 5 %.

2.2.4. ICP-OES

The Inductively Coupled Plasma Optical Emission Spectrometry (ICP-OES) is a trace-level elemental analysis technique that uses the emission spectra of a sample to identify, and quantify the elements through the measurement of the intensity of radiation emitted for element-specific.

Sample introduced into the ICP as liquid form is the typical procedure for sample introduction, while the solid sample is converted into liquid by dissolving it into proper solvent. Liquid sample undergoes through different steps when injected to the ICP (Fig. 2.5).

The first process is called nebulisation, and it takes place when the sample is converted to an aerosol, a mist of finely divided droplet. The most common nebuliser is a concentric tube, where the sample is sucked into capillary tube by a high-pressure stream of Argon gas flowing around the tip of the tube. This pressure breaks the liquid into fine droplets in various sizes in the spray chamber.

In the spray chamber the large droplets go to drain the fine droplet carried to the torch. More than 99 % of the injected sample goes to drain and less than 1 % carried out to the torch.

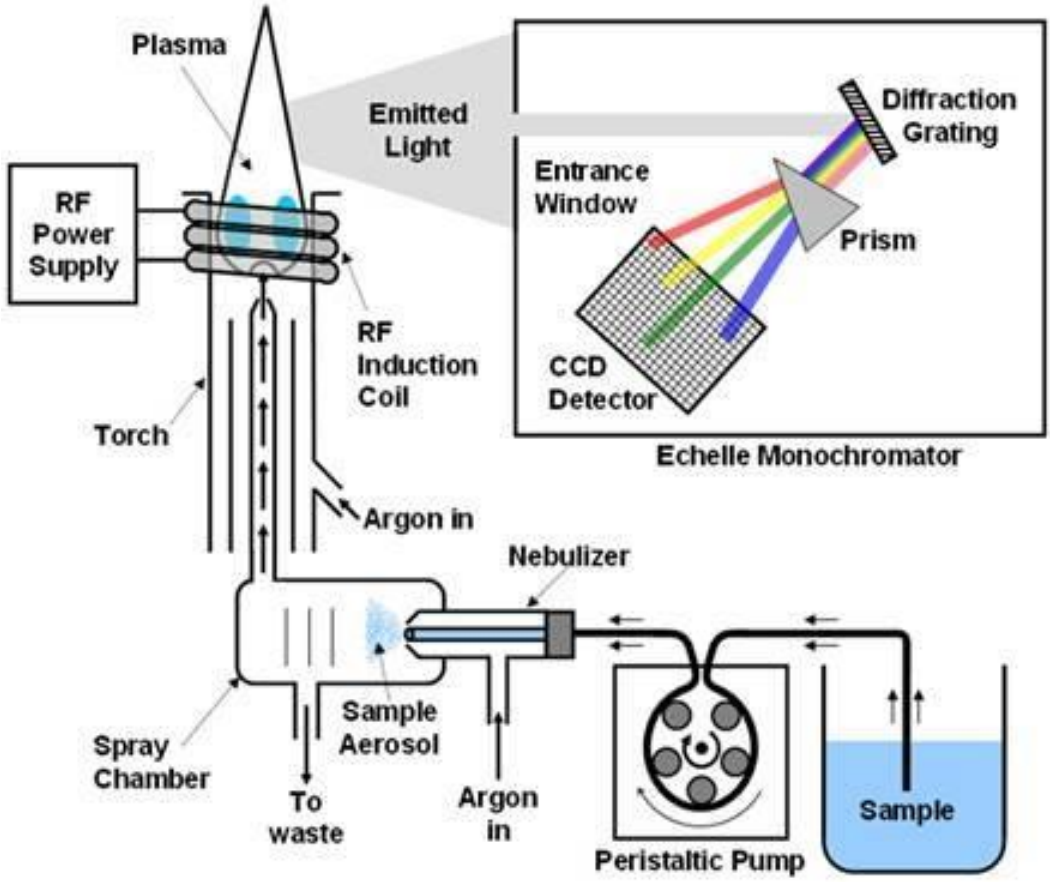

Figure 2.5. *Diagram of Sample introduction to ICP-OES*

The torch often is formed by three concentric quartz tubes through which streams of argon gas flow. A spark from a Tesla coil initiates ionisation resulting ions and their associated electrons interact with the fluctuating magnetic field produced by the induction coil. Adding mechanical energy to the electrons/ions by the use of the induced field within the heart of the plasma is called "Inductively Coupling".

A stable high temperature plasma of about 7000 K is then generated as the result of the inelastic collisions created between the neutral argon atoms and the charged particles. The sample immediately collides with the electrons, charged ions in the plasma and is itself broken down into charged ions. The molecules break up into their respective atoms, which then lose electrons and recombine repeatedly in the plasma, giving off radiation at the characteristic wavelengths of the elements involved.

Transfer lenses are then used to focus the emitted light on a diffraction grating where it is separated into its component wavelengths in the optical emission spectrometer.

Within the optical chamber, after the light is separated into its different wavelengths, the light intensity is measured with a photomultiplier tube or tubes physically positioned to "view" the specific wavelength for each element line involved.

The intensity of each line is then compared to previously measured intensities of known concentrations of the elements, and their concentrations are then computed by interpolation along the calibration lines.

ICP-OES is suitable for the trace elements analysis present at high concentrations (100 ppb-1000 ppm), and is used for much type of matrices of environmental samples especially for high effect-matrix samples. Therefore, this technique is more robust than ICP-MS for analysing samples as ground water, wastewater, soil, and solid waste. The element concentrations were carried out at the Activation Laboratories Ltd (ACTLABS, Ontario, Canada), by using an ICP-OES Varian 735ES spectrometer.

Previous to the analysis, the solid samples were homogenized and grounded, and then digested following the four-acid method, requiring HCl, $HClO_4$, HNO_3 and HF, also called the "near total dissolution method". In this method, 0.25 g samples were taken and digested with four acids beginning with hydrofluoric, followed by a mixture of nitric and perchloric acids, heated using precise programmer controlled heating in several ramping and holding cycles which takes the samples to incipient dryness. After incipient dryness

is attained, samples are brought back into solution using aqua regia. Subsequently, the samples are diluted and analysed.

Multielement standard solutions were prepared from single certified standards supplied by SCP SCIENCE and prepared in a matrix of Milli-Q ultrapure water and nitric acid suprapur 2 % (v/v) for the calibration of the equipment. The concentration of elements in the prepared standard were 0 (instrumental blank), 0.05, 0.5, 1, 5, 10, 25 and 50 ppm for all elements except Al and Fe. In these cases, 100 and 150 ppm respectively of each element were added to the previous concentrations. Detection limits were calculated from the average and the standard deviation obtained by the measuring of at least 5 blanks. Detection limits were below 0.1 mg L^{-1} for these elements.

A triplicate analysis was performed in order to evaluate the analytical precision (repeatability), showing differences below 5 % in all case. The analytical accuracy was checked by the analysis of different certified reference material, such as GXR4, OREAS 45d, FC-1 and FC-2, etc. In addition, the quality control included the use of a reagent blank and replicates.

2.2.5. ICP-MS

While ICP-OES technique measures the radiation emitted by the different atoms through an optical detector, the ICP-MS detects and counts the number of ions by using the mass spectrometer based on the mass-to-charge ratio (m/z).

In the same way as in ICP-OES, solid samples are previously digested following the four-acid method. The sample solution is introduced into the device by means of a peristaltic pump, then it becomes nebulised in a spray chamber, and then the aerosol is injected into an argon-plasma with a temperature of 6000-8000 K.

Then, the ions from the ICP source are collimated and focused into the entrance aperture of the mass spectrometer by the electrostatic lenses. Only a small amount part of the ions produced in the plasma further penetrate to the mass-spectrometer part.

The quadrupole mass spectrometer is a mass filter that only allows ions having a limited range of m/z values reach the transducer. Ions that are not of the correct m/z collide with the rods or exit the path between the rods and are pumped out of the system. Quadrupole instruments easily resolve ions that differ in mass by one unit.

Each ion that exits from the mass spectrometer system hits the detector producing an electrical amplified signal, which is proportional to its m/z ratio, producing a mass spectrum with peaks corresponding to the different mass/z ratios. The quantification is achieved by comparing the measured counts in an unknown sample with a standard containing a known amount concentration of the problem element (Fig. 2.6).

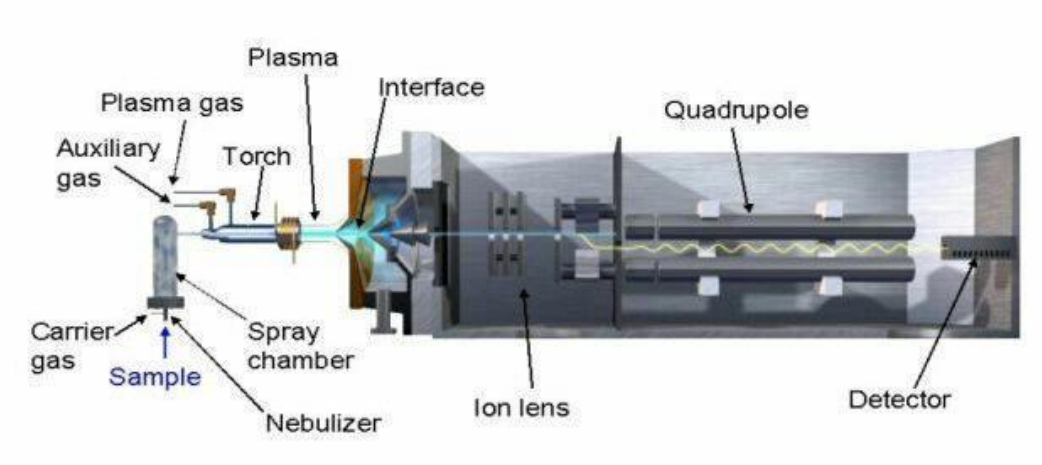

Figure 2.6 *Schematic cross-section of a quadrupole ICP-MS*

ICP-MS is particularly suitable for isotope ratio studies and ultra-trace analysis of elements, being the instrumental detection limits (IDL) in the range from 1 ppt to 10 ppb, depending of each particular element. In addition, this technique shows a wide dynamic range. On the contrary, this technique is not able to measure some non-metallic elements (e.g. S, P, Ti, Sc), which can be determine by ICP-OES.

Trace elements were determined by ICP-MS (inductively coupled plasma mass spectrometry) at the Activation Laboratories Ltd (ACTLABS, Ontario, Canada) using Perkin Elmer Sciex ELAN 9000 spectrometer. The quality control method included the use of a reagent blank, standard reference materials (GXR-6, SAR-M and SBC-1) and replicates. The accuracy of the analytical data ranges from ± 5-10 %.

2.2.6. Scanning Electron Microscope (SEM)

The scanning electron microscopy (SEM) uses a focused beam of high-energy electrons to generate a variety of signals at the surface of solid specimens. The signals that derive from electron-sample interactions reveal information about the sample including external morphology (texture), chemical composition, and crystalline structure and orientation of materials making up the sample. In most applications, data are collected over a selected

area of the surface of the sample, and a 2-dimensional image is generated that displays spatial variations in these properties. Areas ranging from approximately 1 cm to 5 μm in width can be imaged in a scanning mode using conventional SEM techniques. The SEM is also capable of performing analyses of selected point locations on the sample; this approach is especially useful in qualitatively or semi-quantitatively determining chemical compositions by using Energy-Dispersive X-Ray Spectroscopy (EDS).

Accelerated electrons in an SEM carry significant amounts of kinetic energy (30-300 KeV), and this energy is dissipated as a variety of signals produced by electron-sample interactions when the incident electrons are decelerated in the solid sample. These signals include secondary electrons (that produce SEM images), backscattered electrons (BSE), diffracted backscattered electrons (EBSD that are used to determine crystalline structures and orientations of minerals), photons (characteristic X-rays that are used for elemental analysis and continuum X-rays), visible light (cathode luminescence–CL), and heat.

Secondary electrons and backscattered electrons are commonly used for imaging samples. Secondary electrons are most valuable for showing morphology and topography on samples, while the backscattered electrons are most valuable for illustrating contrasts in composition in multiphase samples, i.e. for rapid phase discrimination, since the brightness is directly related with the atomic number of the study zone (whither zones present higher Z). Secondary electrons are emitted from the surface with a certain velocity that is determined by the levels and angles at the surface of the sample. The secondary electrons, strike the scintillator (fluorescing mirror) that produces photons. The location and intensity of illumination of the mirror vary depending on the properties of the secondary electrons. The signal produced is amplified and transduced to a video signal with the “topography” of the sample.

Moreover, there is a probability that some of the incident electrons will suffer a large deviation from the incident direction and be “reflected” backwards. These electrons are called “backscattered” electrons (BSE) and provide compositional information, since the BSE signal intensity of a material is proportional to its average atomic number. This implies that parts of a sample having different composition generate different intensity of backscattered electrons, although there is no difference of topography between them.

If an X-ray detector is incorporated, the characteristics X-rays generated by the electron beam are detected and analysed with an energy dispersive X-ray spectrometer (EDS). The

EDS spectra can be used to obtain a qualitative and/or semi-quantitative elemental analysis at micrometre spatial resolution (Fig. 2.7).

The microstructure was examined by scanning electron microscopy in the University of Huelva (Spain) using a Fei-QUANTA 200 microscope and JEOL 6460LV in the University of Seville (Spain), both equipped with an Energy Dispersive Spectrometer (EDS).

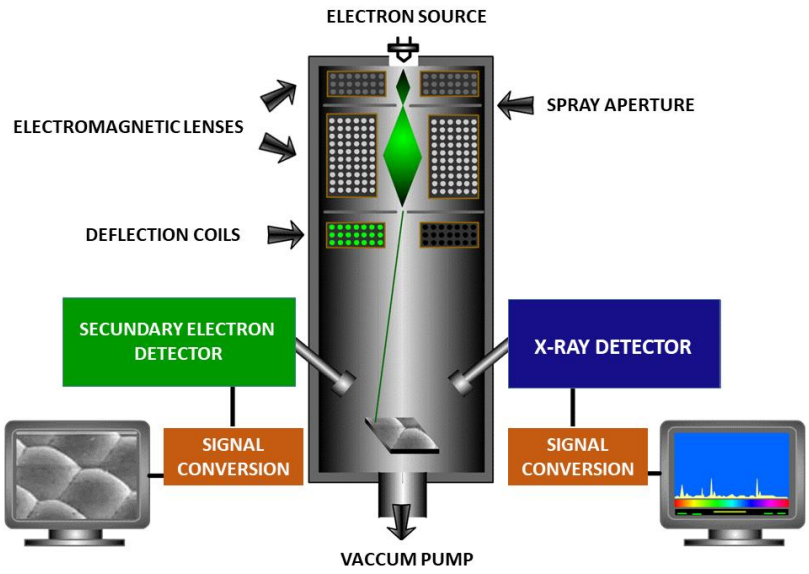

Figure 2.7. *SEM-EDS scheme overview.*

SEM specimens were embedded in epoxy resin (Araldite®), grinded with silicon carbide paper (SiC paper) and polished with 6, 3 and 1 µm diamond pastes after. The samples were washed with deionised water and attacked with 5 % HF for 10 seconds, to highlight the developed phases. Chemically fixed material were ultrasonically washed with distilled water and ethyl alcohol and dried below the critical point to avoid damage of the fine structures due to surface tension. To facilitate their observation under the microscope, the samples are made conductive for current, and so, the specimens were coated with a thin layer of Au-Pd in a Blazers SCD 050 sputter (Fig. 2.8).

***Figure 2.8**. Sample holders for SEM analysis*

2.2.7. Thermogravimetric Analysis (TGA) and Differential Thermal Analysis (DTA)

Thermal analysis studies how the properties of materials change with temperature. This analysis typically measures heat flow, weight loss, or mechanical properties as a function of temperature. Several methods are frequently used, which are distinguished from one another by the measured property.

In this thesis were used two of these methods, Thermogravimetric Analysis (TGA) and Differential Thermal Analysis (DTA).

- TGA is a technique in which the mass of the sample is monitored against time or temperature in a specified atmosphere. The first derivative of the TG curve (DTG) is very useful, because it makes the noticing of small features/boulders on the curve much easier.

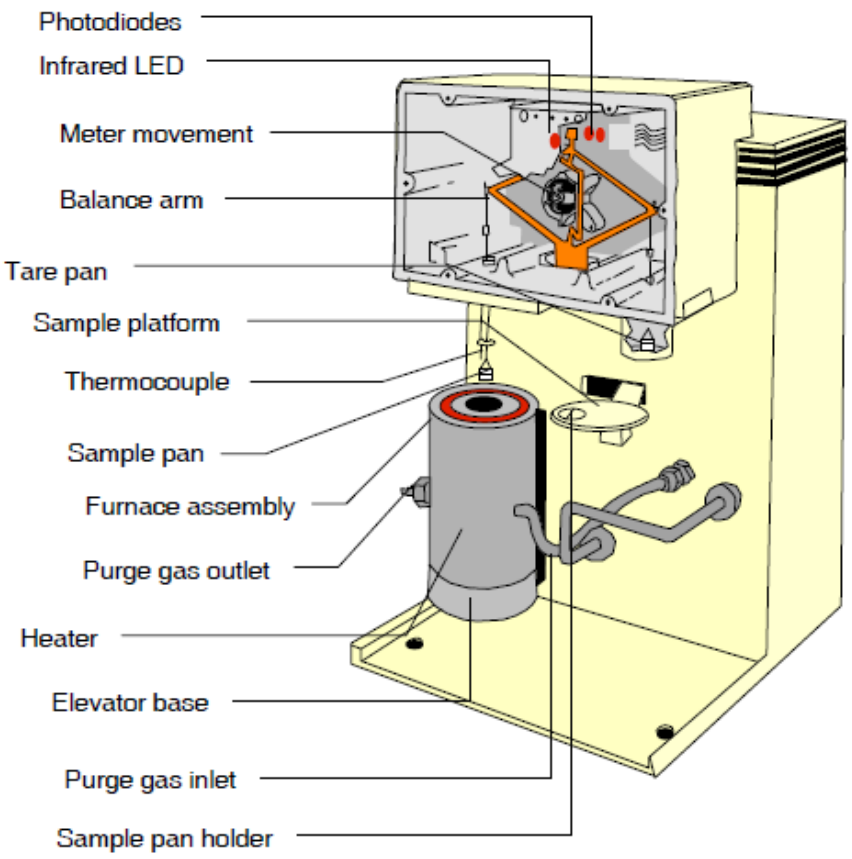

Figure 2.9. *Chart diagram of the TG*

A TGA analyser consists of a sample pan that is supported by a precision balance (± 0.0001 mg) (Fig. 2.9). The pan resides in a furnace while is heated or cooled during the experiment. The furnace can be programmed either for a constant heating rate, or for heating to acquire a constant mass loss with time. The atmosphere in the sample chamber may be purged with an inert gas to prevent oxidation or other undesired reactions or a reactive gas. This gas flows over the sample and exits through an exhaust. In addition, a cooling device is installed to cool down the sample.

Figure 2.10 shows TG and DTG curves of a solid sample, in which four peaks are observed, corresponding to different thermic events. The determination of these events as well as the mass losses that take place in them, make possible the quantification of species that composed the sample.

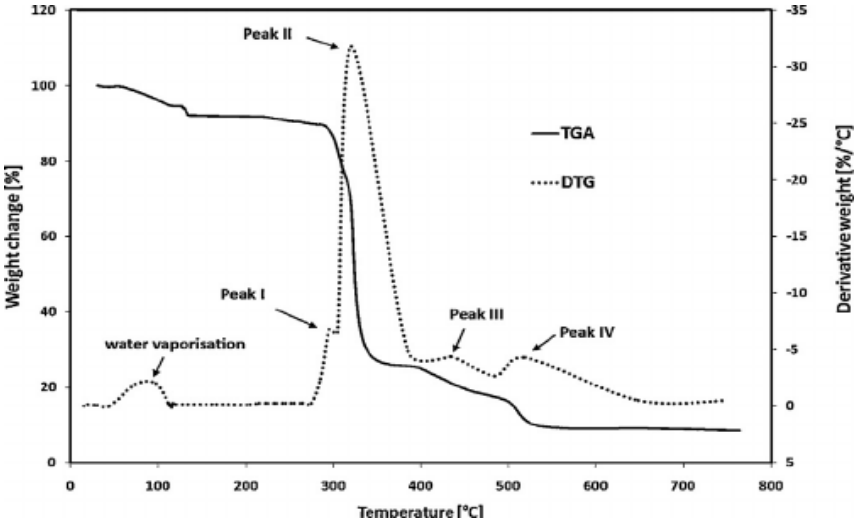

Figure 2.10. *Example of TG/DTG curves*

- DTA is a technique in which the difference in temperature between the sample and a reference material is monitored against time or temperature while the temperature, in a specified atmosphere, is programmed. DTA curve can provide information about physical phenomena, such as exothermic (i.e. oxidation process, crystallization) and endothermic (i.e. melting point, decomposition) phenomena (Fig. 2.11). This is a qualitative method.

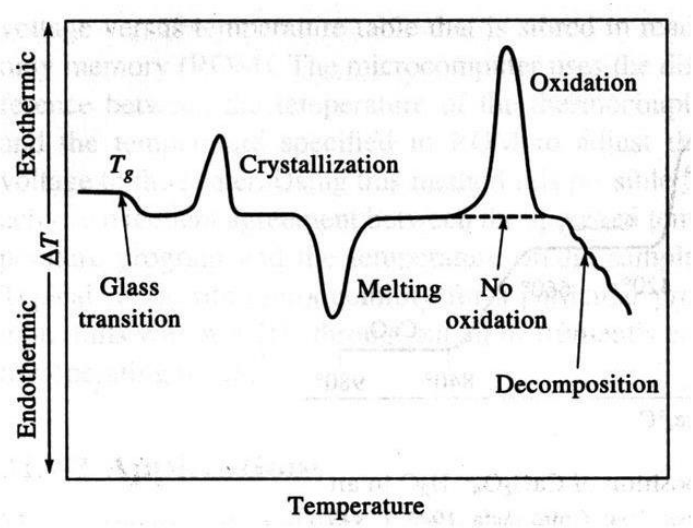

Figure 2.11. *Typical DTA curve*

The sample and the reference are placed symmetrically in the furnace. The furnace is controlled under a temperature program and the temperature of the sample and the reference are changed. During this process, a differential thermocouple is set up to detect the temperature difference between the sample and the reference. A diagram of the process is shown in Fig. 2.12.

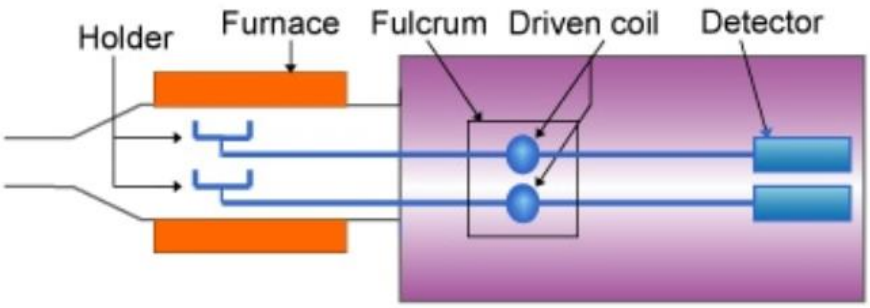

Figure 2.12. *Block diagram of horizontal differential DTA*

The thermal behaviour on samples was performed in the University of Oviedo (Spain) using a TG-SDTA Mettler 851E. TGA/DTA scans were performed between 25 ºC and 1000 ºC at 10 ºC min^{-1} in N_2 inert atmosphere (50 ml/min), platinum pan and calcined Al_2O_3 as reference material. In addition, the thermal analyser was coupled to an ICP-MS equipment (Pffeifer Thermostar) to determine the composition of off-gasses. The analysed material was previously finely ground and homogenised.

To obtain accurate experimental results the thermal analyser was calibrated when running experiments and periodically thereafter. As a minimum, it was recalibrated anytime the beam set, experimental heating rate, or purge gas is changed. In addition, a blank test was performed.

The temperature calibration is carried out using high purity standards (In, Sn, Bi, Pb and Au) with well-defined heat capacities.

TGA/DTA standard calibration includes the following procedures:

- TGA Weight Calibration: Calibration of the TGA weight signal.
- TA Baseline Calibration: Calibration of the Delta T signal. Baseline correction for a given scan rate (1 – 40 ºC min^{-1}).

- Temperature Calibration: Calibration of the temperature, heat of reaction, heat capacity scale.

2.2.8. Alpha spectrometry

Alpha spectrometry is a technique based on the interaction of α-particles with matter, being its aim to determine the activity concentration of a specific radionuclide in a sample (Bq kg^{-1} or Bq m^{-3}). It is a powerful analytical method, extremely sensitive and specific for a large number of both alpha-emitter natural radionuclides (^{210}Po, U-isotopes, Th-isotopes, etc.), and anthropogenic (Pu-isotopes, Am-isotopes, etc.) in any type of samples. The application of this method requires minimisation of the alpha particle self-absorption effects at the source, since the alpha particles are absorbed in a few microns of solid material.

To avoid spectrometric interferences, the radioelements are firstly isolated and purified chemically, and then they are electroplated or self-deposited on a thin layer of the sample uniformly and quantitatively onto an acceptable backing material in order to avoid the self-absorption of the emitted alpha particles in the radioactive source. These two steps are covered by applying a radiochemical procedure.

2.2.8.1. Radiochemical method

The main steps of a radiochemical method to apply the radiometric technique of the alpha-particle spectrometry with PIPS (Passivated Implanted Planar Silicon) detectors in Fig. 2.9 is shown. After the sample pre-treatment (homogenisation, calcination, co-precipitation, etc.), the tracers are added to quantify the yield of the global procedure, and then the sample is dissolved with inorganic acids or by fusion.

The next step is the isolation of the different radioelements of interest (in our case, U-isotopes, Th-isotopes, ^{210}Po and ^{226}Ra). The radiochemical process ends with the manufacturing of the very thin radioactive source, usually by electrodeposition or micro-precipitation (Fig.2.13).

The last step of the radiometric technique will be to take the alpha spectrum (counting), and posterior calculation of the activity concentration of each radionuclide of interest, and its uncertainty.

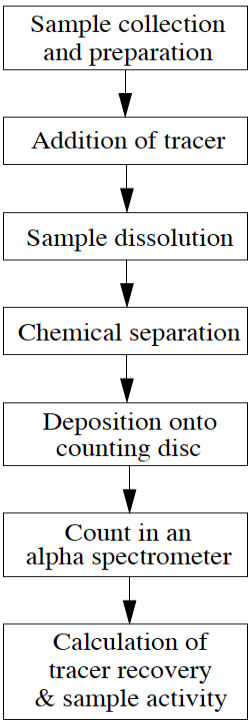

Figure 2.13. *Blocks diagram of a generic radiometric method to measure radionuclides by alpha-particle spectrometry with PIPS detectors.*

In our case, the method begins with addition of the radiochemical tracers, and dissolution of the sample by using four strong acids (HCl, HNO_3, HF and $HClO_4$). Later, actinides are isolated by using tributilphosphate (TBP), and purified with exchange resins. Then, the U- and Th-isotopes are electrodeposited onto stainless steel discs, ^{226}Ra were micro-precipitated and, Po is self-deposited onto silver discs. Finally, the obtained discs are counted in an alpha spectrometer and the activity concentration calculated.

Step 1. Selection of the tracers

Due to the losses of radionuclides during the analytical separation processes, a known activity of an artificial radioactive isotope (same chemical behaviour to the radionuclide of interest) was added in order to evaluate the recovery of the radiochemical process. The tracers used in this method (^{209}Po, ^{232}U and ^{229}Th), are shown in the Table 2.1. In case of radium tracer, ^{225}Ra was used, being direct daughter of ^{229}Th. However, ^{225}Ra is a β emitter and decays to ^{225}Ac, which in turn decays to a series of short-lived α-emitting progeny; of these, ^{217}At is the most convenient to measure, when the ^{225}Ac activity reaches a maximum after 20 days. The measuring method of Ra-isotopes is described in the section 2.2.8.3.

In addition, three conditions must be fulfilled in the selection of the tracers. Firstly, the emission energy must be different between the radionuclide subject of study and its tracer. Secondly, the tracer will be an isotope of the selected radionuclide (the same chemical behaviour) and finally the tracer must be artificial radionuclide, to ensure that the sample does not contain it.

Table 2.1. *Information about the isotopes used as tracers in alpha spectrometry. With ± S is indicated the combined standard uncertainty of the Certified Reference Material (CRM).*

Radionuclide	a (Bq L^{-1}) and Reference Date	$T_{1/2}$ (years)	Energy (MeV) and emission probability (%)
^{209}Po	105.6 ± 0.1 (15/03/1994)	102	4.88 (99 %)
^{229}Th	177.6 ± 1.1 (31/12/2007)	7340	4.797 (1.2 %), 4.814 (9.30 %); 4.837 (4.8 %); 4.845 (56.2 %); 4.901 (10.20 %); 4.967 (5.97 %); 4.978 (3.17 %); 5.050 (5.2 %); 5.052 (1.6 %)
^{232}U	72.5 ± 0.3 (25/03/2003)	69.8	5.32 (68 %) 5.27 (32 %)

Step 2. Digestion of the samples

The samples were subjected to acid digestion in microwave according to EPA 3052 method (EPA, 1996) until near total dissolution. It was taken 0.2-0.5 g of sample and transferred to the reaction vessel with the tracers (^{209}Po, ^{229}Th and ^{232}U), in amounts according to the expected activity concentrations of the samples, and the addition of 9 mL HNO_3, 2 mL HCl, 3 mL HF and 2 mL H_2O_2. The vessels were sealed and heated in the microwave system. The samples were heated to at least 180 °C over 5.5 minutes and then held at 180 °C for at least 9.5 minutes.

After this, they were taken from the oven, cooled, opened, and the samples were transferred to a Teflon vessel, being washed with 5 mL of HCl. Then, the samples were evaporated to dryness and 6 mL of $HClO_4$ were added and evaporated again, with the aim to dissolve the silicates (SiO_2).

Finally, it was added 10 mL of HNO_3 and transferred the sample to a beaker, where the sample was conditioned to 5 mL of 8M HNO_3.

Step 3. Radioelements sequential isolation based on TBP and Ion-exchange resins

This radiochemical method has been performed by our research group (Bolívar et al., 1995) (Fig. 2.12), and is based on the property of TBP (tributyl phosphate, $C_{12}H_{27}PO_4$) to absorb the actinides.

The previous digested sample was added into a funnel with others 5 mL of 8 M HNO_3 used to clean the beaker. Five millilitres of TBP was added in the funnel and shaken for about 10 min, and settled for another 10 min without covering it until the complete separation of phases. The previous two steps were repeated adding 10 mL of 8 M HNO_3 to the funnels to ensure complete separation. The aqueous phase (8 M HNO_3), which contains polonium and radium isotopes, was collected in clean beakers and pass to the self-deposition stage. Radium contained in this phase were isolated after Po self-deposition (Fig. 2.12). The radium isolation was performed with ion exchange resin AG50x8 (3 g) previously conditioned to HCl medium (10mL deionized water, 20mL 6M HCl, and 10mL 0.5 M HCl). The aqueous phase, in which sample was content, was previously conditioned to 1.5M HCl and was loaded into the resin. Some interferences, such as calcium and actinium, were eluted with different solutions (3M HCl and 1.5M NH_4Ac in 0.1M HNO_3) and finally radium was extracted with 20 mL of 5M HNO_3. Later, the solution passed to the micro-precipitation step, Figure 2.12.

On the other hand, the organic phase that remains into the funnel contain the actinides (U and Th). The back-extraction of Th was conducted by adding 20 mL of xylene ($C_6H_8O_6$) and 15 mL of 1.5 M HCl to the organic phase in the funnel, shaken and settled for 10 min, each. The aqueous phase was separated (Th fraction) and this was repeated twice, using 15 mL of 1.5 M HCl (Fig 2.12). The beakers with aqueous solution pass to the thorium purification and separation by anion exchange resin.

A chromatography column was used to purify the Th fraction, which contains trace of U. Previously, the sample was conditioned to 10 mL of 8M HNO_3 (65 %). Then, the column was prepared with the addition of 3 g of AG1X8 Resin (100-200 mesh) and washed with 20 mL of 8 M HNO_3 with a flow of 0.8-1.0 mL min^{-1}. Then, the Th fraction was passed through the column to elute U and other interfering ions, then this solution was discarded.

The thorium was extracted from the column with 40 mL of 9 M HCl. Finally, aqueous solution containing Th was saved until the electro-deposition stage.

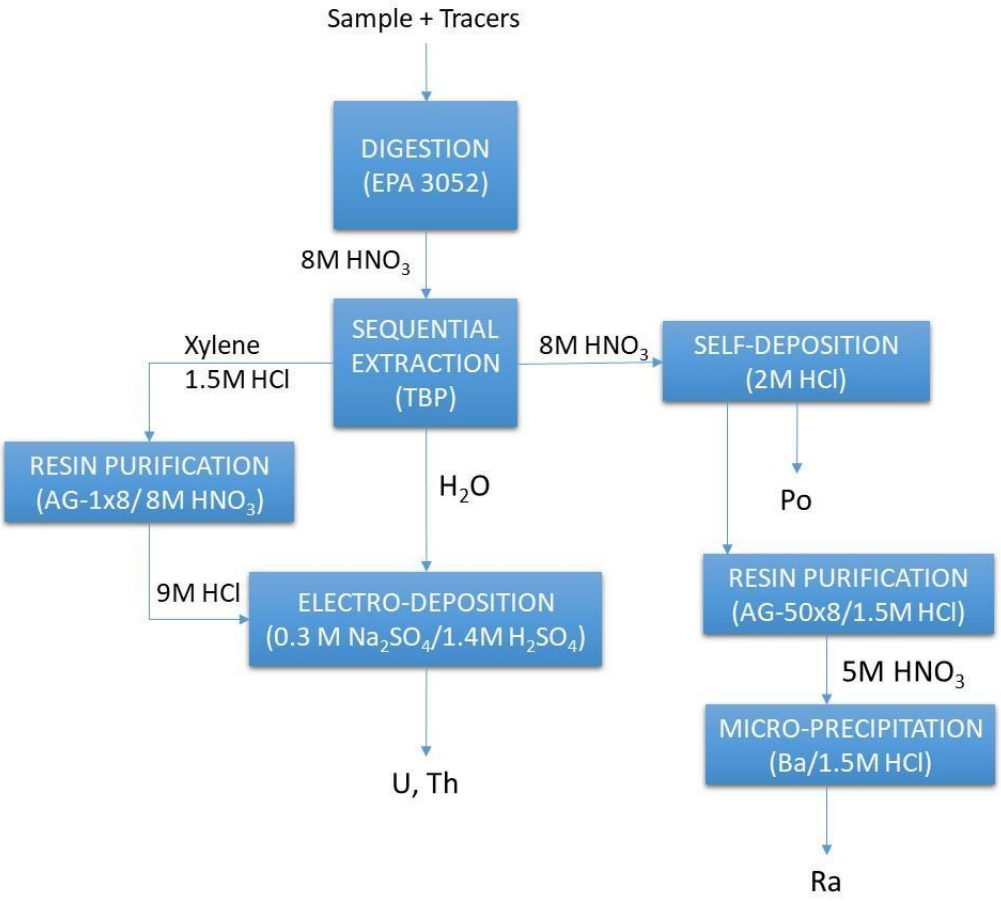

Figure 2.12. *Diagram of TBP radiochemistry method.*

At last, 15 mL of distilled water was added to phase that remains into the funnel to extract and isolate the uranium from organic phase. Then, the funnel was agitated for 10 min and settled for another 10 min. The uranium was back-extracted with water. The agitation steps were repeated with the previous addition of 15 mL of distilled water. Finally, the beakers with the aqueous solution containing U passed to the electro-deposition stage.

Step 4. Thin source preparation by self-deposition, electro-deposition and micro-precipitation

The isolation of ^{210}Po by self-deposition begins evaporating the sample to dryness. The temperature must be approximately 70-80 °C in order to avoid losses of polonium. The sample was conditioned to 10 mL of 2 M HCl, and about 50 mg of ascorbic acid were added for reducing Fe^{3+} to Fe^{2+}. Then, the sample was filtered and transferred to self-

deposition bottle. The bottles were placed in a mechanical agitator for at least 5 hours to ensure a high recovery of the Po isotopes in a silver disc. Finally, the disc was measured by alpha spectrometer.

Micro-precipitation method was performed in order to gain radium alpha source. The sample was conditioned to 1.5M HCl. The micro-precipitation took place with 50 µg Ba carrier and 3g $(NH_4)_2SO_4$, which were added into the sample solution. Later, the solution were filtrated using a resolve filter (Ø 25 mm, 0.1µm polypropylene), which was measured by alpha spectrometer.

Electrodeposition technique were used for obtaining the thorium and uranium thin alpha sources. The sample was evaporated until 1 or 2 mL remained, and 1mL of 0.3 M Na_2SO_4 was added. Then, the sample was evaporated to dryness and the residue was dissolved with 0.3 mL of H_2SO_4 (96 %), 4 mL of distilled water (~1.4M H_2SO_4) and 2 drops of Thymol blue (indicator). Later, the electrodeposition cells were prepared and the sample was transferred into it, washing the beaker with approximately 5 mL of 1 % H_2SO_4. Drops of NH_3 (5 %) were added until pH 2.1-2.4 (orange colour). The electrodeposition was performed during 2 hours with 1.2 A electric current for Th, while it was reduced for U (conditions: 1 hour with 1.2 A electric current). After the electrodeposition, the stainless steel disc was washed with distilled water, followed by iso-propanol, and dry at room temperature. Finally, the disc was analysed in an alpha spectrometric system with passivated implanted planar silicon (PIPS) detectors.

2.2.8.2. Alpha spectrometric system with passivated implanted planar silicon (PIPS) detectors

The silicon is a semiconductor very used for charged particle detector. The silicon charged particle detector is a wafer of silicon having surface contacts forming a p-n junction. On the surface of the Si semiconductor, thin metal layers (gold and aluminium) are evaporated as doping impurities after chemical etching, as in the modern high-performance Passivated Implanted Planar Silicon (PIPS) detector.

In the detection process when an alpha particle enters the detector, it loses a small amount of energy in the thin entrance window. The vast majority of its energy is deposited in the depleted region of the detector diode (p-n junctions) by causing ionisation of the silicon atoms and free electron hole pairs (charge carriers). The electric field in this region sweeps the electrons to one terminal and the holes to the other. This charge pulse is

integrated in a charge sensitive preamplifier to yield the observed voltage pulse and perform the alpha spectrum.

The alfa spectrometry was performed using an EG&G Ortec system with an integrated Octete PC PLUS with eight chambers. Each chamber consists of 450 mm^2 ion-implanted silicon PIPS detector, each one housed inside a vacuum chamber. In addition, each alpha spectrometer chamber includes a vacuum gauge, variable detector bias supply, a preamplifier, a shaping amplifier with adjustable gain, pulse stretcher and bias amplifier, a test pulse generator with variable amplitude, and leakage current monitor. The detectors have a maximum FWHM (Full Width Half Maximum) of 20 keV by using a mono-energetic emission of ^{241}Am, with detection efficiency close to 25 % for distances less than 10 mm. A background counting rate less than 30 counts per day is expected in the energy range from 3-8 MeV, about $(1\text{-}2)\cdot10^{-5}$ cps under a typical alpha peak, energy interval for the most interest natural alpha particle emitters. The detectors operate at a polarisation voltage of 50 V. The program used to control individually the spectrometer and for spectrum analysis and data evaluation was Maestro.

In order to quantify the activity concentrations of the different alpha particle emitters, previously it is needed to identify them in the spectrum using an energy-channel calibration in the energy range 3-8 MeV.

2.2.8.3. Counting efficiency

The absolute counting efficiency (ε) is defined as the number of detections without background (counts, N) in relation to the number of emissions of the radioactive source (N_0):

$$\boldsymbol{\varepsilon = \frac{N}{N_0}} \qquad \text{[Eq. 2.2]}$$

Several factors affect the absolute counting efficiency, as the detector size, the source-detector solid angle, and the intrinsic detention efficiency are the main factors. It is well known that for PIPS detectors the intrinsic detention efficiency is the unit (Aguado, 2003). Therefore, to determine experimentally the counting efficiency, a certified standard source with known activity (A_s) in the same geometry that sample is used, being the counting efficiency obtained from the formula of the activity of the standard sample:

$$\varepsilon = \frac{(G - B)}{A_s \cdot P_S \cdot t} \qquad \text{[Eq. 2.3]}$$

, where *G* is the gross count of the peak, *B* the background, P_s is the emission probability of the standard source, and *t* the counting time.

2.2.8.4. Activity concentration calculation

The Yield (*Y*) of the radiochemical procedure is calculated as:

$$Y = \frac{G_0 - B_0}{\varepsilon P_0 m_0 a_0 t} \qquad \text{[Eq. 2.4]}$$

The average chemical yields obtained to ^{210}Po, Th and U radionuclides were around 90, 60 and 80 %, respectively.

The activity concentration (*a*) at the moment of the isolation (date, F_0) for a given alpha-emitter radionuclide can be calculated by applying the equation:

$$a = \frac{(G - B) \cdot P_0 \cdot m_0 \cdot a_0}{(G_0 - B_0) \cdot P \cdot m} \cdot e^{-\lambda_0 (F_0 - F_r)} \cdot e^{\lambda (F_1 - F_0)} \qquad \text{[Eq. 2.5]}$$

, where *G* is the total alpha counts in the peak of the radionuclide of interest taken during a counting time *t*, G_0 is the net counts at the peak of tracer, *P* is the probability of the alpha emission in the peak of interest, P_0 probability of the alpha emission in the peak of interest for tracer (often is 1), *m* is the mass (or volume) of the sample, m_0 is the mass (or volume) taken from the certified standard tracer solution, a_0 tracer activity concentration at the reference date of the certificate, F_0 is the isolation date, F_1 is the counting date, F_r is the reference date for tracer activity concentration of the certificate (a_0).

The previous equation is valid if the contribution of the blank sample is negligible (blank activity = A_b), but in general this one has to be considered. Therefore, the activity concentration of the sample (a_s) will be calculated trough the next expression:

$$a_s = a - A_b/m \qquad \text{[Eq. 2.6]}$$

In case of 226Ra, the activity concentration is calculated as follows, due to ^{225}Ra, daughter of ^{229}Th (α-emitter) used as tracer, is a pure beta emitter and the recovery yield must be evaluated by its short half-life α-emitter progenies, ^{217}At which it is free of interference.

Let a_0 be the activity of ^{225}Ra at the t_0 of separation from ^{229}Th. If t_1 is the latest time in the procedure at which radium and actinium are separated, then the activity of ^{225}Ra at this point is given by:

$$\boldsymbol{a_1 = a_0 e^{-\lambda_1 (t_1 - t_0)}} \qquad \text{[Eq. 2.7]}$$

Where λ_1 is the decay probability of ^{225}Ra. The subsequent activity of ^{225}Ac at the counting period from t_2 to t_3 gives:

$$\mathbf{a(t_2, t_3) = \frac{a_1 \lambda_2}{(\lambda_2 - \lambda_1)(t_3 - t_2)} \left[\frac{e^{-\lambda_1 (t_2 - t_1)} - e^{-\lambda_1 (t_3 - t_1)}}{\lambda_1} - \frac{e^{-\lambda_2 (t_2 - t_1)} - e^{-\lambda_2 (t_3 - t_1)}}{\lambda_2} \right]} \qquad \text{[Eq. 2.8]}$$

Hence the yield of ^{225}Ra is calculated according to next equation:

$$\mathbf{Y}(\%) = \frac{\mathbf{N_0}}{\boldsymbol{\varepsilon} \cdot \mathbf{a(t_2, t_3)} \cdot \mathbf{(t_3 - t_2)} \cdot \mathbf{m}} \qquad \text{[Eq. 2.9]}$$

Where N_0 is the counts of ^{217}At and Ɛ is the detector efficiency. So, the activity of ^{226}Ra can be determined following the next equation:

$$\mathbf{a(^{226}Ra,)} = \frac{\mathbf{N_{^{226}Ra}} \cdot \mathbf{a(t_2, t_3)}}{\mathbf{Y} \cdot \boldsymbol{\varepsilon} \cdot \mathbf{a(t_2, t_3)} \cdot \mathbf{(t_3 - t_2)} \cdot \mathbf{m}} \qquad \text{[Eq. 2.10]}$$

Figure 2.13 shows the theoretical decay curve of ^{225}Ra and ^{225}Ac and the theoretical ingrowths curve of ^{217}At obtained in a period of 60 days after alpha source preparation. So, in order to obtain the maximum yield, the measurement is done 20 days after the alpha source preparation.

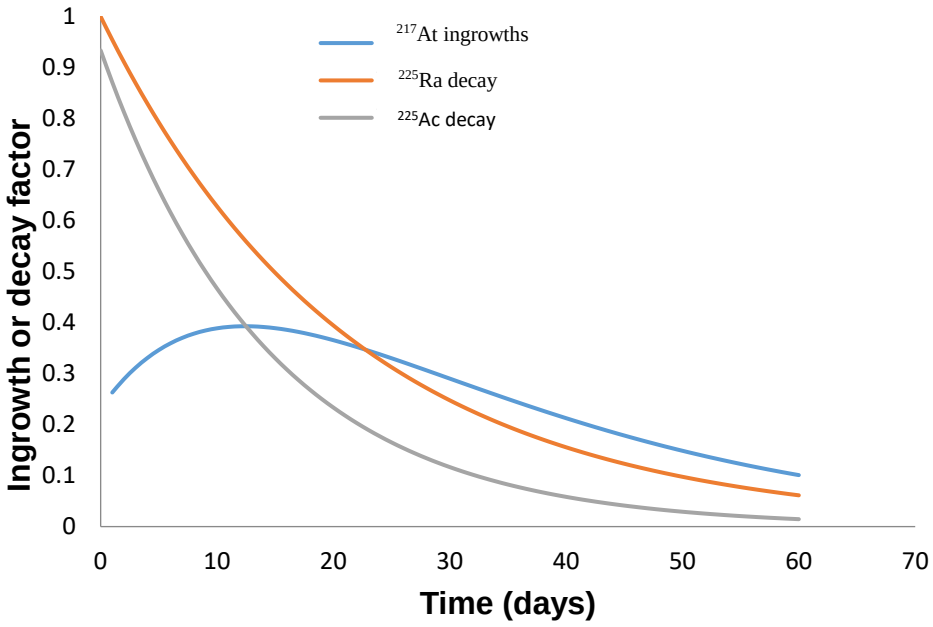

Figure 2.13. *Theoretical decay curve of ^{225}Ra and ^{225}Ac and the theoretical ingrowths curve of ^{217}At.*

2.2.8.5. Lower limit of detection (LLD) and Minimum Detectable Activity (MDA)

The lower limit of detection (LLD) for any radionuclide is critically dependent on the detector background (*B*, counts), and procedure blank count rates. However, an attempt has been made to give typical limits for low background detectors, which is called the Instrumental LLD (ILLD) (Currie, 1968).

The ILLD (in counts) can be calculated by using the next formula derived by Lochamy (1981).

$$\boldsymbol{ILLD = k^2 + 2.8 \cdot k\sqrt{B}} \qquad \text{[Eq. 2.11]}$$

, where *k* is the one-sided confidence factor, being k = 1.65 if a 95 % of confidence level is taken.

$$\boldsymbol{MDA = \frac{ILLD(counts)}{\varepsilon \cdot Y \cdot t} = \frac{k^2 + 2.8 \cdot k\sqrt{B}}{\varepsilon \cdot Y \cdot t} = \frac{2.7 + 4.6\sqrt{B}}{\varepsilon \cdot Y \cdot t}} \qquad \text{[Eq. 2.12]}$$

But it is very common to find that the sample blank contains significantly activity above the detector background, and for these cases a valid alternative to assess the LLC is to use

n replicate measurements of the sample blank by using an equation similar to the previous one (MARLAP, 2004):

$$LLD = k\sqrt{1 + \frac{1}{n}}\sigma_b \qquad \text{[Eq. 2.13]}$$

, where σ_b denotes the standard deviation of the sample blank activity, *n* is the number of replicate blank measurements, and k is the quantile t-Student according to the number of freedom degrees (f = n-1), one side test, and the statistical significant level established. For example, for n = 10 blank samples, f = n-1 = 9, and k = 1.83 if a significant level ⟨ = 0.05 is taken. Therefore, a detection decision is made for a real sample by comparing the measured net activity to the critical net activity. This approach should work best if all samples and blanks are analysed under similar conditions, using instruments with similar counting efficiencies and background levels. It is important to point out that all samples and blanks must be corrected for instrument background (MARLAP, 2004).

The MDA is calculated by applying previous equation 2.9. In our laboratory the background counts is determined every month, and the blank average activity was calculated for five blanks (n = 4, f = 3, ⟨ = 0.05), which gives k = 2.3. Considering an average yield of 80 %, the typical counting times of two days ($1.7 \cdot 10^5$ s), and a counting efficiency of 25 %, the MDA obtained for the radionuclides considered in this work ranged from 0.5 to 2.2 mBq.

2.2.8.6. Quality Control (QC)

The radiochemical method implemented at our laboratory is validated under a quality control system (QC) conformed by replicates, blanks, certified standard materials, and by participating in international and national intercomparison exercises.

The reference materials H1 (^{238}U), C1 (^{232}Th), and IAEA-327 have been used. Tables 2.2 shows that results obtained through TBP method were in agreement with the certified values IAEA-327 a soil from Moscow containing certified activity concentrations of ^{238}U, ^{234}U, ^{230}Th and ^{232}Th at 95 % of confidence. Furthermore, the statistical parameter Z_{Score} was calculated as follow:

$$Z_{Score} = \frac{|x_{meas} - \mu_{ref}|}{\sqrt{\sigma_{meas}^2 + \sigma_{ref}^2}} \qquad \text{[Eq. 2.14]}$$

, where x_{meas} is the measured value, μ_{ref} is the reference value, σ_{meas} is the standard deviation of the measured value and σ_{ref} is the reference standard deviation.

Table. 2.2. *Average activity concentrations (Bq kg^{-1}) of reference material IAEA-327 obtained through TBP radiochemical method and analysed by alpha spectrometry. Uncertainties are indicated as Standard Combined Uncertainty.*

Radionuclide	Reference*	TBP	Z_{Score}**
^{238}U	32.8 ± 1.4	30 ± 3	0.76
^{234}U	32.4 ± 1.0	30 ± 2	1.11
^{232}Th	38.7± 1.5	38.5 ± 1.5	0.10
^{230}Th	34.1 ± 1.7	35.5 ± 1.4	0.63

* Certified activity concentration of the reference material IAEA-327

** $|Z_{Score}| \leq 2$ (no significant differences with a confidence level of 95 %)

All the results obtained shown $Z_{Score} \leq 2$ thus no significant differences between the reference material and the values measured with a confidence level of 95 %.

Tables 2.3 shows the activity concentrations obtained through TBP method compared to C1 and H1 secondary reference materials. Both reference materials are solutions with known activity concentrations of ^{238}U (H1), and ^{232}Th (C1). The results were in agreement with the certified values.

Table. 2.3. *Activity concentrations (Bq kg^{-1}) of reference materials C1 and H1. Uncertainties are indicated as Standard Combined Uncertainty.*

Radionuclide	Reference*	TBP	Z_{Score}**
^{238}U	153.9 ± 1.0	157 ± 3	0.98
^{232}Th	97.1 ± 0.7	95.7 ± 1.6	0.42

* Certified activity concentration of the reference materials C1 and H1

** $|Z_{Score}| \leq 2$ (no significant differences with a confidence level of 95 %)

The Nuclear Safety Council (CSN) organises every year an intercomparison exercise with different type of samples (sediment, soil, filters, water, etc.). The results obtained in our laboratory and the reference values for a food ash are reported in Table 2.4, which are in accordance within 1σ of their nominal values.

Table. 2.4. *Average activity concentrations (Bq kg^{-1}) of the food ash in the CSN-2010 inter-comparison exercise.*

Radionuclide	Reference*	TBP	Z_{Score}**
^{238}U	27.3 ± 4.9	27.9 ± 1.0	0.13
^{234}U	28.5 ± 5.1	28.8 ± 1.0	0.07
^{230}Th	3.65 ± 0.66	4.30 ± 0.80	0.99

* Certified activity concentration of the reference material supplied by CSN

** $|Z_{Score}| \leq 2$ (no significant differences with a confidence level of 95 %)

2.2.9. Gamma spectrometry with Ge detectors

Gamma ray spectrometry is an analytical non-destructive method that allows the identification and quantification of γ-emitting radionuclides in a high variety of matrices. In one single measurement and with little physical sample preparation (efficiency is only dependent on physical parameters), gamma ray spectrometry detects several gamma-emitting radionuclides in the sample (multi-elemental). The measurement gives a spectrum of lines, being the net areas of the peaks proportional to the activity of the radionuclides contained in the sample.

Opposite the alpha-particle spectrometry, this method requires higher sample masses (1-2 orders of magnitude), background gamma spectrum is more complex, detection efficiency varies with gamma energy, self-absorption in the sample, being generally less sensitive than the alpha-particle spectrometry with PIPS detectors, being its detection limits 2 orders of magnitude higher.

Radioactive nuclei (radionuclides) commonly emit gamma rays in the energy range from a few keV to 10 MeV, corresponding to the typical energy levels in nuclei with reasonably long lifetimes. Such sources typically produce gamma-ray “line spectra” (i.e., many photons emitted at discrete energies).

In that range of energies, there are three mechanisms of interaction between gamma rays and matter (photoelectric, Compton, and pairs production), which have an important role

in the measurement of radiation inside the detectors. In all these processes the total, or partial, transfer of the energy from the gamma photon into the electrons of the detector takes place, so that the photon changes its path or disappears.

In the photoelectric absorption process, all the energy of the incident photon is transferred in its entirety to a bound electron of an atom of the material that is expelled from it with a kinetic energy and the photon disappears completely. This electron, by collisions, yields its energy to other electrons producing an excitation of multiple electrons of the material. The final effect is that all photon energy is transmitted to the electrons of the material. This mechanism is the dominant for gamma rays (or X-rays) when the energy of the rays is relatively low (KeV).

In a Compton scattering process, the incident photon is deflected a certain angle from its initial direction, transferring some of its energy to the electron, which is assumed initially at rest. Because all scattering angles are possible, the transferred energy can range from zero to a maximum energy that is much of the initial energy of the photon. Unlike the photoelectric effect, which requires the presence of the nucleus to convert the momentum and energy, the Compton effect can also occur in electrons not connected to the nuclei. The Compton effect is the most important absorption mechanism for gamma radiation with intermediate energy (0.5-10 MeV).

In the producing pairs process, the incident photon, in the vicinity of an atomic nucleus, disappears and is replaced by an electron-positron pair. The excess photon energy is transformed into kinetic energy of the pair. Of the two particles produced, the electron yields its energy in the material while the positron loses its energy by successive collisions until practically at rest. At that time, it can interact with an electron, disappearing both particles and giving rise to two photons that move in opposite directions. This secondary radiation is known as annihilation radiation, and normally accompanies the absorption of high energy gamma rays by matter.

Gamma radiation detectors use the interaction phenomena of radiation with the matter to detect and measure the incident radiation. The detector transforms the effect generated by the interaction into a measurable signal (either light, electrical pulses, etc. depending on the type of detector) so that it can be processed to obtain the desired information.

The gamma spectrometry system used contains an Extended Range coaxial Ge Camberra detector (XtRa), model GX3519. The detector has a unique carbon composite thin-window (0.5 mm thick), 153 cm^3 active volume and 4 mm length from the detector to the carbon window, which extends the useful energy range down to 3 keV. Its relative efficiency in relation to a 3 x 3“ NaI(Tl) detector is 38 % and have FWHMs (Full Width Half Maximun) of 0.95 keV at 122 keV and 1.9 keV at 1330 keV. The detector is cooled to liquid nitrogen temperatures and coupled to a conventional electronic chain, including a PC-based 8K multichannel analyser and an ADC with Genie 2000 for data acquisition and analysis.

The background is reduced by applying a shield constituted by an iron layer of 15 cm. The iron shield is covered internally by a thin copper layer of 2 mm, whose mission is the attenuation of X-rays generated as consequence of the interaction between the outer radiation and the lead layer.

As the gamma spectrometry is a multi-element and non-destructive technique, the sample preparation was reduced to two main steps. The sample was dried to constant weight and grinded to homogenise the particle size. A representative aliquot between 50-100 g is placed in a cylindrical polyethylene container calibrated with 25 mm in height. The gamma spectrometric measurements were carried by using typical counting times of 48 h.

The full-energy-peak-efficiency calibration was made by other members of the FRYMA research group following the methodology of Pérez-Moreno et al (2002).

The gamma spectrometry quality control has been performed by taken periodic blanks, certified reference materials (i.e., IAEA-327) and replicates.

2.3. TECHNIQUES FOR ENVIRONMENTAL RISK EVALUATION

Environmental implications and potential human risk of the studied materials were evaluated according to the following methods:

2.3.1. Leaching test

2.3.1.1. TCLP

The potential environmental impact was evaluated according the method US EPA SW846-1311:1997 TCLP tests (Toxicity Characteristic Leaching Procedure), established

by the Environmental Protection Agency (EPA). TCLP is designed to determine the mobility of both organic and inorganic pollutants present in solid and multi-phase wastes.

This method classifies waste as hazardous or non-hazardous based on its potential toxicity. If the extract from a representative sample contains any of the contaminants listed in U.S. EPA 40 CFR 261.24:2011 at the concentration equal to or greater than the respective value given is classified as hazardous from the toxicity point of view.

The leaching procedure follows the next steps:

Step 1. Preliminary Evaluations

Preliminary evaluation is performed on 100 g of waste. This aliquot may not actually undergo extraction.

Calculation of the percent solids was according the following equation:

$$\boldsymbol{Percent\ solids} = \frac{\boldsymbol{Weight\ of\ Solid}}{\boldsymbol{Total\ Weight\ of\ Waste}}\ \boldsymbol{x100} \qquad \text{[Eq. 2.15]}$$

Any material that did not pass through a 9.5 mm (0.375 inch) standard sieve required size reduction.

The amount of extraction fluid was determined as follows, using an L/S relation of 20:

$$\boldsymbol{Weight\ of\ Extraction\ Fluid} = \frac{\boldsymbol{20\ x\ \%\ Solids^{4}\ x\ Weight\ of\ Waste\ Filtered}}{\boldsymbol{100}} \qquad \text{[Eq. 2.16]}$$

Step 2. Selection of the Extraction Fluid

Determination of which of the two extraction fluids are to be used for the TCLP extraction of the waste. Extraction fluid is prepared in batches by the total number of extractions required.

Firstly, 5 g of the waste are transferred into a 500 mL Erlenmeyer flask with 96.5 mL of reagent water. It is covered with a watch glass, and stirred vigorously for 5 minutes using a magnetic stirrer. The pH is measured and recorded. If the pH < 5.0, then the extraction fluid #1 is used. If the pH > 5.0, then 3.5 mL 1N HCl is added, slurred briefly, covered

with a watch glass and heated to 50 ºC for 10 minutes. The solution is cooled to room temperature and the pH measured. If the pH < 5.0, then the extraction fluid #1 is used. Oppositely, if the pH > 5.0, extraction fluid #2 has to be used.

Step 3. Preparation of the Extraction Fluids

- Extraction Fluid #1 is prepared with the addition of 5.7 mL of glacial CH_3CH_2OOH and 64.3 ml of 1N NaOH diluted to a volume of 1L. When correctly prepared, the pH of this fluid is 4.93 ± 0.05.

- Extraction Fluid #2 is formulated diluting 5.7 mL of glacial CH_3CH_2OOH with reagent water to a volume of 1 L. When correctly prepared, the pH of this fluid is 2.88 ± 0.05.

Step 4. Extraction procedure

Slowly this amount of appropriate extraction fluid was added to the extractor vessel with the waste. A Teflon tape to the threads of the bottle was used and the vessels secured in the rotary agitation device, and rotate at 30 ± 2 rpm for 18 ± 2 hours. Then, the material in the extractor vessel was separated into its component liquid and solid phase by filtering through a glass fibre filter.

Finally, the pH of the extract was recorded. Immediately it was aliquoted and preserved the extract for farther analysis. Metals aliquots were acidified with nitric acid to pH < 2. All aliquots were stored under refrigeration (4 ºC) until analysis.

The concentrations of metals and radionuclides in the leachates were determined by ICP-MS/OES and alfa spectrometry, respectively.

The following general quality assurance procedures were applied during this procedure:

- A minimum of one blank (using the same extraction fluid as used for the samples) was analysed for every extractions series.

- Duplicate were processed for each sample. Duplicate samples were used to determine the precision of the procedure.

2.3.1.2. UNE-EN 12457/4

UNE-EN 12457/4 testing method is part of the procedure established in the R.D. 1481/2001 of 27 December, which regulates the disposal of waste by landfill. The test consists on the evaluation of the behaviour of wastes in relation to leaching. This standard considers leaching as the release of soluble constituents upon contact with water, the main release mechanism, which may give rise to a potential risk to the environment during the disposal of waste. This test is intended to identify the leachate properties of the wastes and provides information on the leaching of granular waste and sludge at a liquid-solid ratio of 10 L/ kg dry matter. It is applied to wastes having a particle size of less than 10 mm with or without size reduction. This European standard has been developed to primarily investigate inorganic waste components.

The limit values are defined for each type of waste, which are classified as inert, non-hazardous and hazardous, in the R.D. 1481/2001, as well as the admission criteria for each type of landfill.

The leaching procedure follows the next steps:

Step 1. Sample preparation

The tests must be carried out on materials with a particle size of at least 95% (mass) of less than 10 mm. Therefore, the laboratory sample should be sieved. If the fraction of material that is too thick exceeds 5% (mass), this fraction as a whole must be crushed with a grinding equipment. The material should not be finely ground.

Step 2. Preliminary evaluations

The drying temperature must not exceed 40 °C. The mass of the dry residue must be determined at 105 °C in the case of sludge.

The dry matter content is calculated as follows:

$$DR = 100 \times MD / MW \quad \text{[Eq. 2.17]}$$

Where D_R is the dry matter content rate (%), M_D is the mass of the test portion once dry (kg); M_W is the test portion masses before drying (kg).

The moisture content rate (MC in%) is calculated as follows:

$$MC = 100 (M_W - M_D) / M_D \quad \text{[Eq. 2.18]}$$

A test portion is prepared from the test sample a total mass M_W (measured to a precision of 0,1 g) containing 0,090 kg ± 0,005 kg of dry matter (M_D).

$$MW = 100 \times MD / DR \quad \text{[Eq. 2.19]}$$

Where D_R content in dry matter; M_D is the mass of the dried test portion (kg); M_W is the no-dry test portion mass (kg).

Step 3. Leaching

The test portion was placed in a glass or high density polyethylene bottle. A quantity of leachant (L) which establishes a liquid / solid ratio (L / S) = 10 l / kg ± 2% was added during the extraction.

$$L = (10 - MC / 100) \times MD \quad \text{[Eq. 2.20]}$$

Where L is the volume of the leachate used (in L); MD is the dry mass of the test portion (kg); MC is the rate of moisture content (in %).

The bottle was covered and stirred for 24 h ±40.5 h. Later, suspended solids are allowed to settle for 15 min and separated from de solution by vacuum filtration, using membrane filters of 0.45µm. immediately, pH, conductivity and temperature of the leached were measured. Finally the solution were preserved for farther analysis.

The quality assurance procedures were performed in the same way as in TCLP.

2.3.1.3. BCR Extraction Procedure

The mobility of contaminants, as well as their bioavailability and related eco-toxicity to the environment, depends strongly on their specific chemical form and methods of binding. Consequently, these have to be determined rather than the total element contents in order to assess the toxic effects. Therefore, determinations of binding forms, using extraction procedures can be good compromise to give information on environmental risk. The most significant advance in sequential extraction studies came in 1987 when the European Commission launched a program (under the BCR, Community Bureau of Reference) aimed at the harmonization of extraction procedures. In 1993 a standard sequential extraction procedure known as BCR was proposed.

The BCR procedure is summarized below, and its specific details can be found elsewhere (Sahuquillo et. al., 1999; Rauret et. al., 1999). Proximately, 1.0 g of sample, previously dried and homogenized, was taken and subjected to the optimized BCR sequential extraction procedure.

Step 1. Water/acid soluble and exchangeable fraction

For each solid sample, 40 mL of 0.11 M acetic acid was added to 1.0 g aliquot in a 60 mL centrifuge tube and shaken end-over-end (30 ± 10 rpm) for 16 h at 22.5 °C (overnight). The liquid extract was separated from the solid residue (S1) by centrifugation for 20 min, and stored at 4 °C until analysis. The residue was washed with 20 mL distilled water, shaken for 20 min, and centrifuged, and the washing was discarded. This extraction step (water/acid soluble and exchangeable fraction) is designed to extract exchangeable metals and those soluble in water or in slightly acidic conditions. This fraction is the most labile in environmental samples, and therefore, the most bio-available and dangerous for the environment.

Step 2. Reducible fraction

40 mL of 0.5 M $NH_2OH{\cdot}HCl$ (adjusted to pH of around 2 by adding HNO_3) was added to the solid obtained in Step 1 in the centrifuge tube and shaken for 16 h at 22.5 °C. The extract was separated as for Step 1 as well as the solid wash procedure. The reducible fraction would represent all metals bound to Fe and Mn oxi-hydroxides that can be released if the conditions change from an oxic to an anoxic state.

Step 3. Oxidizable fraction

Small aliquots of 10 mL of H_2O_2 were added carefully to Step 2 residue. The tubes were covered and digested for 1 h at room temperature with occasional manual shaking, and then heated to 85 ± 2 °C for 1 h in a water bath. The volume was reduced to < 3 mL (uncovered) by further heating of the uncovered tube. A further 10 mL of H_2O_2 was added and heated again to 85 ± 2 °C for 1 h (covered vessel). Later, the volume of liquid was reduced to about 1 mL. Finally, 50 mL of 1 M NH_4OAc (pH 2) was added and shaken for 16 h at 22 ± 5 °C. The extract was separated from the solid residue by centrifugation as described in Step 1, as well as the procedure for washing the solid. The oxidizable fraction is mainly composed of metals bound to organic compounds and sulphides that could be released under oxidizing conditions.

Step 4. Residual fraction

Additionally, as an internal check on the procedure, it is recommended that the residue from Step 3 be digested in aqua regia and the total amount of metal extracted (Step 1 + Step 2 + Step 3 + Step 4) be compared with that obtained with "direct analysis" by aqua regia, trying be similar both amounts.

The residue from Step 3 was digested by adding 10 mL of aqua regia (a mixture of 12 M HCl and 15.8 M HNO_3 in the ratio 3:1), and allowed to stand for 16 h at room temperature. After that, samples were heated slowly under reflux conditions maintained for 2 h. The extract was separated as in Step 1. The non-mobile fraction, or fraction 4, corresponds to those metals that are strongly associated with crystalline structures of minerals and are therefore unlikely to be released from the samples unless they are exposed to extreme conditions.

This procedure was tested for metals and radionuclides mobility. The quality control has been performed using the BCR-701 certified reference material and replicates.

2.3.2. Radiological implications in building materials

It is necessary to evaluate the environmental impact when NORM (Naturally occurring radioactive materials) wastes are incorporated in building materials. In this sense, it is worth highlighting that tionite and red gypsum are considered as NORM waste. Moreover, the activity concentrations of the nuclides in the final product should be measured in order to ensure the negligible environmental impact.

To this end, Directive 2013/59/EURATOM laying down basic safety standards for protection against the dangers arising from exposure to ionising radiation, defines an external risk index (I), also called an activity concentration index (Eq. 2.38).

$$I = \frac{C_{226_{Ra}}}{300\ {}^{Bq}/_{kg}} + \frac{C_{232_{Th}}}{200\ {}^{Bq}/_{kg}} + \frac{C_{40_K}}{3000\ {}^{Bq}/_{kg}} \qquad \text{[Eq. 2.21]}$$

, where C(^{226}Ra), C(^{232}Th) and C(^{40}K) are the respective activity concentrations for ^{226}Ra, ^{232}Th and ^{40}K in the building material considered (expressed in Bq kg^{-1}).

The activity concentration index shall not exceed the following values depending on the dose criterion and the material amount used in a building (Table 2.5). It is therefore

recommended that controls should be based on a dose in the range 0.3-1 mSv a^{-1} (Kovler et al., 2009).

Table. 2.5. *External risk (I) depending on the dose criterion and the way and the amount the material is used in a building.*

Dose criterion	0.3 mSv a^{-1}	1 mSv a^{-1}
Materials used in bulk amounts, e.g. concrete	I ≤ 0.5	I ≤ 1
Superficial and other materials with restricted use: tiles, boards, etc.	I ≤ 2	I ≤ 6

2.4. TECHNIQUES FOR TECHNOLOGICAL PROPERTIES

The following section shows the procedure establish and equipment used to evaluate the technological properties of the applications performed.

2.4.1. Fire resistance Test

Protection against fire hazard and assessment of reaction to fire as well as fire resistance is a basic presumption when planning buildings construction and is therefore an imperative requirement from both, national and EC regulations. The basic requirement in fire safety is to reduce to acceptable limits the risk of damage to users of building from accidental fire, due to the characteristics of its design, construction, use and maintenance.

Fire prevention has generated broad regulation and legislation, based fundamentally on experience, technological advances and the unification of criteria. Fire testing methods are generally designed to simulate the different phases of the fire process. In that sense, there is applicable European legislation, UNE-EN 13501-1: 2007 + A1: 2010 "Classification according to fire behaviour of construction products and elements for building", which defines the term reaction to fire as the response of a product, contributing with its own decomposition to a fire to which it is exposed, under specific conditions. This European regulation is included in Spanish regulation by R.D 110/2008, which establishes the classification of products of construction and of the constructive elements in function of their reaction properties and fire resistance.

Complete building elements (doors, floor structures, partitions etc.) which are used for separating fire compartments are tested for the case of a fully developed fire. The behaviour of these building elements are evaluated by fire resistance tests, assessing for how long an element continues to fulfil the function for which it was intended when subjected to the high temperatures that develops a fire. The temperature in the test furnace follows the so-called "standard fire curve" (Eq. 2.39) which is designed to represent a fully developed fire. The nominal curve is defined in UNE EN 1363-1: 2000 "Fire resistance tests. Part 1: General Requirements " as follows:

$$\boldsymbol{T = 20 + 345\ \log_{10}(8t + 1)} \qquad \text{[Eq. 2.22]}$$

Where T is the temperature in ° C and t is the time in minutes. The properties which are evaluated in this test are:

- ✓ Insulation (ability to reduce the heat transfer)
- ✓ Integrity (ability to prevent leakage of flames and hot gases)
- ✓ Load bearing capacity

Building elements classified as "fire resistant" with respect to integrity and insulation are used as a means to prevent fire being spread between fire compartments.

Generally, the fire resistance of the elements of construction can be defined as the time it takes for this element to lose its bearing capacity, or stability to fire, its integrity and its thermal insulation.

The conditions of fire exposure were simulated using a specially designed furnace for the manufactured plates, where were exposed to the normalized curve. The oven door was replaced by a special door in which the plates were inserted. The furnace allowed to record the temperature of the surface exposed by thermocouples inside the furnace, which was used to regulate the temperature by a controller. And on the unexposed side, the temperature was recorded by three Pt-100 probes with a stainless steel contact surface.

The test is completed when the temperature of one of the thermocouples on the surface of the unexposed side of the material exceed 180 ° C or when the average temperature of all thermocouples on the surface of the unexposed side is greater than 140 ° C plus ambient temperature, being the ambient temperature of 23 ° C when the product

was tested. In addition, the test would be finished if the material studied results fractured or losing its structural stability.

Chapter 3. Results and Discussion

3.1. THERMAL CHARACTERIZATION OF NEW FIRE-INSULATING MATERIALS FROM INDUSTRIAL INORGANIC TiO_2 WASTES

S.M Pérez-Moreno[1], M.J. Gázquez[1], A.G. Barneto[2], and J.P. Bolívar [1]

[1)] Department of Applied Physics, University of Huelva, Huelva, Spain

[2)] Department of Chemical Engineering, University of Huelva, Huelva, Spain

Journal of Thermochimica Acta 552 (2013) 114– 122

Abstract

Two wastes, red gypsum (RG) and unattacked ilmenite (known as tionite), from the titanium dioxide production industry have been used to study the possibility of manufacturing new fire-isolating materials, and for that they were characterized for mineralogical composition and thermal behaviour. Tests have demonstrated that these wastes could be used for fire insulation. Thermogravimetric analysis (TGA) of the thermal behaviour of these wastes and tests on the new isolating materials against temperature indicate that they do not undergo significant chemical and structural changes up to about 1000 ºC.

Keywords: *Norm Industry, Titanium Dioxide, Waste, Ilmenite, Undissolved Muds, Red Gypsum.*

3.1.1. INTRODUCTION

The current trend towards recycling the waste material generated in most industrial production processes makes this an important field for research. In this sense, the development of technologies and new applications to valorise these wastes in order to cut disposal costs and avoid environmental pollution environment is of increasing importance. In addition, the appropriate treatment of industrial wastes could lead to the generation of co-products of economic value and broad application (Colombo et al., 2003; Liu et al., 2007), especially when the waste properties are manufactured for specific applications with high added value and can successfully compete with products made from traditional raw materials (Leiva et al., 2005).

In our case, we valorise two wastes generated by an industrial manufacturer of titanium dioxide pigment for plastics in the province of Huelva (southwestern Spain). The pigment is produced by applying the "sulphate method" that uses ilmenite (Fe_2TiO_3) as raw

material, which is a heavy mineral containing approximately 43–65% titanium dioxide (Chernet, 1999; Sahoo et al., 1999; Pistorius and Coetzee, 2003).

The first of these two wastes (unattacked mud or tionite) originates in the digestion stage of the ilmenite with sulphuric acid (98% concentration). The tionite is obtained by filtration of the liquor from digestion, making this mud highly acidic, with large concentrations of heavy metals that could potentially damage health and the environment if not adequately managed (Gázquez et al., 2011).

The second waste, red gypsum (RG), emerges in the final stage of the industrial process, where a low acidic liquid stream composed primarily of sulfuric acid (H_2SO_4) and iron sulphates ($FeSO_4$, $Fe_2(SO_4)_3$) is treated in a neutralization plant. Here calcium hydroxide and magnesite are added to the weak acid stream in order to precipitate the dissolved materials in the stream, and the red gypsum is finally obtained by filtration (Gázquez et al., 2009). In this process the following reactions occur:

$$H_2SO_4 + Ca(OH)_2 \rightarrow CaSO_4 \cdot 2H_2O \quad \text{[Eq. 3.1]}$$

$$Fe^{3+} + OH^- \rightarrow Fe(OH)_3 \quad \text{[Eq. 3.2]}$$

$$Ca^{2+} + CO_3^{2-} \rightarrow CaCO_3 \quad \text{[Eq. 3.3]}$$

$$Mg^{2+} + SO_4^{2-} \rightarrow MgSO_4 \quad \text{[Eq. 3.4]}$$

This factory produces about $7 \cdot 10^4$ tons of red gypsum and $3 \cdot 10^4$ tons of mud, which contain about 40% humidity; currently these wastes have no commercial value and are disposed of in an authorized and controlled repository area. Furthermore, the management of this waste represents a high cost to the company. The potential commercial applications of these wastes are what motivate this research. Due to this problem and the previous chemical and mineralogical characterization of these wastes, this study analyses the possibility of using these wastes (or their mixes) as insulating material in the construction sector.

It is noteworthy that the feedstock used in the process (ilmenite) presents enhanced levels of radionuclides from the natural uranium and thorium series (about ten times more radioactive than a typical soil), and as a result the TiO_2 production industry is considered a NORM (Naturally Occurring Radioactive Material) industry (IAEA, 2004). Previous studies (Gázquez et al., 2011) have shown that the mud contains a concentration of about 3000 Bq kg^{-1} in equivalent radium, which is greater than the 1 Bq g^{-1}, the reference level for a material to qualify as a NORM waste according to the IAEA.

On the other hand, The European Union (Directive EURATOM, 2013) has proposed to the European countries to control the radioactivity content in building materials. The purpose of these recommendations is to limit radiation exposure from materials with high levels of natural radionuclides. For that an "external risk index" (I) is defined to ensure that external dose received by population from building do not exceed 1 mSv per year. In this document is indicated that surface and other materials with restricted use such as tiles, boards, etc. should not exceed the threshold value of I = 6.

Taking into account the previous facts, the main objective established for this work was to study the possibility of knowing if the tionite and red gypsum wastes have promise in future as potential building materials for fire wall insulation or as fire-resistant panels. In order to develop this objective physicochemical characterization and TGA thermal analysis of these wastes, as well as a study of the materials obtained from them, is required. In addition to predicting the burning behaviour of the wastes, a preliminary fire resistance test was carried out with the aim of using them as internal building partitions with good isolation properties.

3.1.2. MATERIALS AND METHODS

3.1.2.1. Materials

3.1.2.1.1. Waste

The wastes (mud and red gypsum) used in this study were collected from a titanium dioxide production plant 12 km from the city of Huelva (southwestern Spain). Five sampling campaigns were organized for one month, with a sampling taking place every six days to evaluate the possible temporal variability of the characteristics of these wastes. After collection, all samples were dried at 60 °C (at this low temperature red gypsum does not dehydrate) until reaching constant weight before analysis.

3.1.2.1.2. Additives

Vermiculite is composed primarily of silicates of aluminium, iron and magnesium. Its structure is foliated in yellowish crystalline plates whose particle diameter ranges from 1 mm to 1 cm (El Mouzdahir et al., 2009). This mineral is also used as building insulation (Al-Homoud, 2005). Its structure's shiny surface sheets become large reflectors of radiation which disperse heat and increase the thermal insulation capacity of materials that contain it. This makes it a suitable additive to increase the insulating capacity of the materials under study.

3.1.2.1.3. Blends

Several plates with different compositions were produced by using a low-cost manufacturing method with no prior waste treatment. The manufacturing process was as follows: firstly, the components of different plates were mixed according to the percentages shown in Table 3.1; secondly, the components were mixed with water so that the mixture was homogeneous, and the pastes obtained were poured into 25 x 25 cm by 1.8 and 2.8 cm thick moulds. Fire resistance generally depends on thickness, and in many applications for fire resistance panels that thickness is usually between 1.5 and 2.5 cm. The plates were dried for more than 20 days at ambient temperature, and the pastes were used to make test panels of different shapes and sizes for the insulation test.

Name	Red gypsum	mud	Vermiculite	$I \leq 6$
Plate 1	100	-	-	0.7
Plate 2	75	25	-	4.7
Plate 3	80	15	5	3.9

Table 3.1. *Proportions of red gypsum, tionite and vermiculite used in the different plates made for this study, and their external risk index value.*

The percentages of tionite in the plates were below 25 % in order to comply with European Union requirements, which stipulate that building materials should not exceed 1 mSv per year, so surface and other materials with restricted use such as tiles, boards, etc. ought not to remain within $I \leq 6$, as shown in Table 3.1. This index is defined as follow: $I = C(^{226}Ra)/300 + C(^{228}Ra)/200 + C(^{40}K)/3000$; where $C(^{226}Ra)$, $C(^{228}Ra)$ and $C(^{40}K)$ are the activity concentrations for ^{226}Ra, ^{228}Ra and ^{40}K, respectively, in the building material considered, expressed in Bq kg^{-1}.

3.1.2.1.4. Pladur®

A plate of Pladur® was used as reference material in order to compare the behaviour of each plate against fire; Pladur® is one of the most widely used materials in construction.

Pladur® is plasterboard consisting of a natural gypsum core manufactured to UNE - 102,023 standard specifications. Pladur® is classified with respect to its reaction to fire as

A1-Non-combustible material according to the UNE-13501-2002 standard (Ang and Wang, 2004; Thomas, 2002).

3.1.2.2. Methods

3.1.2.2.1. X-Ray Diffraction (XRD)

The mineralogical study was performed by applying the disoriented dust method with a Bruker laser diffraction instrument, and with the Kα radiation of Cu (filtered by a Ni film) excited by 30 mA of intensity and 40 kV of tension. The mineralogical quantification was carried out using Bruker EVA software with internal standard.

3.1.2.2.2. X-ray Fluorescence (XRF)

The major elements were measured for X-ray fluorescence (XRF) with a Bruker S4 Pioneer system with the following characteristics: 4 kW, front window and Rh anode; five analysing crystals - LIF200, Ge, PET, OVO55 and OVOC, and two X-ray detectors. In our case 1 g aliquot of each dry sample was taken and mixed with 10 g of lithium tetraborate (material used for melting), and 5 drops of lithium iodine at 20 %. Each mixture was placed in a Pt-Au crucible and placed in a special furnace for fusion. The final result for each sample is a homogenous glass called “pearl”, ready to be measured in the XRF system.

3.1.2.2.3. TGA

Thermogravimetry analysis (TGA) runs were carried out with a Mettler Toledo model TGA/SDTA851e/LF1600 on samples of around 5 mg supported in a crucible without lid. In nitrogen and synthetic air (N2:O2 4:1) environments a heating rate of 10 ºC/min was applied from 25 ºC up to 900 ºC. TGA results were presented as mass loss versus time or temperature (TG curve), and mass loss rate versus time or temperature (DTG - derivative thermogravimetric curve).

3.1.2.2.4. Fire-resistance tests

The basic safety requirement in case of fire is to reduce the risk for users of a building damaged by a fire of accidental origin that could result from its design, construction, operation or maintenance. Generically we define the fire resistance of a building’s assembly as the time it takes for this element to lose its bearing capacity or stability with regard to fire, integrity and insulation. In Spain, fire-resistance test standards are stipulated in regulation UNE-EN 13501-1:2007.

This fire-resistant test requires that one of the sides of the plate be exposed to a standard temperature curve defined by the equation $T = 20 + 345 \log_{10}(8t+1)$, where T is the oven temperature (°C), and t is the time (minutes) from the beginning of the test. The temperature of the unexposed side is measured by means of three Pt-100 probes with a stainless steel contact surface (see Fig. 3.1). This test was done in laboratory scale.

Figure 3.1. *Thermal Resistance Test.*

The test is concluded when the temperature of one of the thermocouples on the unexposed surface of the plate is either above 180 °C, or the average temperature of all the thermocouples exceeds 140 °C + T_{Env}, where T_{Env} is the environment temperature when the product was tested at 23 °C.

The trial would have been discontinued if the test material had fractured or lost structural stability, but this did not occur in any of the tests performed.

3.1.3. RESULTS AND DISCUSSION

3.1.3.1. Characterization of materials

3.1.3.1.1. Mineral composition

In the tionite sample, several crystalline phases present ilmenite ($FeTiO_3$) and rutile (TiO_2) as main components, being minerals that are left over from the used raw material. Other phases detected are zircon ($ZrSiO_4$), quartz (SiO_2) and Fe and Ti oxides ($Fe_3Ti_3O_{10}$). The presence of rutile and the occurrence of the zircon and quartz mineral phases in the tionite are hardly surprising since all these species in the raw material are insoluble in sulphuric acid (McNulty, 2007). Another important feature of this waste is that all the mineral phases are highly refractory, which is interesting for their potential use in heat insulation materials

In the red gypsum sample, the crystalline phases observed are mainly gypsum (calcium sulphate dehydrate, $CaSO_4 \cdot 2H_2O$), iron and titanium oxides. We acknowledge that the amorphous sample is not detectable in this type of analysis. Based on the composition of

the major elements and their stoichiometry, it can be shown that the red gypsum sample is made up of approximately 76% $CaSO_4 \cdot 2H_2O$, indicating an amorphous phase of about 24 % (Gázquez et al., 2009).

In relation to the raw materials used, Pladur® and vermiculite, the mineralogy obtained by XRD is similar to that found in the literature (Pérez-Maqueda et al., 2003). Pladur consists solely of drywall gypsum ($CaSO_4 \cdot 2H_2O$) and vermiculite, a mineral composed mainly of aluminium silicates, contains iron and magnesium.

3.1.3.1.2. Major elements

Table 3.2 shows the concentrations of the major elements (%) of the studied samples. The mud sample (tionite) is mainly composed of TiO_2 (53 %), which corresponds to approximately 5 % of the total titanium contained in the ilmenite (raw material). In addition, this waste has a high percentage of SiO_2 (18 %), from the quartz phase, and ZrO_2 (4 %) associated with the zircon phase. The high content of Fe_2O_3 (11 %) derives from the iron and titanium oxides ($Fe_3Ti_3O_{10}$) and ilmenite ($FeTiO_3$), previously identified as crystalline phases in the XRD analysis.

	Mud (*)	Red gypsum (*)	Vermiculite	Pladur ®
SiO_2	18 ± 1	1.2 ± 0.2	40 ± 4	1.5 ± 0.1
Al_2O_3	2.5 ± 0.2	1.4 ± 0.2	9.2 ± 0.9	0.45 ± 0.05
Fe_2O_3	11 ± 1	14 ± 2	8.8 ± 0.9	0.20 ± 0.02
MnO	0.36 ± 0.01	0.35 ± 0.04	0.04 ± 0.01	< 0.01
MgO	0.38 ± 0.02	1.4 ± 0.2	23 ± 2	0.58 ± 0.06
CaO	0.75 ± 0.01	33 ± 2	4.8 ± 0.5	37 ± 4
TiO_2	53 ± 1	7.6 ± 1.2	1.1 ± 0.1	0.03 ± 0.01
SO_3	6.1 ± 0.7	27 ± 1	< 0.01	37 ± 4
K_2O	0.56 ± 0.07	< 0.01	5.8 ± 0.6	0.18 ± 0.02
ZrO_2	4.2 ± 0.1	< 0.01	< 0.01	< 0.01
LOI	< 0.01	13 ± 1	< 0.01	23 ± 2

Table 3.2. *Concentration (%) of major elements in the materials under study. The total iron content is given as Fe2O3. (*) The uncertainty is given by the standard deviation of the mean.*

The composition of red gypsum is in line with the literature (Gázquez et al., 2009) and consistent with the mineralogy reported in other papers, having SO_3 and CaO as major

components, with 27 and 33 % respectively, similar to natural gypsum. We must also remember that this waste is generated by neutralization of the weak acid effluent obtained in the latter stages of the washing and leaching of TiO_2 pulp with calcium hydroxide and magnesite ($MgCO_3$). This explains the high titanium content in this waste, 7.6 % TiO_2. This weak acid is also composed of sulfuric acid (H_2SO_4) and trace amounts of iron sulphate.

In relation to the composition of the vermiculite (Table 3.2) as expected there is a high percentage of silicon oxide (40 %), magnesium (23 %), aluminium (9.2 %) and iron (8.8 %), confirming that it is mainly formed of aluminium silicates, iron and magnesium (Leiva et al., 2005).

The composition of Pladur® as shown in Table 3.2 confirms that this material is mainly composed of $CaSO_4 \cdot 2H_2O$ as well as non-negligible amounts of SiO_2 (1.5 %), Al_2O_3 (0.48 %) and MgO (0.58 %).This material also suffers a fire loss on ignition (LOI) of 23 % (Table 3.2) consistent with gypsum's loss of water structure.

3.1.3.2. Thermogravimetric analysis (TGA)

As mentioned previously, the valorisation of these wastes is based on their manufacture as fire insulation materials. Therefore, the first step is to measure the behaviour of these materials when exposed to temperatures up to 1,000 ºC by means of thermogravimetric analysis (TGA).

3.1.3.2.1. Tionite

Figure 3.2 shows the TG and DTG curve for the mud waste, in which DTG is calculated by the first derivative of the mass loss in relation to the time (rate of mass changes with respect to the time t or temperature T).

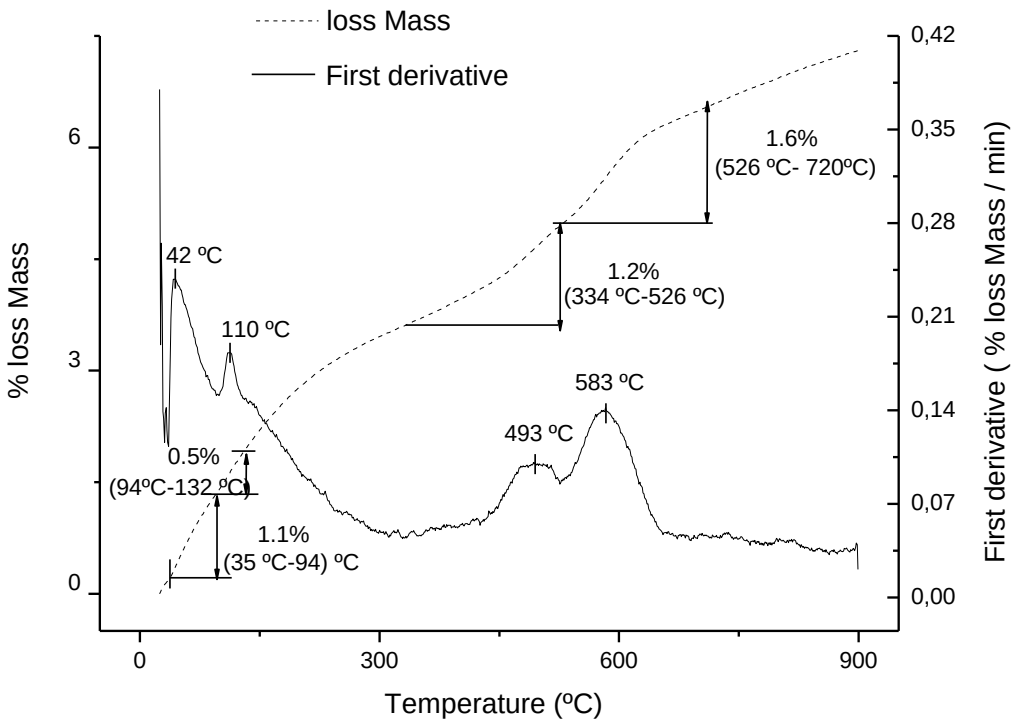

Figure 3.2. *TG and DTG of Tionite.*

In the previous Figure, a first peak on the DTG curve at 42 ° C is observed, which corresponds to the loss of moisture in the sample. The next three peaks can be attributed to the decomposition of $FeSO_4 \cdot xH_2O$ and $Fe_2(SO_4)_3$. The first thermal event happens at 110 °C, from the loss of the chemically-bound water in the iron sulphate (II) (Mass et al., 2006) probably as a result of the dehydration mechanism described by the following reaction (Gázquez et al., 2009):

$$FeSO_4 \cdot xH_2O \rightarrow FeSO_4 + xH_2O \qquad \text{[Eq. 3.5]}$$

Siriwardane et al. (1999) and Thomas et al. (2003) studied the decomposition of $FeSO_4$ and obtained a similar result. The following peaks appear at 493 °C and 583 °C, and are probably due to the thermal decomposition of $FeSO_4$ and $Fe_2(SO_4)_3$. The thermal decomposition (reactions) of $FeSO_4$ takes places in two stages (Masset et al., 2006):

$$6\ FeSO_4 \rightarrow Fe_2(SO_4)_3 + 2\ Fe_2O_3 + 3\ SO_2 \qquad \text{[Eq. 3.6]}$$

$$Fe_2(SO_4)_3 \rightarrow Fe_2O_3 + 3\ SO_2 + 3/2\ O_2 \qquad \text{[Eq. 3.7]}$$

The $Fe_2(SO_4)_3$ is then added to the decomposition of $Fe_2(SO_4)_3$ in the waste, which occurs at 550 °C. The final product of the thermal decomposition of iron sulphate (III) is magnetite Fe_2O_3.

The previous mechanism agrees with TGA data for ferric sulphate hydrate ($Fe_2(SO_4)_3 \cdot xH2O$) produced by the oxidation of ferrous sulphate heptahydrate ($FeSO_4 \cdot 7H_2O$), which is a co-product of the titanium dioxide production industry (Figure 3.3). There are two losses of mass at 180 °C and 290 °C, corresponding to the dehydration of ferric sulphate, while the peak at 670 °C results from the thermal decomposition of $Fe_2(SO_4)_3$.

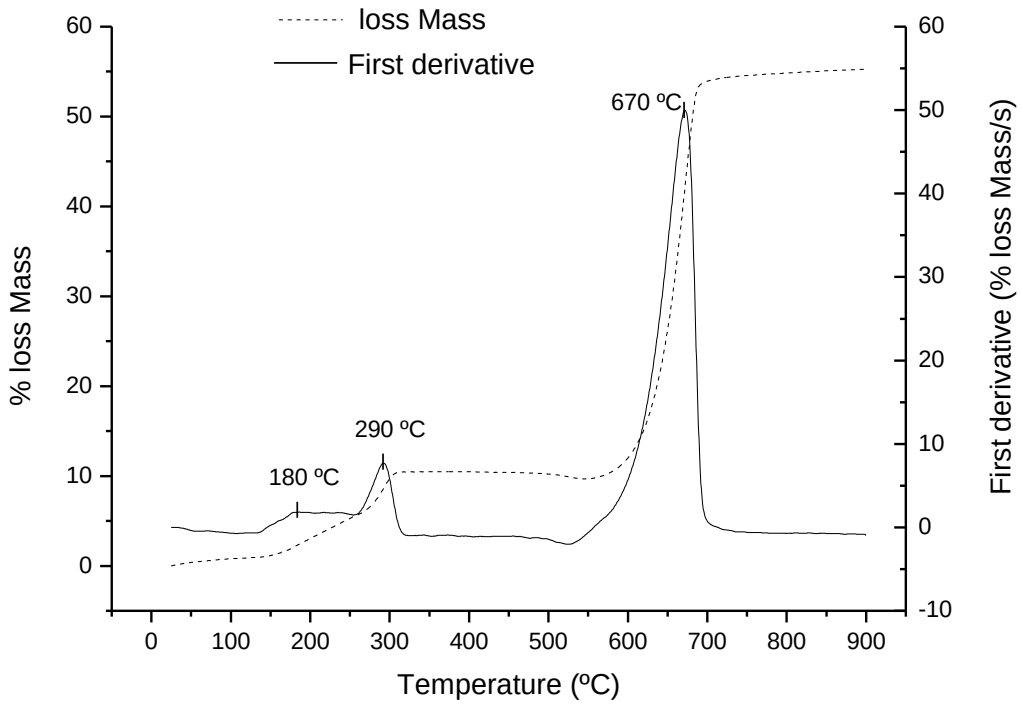

Figure 3.3. *TGA and DTG of $Fe_2(SO_4)_3 \cdot xH2O$.*

3.1.3.2.2. Red gypsum

In Figure 3.4 we see that the most significant thermal event takes place at 138 °C, and is related to the loss of chemically-bound water of hydration to calcium sulphate ($CaSO_4 \cdot 2H_2O$) (Paulik et al., 1992; Hudson-Lamb et al., 1996). This thermal event is similar to the one observed in the reference sample (Pladur®), as shown in Figure 3.7.

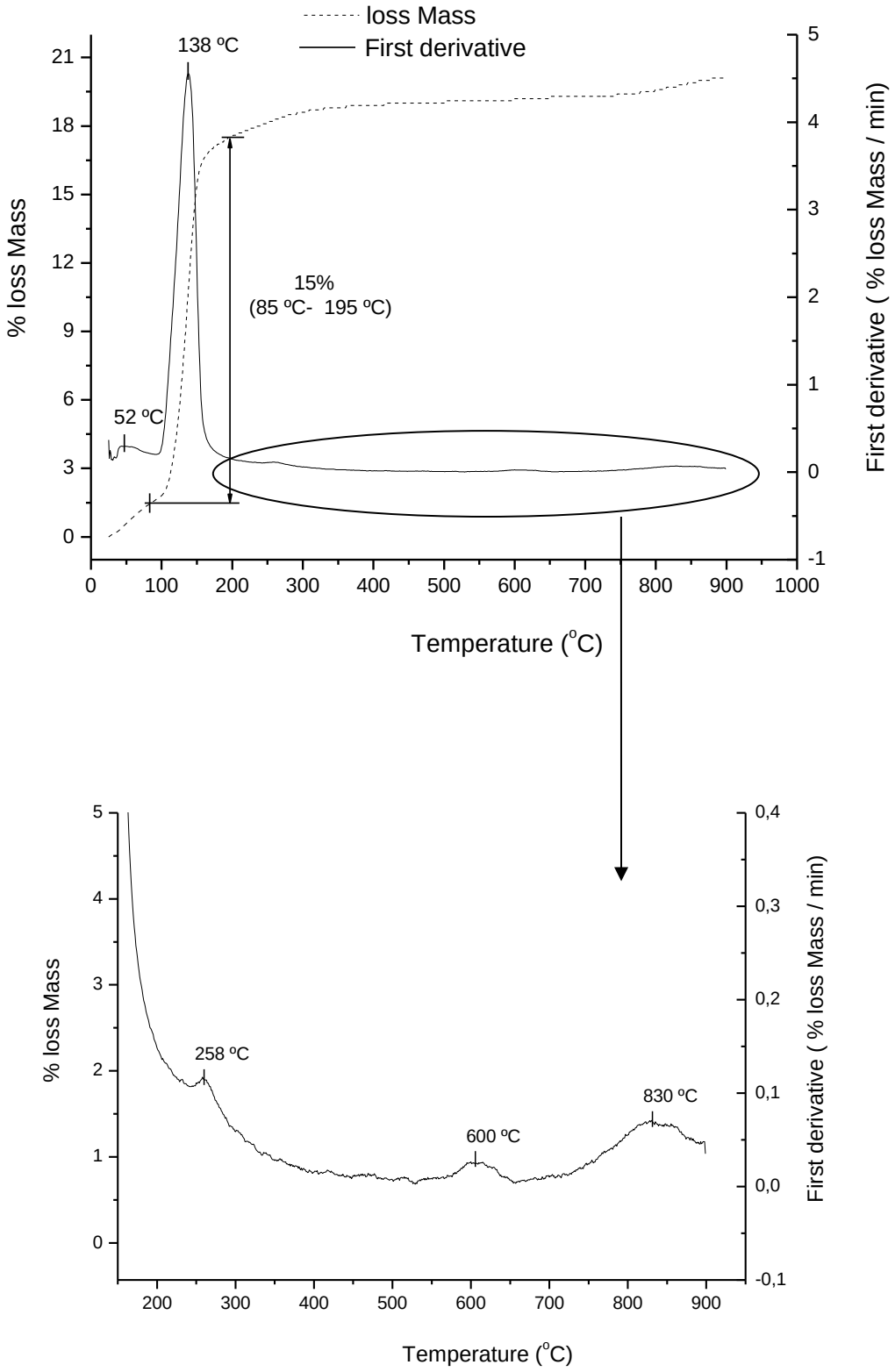

Figure 3.4. *TGA and DTG of Red gypsum.*

According to the variation in the mass measured the mass loss in the sample is 15%, which corresponds approximately to the loss of two water molecules bound to the calcium sulphate in the red gypsum sample, according to the next chemical reaction:

$$CaSO_4 \cdot 2H_2O \rightarrow CaSO_4 + 2\ H_2O \qquad \text{[Eq. 3.8]}$$

Above 150 °C the mass loss in the waste is almost negligible although, as shown in Figure 3.4, but there is a small mass loss at certain temperatures: 258 °C, 600 °C and 830 °C (Figure 3.4b).

The corresponding peak to 258 °C can be attributed to the decomposition of hydroxides formed in the neutralization of acidic waters, specifically the thermal decomposition of iron hydroxide (III) ($Fe(OH)_3$), as demonstrated by various tests on reference samples prepared in our laboratory, as well as by the literature (Said et al., 1993). The thermal decomposition of $Fe(OH)_3$ into Fe_2O_3 occurs at around 240 °C with heat absorption, as shown in equation:

$$2\ Fe(OH)_3 \rightarrow Fe_2O_3 + 3\ H_2O \qquad \text{[Eq. 3.9]}$$

This hypothesis has been confirmed by thermogravimetric analysis of a mixture of red gypsum and $Fe(OH)_3$. The $Fe(OH)_3$ was obtained in our laboratory after neutralizing Fe^{3+} dissolved ($FeCl_3 \cdot 6H_2O$ solution) with NH_4OH to basic pH. The result of this analysis is presented in Figure 3.5, where mass loss is observed at 54 °C due to the initial moisture of the sample, while the loss at 140 °C corresponds to the dehydration of the calcium sulphates (a major component of red gypsum).We also observe a peak at 270 °C produced by the thermal decomposition of $Fe(OH)_3$.

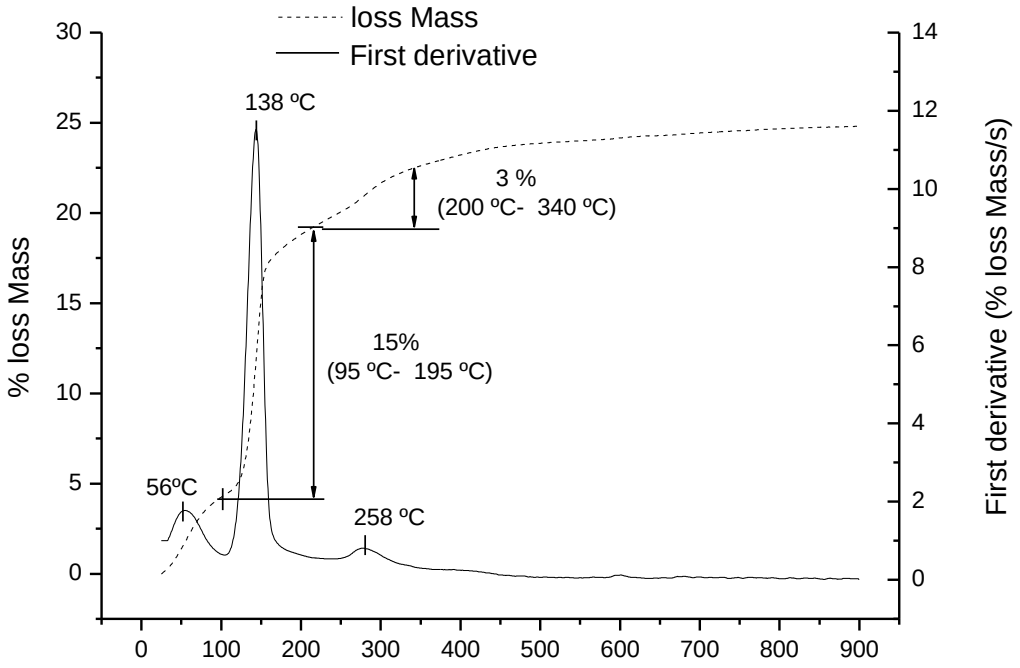

Figure 3.5. *TG and DTG of a mixture of 75% red gypsum and 25% $Fe(OH)_3$*

In addition, Figure 3.4 clearly shows two peaks at higher temperatures. The peak at 600 °C traces the magnesite ($MgCO_3$) in the waste coming from the magnesite added in the neutralization process of the final weak acid effluent. This is ratified by the analysis of magnesite in our laboratory and by other studies such as Demir et al. (2003), according to the process:

$$MgCO_3 \rightarrow MgO + CO_2 \qquad \text{[Eq. 3.10]}$$

The mass loss occurs between 590 °C and 650 °C, corresponding to the loss of CO_2.

The second peak observed in Figure 3.4 is associated with the decomposition of carbonates at about 700 °C. The presence of these carbonates in the red gypsum comes from the neutralization of the acidic waters with calcium hydroxide and magnesite, as follows:

$$Ca^{2+} + CO_3^{2-} \rightarrow CaCO_3 \qquad \text{[Eq. 3.11]}$$

This reaction is favoured by the acidity of the water, leading to calcium carbonate, as described in Equation 10. According to previous studies (L'vov et al., 2002) the thermal decomposition of $CaCO_3$ takes place within a range of 800 - 900 °C (maximum at 830 °C), which matches our results (Figure 3.5).

3.1.3.2.3. Vermiculite

The vermiculite TGA plot (Figure 3.6) shows a significant mass loss at 75 °C, 180 °C and between 600-800 °C.

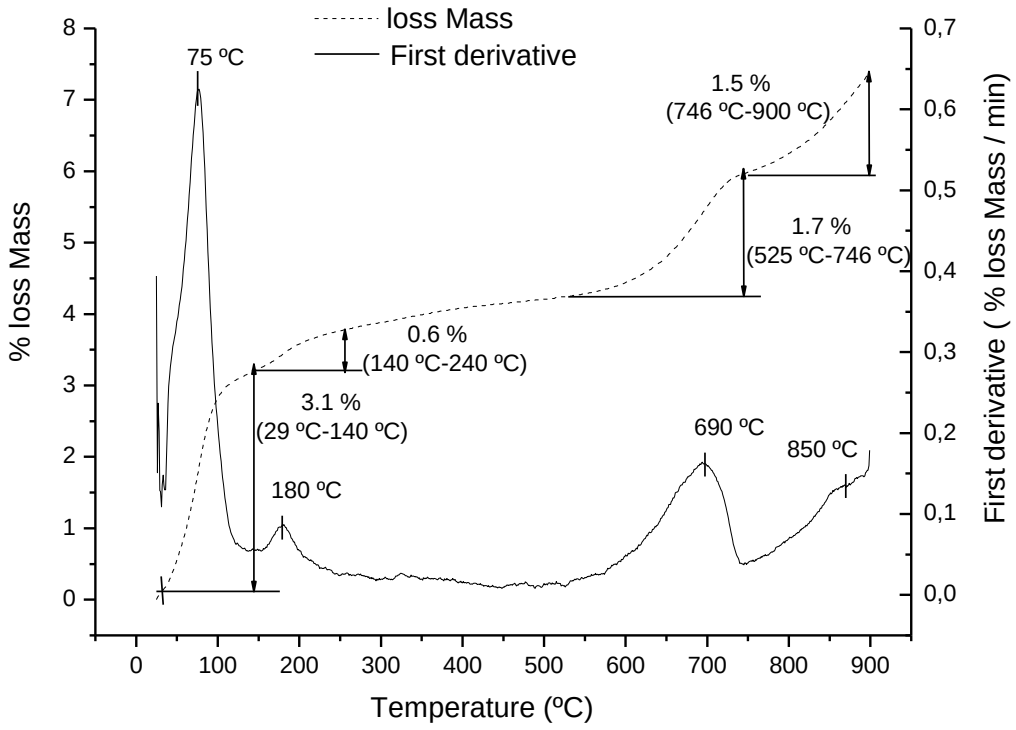

Figure 3.6. *TG and DTG of vermiculite.*

According to published studies (Pérez-Maqueda et al., 2003; El Mouzdahir et al., 2009), the first peak (75 °C) corresponds to the initial moisture content of the sample. The second event (180 °C) is produced by the loss of the interlaminar water in the mineral structure, whereas at 690 °C the silicate structure is destroyed together with a loss of the hydroxyl molecules that were part of the original structure. Beyond 800 °C, a re-crystallization occurs in the structure with the formation of enstatite (Poyato et al., 2002).

3.1.3.2.4. PLADUR®

The Pladur® used in this study consists of a core of natural gypsum manufactured according to standard UNE - 102,023 specifications. Table 3.2 shows that is mainly composed of S and Ca in the stequiometric form of $CaSO_4 \cdot 2H_2O$.

The Pladur® TGA plot is similar to the expected one for natural gypsum (Figure 3.7). Sample mass is almost constant up to 100 °C, then a mass loss occurs corresponding to the chemically-bound water of the material mainly present in the form of $CaSO_4 \cdot 2H_2O$ (Eq. 3.8).

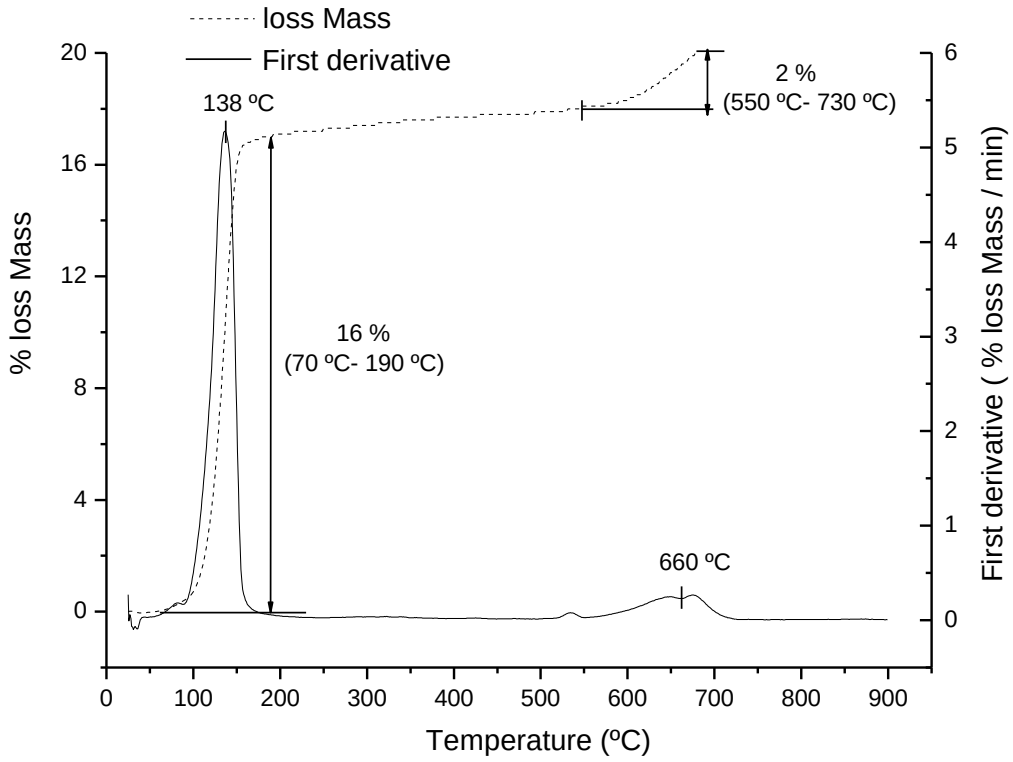

Figure 3.7. *TG and DTG of Pladur®*

According to previous studies (Paulik et al., 1992; Hudson-Lamb et al., 1996), the decomposition of calcium sulphate dihydrate takes place in two stages. In the first (100 °C - 150 °C), the calcium sulphate dihydrate loses 3/2 water molecules, as follows:

$$CaSO_4 \cdot 2H_2O \rightarrow CaSO_4 \cdot 1/2H_2O + 3/2H_2O \qquad \text{[Eq. 3.12]}$$

A calculation with the TGA data reveals that this peak is the result of a mass loss of 16% equivalent to the loss of 3/2 water molecules in the calcium sulphate dihydrate sample, according to the above equation.

A second thermal event occurs with the decomposition of the sulphate hemihydrate with the loss of 1/2 water molecules, as follows (Ang and Wang, 2004):

$$CaSO_4 \cdot 1/2H_2O \rightarrow CaSO_4 + 1/2H_2O \qquad \text{[Eq. 3.13]}$$

A mass loss of about 5% is caused by this reaction. The temperature at which this reaction takes place varies greatly depending on the matrix in which the calcium sulphate is mixed, and the heating rate to which the sample is subjected. Andersson and Jansson (1987) found that reaction occurred at 210 °C, Groves (1958) at around 300 °C, and Sultan (1996) at 600 °C, a similar temperature to the one in this work.

3.1.3.2.5. Plate 2 (75% red gypsum, 25% tionite)

In order to obtain a material with the best fire behaviour (stable when subjected to high temperatures), we prepared a mixture of 75% red gypsum and 25% tionite, which roughly corresponds to the industrial production of both wastes. This composition was also conditioned by the fact that the mud proportion is restricted by the high concentration of natural radionuclides in the tionite (Gázquez et al., 2011) and EU regulations on radioactivity (Directive EURATOM, 2013).

Figure 3.8 shows the TGA results for Plate 2 compared with those obtained for the red gypsum and mud.

An initial loss of mass takes place at around 50 °C due to moisture in the mixture, and at about 136 °C there occurs the peak of the loss of structural water in the $CaSO_4 \cdot 2H_2O$ (equation 8), which is the main constituent of red gypsum (around 57%).

Above 150 °C the mass loss in Plate 2 is almost negligible, meaning that the board demonstrates good behaviour as a building material because it does not contain volatile compounds. There are some small mass losses at different temperatures (Figure 3.8), with thermal events at 258 °C and 700 °C.

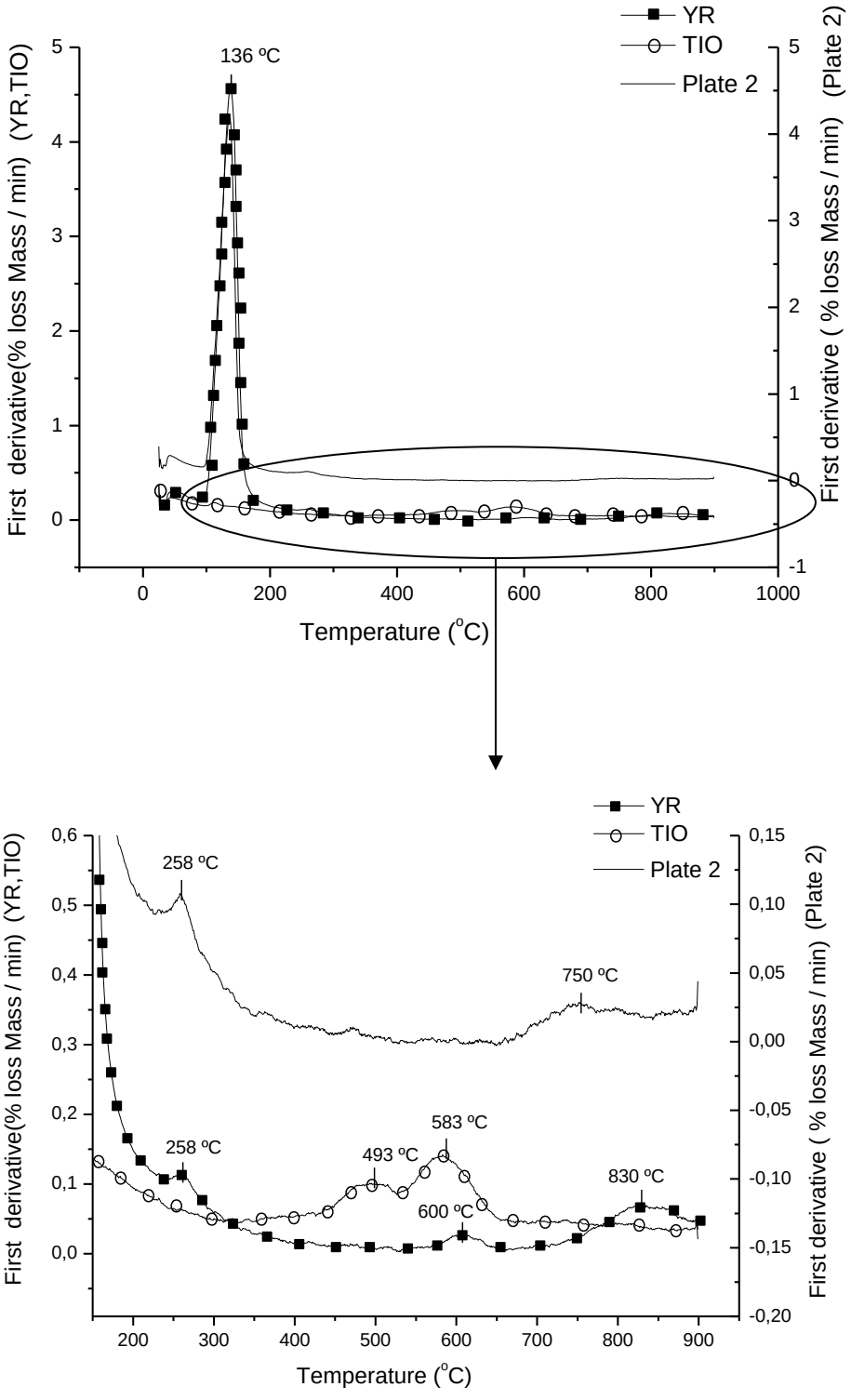

Figure 3.8. *DTG of the mixture 75% red gypsum and 25% tionite.*

The peak at 258 °C is the same event at the same temperature as in the red gypsum sample (Figure 3.4), and is due to loss of water in the thermal decomposition of the iron hydroxide (III) in the waste.

Thermals events are also observed between 400-650 °C corresponding to the decomposition of sulphates in the mud and of the magnesite in the red gypsum, but these thermal events do not appear in Plate 2. This is due to chemical reactions between sulphates in the mud and carbonates such as magnesite in the red gypsum at the setting of the plate. These reactions are favoured by the high acidity of the mud (pH = 1.9), which was measured by established reference methods for soils (Gázquez et al., 2011). The chemical reactions that occur during the setting of Plate 2 can be expressed as:

$$Mg^{2+} + SO_4^{2-} \rightarrow MgSO_4 \qquad \text{[Eq. 3.14]}$$

$$Fe^{2+} + CO_3^{2-} \rightarrow FeCO_3 \qquad \text{[Eq. 3.15]}$$

Due to the formation of these compounds during plate setting, the mass losses occur at about 700 - 800 °C (Figure 3.8) as a result of the decomposition of carbonates. Previous studies confirm that the thermal decomposition of iron carbonate (II), also known as siderite, occurs in the temperature range of 475-540 °C (Alkaç and Atalay, 2008) by the following reaction:

$$FeCO_3 \rightarrow FeO + CO_2 \qquad \text{[Eq. 3.16]}$$

Therefore, we consider that the nature of the matrix in which the iron carbonate (II) is immersed can lead to decomposition within a higher temperature range. This causes the peak corresponding to the loss of mass of CO_2 (Figure 3.8) to shift to a higher temperature range, overlapping with the loss of mass resulting from the thermal decomposition of $CaCO_3$.

3.1.3.2.6. Plate 3 (80% red gypsum, 15% mud, 5% vermiculite)

In order to increase the insulating capacity of the materials under study, we used vermiculite as an additive for its refractory qualities (Addison, 1995), and to increase the insulating capacity of the mixture. Plate 3 (80% red gypsum, 15% mud and 5% vermiculite), is a blend that also complies with EU requirements on radioactivity (Directive EURATOM, 2013).

Figure 3.9 shows an initial loss of mass due to moisture in the mixture, with the most significant thermal event occurring between 100 and 150 ° C due to the hydration water loss in the calcium sulphate dehydrate (Eq 3.8).

In addition, two minor thermal events occurred at 258 °C and 700 °C, the former being the same as that obtained on Plate 2 and the red gypsum (Figure 3.9), and identified above as the loss of water generated by the thermal decomposition of iron hydroxide (III).

As on Plate 2, new carbonates are formed as confirmed by the slight increase in the first derivative from 700 °C (Figure 3.9); this is due to their decomposition but too a much lesser extent than on Plate 2, which results from the addition of vermiculite.

So, we can state that adding vermiculite to the mixture increases the plate's thermal stability due to the shifting of the decomposition of carbonates to higher temperatures which improves the thermal behaviour of these plates against fire.

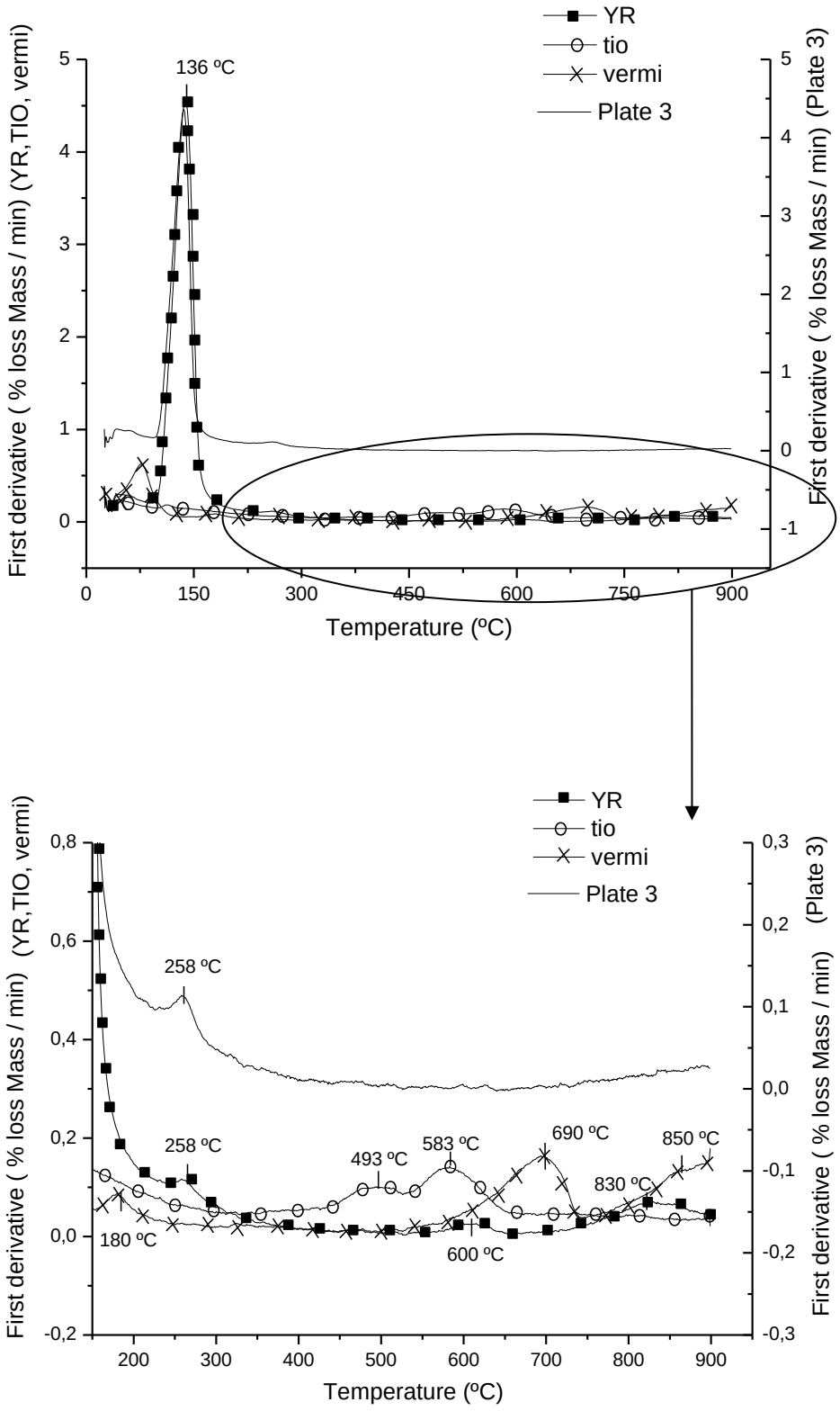

Figure 3.9. *DTG of mixture 80% red gypsum, 15% tionite and 5% vermiculite.*

In order to summarize all the obtained results on TGA analysis, the following Table 3.3 it has been conformed showing the peaks of the mass loss rates and temperature ranges where they occur.

Sample		Temperature range (ºC)	Mass lost (wt. %)
Tionite	Peak 1	35 -94	1.1
	Peak 2	94-132	0.5
	Peak 3	334-526	1.2
	Peak 4	526-720	1.6
Red gypsum (Plate 1)	Peak 1	30- 93	1.5
	Peak 2	85-195	15
	Peak 3	240-300	0.6
	Peak 4	530- 660	0.2
	Peak 5	725-900	0.8
Vermiculite	Peak 1	29-140	3.1
	Peak 2	140-240	0.6
	Peak 3	525-746	1.7
	Peak 4	746-900	1.5
Pladur®	Peak 1	70-190	16
	Peak 2	550-730	2
Plate 2	Peak 1	97-200	13
	Peak 2	225-300	0.6
	Peak 3	650-840	0.3
Plate 3	Peak 1	93-190	13
	Peak 2	220-300	0.6

Table 3.3. ***Summary of the mass loss rates and temperature ranges.***

3.1.3.3. Fire-resistance tests

Once the plates were designed and studied for thermal characteristics by TGA testing, the fire resistance test results helped to describe the behaviour of a building system during the development of a fire.

The fire resistance of a building element is defined as the time it takes the element to lose a certain property, the most important of which are: a) carrying capacity, b) heat stability, c) integrity, and d) thermal insulation.

Thermal insulation capacity was evaluated approximately by laboratory experiments in agreement to EN-1363-1 standard, which establishes a temperature (T) versus the time (t) inside the oven by the equation $T = 20 + 345 \log_{10}(8t+1)$, and by measuring the time required by the unexposed side to meet one of these two criteria; a) the temperature of one of the thermocouples on the unexposed surface of the material is above 180 ºC or, b) the average temperature of all the thermocouples on the unexposed surface is above 140 ºC + T_{env}, with T_{env} being the environmental temperature when the plates were tested (23 ºC).

Figure 3.10 shows the results from the insulating test for Plate 1 (100% red gypsum), Plate 2 (75% red gypsum, 25% mud), Plate 3 (80% red gypsum, 15% mud and 5% vermiculite) and Pladur®, as well as for a commercial product and the reference material.

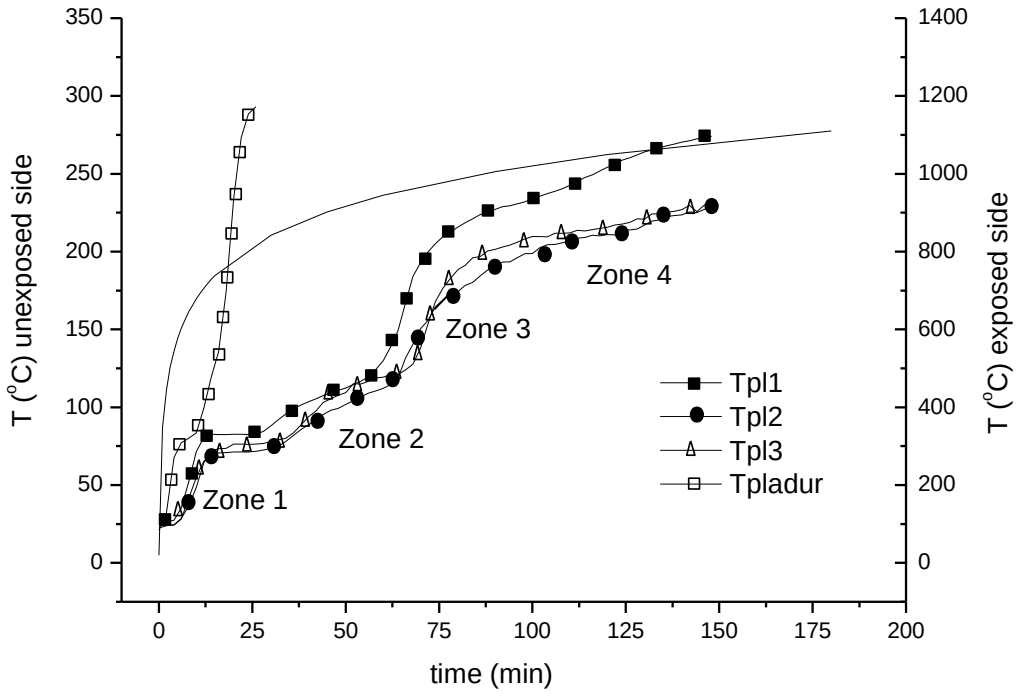

Figure 3.10. *Insulating capacity of the plates tested.*

Plates 1, 2 and 3 have similar insulating behaviour, much better and more varied than Pladur®, whose temperature increased rapidly, indicating its very low thermal insulation.

The different thermal zones observed in Figure 3.10 are characterized by their slopes (see Table 3.4), and they are discussed as follows. The curves of Plates 1, 2 and 3 show that the temperature does not vary in the unexposed side during the first 5 minutes of the test, fact due to the time of the thermal wave generated on one side takes to get exposed to the other side, which varies according to the moisture content of the plate. From this moment the temperature begins to rise (Zone 1) linearly up to 70-80 °C during 15 minutes, depending on the composition of the plate. So, Plate 1 (100% YR) reaches a higher temperature of around 80 °C. At this moment, the temperature remains constant for 30 minutes and then starts to increase up to 125 °C, reaching 60 minutes (Zone 2). In addition, the temperature of the unexposed side remains within the range of 80-125 °C, while inside the plate the loss of structural water chemically joined to the calcium sulphate dihydrate ($CaSO_4 \cdot 2H_2O$) takes place, as seen from the thermogravimetric analysis results. From 60 to 80 minutes (Zone 3), the temperature newly increases linearly up to about 200 °C, which can be associated with heat transfer by conduction through the solid (Leiva et al., 2009). Then the slope falls (Zone 4), probably due to a change in the plate composition resulting from the decomposition of the iron hydroxides (III) in the red gypsum, as previously analysed. The results shown in Figure 3.10 have been found by other authors (Leiva et al., 2005, 2008, 2009, 2010; Vilches et al., 2003, 2005; García Arenas et al., 2011).

		Zone 1	*Zone 2*	*Zone 3*	*Zone 4*
	Slope (°C min^{-1})	7.7 ± 0.7	1.2 ± 0.1	7.8 ± 0.6	0.92 ± 0.01
Plate 1	*T^a range (°C)*	28 - 83	83 – 119	129 - 215	215 - 274
	Time range (min)	4 - 14	26 – 56	60 - 80	80 - 148
	Slope (°C min^{-1})	6.3 ± 0.2	1.3 ± 0.1	3.8 ± 0.3	0.61 ± 0.01
Plate 2	*T^a range (°C)*	24 - 70	75 – 118	118 - 188	188 - 228
	Time range (min)	4 - 16	32 – 64	64 - 88	64 - 148
	Slope (°C min^{-1})	6.9 ± 0.6	1.9 ± 0.1	5.2 ± 0.4	0.49 ± 0.01
Plate 3	*T^a range (°C)*	25 - 73	80 – 127	120 - 196	196 - 232
	Time range (min)	4 - 16	34 – 68	64 - 86	86 - 148

Table 3.4. ***Slopes (°C min^{-1}) of the temperature-time curve for the different plates. The uncertainties are given at 1 sigma.***

One final point is that no smoke or odours from the plates were emitted at any time during the test. As a summary, Table 4 shows the slopes' various thermal zones for the different plates undergoing fire resistance tests.

The slope for Plates 2 (6.3 $°C\ min^{-1}$) and 3 (6.9 $°C\ min^{-1}$) are similar in Zone 1 (a range of 5-15 minutes) and lower than the slope of Plate 1 (7.7). In the second time range (30-60 minutes), Zone 2, the slopes of Plates 1 (1.2) and 2 (1.3) are similar and fall below that of Plate 3 (1.9). In Zone 3, the best plate is 2 as its slope has the lowest value (3.8), with Plate 1 presenting worst behaviour. In the final temperature range shown in Table 4 (around 200 *°C)*, Plate 3 presents the lowest slope (0.49 $°C\ min^{-1}$), and Plate 1 the worst behaviour. So, we can state that Plates 2 (75% red gypsum, 25% tionite) and 3 (80% red gypsum, 15% tionite and 5% vermiculite) have the best fire resistance in most thermal ranges.

Moreover, the addition of mud improves thermal insulation significantly, mainly due to its highly refractory mineral phases. When vermiculite is added, we note that the improvement in the thermal behaviour is not significant because there is only a slight decrease in the slope after 80 minutes of testing at approximately 200 °C. We believe that the influence of vermiculite on the material is only seen at higher temperatures that were not measured in this study.

3.1.4. CONCLUSIONS

The present study focuses on the characterization of waste (tionite and red gypsum) generated by the titanium dioxide production industry near the city of Huelva, with the aim of ascertaining their mineralogical composition and behaviour as insulating material. The main objective was to increase knowledge of these industrial wastes for commercial applications in the construction industry.

The possibility of recycling these materials as passive fire protection has been evaluated by thermogravimetric analysis and a preliminary fire resistance test. This study covers materials that have been used previously so that we could compare these analyses, and we have established which of these materials performs better at high temperatures.

Thermogravimetric analysis shows that adding tionite to the red gypsum sample plate makes it behave in a more stable way when subjected to high temperatures, due to the different chemical reactions that occur in the mixture process, making the final solid obtained more unalterable. In relation to the addition of vermiculite to the mixture of red gypsum and tionite, it has been shown that its influence makes for better behaviour in the

mixture when subjected to high temperatures, causing the decomposition of carbonates as observed on Plate 2 (75% red gypsum, 25% tionite) to shift to much higher temperatures.

Experimental results from fire resistance tests indicate that Plate 2 (75% red gypsum, 25% tionite) and Plate 3 (80% red gypsum, 15% tionite and 5% vermiculite) are those with better fire resistance than Plate 1 (100% red gypsum), when subjected to the standard temperature-time curve, mainly due to the high content of refractory material in the tionite. The test material also possesses acceptable mechanical properties that showed no noticeable distortion or breakage during the fire endurance test, although the study of these properties is a future research line study. These results demonstrate that the plates perform better than some materials used in construction such as Pladur®, used as reference material in this study.

As a complementary conclusion, it has been proven that the plates are agree to EU radioactivity requirements, since the use of these wastes as building materials not exceeded the radioactive thresholds.

Finally, while this article is primarily focused on the application of two inorganic industrial wastes (tionite and red gypsum) in the development of new materials for passive fire protection, other possible uses are not ruled out. The thermogravimetric analysis and fire resistance tests to which the materials were subjected may be used to determine other applications and provide useful data for future research.

Acknowledgments

This work was partially supported by the following projects: a) "Valuation of Red Gypsum waste from industry production of titanium dioxide" (CIT-310200-2007-47), b) "Modelling and characterization of Huelva phosphogypsum stacks for its management and environmental control" (RNM-6300). I would also like to give our acknowledgements to the Hutsmann-Tioxide (factory of Huelva), and to their technical staff by the collaboration in the explanation of the obtained results.

3.2. CO_2 SEQUESTRATION BY INDIRECT CARBONATION OF ARTIFICIAL GYPSUM GENERATED IN THE MANUFACTURE OF TITANIUM DIOXIDE PIGMENTS

S.M Pérez-Moreno[1], M.J. Gázquez[1,2], and J.P. Bolívar[1]

[1]Departmento de Física Aplicada, Universidad de Huelva, Huelva, Spain

[2]Departamento de Química, Universidad Técnica Particular de Loja, Loja, Ecuador

Chemical Engineering Journal 262 (2015) 737–746

Abstract

In this paper, the use of red gypsum (RG), waste from the naturally occurring radioactive materials industry that is devoted to the production of the TiO_2 pigment, was evaluated as a source of calcium for CO_2 sequestration by an indirect carbonation process. The main objective was to valorise this waste and, at the same time, analyse the reduction of greenhouse gas emissions (CO_2) emitted by industrial sources that use this process. In order to induce the carbonation process, the extraction of calcium from the sample was required beforehand. For this, two different extraction routes were applied (the NaOH and NH_4OH pathways). The obtained results demonstrate that RG has high carbonation reactivity, depending on the extraction agent used at room temperature and pressure. The conversion of RG to calcium carbonate was 92% when using sodium hydroxide, whereas 64% was obtained with ammonium hydroxide extracting. The behaviour and fluxes of the radionuclides and trace elements, initially contained in the RG, were also evaluated during the full carbonation process. In general, the levels of pollutants in the final calcite (calcium carbonate) were comparable to the ones found for typical unperturbed soils.

Keywords: *Red gypsum, Titanium Dioxide, CO_2 sequestration, Carbonation, Calcite.*

3.2.1. INTRODUCTION

Mineral carbon sequestration technology is based on the process carried out by natural rock, in which carbonic acid, generated through the dissolution of CO_2 in rain water, is neutralised with mineral alkalinity to form carbonate minerals (Huijgen and Comans, 2003). The products of mineral carbonation remain, naturally, in the solid state and, thus, there is no possibility of CO_2 release after sequestration. Therefore, this technique represents the most stable form for carbon capture and storage.

This form of CO_2 capture is not a new technological concept. The technologies and practices associated with mineral carbon capture have previously been studied by several authors (Praetorius and Schumacher, 2009; Mai et al., 2009; Muriithi et al., 2011; Erin et al., 2012; López-Periago et al., 2013) and, currently, a pilot-scale plant is being developed (Hawthorne et al., 2011; Hwanju et al., 2012; Wang et al., 2013), because this carbon capture technique promises to decrease CO_2 emissions from industrial processes (Ho Young et al., 2012).

The need for CO_2 capture has been influenced by the concern for the environment and alarm over global warming, triggered by the rise in greenhouse-gas emissions. And this fact must not be ignored. Currently, the atmospheric concentration of CO_2 is about 395 parts per million (ppm) by volume (NOAA, 2013), which is approximately 1.4 times higher than the concentration of CO_2 in the pre-industrial stage. Moreover, this level is expected to increase over the next few decades, owing to the burning of fossil fuels and land-use changes. The rate of this increase will depend on uncertain economic, sociological, technological and natural developments, but may ultimately be limited by the reduced availability of fossil fuels or CO_2-reduction strategies (Mehdi et al., 2012).

Mineral sequestration of CO_2, such as carbonation of alkaline materials with high content in Ca, is a feasible technology for the reduction of carbon dioxide emissions to the atmosphere (Fernández Bertos et al., 2004; Kaithwas et al., 2012). Carbon capture could be an effective means for mitigating global climate change and a form of CO_2 storage for a long time period. Moreover, it is the safest and most permanent form of fixing the CO_2 emitted into the atmosphere, because the CO_2 becomes part of stable and slightly soluble carbonates, mainly as calcium carbonate. The calcium carbonate can be used as a raw material (i.e. substituting to natural calcium carbonate), for example in the manufacture of cement (Matschei et al., 2007) or as a removal agent for heavy metals in contaminated effluents (Minhee et al., 2007).

In the southwest of Spain, there is a naturally occurring radioactive material (NORM) industry, which generates waste with a high content of Ca (usually called red gypsum (RG) and, in the same way, it releases large amounts of CO_2 into the atmosphere. The industry is engaged in the production of titanium dioxide, a pigment that delivers whiteness, brightness and opacity to a vast range of products from coatings and polymers to cosmetics and food (Gázquez et al., 2014). This industry generates of about 7.0×10^4

tons of RG per year, containing around 33% CaO (Gázquez et al., 2009), and emitted 1.5 × 10^5 tons of CO_2 into the atmosphere in 2011 (PRTR, 2013).

Previous studies have promoted the use of this residue in different applications such as in soil remediation (Fauziah et al., 1996), cement production (Gázquez et al., 2013) and as a new fire-insulating material (Pérez-Moreno et al., 2013). The new proposal discussed in this work concerns the utilisation of RG as a CO_2 sequestering agent by indirect carbonation. Indirect carbonation involves the extraction of a reactive component (Ca^{2+}) from the minerals, using sodium hydroxide or ammonium as the solvent, followed by the reaction of the extracted component with CO_2 in the aqueous phase. The treatment proposed is especially attractive, because there are no references of previous studies in which RG is used in the capture of CO_2 and, until now, RG has not been found in any commercial market application, being eliminated in a legal waste repository plant where it is properly disposed.

The aim of the present study is to evaluate the use of RG as a calcium source for carbon dioxide sequestration and to analyse the advantages and disadvantages of using sodium hydroxide or ammonium as extracting agents. This work also studies the behaviour of radionuclides as well as the trace and major elements contained in the waste during the capture process, determining the transfer factor (%) of them in the carbonation process.

3.2.2. MATERIALS AND METHODS

3.2.2.1. Materials

The sample of RG used in this study was collected from a titanium dioxide production plant located 12 km from the city of Huelva (southwest Spain), and it was dried at 50 °C (at this low temperature, RG does not dehydrate) until reaching a constant weight before the experiments. RG emerges in the final stage of the industrial process of titanium dioxide manufacturing, where a weakly acidic liquid stream, composed primarily of 1.36 % of sulfuric acid (H_2SO_4) and 0.28 % iron sulphates ($FeSO_4$, $Fe_2(SO_4)_3$), is treated in a neutralisation plant. In this plant, calcium hydroxide and magnesite are added to the weak acid stream in order to precipitate the dissolved materials. Finally, the RG is separated from the stream by filtration (Gázquez et al., 2009).

3.2.2.2. Measurement techniques

3.2.2.2.1. X-Ray Fluorescence (XRF)

The major elements were measured using XRF with a Bruker S4 Pioneer system, which has the following characteristics: 4 kW, front window and anode of Rh, five analysing crystals, LIF200, Ge, PET, OVO55 and OVOC, two X-ray detectors. In our case, a 1 g aliquot of each dry sample was taken and mixed with 10 g of lithium tetraborate (material used for melting), with five drops of lithium iodine at 20% added. Each mixture was placed in a crucible of Pt–Au and introduced into a special furnace for fusion. The final result for each sample is a homogenous glass, called "pearl", ready to be measured in the XRF system.

3.2.2.2.2. X-Ray Diffraction (XRD)

The mineralogical study was performed by applying the disoriented-dust method with a Bruker laser diffraction instrument, and using the Kα radiation of Cu (filtered by a Ni film) excited by 30 mA intensity and 40kV tension. A semi-quantitative mineralogical determination was estimated with the XPowder software.

3.2.2.2.3. Scanning Electron Microscopy (SEM)

The scanning electron microscope is a type of electron microscope that creates an image of the sample surface by scanning it with a high-energy beam of electrons in a raster-scan pattern. The electrons interact with the atoms that constitute the sample, thereby producing signals that contain information about the surface topography, composition and other properties of the sample, such as its electrical conductivity. Aliquots of each sample were embedded in epoxy resin mounts, polished and covered with a carbon layer prior to analysis. The SEM analyses were carried by a JEOL JSM-5410 system, working at 20 kV. It has a backscattered electron detector (BSE), by Tetra Link of Oxford, and a dispersive X-ray spectrometer for EDS (energy-dispersive X-ray spectroscopy).

3.2.2.2.4. Inductively coupled plasma–mass spectrometry (ICP-MS)

Trace elements were determined by ICP-MS using a Perkin Elmer Sciex ELAN 6000 at the Activation Laboratories Ltd. (ACTLABS, 2013) in Canada. To this end, representative aliquots (0.25 g) of the samples were subjected to hard acid attack until near total dissolution. The digestion method was carried out using four acids, beginning

with hydrofluoric, followed by a mixture of nitric and perchloric acids, heated using precise programmer-controlled heating in several ramping and holding cycles, which takes the samples to dryness. After dryness was attained, samples were brought back into solution using hydrochloric and nitric acids. Finally, digested samples were diluted and analysed.

3.2.2.2.5. Thermogravimetric Analysis (TGA)

The TGA runs were carried out with a Q50 thermogravimetric analyser on samples of around 10 mg. Under nitrogen (N_2) environments, a heating rate of 10°C/min was used between 25 and 1000°C. TGA results were depicted in two ways, that is, mass loss versus time or temperature (TGA curve) and mass-loss rate versus time or temperature (differential TGA curve, or DTG).

3.2.2.2.6. Alpha-Particle Spectrometry

^{210}Po, Th and U isotopes contained in the solid samples were initially dissolved and then isolated using a well-established sequential radiochemical method based on tributilphosphate extraction. After isolation, the U and Th isotopes were electrodeposited, independently, onto stainless-steel discs. The thin ^{210}Po source was obtained by self-deposition of polonium onto silver discs. Then, the radioactive sources were counted in an EG&G Ortec alpha-particle spectrometer system, and finally the activity concentrations of these radionuclides were calculated. In order to control the radiochemical recovery, ^{209}Po, ^{232}U and ^{229}Th certified standards were used.

3.2.2.3. Carbonation Method

Using the same methodology as previously published work, the experimental procedure begins by dissolving the sample (50 g), earlier dried at 50°C, in either alkaline solution (NaOH) (Cárdenas-Escudero et al., 2011) or NH_4OH (Song et al., 2012), where the following simplified reactions occur:

$$CaSO_4 \cdot 2H_2O(s) + 2NaOH\ (aq) \rightarrow Ca(OH)_2(s) + Na_2SO_4(aq) + 2H_2O \quad \text{[Eq. 3.17]}$$

$$CaSO_4 \cdot 2H_2O(s) + 2NH_4OH\ (aq) \rightarrow Ca(OH)_2(aq) + (NH_4)_2SO_4(aq) + 2H_2O \quad \text{[Eq. 3.18]}$$

In the first experiment, approximately 20 g of NaOH was added to 1 L of water (eq. 3.17) and, in the second experiment, the same amount of sample was added to 1 L of ammonia solution 3.8% (v/v) (eq. 3.18). By considering that the content of calcium sulphate ($CaSO_4 \cdot 2H_2O$) in RG is around 70–80% (Gázquez et al., 2009; Pérez-Moreno et al., 2013), an amount of ammonia that was equal to a slight excess (120 %) of the stoichiometric ratio was used, because previous studies (Song et al., 2012; Myung Gyu et al., 2012) suggest that excess ammonia (110–120 %) would be desirable for the stability of the reaction and for obtaining $CaCO_3$ with higher purity. Both mixtures were kept at room temperature for 3 h under constant stirring.

Subsequently, the solid $Ca(OH)_2$ formed was dissolved in water with a flow of CO_2 through the suspension for 1 h, and the carbonation reaction took place:

$$CO_{2(g)} + H_2O \rightarrow H_2CO_{3(aq)} \rightarrow 2H^+_{(aq)} + CO_3^{2-}{}_{(aq)} \quad \text{[Eq. 3.19]}$$

$$Ca(OH)_{2(s)} \rightarrow Ca^{2+}{}_{(aq)} + 2\,OH^-{}_{(aq)} \quad (2.2) \quad \text{[Eq. 3.20]}$$

$$CO_3^{2-}{}_{(aq)} + Ca^{2+}{}_{(aq)} \rightarrow CaCO_{3(s)} \quad (2.3) \quad \text{[Eq. 3.21]}$$

These partial reactions give the following global reaction:

$$Ca(OH)_{2(s)} + CO_{2(g)} \rightarrow CaCO_{3(s)} + H_2O \quad \text{[Eq. 3.22]}$$

The carbonation process was performed at a constant temperature of about 75°C, since according to previous experiments (Wouter et al., 2005) is considered a suitable temperature to obtain a good conversion in the carbonation process. . When the carbonation was complete, the pH approached a constant value of approximately 7.0, being the most apparent indication of the completion of the carbonation reaction (eq. 3.22) (Song et al., 2012; Myung Gyu et al., 2012).

Afterwards, the samples were filtered, washed with 200 mL distilled water and finally dried at 60°C. Moreover, the resulting liquid was evaporated at 80°C, and the obtained white-coloured crystals were characterised in order to ensure that the expected

composition was obtained and to evaluate the yields in all steps. Two replications were performed for each experiment in order to assess the reproducibility of the results.

In Figure 3.11, the full experimental procedure is summarised. The RG sample (waste generated in the titanium dioxide industry) is the raw material of this work. The calcium carbonate from the RG (C) is the final product of the carbonation process ($CaCO_3$ plus other unknown products) and is called C1 when sodium hydroxide (NaOH) is used as the solvent to extract calcium (eq. 3.17), whereas the code C2 is assigned when ammonium (NH_4OH) is used (eq. 3.18). In the process, a co-product (S) is generated, that is sodium sulphate (Na_2SO_4), or S1, according to eq. 3.17 and ammonium sulphate ($(NH_4)_2SO_4$), or S2, according to eq. 3.18.

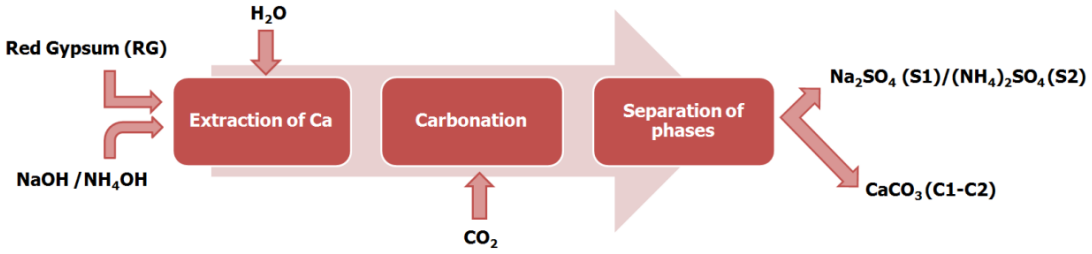

Figure 3.11. *Flowchart of the experimental methodology.*

3.2.3. Results and discussion

3.2.3.1. Mineral Composition

Figure 3.12 shows the diffraction pattern obtained by XRD for all the samples under study. In this figure, the main crystalline phase observed in RG is mainly formed of gypsum ($CaSO_4 \cdot 2H_2O$), approximately 90%, which is a similar result to that obtained in previous studies (Gázquez et al., 2009; Pérez-Moreno et al., 2013). Other traces phases detected in RG are basanite ($CaSO_4 \cdot 1/2H_2O$) and magnesian calcite ($(Ca,Mg)CO_3$), which is a variety of calcite consisting of randomly substituted magnesium carbonate in a disordered calcite lattice. The presence of magnesian calcite can be justified by taking into account that magnesite is added to the calcium hydroxide in the neutralisation of the weak acid stream and, therefore, a small amount remains un-reacting in the production

process of RG. This has been confirmed in previous work by TGA analysis (Pérez-Moreno et al., 2013).

The C1 sample (carbonate by NaOH) contains between 70-80% calcite ($CaCO_3$) as the main crystalline phase, 15-20% magnesian calcite and <5% rutile (TiO_2), with this last compound coming from the RG. In the C2 sample (carbonate by NH_4OH), the main crystalline phases are gypsum (50-55%) and calcite (25-30%), with -trace phases of basanite, magnesian calcite and rutile.

The obtained results lead us to think that the carbonation process with ammonium is less effective than the sodium process, as a part of the gypsum present in the sample remains unreacted. This is due to the fact that ammonium hydroxide is a weak base and does not dissociate completely, which produces an unsatisfactory concentration of hydroxyl ions to react with the whole sample (ATSDR, 2004). This has been experimentally shown (eq. 3.18), as the pH value achieved using ammonia (pH 11) was smaller than that using sodium hydroxide (pH 13).

The results of XRD for the co-products coming from the carbonation process (solid samples with code S) are as expected, according to eqs. 3.17 and 3.18. In the S1 sample, the only crystalline phase detected was thenardite (Na_2SO_4), and the S2 sample contained mainly mascagnite ($(NH_4)_2SO_4$), which correspond to the more stable phases minerals according to experimental conditions (Armarego and Chai, 2009).

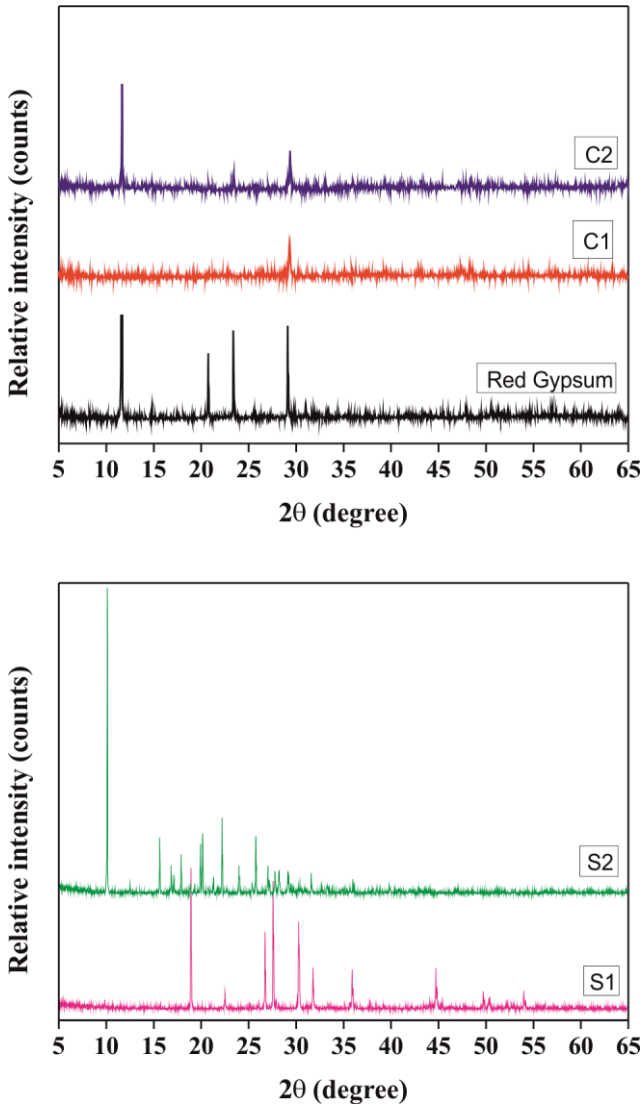

Figure 3.12. *XRD analysis on the raw material (RG) and precipitated obtained from carbonation process (C1, C2, S1 and S2).*

3.2.3.2. Major and Trace Elements

Table 3.5 shows the concentrations of the major elements (% dry weight) of the studied samples, being in agreement to the results obtained by XRF. It is observed that the RG is mainly composed of Ca (28% of CaO) and sulphur (34% of SO_3) as the major elements, which are very similar to the results obtained in previous studies (Pérez-Moreno et al., 2013). This confirms that RG is mainly formed from calcium sulphate (70%) if all of the calcium is in the form $CaSO_4$. As expected, the C1 and C2 samples show high concentrations of CaO (47 and 42%, respectively). The RG, C1 and C2 samples contain several major elements, but in a lower proportion, as are the cases for iron (Fe_2O_3, 7–9%)

and titanium (TiO2, 4–5%). These elements come from the raw material (ilmenite, $FeTiO_3$) used in the titanium dioxide manufacture, remaining as a significant fraction in the RG, which will finally be bound to C1 and C2 co-products (Gázquez et al., 2009). In relation to the S1 sample, the major elements observed were Na (Na_2O, 37%) and S (SO_3, 35%), which form thenardite according to the XRD pattern. The S2 sample contains 53% SO_3, which is directly linked with the higher proportion of ammonium in the ammonium sulphate.

	RG	C1	S1	C2	S2
SiO_2	0.74±0.05	1.2±0.1 (103±11)	0.35±0.03 (38±4)	0.91±0.06 (85±8)	0.22±0.02 (12±1)
Al_2O_3	0.75±0.02	1.0±0.1 (84±8)	0.04±0.01 (4.4±1.1)	0.89±0.03 (82±4)	0.03±0.01 (1.6±0.5)
Fe_2O_3	7.3±2.0	9.0±2.5 (79±30)	0.03±0.01 (0.34±0.15)	9.3±2.6 (88±34)	0.02±0.01 (0.11±0.06)
MnO	0.25±0.07	0.30±0.08 (76±29)	0.01±0.01 (3.3±3.4)	0.31±0.09 (86±34)	0.01±0.01 (1.6±1.6)
MgO	0.77±0.05	0.30±0.02 (25±2)	0.95±0.06 (101±9)	0.37±0.02 (33±3)	1.1±0.1 (57±6)
CaO	28±2	47±3 (106±10)	1.8±0.1 (5.3±0.5)	42±3 (103±10)	4.2±0.2 (5.9±0.5)
Na_2O	0.18±0.01	0.50±0.03 (0.84±0.07)	37±3 (80±8)	0.09±0.01 (34±4)	0.29±0.02 (64±6)
K_2O	0.03±0.01	0.04±0.01 (84±35)	0.01±0.01 (27±20)	0.04±0.01 (92±38)	0.02±0.01 (26±15)
TiO_2	3.8±0.1	4.7±0.1 (79±3)	0.02±0.01 (0.43±0.21)	4.9±0.1 (89±3)	0.01±0.01 (0.10±0.10)
P_2O_5	0.05±0.01	0.05±0.01 (64±18)	0.01±0.01 (17±17)	0.05±0.01 (69±19)	0.01±0.01 (15±8)
SO_3	34±1	2.1±0.1 (4±1)	35±1 (85±4)	11±1 (22±2)	53±1 (62±2)
LOI	23±5	33±6	24±3	29±6	39±2

Table 3.5*. Concentration (%) of major elements in the materials under study and in the brackets the transfer factor (%) of major elements in the experimental process. The total iron content is given as Fe_2O_3.*

Furthermore, in Table 3.5 the transfer factors (in brackets) of the major elements in the experimental process are also shown, in order to know their chemical behaviour and their distribution throughout the carbonation process. The transfer factor (η_i) for an element "i" has been defined as the fraction of each element that remains in each one of the products in relation to the initial input, and it is given by the following equation:

$$\eta_i(\%) = \frac{C_{Pi} \times f_{Pi}}{\sum C_{Rj} \times f_{Rj}} \times 100 \qquad \text{[Eq. 3.23]}$$

Where C_{Pi} and C_{Rj} are the concentrations of the element (i) of interest in the products and reactants for each reaction of the carbon mineral sequestration process, f_i is the 'mass factor' of each reactant (i), i.e. the experimentally involved mass in the chemical reaction for each reactive added (R_i) or each product generated (P_i). So, It can be seen that the majority of the major elements (SiO_2, Al_2O_3, Fe_2O_3, MnO, CaO, K_2O, TiO_2 and P_2O_5) contained in the RG are almost entirely transferred into calcite (C1 or C2), whereas other elements, such as Mg, Na and S, remain in solution; therefore, they will be transferred into the co-product (S1 or S2) of the carbonation process.

The samples (RG, C1 and C2) contain around 7–9% iron as Fe_2O_3 (Table 3.6). Iron minerals have not been identified in the XRD, probably because the Fe fraction is associated with amorphous phases. A study published by Acevedo-Sandoval et al. (2004) demonstrated that, at high pH values (>8), a stable environment for ferric iron is generated. Therefore, the precipitate formed by rapid addition of a basic solution to a solution of Fe (III) at room temperature will be constituted for amorphous ferric hydroxides. Thus, the precipitate formed by rapid addition of a basic solution to an effluent containing Fe (III) at room temperature, will be constituted by amorphous ferric hydroxides. In our case, the generation of red gypsum meets the above mentioned conditions, because the neutralisation process of weak acid effluent, is carried out to a high pH value, around 8.5. This suggests that Fe is present as amorphous ferric hydroxides and, therefore, it is unperturbed during the carbonation process, transferring them to the carbonation product.

	RG	C1	S1	C2	S2	Soil (*)
Cr	109±4	142±8 (83±6)	42±24 (32±18)	142±12 (90±8)	16±5 (6±2)	92±17
Ni	25±3	37±2 (94±12)	1.2±0.2 (3.9±0.8)	33±1 (91±11)	1.3±0.1 (2.1±0.3)	47±11
Co	9.4±0.5	14±1 (94±8)	<0.1	13±1 (96±9)	0.17±0.07 (0.7±0.3)	17±3
Zn	626±10	891±47 (90±5)	15±2 (1.9±0.3)	803±3 (89±1)	18±7 (1.1±0.4)	67±6
Sr	61±4	83±3 (86±6)	8.4±2.5 (11±3)	69±8 (78±10)	9.4±1.2 (6.1±0.9)	320±46
Ba	60±3	83±3 (88±5)	1.7±0.3 (2.3±0.4)	71±4 (82±6)	1.7±0.3 (1.1±0.2)	628±83
Cu	36±2	50±4 (88±9)	1.6±0.2 (3.6±0.5)	44±1 (84±5)	2.8±0.61 (3.1±0.7)	28±4
Pb	40±2	64±4 (101±8)	<0.5	61±1 (105±6)	<0.5	17±1
Th	41±1	69±1 (106±7)	<0.1	54±9 (91±15)	<0.1	11±1
U	1.6±0.1	2.1±0.1 (83±6)	0.43±0.18 (20±10)	2.1±0.1 (90±7)	0.27±0.03 (6.7±0.9)	2.7±0.6

Table 3.6. *Concentrations of trace elements (mg kg^{-1}) in the solid samples from experimental process and in the brackets the transfer factor (%) of trace elements in the experimental process. (*) Global concentration contaminated soils. (The uncertainties are given as standard deviation).*

Trace-element concentrations of RG, C1, S1, C2 and S2, analysed by ICP-MS, are compiled in Table 3.6. In order to know the environmental implications that the samples under study may produce, depending on its use, the results were compared to the global concentration of trace elements for a typical soil (Rudnick and Gao, 2003). Some of the trace elements contained in the samples (Ni, Co, Sr, Zr, Ba and U) are below the concentration of a typical soil, except for the Cr content, which can be considered as a similar concentration (100 mg kg^{-1}, approximately). Others trace elements, such as Cu (44–50 mg kg^{-1}), Pb (61–64 mg kg^{-1}) and Th (54–69 mg kg^{-1}), can be considered as moderate, although higher than those of a typical soil. The concentrations Zn (803–891 mg kg^{-1}) is also higher, even by a factor of 10.

There is a multiplicity of the limit values, or references, regarding trace metals, depending on each country or even each region, because the maximum permissible levels for each soil differ depending on the local conditions, use, soil type, climate, and so forth. The regional legislation in the area of study (Andalusia) describes levels for certain trace elements according to the use of the soil (CMAJA, 1999). The methodology for calculating the value is based on models proposed by US-EPA (Guidance for Developing

Soil Screening Levels for Superfund Sites), using data from the EPA (Environmental Protection Agency) and ATSDR (Agency for Toxicity Substances and Disease Registry). According to this regional legislation, we found that the trace-element concentrations of RG, C1 and C2 were lower than the reference values, and is thus considered a non-polluted soil for agricultural land use. Only the Zn value exceeds, four times, its reference level; however, the samples may be used if the dose added is controlled. If the final use of the products of carbonation is in the manufacture of cement (Matschei et al., 2007), the regional legislation establishes others threshold values for the concentration of trace elements in soil (>3000 mg kg^{-1} for Zn), these are much higher than those found in the samples studied. Therefore, the environmental implications of carbonation products due to trace elements, associated with the use as a building material, are negligible.

Finally, Table 3.6 also shows the transfer factor (in brackets) of trace elements in the carbonation process, in order to know their behaviour and to verify the carbonation methodology. It can clearly be seen that the trace elements contained in the RG are transferred almost entirely to calcite (see transfer factor in Table 3.6). In this sense, it is well known that the iron oxides and hydroxides generate colloids, which absorb large quantities of trace metals (Acevedo-Sandoval et al., 2004). Some authors (Randall et al., 1999; Nia et al., 2011) affirm that iron–manganese oxides are important components in soil and sediments, regulating the mobility of several essential elements for the growth of the plants. These components have a high specific surface area and are able to absorb metal compounds. Taking into account the high percentage of iron (given as Fe_2O_3) contained in the RG (7%, see Table 3.5) and calcite samples (9% of Fe_2O_3), this fact could explain how the trace elements are fully transferred into these "C" samples. This means that the "S" samples remain substantially exempt of trace elements, indicating that the use of these co-products as raw material in several commercial applications will not cause environmental implications.

3.2.3.3. Morphologic Characterisation

Highly relevant information on the morphology of the samples and, in particular, their particle-size distribution, texture and porosity is gained by applying the SEM with EDS. A representative SEM image, corresponding to RG, is shown in Figure 3.13. It is possible to observe in this figure that the RG is composed of tabular crystals with extended morphologies and, in some cases, symmetrical crystal groupings occur in different

directions. The corresponding representative EDS spectra (Fig. 3.13) indicates that these samples are formed mainly of Ca and S (point 1), similar to natural gypsum (Kuryatnyk et al., 2008) and consistent with previous studies (Fauziah et al., 1996; Gázquez et al., 2009). However, it can also be observed that there are very small particles (amorphous material) deposited onto the calcium sulphate crystals, which contain high iron concentrations and significant levels of titanium (point 2), with the additional presence of several metals such as Al, Si, Mn and Mg. This information is in agreement with the results obtained previously by means of XRF, see Table 3.5.

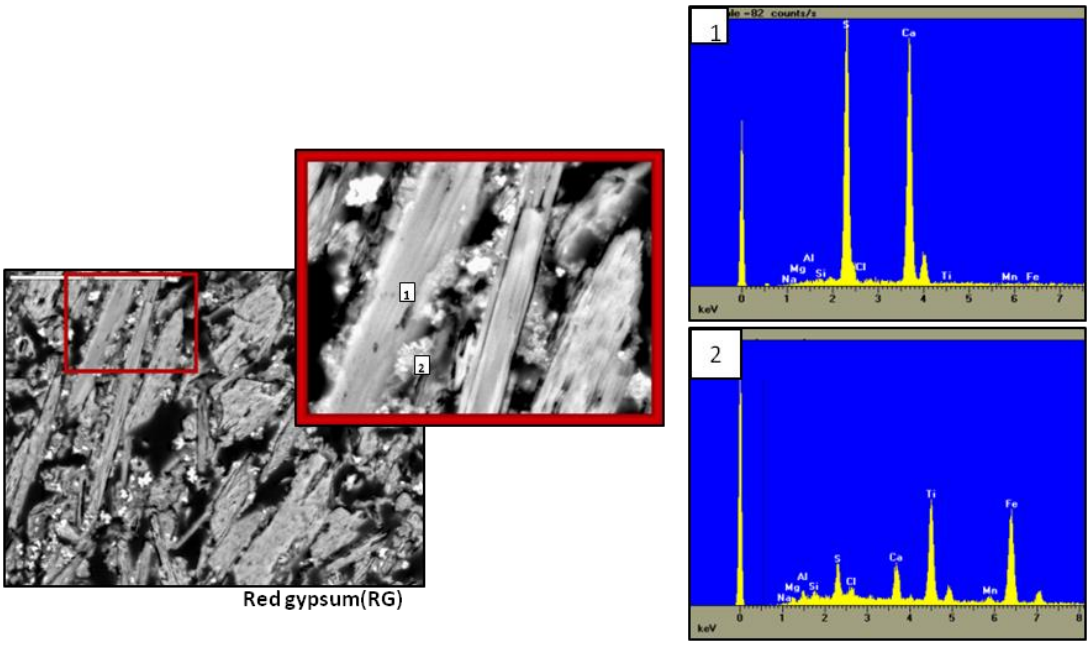

Figure 3.13. *SEM analysis of red gypsum sample and their corresponding X-ray spectra.*

Figure 3.14 shows SEM images of the C1 sample. It can be observed that the particles present a poorly developed rectangular or rhombohedral shape (point 1), which is characteristic of calcite ($CaCO_3$) (Myung Gyu et al., 2012). Further examination of the polished sample revealed two other phases: (a) a titanium-rich phase (point 2) and (b) an iron-rich phase (point 3). Both phases are in the presence of several metals, as in the RG (Fig. 3). Therefore, as indicated previously, we have demonstrated that the gypsum ($CaSO_4$) is the only compound that reacts during the carbonation process and, therefore, that the iron acts as a sequestering agent for trace elements in the formation of RG.

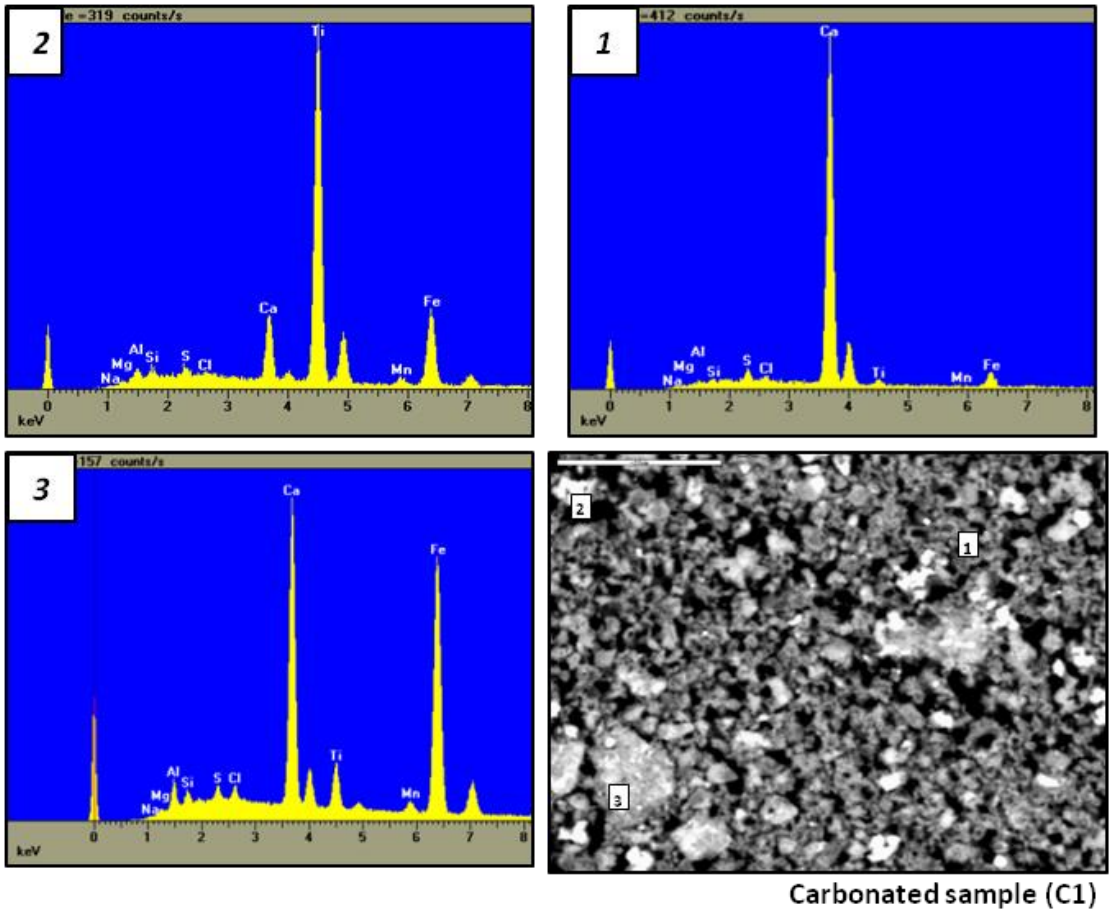

Figure 3.14. *SEM analysis of carbonated sample C1 and their corresponding X-ray spectra.*

Finally, the SEM image of the carbonated sample obtained by the ammonium route (C2) is shown in Figure 3.15. It can be observed that there is a portion of gypsum present in the sample (point 1), ratifying that a significant fraction of RG remains unreacted, as was concluded from the previous analysis (Figure 3.12 and Table 3.5). In addition, the C2 sample has similar phases to C1, that is, (a) iron- and titanium-rich phases (point 2) in the presence of several metals and (b) poorly developed rectangular or rhombohedral phases ($CaCO_3$) (point 3).

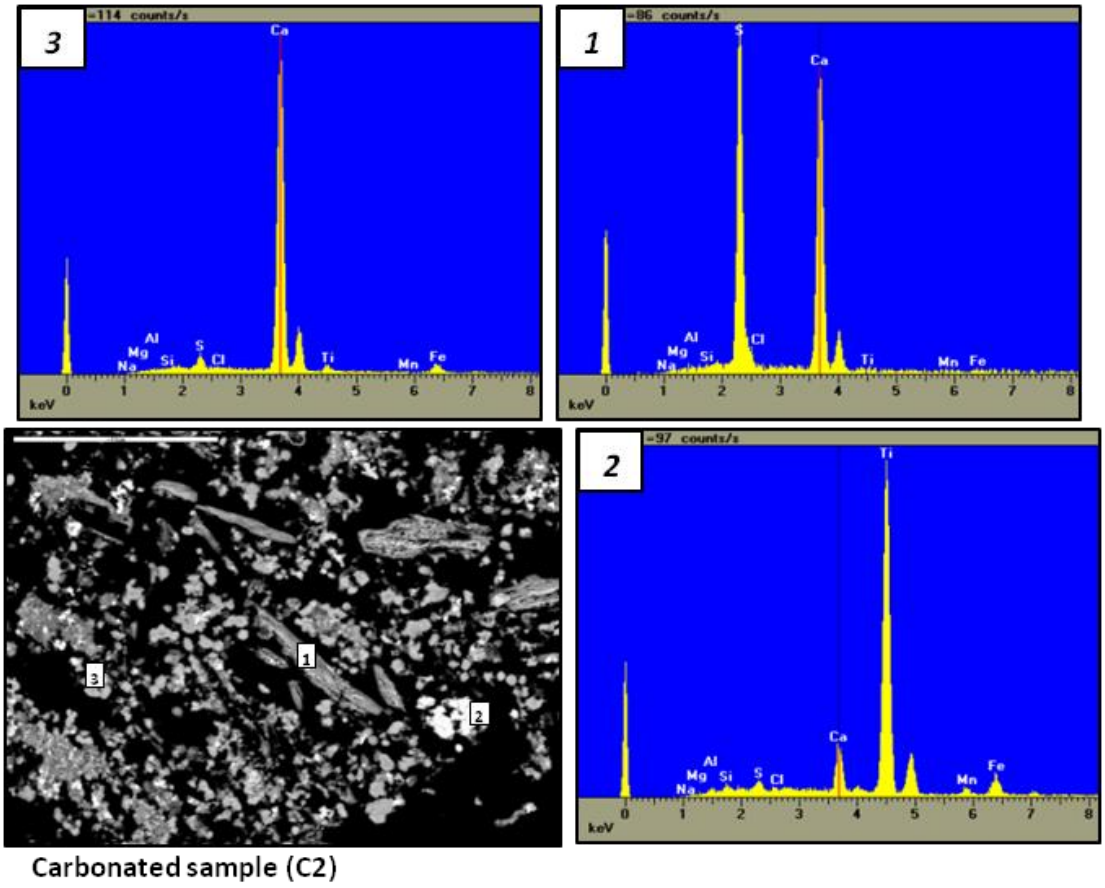

***Figure 3.15**. SEM analysis of carbonated sample C2 and their corresponding X-ray spectra.*

3.2.3.4. Radiological Characterisation

Previous studies (McNulty, 2007; Gázquez et al., 2011; Mantero et al., 2013) have demonstrated that the production of titanium dioxide is a NORM industry, because the raw material used in the industrial process, ilmenite, is enriched in natural radionuclides from both Th- and U-series radionuclides, with all of them in secular equilibrium. Therefore, radiological analysis of RG and its carbonation products is needed in order to determine their environmental implications.

Table 3.7 shows the activity concentrations of several natural radionuclides belonging to the uranium and thorium series, whose half-lives are longer than one month and, therefore, could be relevant from a radiological point of view. The activity concentrations for ^{40}K were calculated from the potassium content in the samples (Table 3.5), taking into account that 1% of K equals 320 Bq kg^{-1} of ^{40}K. In Table 3.7, it can be observed that the C1 and C2 samples contain moderate concentrations of natural radionuclides, with values similar to the RG. These samples (RG, C1 and C2) are only enriched in ^{232}Th, in relation

to an unperturbed soil, containing the studied samples around $2 \cdot 10^2$ Bq kg^{-1} of ^{232}Th. But, such contents are far from being able to consider C1 and C2 as NORM samples, because the concentration does not exceed the IAEA criterion of 1 Bq g^{-1} (IAEA, 2004). On the another hand, the ^{232}Th/^{230}Th activity ratio of the samples "C" is around 4, which is similar to that found in the feedstock for the production of titanium dioxide, ilmenite (Gázquez et al., 2011); this shows the similar behaviour of both radionuclides through the carbonation process, as they belong to the same chemical element (Th).

	^{210}Po	**^{230}Th**	**^{232}Th**	**^{234}U**	**^{238}U**	**^{226}Ra**	**^{40}K**
RG	27±1	32±2	138±4	18±1	16±1	14±2	19±6
C1	35±2 (82 ± 6)	50±2 (98±6)	208±5 (95±3)	26±2 (92±8)	24±1 (94±9)	25±3 (113±21)	26±6 (87±34)
S1	1.3±0.3 (3.9±0.8)	2.2±0.3 (5.8±0.8)	0.6±0.2 (0.3±0.1)	4.1±0.5 (18±3)	3.6±0.5 (18±3)	<1.5	6.4±6.4 (22±22)
C2	31±2 (79±6)	50±2 (108±7)	219±6 (109±5)	27±3 (104±12)	24±2 (104±13)	24±3 (119±22)	26±6 (95±37)
S2	1.1±0.2 (1.6±0.3)	1.5±0.3 (1.8±0.4)	0.6±0.2 (0.2±0.1)	5.3±0.6 (11±2)	4.7±0.6 (12±2)	<1.5	6.4±6.4 (24±24)

Table 3.7. *Summary of reported activity concentrations (Bq·kg^{-1} dry weight) of α -emitting radionuclides studied from RG, C1, S1, C2, S2; and the transfer factor (%) of α -emitting radionuclides in the experimental process*.

The concentrations of uranium and its descendants in the C samples are similar to typical undisturbed soils (20–30 Bq kg^{-1}) (UNSCEAR, 2000). In addition, the activity concentration of U and Th isotopes obtained in the second co-product "S" is about one order of magnitude lower than a typical soil. Taking into account that 1 mg kg^{-1} of U and Th corresponds to 12.33 Bq kg^{-1} of ^{238}U and 4.05 Bq kg^{-1} of ^{232}Th, the concentrations of the U and Th isotopes are consistent with those measured by ICP-MS.

Table 3.7 also shows (in brackets) the transfer factor of radionuclides in the carbonation process. It can be seen that the total content of radionuclides present in RG are transferred to the calcite samples (C) (between 80–100% of the initial activity remains in calcium carbonate). This means that the sodium sulphate (S) is practically free of alpha-emission radionuclides.

On the other hand, in order to determine the environmental implications arising from the use of the samples studied in the building field, the European legislation establishes a radioactive risk index (*I*). This index is defined as follow:

$$I = \frac{C(^{226}\mathrm{Ra})}{300} + \frac{C(^{232}\mathrm{Th})}{200} + \frac{C(^{40}\mathrm{K})}{300} \qquad \text{[Eq. 3.24]}$$

Where $C(^{226}\mathrm{Ra})$, $C(^{232}\mathrm{Th})$ and $C(^{40}\mathrm{K})$ are the activity concentrations for $^{226}\mathrm{Ra}$, $^{232}\mathrm{Th}$ and $^{40}\mathrm{K}$, respectively, in the building materials considered, expressed in Bq kg^{-1}. This index should not exceed 1 for any material used in bulk quantities, for example concrete, in order to ensure that the additional external dose received by occupants living in the buildings constructed with these materials do not exceed the reference value of 1 mSv $year^{-1}$ (Directive EURATOM, 2013).

Table 3.8 shows the radioactive risk index for the C1 and C2 samples. It can be seen that the results are slightly above the limit set by the European legislation (1 mSv $year^{-1}$) for materials used in large quantities in construction. But, this value is not conclusive, considering that, to use the product of carbonation as a building materials, it would require the addition of other materials (Matschei et al., 2007). Thus, the risk index would depend on the proportion of carbonated material added, causing the radiation dose to be much smaller than 1 mSv $year^{-1}$. Finally, the environmental radioactive impact of the activities performed by the S1 and S2 samples can be evaluated as negligible.

	^{226}Ra(*)	^{232}Th(*)	^{40}K(*)	i
C1	25±3	208±5	26±6	1.1±0.1
C2	24±3	219±6	26±6	1.2±0.1

Table 3.8. *Radioactive risk index (i) (mS a^{-1}) of samples C1 and C2.*
(*)The concentration is given in Bq·kg^{-1}.

3.2.3.5. CO2 Sequestration Efficiency

In order to evaluate the yield of the carbonation process developed in this work, TGA of the RG, C1 and C2 samples was carried out.

Figure 3.16 shows the thermogram of RG. We can see that the most significant thermal event takes place at 127.5°C, which is related to the loss of chemically bound water of hydration to calcium sulphate ($CaSO_4 \cdot 2H_2O$) (Kontogeorgos and Founti, 2012; Pérez-Moreno et al., 2013;). According to the variation in the mass measured, the mass loss in the sample is 16%, which corresponds, approximately, to the loss of the two water

molecules bound to the calcium sulphate (70%) of the RG, according to the chemical reaction:

$$CaSO_4 \cdot 2H_2O \rightarrow CaSO_4 + 2H_2O \quad \text{[Eq. 3.25]}$$

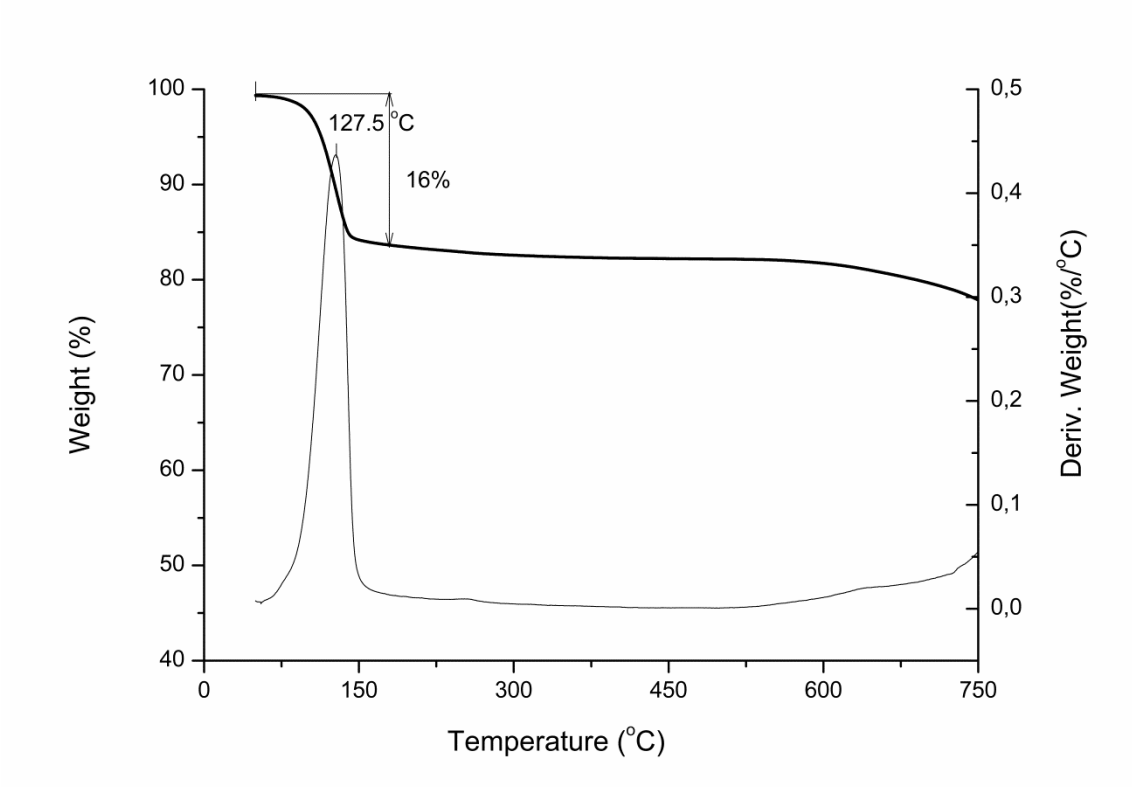

Figure 3.16. *TG and DTG of Red gypsum (RG).*

Figure 3.17 shows the thermal decomposition of the C1 and C2 samples. According to the results of XRD and XRF, they are composed mainly of calcium carbonate. It is known that the loss of $CaCO_3$ occurs in the temperature range 600–800 °C (Maciejewski, 2000; Sanders and Gallagher, 2002), because of the decomposition reaction of calcium carbonate as follows:

$$CaCO_3 \rightarrow CaO + CO_2 \quad \text{[Eq. 3.26]}$$

The TGA of C1 and C2 (Figure 3.17) confirms this. In Figure 3.17a, we can see that there is a single thermal event at 706.8°C, with a weight loss of 31.2%, which corresponds to the loss of a molecule of CO_2 from the calcium carbonate contained within the C1 sample.

Finally, Figure 3.17b shows the thermal decomposition of the C2 sample. Two thermal events were observed; the first at 114.3°C and the second at 714.5°C. The first peak (114.3°C) corresponds to the loss of the hydration water of RG (Figure 3.11), ratifying the result that a portion of RG remains unreacted in the calcite (Fig. 3.15). The second event, which takes place in the range 600–800°C, corresponds to the decomposition of calcium carbonate formed in the carbonation process (eq. 3.26). The weight loss observed (20%) (Figure 3.17) corresponds to the loss of a molecule of CO_2 from the calcium carbonate contained in the C2 sample.

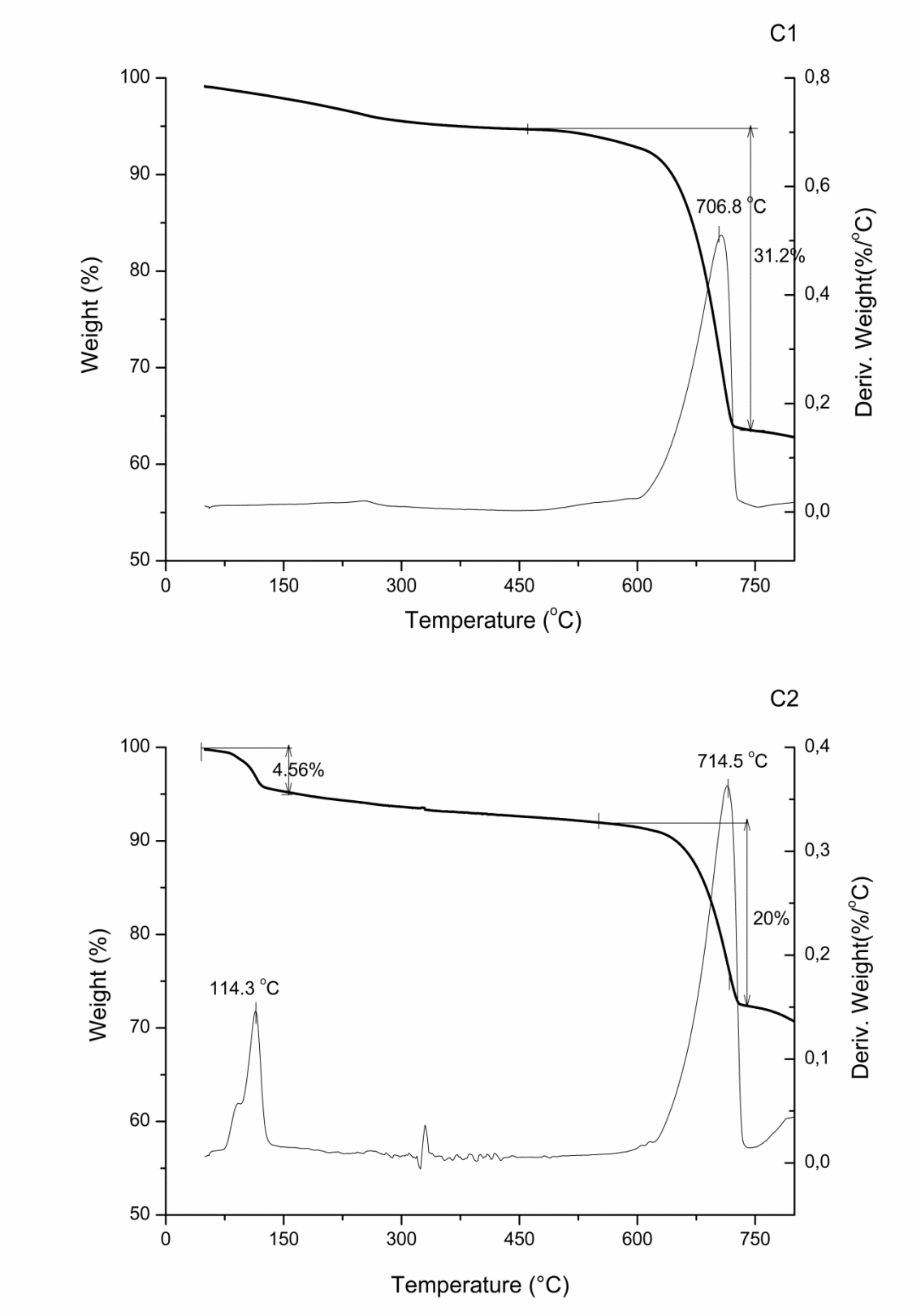

Figure 3.17*. TG and DTG of carbonation products. (a) C1. (b) C2.*

In this work, a CO_2 capture efficiency, for evaluating the degree of carbonation of the C1 and C2 samples, has been defined in order to evaluate the most suitable extracting agent. The carbonation efficiency (C_E) is defined as the ratio between the amount of carbonate formed in the carbonation process (X_{exp}) and the theoretical amount of carbonate (X_{theo}), which could be formed from the total Ca contained in the RG. Generally, the capture efficiency is expressed as follows:

$$C_E\,(\%) = \left(\frac{X_{exp}}{X_{theo}}\right) \times 100 \qquad \text{[Eq. 3.27]}$$

The XRF results of RG were used to determine the theoretical amount of XCO_3 formed ($CaCO_3$ or $MgCO_3$), which depends on the concentration of calcium and magnesium (Ca, Mg) contained in the sample. Considering the low magnesium concentration in the RG sample (approximately 0.77% of MgO, see Table 3.5), it is considered that all of the carbonate formed is present as calcium carbonate ($CaCO_3$). In order to determine the $CaCO_3$ formed, the TGA results of the C1 and C2 samples were used, as the amount of $CaCO_3$ formed in the carbonation process is a function of weight loss, corresponding to one molecule of CO_2, according to the decomposition reaction (eq. 3.26). In the majority of published works related to the carbonation processes, the process efficiency is only estimated. However, in our case, we can determine this value exactly, because we can obtain experimental data from TGA analysis (Table 3.9).

	%CaO (a)	**%CO_2** (b)	**%$CaCO_3$** (c)	**Experimental mass** (d)	**$CaCO_3$** (e)	**C_E (%)**
RG	28±2	-	50±4 (*)	50±2	25±2 (*)	-
C1	-	31±2	71±4	32±1	23±1	92±6
C2	-	20±1	46±2	35±1	16±1	64±5

***Table 3.9**. The carbonation efficiency (C_E) in different experiments. (a) Percent of CaO in red gypsum from XRF results. (b) Percent of CO_2 in C1 and C2 (product of carbonation process) from TGA results. (c) Percent of $CaCO_3$ calculated from %CaO or % CO_2 data. (*) Data of theoretical $CaCO_3$ formed from red gypsum.(d) Mass (g) of samples in the experiment. (e) Mass (g) of $CaCO_3$ calculated in the samples from experimental data.*

Table 3.9 shows the carbonation efficiency for C1 and C2. It can be seen that the capture efficiency is greater for the C1 sample, reaching approximately 92%. The low efficiency in the C2 sample is probably due to the ammonium hydroxide, which is a weak base and does not dissociate completely, thus producing an insufficient concentration of hydroxyl ions to react with the whole sample, causing a decrease in the carbonation efficiency. This problem could be solved in two ways. Firstly, a reduction of pH value could improve the solubility of ammonium, because it is known that its solubility in water is increased with decreasing pH (let us not forget that the pH of RG in solution is around 8). Secondly, a decrease in the temperature of carbonation (currently 75°C) could also improve the efficiency, because this is also a favourable factor for increasing the solubility (ATSDR, 2004).

3.2.4. CONCLUSIONS

This study was carried out to evaluate the use of RG as a CO_2 capture agent, owing to its high content of Ca. This is a fundamental property of the waste, in order to form calcium carbonate, which is currently the most stable form of CO_2 storage. This work intends to provide solutions to two environmental problems: firstly, to consider a possible commercial application for RG, and secondly, to mitigate the CO_2 emissions to the atmosphere.

In order to study this application, two extracting agents (NaOH and NH_4OH) were evaluated. In addition, the behaviour of radionuclides as well as the traces and major element contents in the carbonation process (C and S) were analysed in order to assess the environmental implications associated with the commercial use of the obtained products.

According to the results, the composition of the carbonation product is primarily $CaCO_3$ and, depending on the extraction agent used, the co-product is sodium sulphate or ammonium sulphate, as expected. Furthermore, the results show that the contaminants are transferred almost completely into the carbonate fraction, whereas the sulphate fraction is very clean in relation to pollutants initially contained in the RG. In this sense, we can ensure that the environmental implications associated with the use of $CaCO_3$ as construction materials are negligible.

The carbonation efficiencies obtained indicate that the best extracting agent is NaOH under experimental conditions at room temperature and pressure. Although the conversion in the carbonation process using NH_4OH as the calcium extraction agent is lower than using NaOH, the use of this agent may be attractive from an environmental standpoint. There are many effluents from sewage treatment plants that are high in ammonia, which could be reused in this type of process, preventing liquid discharge into the environment. Therefore, improving the carbonation using NH_4OH may be subject to future research.

Acknowledgements

This work was supported by the Government of Andalusia through a research project "Characterisation and modelling of the phosphogypsum stacks from Huelva for their environmental management and control" (Ref.: P10-RNM6300). It was also partially supported by the National Institution of Higher Education, Science, Technology and Innovation of the Republic of Ecuador (SENESCYT for its acronym in Spanish) as part of the Prometeo Project.

3.3. DIAGNOSE FOR VALORISATION OF REPROCESSED SLAG CLEANING FURNACE FLUE DUST FROM COPPER SMELTING

S.M Pérez-Moreno[1], M.J. Gázquez[2], G. Ríos[3], I. Ruiz-Oria[3] and J.P. Bolívar[1]*

[1]Department of Applied Physics, University of Huelva, Huelva, Spain

[2]Department of Applied Physics, University of Cádiz, Cádiz, Spain.

[3] R&D Department, Atlantic Copper S.L.U, Huelva, Spain.

Submitted to Journal of cleaner Production (Under Review)

Abstract

Slag cleaning furnace flue dust is generated in the cleansing of copper slag and their reprocessing produces wastes considered hazardous materials. Due to their high metals content their disposal not offers any economic either environmental benefit. In view of this fact, the main objective was to gain basic information for the reuse of these wastes in different fields. So, an exhaustive characterization of two wastes have been carry out in order to determine their composition, mineral phases, particle size distribution and leaching capacity of contaminants, as an indispensable preliminary step to choose the best available technology to recover the metals. The results show that both wastes are an important secondary resource of Zn and Pb and pyrometallurgy and hydrometallurgy appears to be attractive options for the management of these hazardous materials.

Keywords: *Slag Cleaning Furnace, Zinc recovery, Waste characterization, Copper smelting, Valorisation.*

3.3.1. INTRODUCTION

The global demand for copper is in continues expansion, around 18.6 million tonnes of copper were reached in 2015 by smelter (ICSG, 2016). And therefore, their production is accompanied of a large amount of dust/sludge, slag and wastewater which represent a great risk to environment and human health (Dudka and Adriano, 1997; USC, 1988; Newhook, et al., 2003; Csavina et al., 2014). This trend seems will be unchanged in the following years.

Atlantic Copper, located in Huelva (Spain), is one of the largest producers in Europe, which produce more than 285.000 tons (per year) of cathodic copper as main product. The pyrometallurgical process involved also generate by-products such as iron silicates or slag (~670.000 tons/year) between others, which is widely marketed in civil engineering (Raposeiras et al., 2016; Prasad and Ramana, 2016). The commercial slag is produced in the slag cleaning furnace (SCF), where under high temperature (1250 °C) and reducing atmosphere its remaining copper content (5%, approximately) decrease (below to 1 %), and flue dust, mainly enriched of Zn and Pb among other metals, is formed (Schlesinger, 2011; Seetharaman, 2014). After treatment of the off gases through a scrubbing with water system, about 2500 tons per year of filtered cake is obtained (SWC) (Rios et al., 2012). The Zn, Pb-rich waste, containing about 60% water, is classified as hazardous material according to the Waste European Directive (Waste Framework Directive, 2008). Currently, the waste is disposal in a controlled landfill, located about 70 km from the factory. However, this simple solution not offers any benefit to the environment either the smelter. Its management implies high cost of transport and storage, as well as a potential contamination source for soil, water, plant, animals and humans.

The literature widely reports that wastes with high Zn and Pb content can be reprocessed to recover these metals, mainly through two options: pyrometallurgy (Suetens et al., 2014; Issa et al., 2016; Lin et al., 2017) or hydrometallurgy (Jha et al., 2001; Shengo et al., 2013; Raza et al., 2016). The incorporation of these wastes into other products, such us construction materials, is also considered as a safe alternative for their final destination (Maslehuddin et al., 2011; Stathopoulos et al, 2013; Ledesma et al., 2017). However, the operational practice methods are rather complex and widely depend on the chemical composition and other physical and mineral features of the waste (Walburga Keglevich de Buzin, et al., 2017). Due to this fact, the smelter suggests new treatment strategies, among which stand out the following: a) reducing the quantity of the waste generated of this stream; and b) recovery of marketable metals.

According to the first plan, a new technology is now being studied which consists of flue-gas desulphurisation in a ceramic sleeve filter (CF) using micronized calcium hydroxide. This operation is based on the adsorption of gas pollutants onto fine-grained solid particles of $Ca(OH)_2$, which is introduced in the gas stream and is finally collected onto the filter. As novelty, a pilot plant has been installed in the factory for this purpose. The

new treatment, which reduce the water consumption, gives lower volume of final dry solid waste (CFD) produced. The second strategy requires an exhaustive physic, chemical and mineralogical characterization of the waste generated in order to stablish and develop the appropriated treatment for metals recovery in view of the potential economic and environmental benefits.

By considering these facts, the central aim of this research was to diagnoses the best available techniques for the metal recovery from the two wastes produced (SWC and CFD) base on their extensive characterization.

3.3.2. MATERIALS AND METHODS

3.3.2.1. Materials

The samples used in this study, SWC and CFD, were collected from Atlantic Copper, the copper smelting plant in Huelva, south-western Spain. Five sampling campaigns were organised over a period of one month in October 2015. After collection, the samples were dried at 60°C until a constant weight was reached.

3.3.2.2. Methods for physical and chemical characterisation

3.3.2.2.1. Granulometry

The particle size range of the samples was determined using a modular analyser, the Mastersizer 2000, with He-Ne laser diffraction technology at a wavelength of 632.8 nm. A representative amount of each sample was placed in water and subjected to ultrasound for 10 min, followed by magnetic stirring for approximately 30 min.

3.3.2.2.2. Mineralogy

X-ray diffraction analysis was performed using a PanalyticalX'Pert Pro diffractometer, equipped with a Cu X-ray source and an X'celerator detector, operating under the following conditions: voltage 40 kV; current 40 mA; range 5–70 deg 2θ; step size 0.017 deg 2θ; time per step 50.165 sec; divergence slit fixed, angle 0.5°. The crystalline mineral phases were identified using an X'PertHighScore Plus with the PDF-4 Minerals 2013 ICDD database. The quantities of the crystalline minerals were determined using the Rietveld method. Corundum was used as an internal standard to determine the amount of amorphous material.

3.3.2.2.3. Chemical analysis

The major elements were measured using an X-ray fluorescence Panalytical spectrometer (AXIOS model) with an Rh tube and two detectors (scintillation and flow). Prior to the analysis, the samples were prepared as pressed tablets of 40 mm diameter and 25 mm thickness.

The trace elements were analysed using two measurement techniques: ICP-MS (Perkin Elmer Sciex ELAN 9000), and ICP-OES (Varian 735ES). Prior to analysis, samples were digested by combining four acids (hydrochloric, nitric, perchloric and hydrofluoric) and some aliquots were dissolved by fusion with sodium peroxide.

3.3.2.2.4. Thermogravimetric analysis

In the thermal gravimetric analysis and differential thermal analysis a TG-851E 11 SDTA Mettler thermobalance was employed, coupled to a Pffeifer Thermostar mass spectrometer. The operating conditions used were 25^{o}C–1000^{o}C with a heating rate of 10^{o}C min^{-1} and an inert atmosphere of N_2 with a flow of 50 ml min^{-1}.

3.3.2.2.5. Scanning electron microscopy

The morphology and microstructure of the samples were studied using an environmental scanning electron microscope (QUANTA Fei-200). This equipment also enabled a multi-elemental semi-quantitative analysis using energy dispersive spectroscopy (EDS). Following this, a mineralogy database (Webmineral, 2016) was used to determine the mineralogical composition.

The spatial distribution of several elements was obtained using a scanning electron microprobe (EPMA) JEOL JXA-8200 model with four wavelength-dispersive X-ray spectrometers and energy-dispersive X-ray spectrometers (EDS).

3.3.2.2.6. Leaching test

Two leaching tests were applied: the toxicity characteristic leaching procedure (TCLP) from USEPA (TCLP, 1992) and the UNE-EN 12457-4 test (2003) from Directive 1999/31/CE.

USEPA test method 1311 was adopted in this experiment. The extraction fluid used was 5.7 mL of glacial acetic acid diluted in water to a volume of 1 L. The pH of the extraction fluid measured with a calibrated pH meter was 2.88±0.05. A liquid/solid ratio of 20:1 and 16 h extraction time was used for the TCLP tests. The agitation apparatus, rotation speeds, extraction vessels and filtration devices were as recommended in the USEPA 1311 method.

The European Commission regulates disposal waste in landfill through Directive 1999/31/CE, and the waste acceptance criteria are established for each class of landfill in Directive UNE-EN 12457-4. The leaching tests set out in this CE Directive were adopted in our experiments. The extraction fluid used was distilled water at a liquid/solid ratio of 10 L/kg ± 2%. The agitation apparatus, rotation speeds, extraction vessels, filtration devices and extraction time (24 h) were as recommended in this Directive.

3.3.3. Results and discussion

3.3.3.1. Granulometry

The particle size distribution (% volume) obtained after granulometry analysis is summarised in Table 3.10. Both samples, SWC and EFD, are characterised by a high concentration of silt (62% in SWC and 73 % in EFD; 4–62 microns) and practically the same proportion of clay particles (14% and 18%, respectively). But, SWD shows higher quantity of sand (24%). Both grain size distribution is a well-defined multimodal distribution, in which the maximum volumes of particles are of 0.6, 7 and 60 microns diameter respectively (Fig. 3.18).

A multimodal distribution may arise from a process involving the breakup of large particles, multiple sources of particles or variable growth mechanisms in the system. There are few studies reporting on the particle formation in a furnace (Guézennec et al., 2005; Machado et al., 2006), where indicate that the dust particles covers a wide range of sizes, but two categories of particle were distinguished: large particles of a few dozen to a few thousand micrometres, and finer particles of lower than 20 μm. These particles distribution are in agreement with our results.

The particle size distribution is a parameter to take into account depending on the final destination of these wastes. In case of incorporation in construction materials, it is noticed that fine particles improve the mechanical properties of final product (Zhao et al., 2014; Braz de Abreu et al., 2017).

		SWC (%)		CFD (%)	
Size (µm)	**Type**	**Average concentration**	**Global**	**Average concentration**	**Global**
<4	Clay	14.1 ± 3.2	14.1 ± 3.2	18.1 ± 4.1	18.1 ± 4.1
4-8	Silt	17.1 ± 1.8	61.8 ± 3.8	26.6 ± 1.8	72.8 ± 3.6
8-16		15.6 ± 2.9		23.5 ± 2.9	
16-32		13.3 ± 1.2		12.8 ± 0.9	
32-62		15.8 ± 1.1		9.87 ± 0.78	
62-125	Sand	14.9 ± 2.1	24.1 ± 2.7	6.77 ± 1.81	9.05 ± 2.02
125-250		7.49 ± 1.67		2.07 ± 0.88	
250-500		1.62 ± 0.56		0.20 ± 0.04	
500-1000		0.08 ± 0.02		-	
1000-2000		-		-	

Table 3.10. *Average grain-size distribution (%V) of the studied samples. Standard uncertainty (1 σ) has been calculated as the standard deviation of the mean,* $\sigma = Sx/(n)^{1/2}$.

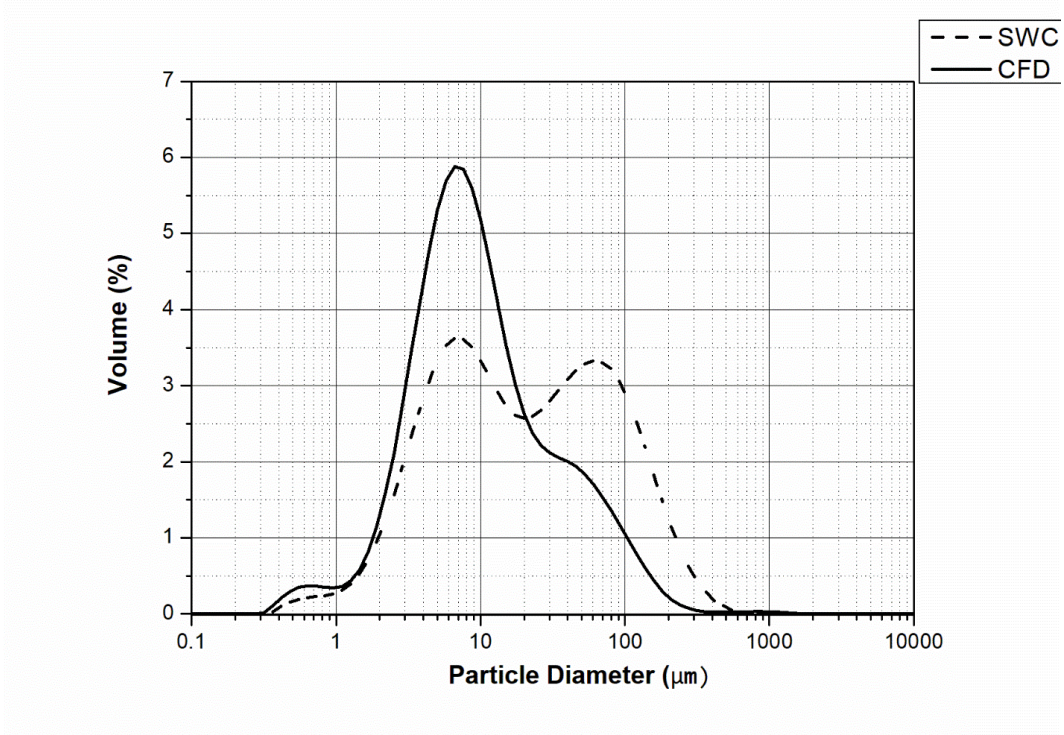

Figure 3.18. *Particle size distribution (%V) of samples.*

3.3.3.2. Elemental composition

The concentrations of the major and trace elements of the samples studied are shown in Table 3.11. The SWC contains Zn (41.4%), Fe (14.1 %) and Pb (7.12 %) as major elements. Also it has Cu (3.62%), As (2.79%) and Si (2.32%). Some trace element, such as Mn, Ni and In are found in concentration higher than 100 ppm, while Cr, Co, Zr, Sr and Se content is in range from 80 to 50 ppm respectively.

The CFD is characterised by its concentrations of Ca (23.2%) and Zn (22.3%). In addition, S (4.94%), Pb (4.45%), Fe (2.60%), Cu (1.75%), As (1.20%) and Si (0.99%) are present in the sample. Furthermore, Ba, Sr (> 100 ppm), Mn, Tl and In (50–80 ppm) are their main trace elements.

The concentrations of the majority of the elements in the SWC are almost twice those of the CFD. However, the main differences between both wastes is found in Fe, Ca and S concentrations, and can be explained given the following considerations:

- The sulphur content in the off-gases from the SFC is dissolved in the water that come from the scrubber system. For this reason, SWC obtained has a low concentration of sulphur. On the other hand, this wastewater along with the wastewater from the slag granulation, which high content of Fe, are depurated in a wastewater treatment plant. So, the iron is transferred to the SWC.

- The CFD is enriched of Ca due to new system used in the treatment of off-gases from SCF, using $Ca(OH)_2$.

On the other hand, the average estimated composition of undisturbed soil is compiled in Table 3.11 (Rudnick and Gao, 2003; Hu and Gao, 2008). Taking into account the composition of both waste, it is notable that most elements exceed the average concentrations for unperturbed soils. In practice, both Cd and Bi concentrations exceed the reference values by four orders of magnitude; As, Cu, Mo, Pb, Sb, Sn and Zn exceed by about three orders of magnitude. In addition, some trace elements exceeds the value stablished by about four orders of magnitude, such as Re; and Ag, In and Se, exceed by about three orders of magnitude.

Element	UNIT	DL	SWC	CFD	Undisturbed soil (*)
As	%	0.01	2.79 ± 0.63	1.20 ± 0.03	$(5.7 \pm 1.2)\cdot10^{-4}$
Bi	%	0.01	0.28 ± 0.01	0.17 ± 0.04	$(2.30 \pm 0.3)\cdot10^{-5}$
Ca	%	0.01	0.57 ± 0.11	23.2 ± 2.2	2.6 ± 0.1
Cd	%	0.01	0.24 ± 0.03	0.15 ± 0.01	$(0.6 \pm 0.2)\cdot10^{-5}$
Cl	%	0.01	0.11 ± 0.01	0.09 ± 0.01	$(3.7 \pm 3.8)\cdot10^{-2}$
Cu	%	0.01	3.62 ± 0.18	1.75 ± 0.14	$(2.7 \pm 0.2)\cdot10^{-3}$
Fe	%	0.01	14.1 ± 1.9	2.60 ± 0.19	3.9 ± 0.4
O	%	0.01	17.8 ± 1.0	25.4 ± 2.4	-
Na	%	0.01	0.26 ± 0.01	0.17 ± 0.01	2.42 ± 0.36
Pb	%	0.01	7.12 ± 1.89	4.45 ± 1.15	$(1.7 \pm 0.1)\cdot10^{-3}$
S	%	0.01	0.43 ± 0.07	4.94 ± 0.01	$(6.2 \pm 0.3)\ )\cdot10^{-2}$
Sb	%	0.01	0.53 ± 0.04	0.30 ± 0.02	$(7.5 \pm 1.1)\cdot10^{-5}$
Si	%	0.01	2.32 ± 0.36	0.99 ± 0.07	31 ± 1
Sn	%	0.01	0.15 ± 0.04	0.09 ± 0.04	$(2.2 \pm 0.2)\cdot10^{-4}$
Zn	%	0.01	41.4 ± 0.3	22.3 ± 4.6	$(7.5 \pm 0.9)\cdot10^{-3}$
LOI	%	-	7.35 ± 0.21	11.5 ± 1.2	-
Ag	ppm	0.05	34.8 ± 1.0	13.2 ± 1.4	0.053 ± 0.003
Ba	ppm	1.0	318 ± 19	160 ± 10	628 ± 83
Co	ppm	0.1	71.4 ± 3.8	30.6 ± 0.5	15 ± 1
Cr	ppm	0.5	76.3 ± 9.1	23.9 ± 7.8	74 ± 8
Ge	ppm	0.1	21.0 ± 10.2	12.9 ± 3.7	1.3 ± 0.1
In	ppm	0.1	120 ± 18	56.6 ± 3.8	0.066 ± 0.003
Li	ppm	0.5	2.74 ± 0.20	2.76 ± 0.07	41 ± 6
Mn	ppm	1.0	648 ± 52	74.0 ± 2.3	775 ± 78
Ni	ppm	0.5	138 ± 14	46.6 ± 3.0	34 ± 4
Re	ppm	0.001	2.03 ± 0.28	2.39 ± 0.42	0.0002
Se	ppm	0.1	55.9 ± 1.4	29.9 ± 1.2	0.09 ± 0.05
Sr	ppm	0.2	64.2 ± 15.2	114 ± 6	320 ± 46
Te	ppm	0.1	4.30 ± 0.41	1.73 ± 0.69	0.027 ± 0.003
Th	ppm	0.1	0.78 ± 0.08	0.36 ± 0.04	11 ± 1
Tl	ppm	0.05	31.2 ± 3.7	72.7 ± 3.9	0.53 ± 0.04
U	ppm	0.1	0.64 ± 0.17	1.53 ± 0.18	2.6 ± 0.1
V	ppm	1.0	13.3 ± 1.0	8.29 ± 0.97	106 ± 7
W	ppm	0.1	4.46 ± 1.83	2.55 ± 0.88	1.4 ± 0.1
Zr	ppm	1.0	68.0 ± 5.6	24.7 ± 1.5	193 ± 28

Table 3.11. *Concentration of major (%) and trace (ppm) element in samples. Standard uncertainty (1 σ) has been calculated as standard deviation of the mean as σ = Sx/(n)1/2. LOI = Loss on ignition. (*)Worldwide average concentrations taken from Rudnick and GaO (2003) and Hu and Gao (2008).*

3.3.3.3. Mineralogy

Both wastes contain zincite (ZnO) as principal mineral according to the diffraction pattern (Fig. 3.19). It is estimated that SWC has about 45 % and approximately 25% is found in CDF, according to their Zn content. But also willemite (Zn_2SiO_4), magnetite (Fe_3O_4) and goethite (FeOOH) are identified. The main differences between them is the presence of portlandite ($Ca(OH)_2$), calcite ($CaCO_3$) and anglesite ($PbSO_4$) in CFD.

The portlandite comes from the unreacted residual chemical agent employed in the neutralisation of the electric furnace gas stream ($Ca(OH)_2$), which is collected in the CF. Otherwise, the existence of forced air ventilation system helps the $Ca(OH)_2$ to react with the CO_2 in the air, producing calcite in the following reaction (Li et al., 2000):

$$Ca(OH)_2 + CO_2 \rightarrow CaCO_3 + H_2O \quad \text{[Eq. 3.28]}$$

The presence of anglesite is probably due to the reaction of SO_2 in the gases with condensing lead vapour (Balladares et al., 2014):

$$PbO + SO_2 + 1/2O_2 \rightarrow PbSO_4 \quad \text{[Eq. 3.29]}$$

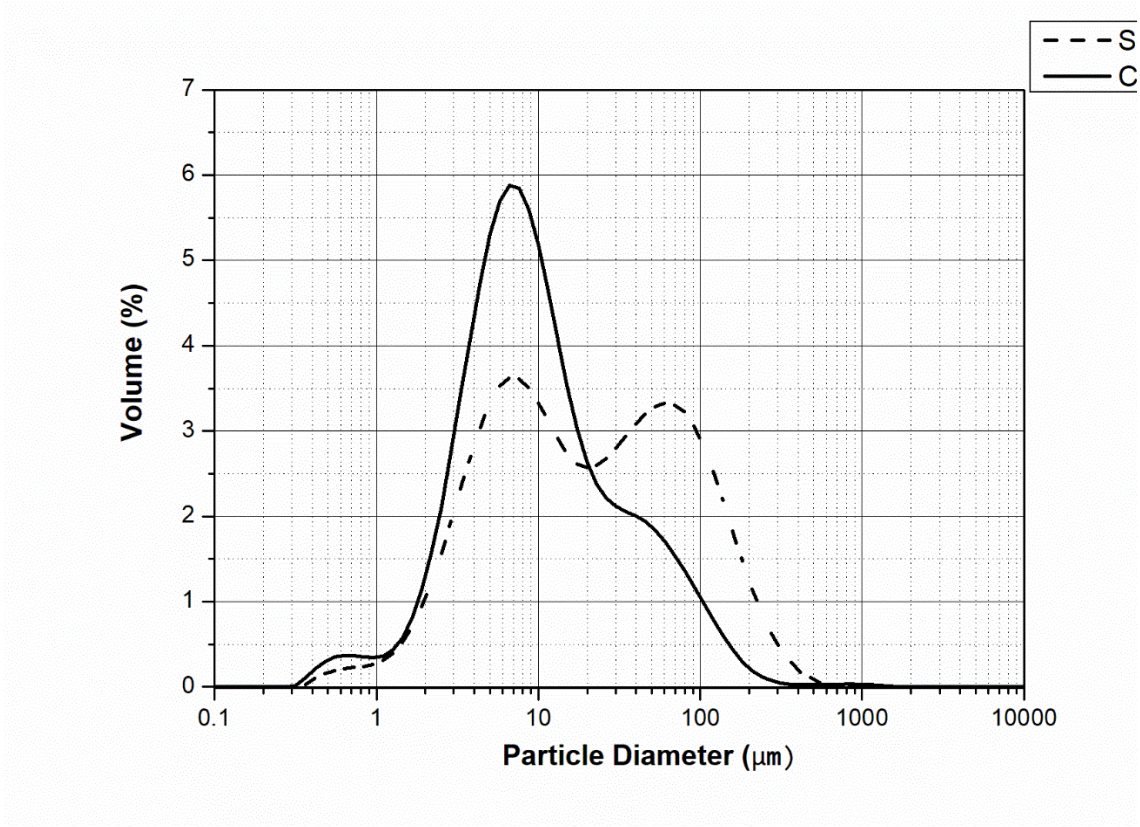

Figure 3.19. *X-ray diffraction (XRD) pattern of SWC and CFD. Mineral phases identified: Zincite – ZnO (Z), Willemite- Zn_2SiO_4 (W), Goethite – FeOOH (G), Magnetite- Fe_3O_4 (M), Portlandite – $Ca(OH)_2$ (P), Calcite- $CaCO_3$ (C) and Anglesite – $PbSO_4$ (A).*

3.3.3.4. Thermogravimetric analysis

The samples were subjected to TGA, and the released gases were analysed using ICP-MS. The results are shown in Figures 3.20 and 3.21.

The SWC presents five thermal events, which take place at temperatures of 134°C, 510°C, 600°C, 834°C, and above 900°C (Figure 3.20). Water is detected in the first event, and this water is likely to come from crystallised water bounded to some hydrated compound or even some hydroxides, which are difficult to identify. At 510°C, CO_2 is released, and probably the decomposition of lead carbonate takes place (Földvári, 2011). It is estimated that sample contains about 9% of $PbCO_3$, approximately in agreement with the Pb concentration measured using FRX analysis.

$$PbCO_3 \rightarrow PbO + CO_2 \quad \text{[Eq. 3.30]}$$

SO_2 is released in the third event at about 600°C, and this probably comes from the decomposition of iron (II) sulphate ($FeSO_4$) (Siriwardane et al., 1999). According to the proportion of mass loss, it is estimated that the sample contains less than 1% of this compound. However, the Fe contained in the sample is much higher, meaning that iron is joined with other elements, such as magnetite and goethite identified by DRX analysis.

$$FeSO_4 \rightarrow FeO + SO_3\ (SO_2 + 1/2\ O_2) \quad \text{[Eq. 3.31]}$$

Further loss of mass associated with the release of CO_2 occurs at 834°C. In this case, calcium carbonate ($CaCO_3$) is decomposed (L'vov, 2022); it has been calculated from the mass loss that the SWC contains around 3.5% of this substance.

$$CaCO_3 \rightarrow CaO + CO_2 \quad \text{[Eq. 3.32]}$$

The final thermal event takes place at a temperature of above 900°C; SO_2 gases are detected again, which are probably due to the decomposition of calcium sulphate (Földvári, 2011).

$$CaSO_4 \rightarrow CaO + SO_3 \quad \text{[Eq. 3.33]}$$

The DTA curve reveals that all events coming from the decomposition of chemical species contained in the CFD are endothermic.

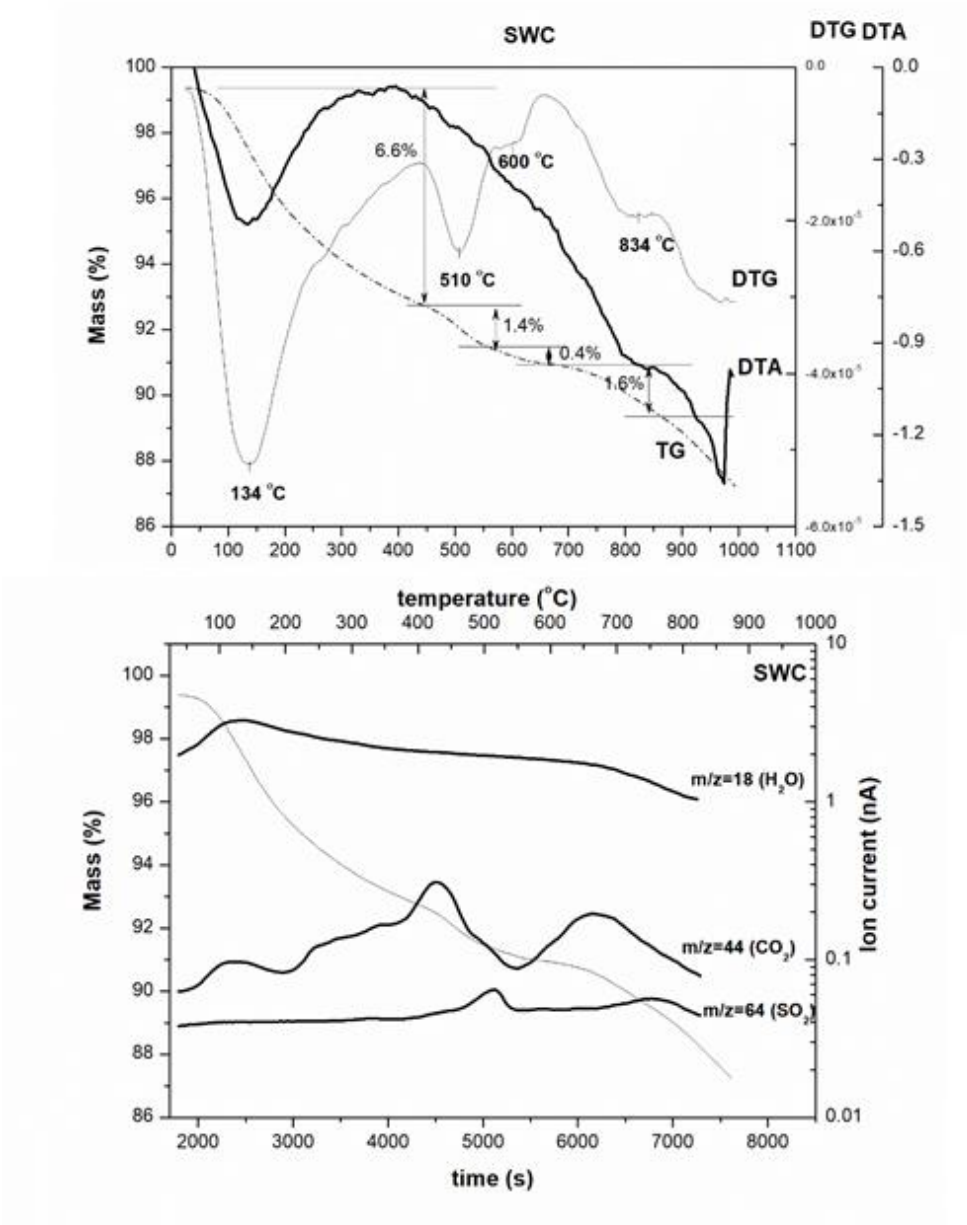

Figure 3.20. *TG-DTG-DTA curve and gases detected in the SWC.*

The CFD presents four thermal events at 132°C, 453°C, 703°C and above 900°C. As can be observed in Figure 3.21, water is released at 132°C and 453 °C. The first event is associated with the evaporation of crystallised water from a hydrated compound, and the second is due to the decomposition of hydroxides. In this case, calcium hydroxide decomposition takes place at this temperature (Gabrovšek et al., 2006). This chemical

species is added into the ceramic filter and a proportion remains unreacted. It was also identified using DRX analysis.

$$Ca(OH)_2 \rightarrow CaO + H_2O \qquad \text{[Eq. 3.34]}$$

CO_2 was detected at 703°C, and this is associated with calcium carbonate decomposition (L'vov, 2002). This is in agreement with the DRX analysis (Eq. 3.32). Taking into account the mass loss obtained in the TG curve, the concentration of both compounds in the sample can be calculated. The CFD contains 26% $Ca(OH)_2$ and 10% $CaCO_3$. However, the proportion of Ca is somewhat lower than that obtained by FRX, and another compound of calcium must therefore be present in the sample. Previous studies (Fernández et al., 1998; Chang et al., 2016) suggest that a fraction of the calcium added into the gas stream of the ceramic filter reacts with the SO_2 gases, generating calcium sulphate ($CaSO_4$), which is decomposed above 900°C (Eq. 3.33) (Földvári, 2011). It is estimated that the sample can contain about 17% of this compound that could be hydrated. The DTA curve reveals that all events coming from the decomposition of chemical species contained in the CFD are endothermic.

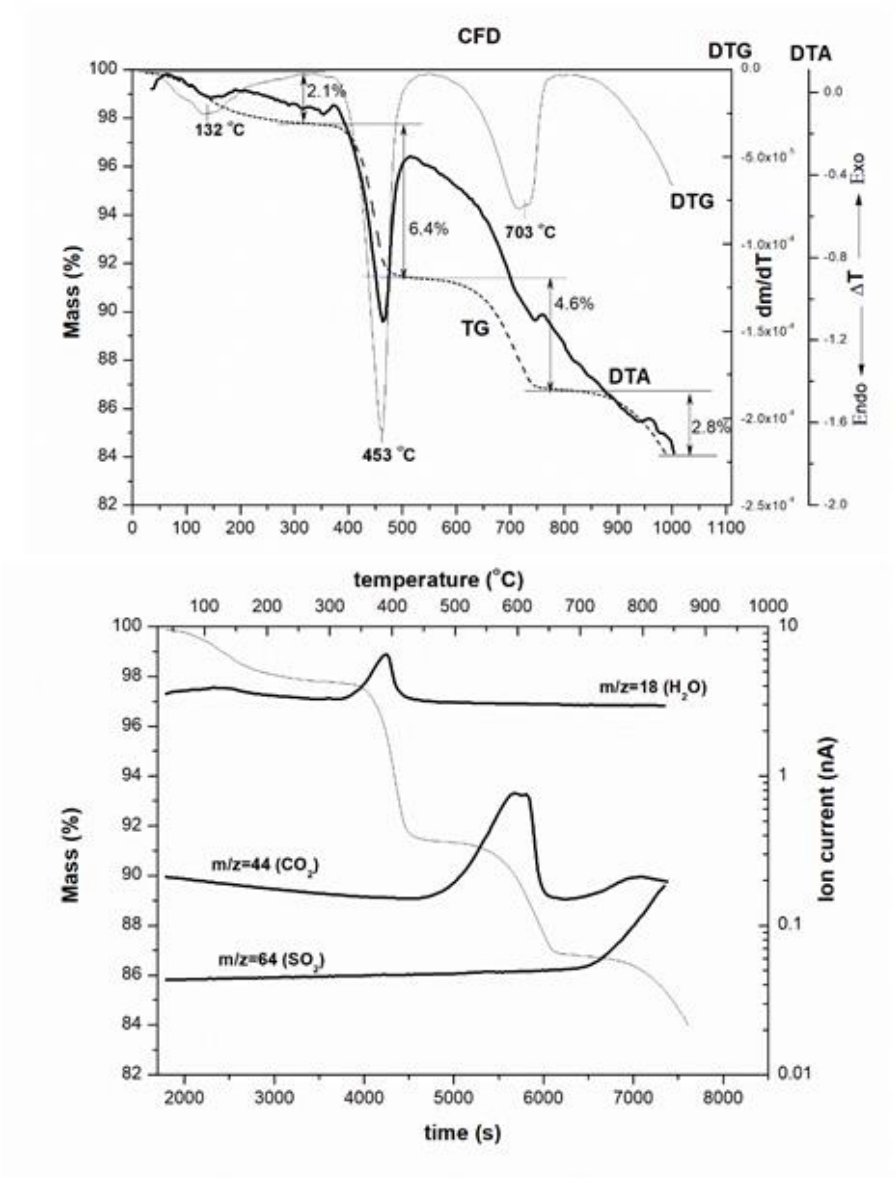

Figure 3.21. *TG-DTG-DTA curve and gases detected in the CFD*

3.3.3.5. Scanning electron microscopy

Figure 3.22 shows an agglomerated morphology for the SWC, with fine particles forming aggregates, although large particles are also present in the sample. This is in agreement with the granulometric analysis, which indicates two main particle distribution sizes. Based on this fact, it can be seen that the fine particles (point 2, Fig. 3.22) have high concentrations of Zn, Fe, Pb, Si, Cu, and As, which correspond to the main composition as measured using FRX analysis. Due to their amorphous morphology, it is impossible to differentiate the compounds that are present in the fine fraction. However, the large particles (point 1, Fig. 3.22) have high concentrations of Fe and Si according to the EDS spectra. Their composition and morphology, in form of smooth sheets, suggest that these

particles are iron silicate (fayalite, Fe_2SiO_4) (Fan et al., 2014; Potysz et al., 2016). The presence of these particles is justified due to the water stream from slag granulation, which is composed of fayalite (Fe_2SiO_4), this is also managed in the WTP, and where SWC is formed.

Fig. 3.23 shows a secondary electron image of an SWC region and the X-ray mapping for the elements S, Pb, Fe, As, Ca, Cu, Zn and Si present in the sample. This figure indicates that Pb, Fe, As, Cu, Zn and Si are uniformly distributed among the samples. Nevertheless, there are regions in which the presence of sulphur and calcium elements is coincident, confirming the existence of a $CaSO_4$ phase. At the same time, areas where iron and silicon are coincident can be observed, proving the existence of Fe_2SiO_4.

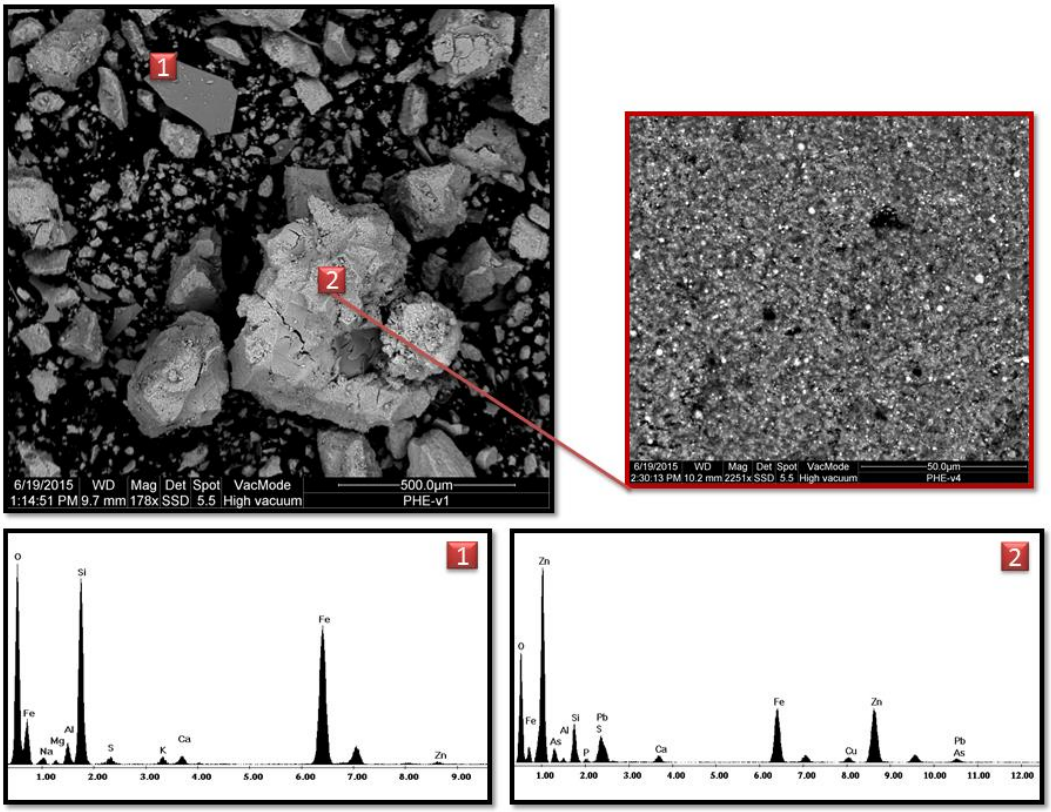

Figure 3.22. *Scanning electron micrograph of SWC particles*

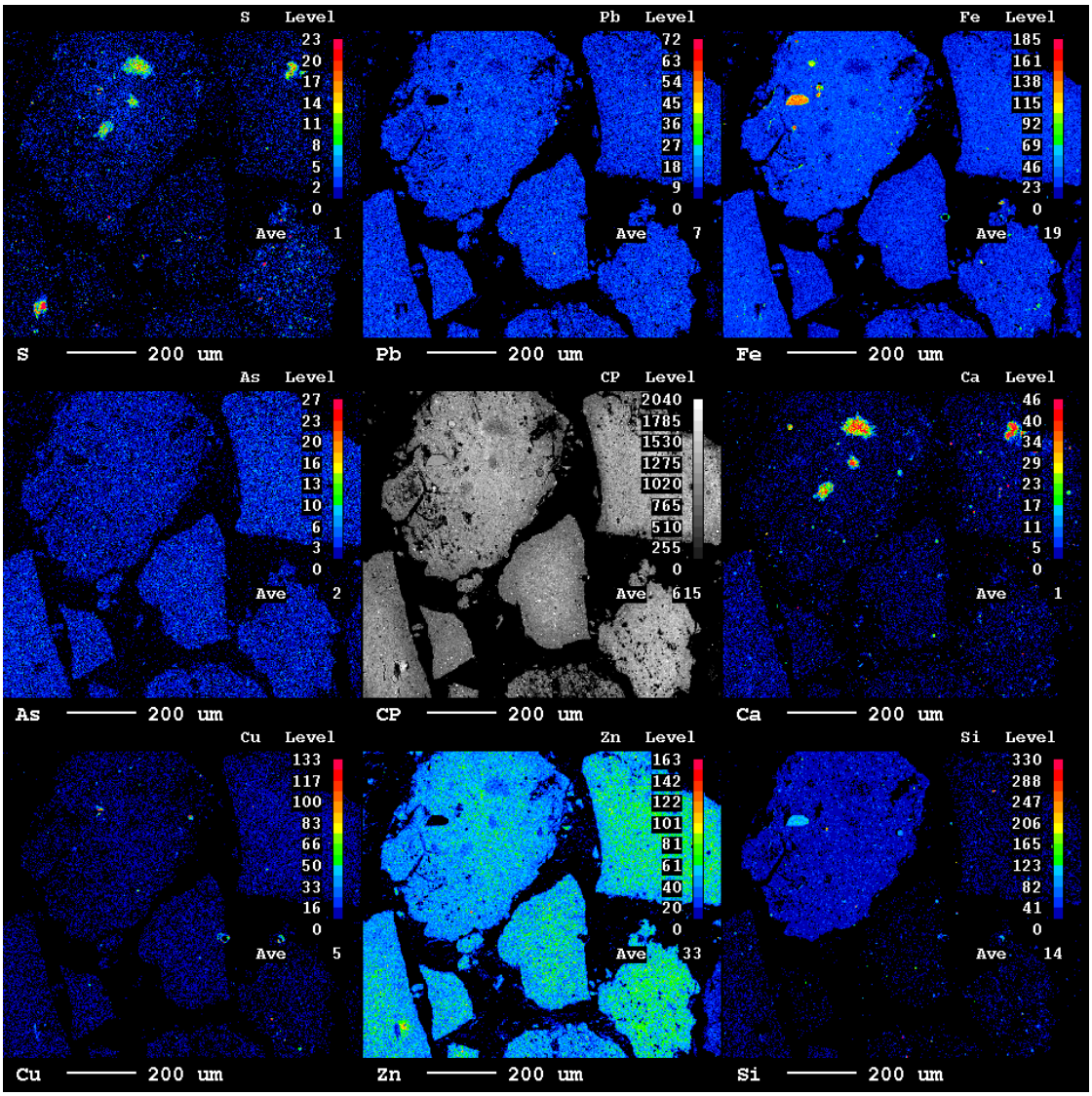

Figure 3.23. *Secondary electron image of the SWC region, and distribution of S, Pb, Fe, As, Ca, Cu, Zn and Si.*

A general distribution and morphology of CFD particles is shown in Fig. 3.24, where it can be seen that the sample is characterised by two kinds of particles: large particles; and very fine particles, fact in agreement with the laser grain-size analysis. According to the EDS results, the fine particles are composed of Zn, Ca, S, Pb, Si and Fe (point 4, Fig. 3.24), in agreement with the FRX results. These fine particles are characterised by their amorphous morphology, which makes the identification of compounds difficult. On the other hand, the large particles (point 3, Fig. 3.24) contain a high proportion of calcium based on the EDS results. These particles therefore correspond to calcium hydroxide ($Ca(OH)_2$), which is also identified using DRX and thermogravimetric analysis.

In this sense, a secondary electron image of the CFD region and X-ray mapping for several elements (S, Pb, Fe, As, Ca, Cu, Zn and Si) were carried out (Fig. 3.25). Pb, Fe, As, Cu, Zn and Si were distributed throughout the sample. However, there are regions in which the concentration of calcium is very high and others where the presence of sulphur and calcium are coincident, confirming that $Ca(OH)_2$ and $CaSO_4$are the main phases related to Ca.

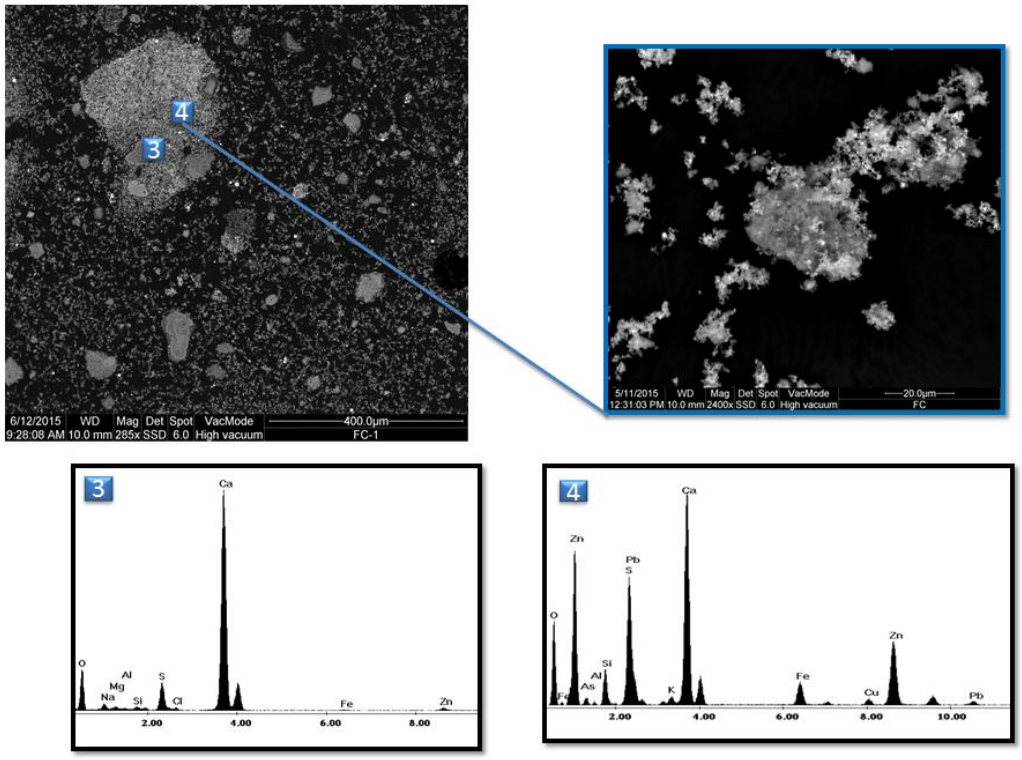

Figure 3.24. *Scanning electron micrograph of CFD particles*

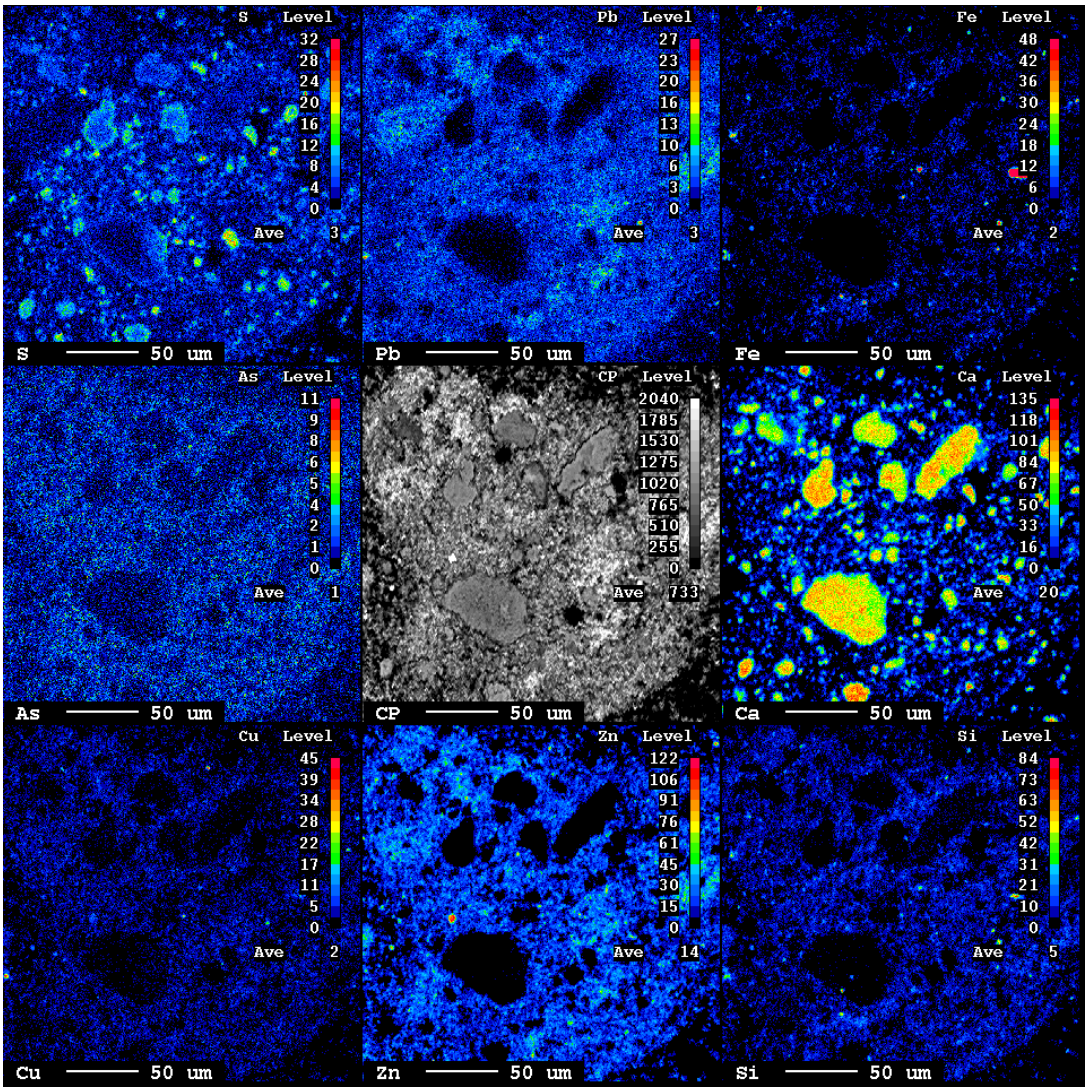

Figure 3.25. *Secondary electron image of CFD region and distribution of S, Pb, Fe, As, Ca, Cu, Zn and Si*

3.3.3.6. Lixiviation Test

The results of the TCLP tests and the limits of TCLP concentration for classification as hazardous waste are shown in Table 3.12. It can be observed that TCLP concentrations for Cd and Pb in the SWC are higher than the threshold (Cd: 1mg/L; Pb: 5mg/L); specifically, Cd exceeds the threshold value by 28 times and Pb by three times. However, the percentage of these elements leached is very low: less than 1.5% in case of Cd and less than 0.05% for Pb.

On the other hand, the CFD exceeds the established limits for Cd (Cd: 1mg/L) almost five times. Furthermore, the As and Pb values should be taken into account since these are

very close to the TCLP limit (As: 5mg/L; Pb: 5mg/L). In the same way, the percentage of each element leached is low.

On the other hand, the results of the UNE tests and the reference limit value for non-hazardous materials are shown in Table 3.13. It can be seen that the UNE test concentrations for As and Cd in the SWC are higher than the UNE limits (As: 2mg/kg; Cd: 1mg/kg); specifically, the As concentration exceeds the value given by two times, and the Cd concentration is slightly higher. It is notable that potassium, sodium and sulphur are highly leached (K = 50%; Na= 100% and S=80%); however, these are below the reference limit values.

The CFD exceeds the established limits for As (two times higher), Cd (slightly higher), Mo (two times higher), Pb (seven times higher), and Zn (1.5 times higher) (As: 2 mg/kg; Cd: 1mg/kg; Mo: 10mg/kg; Pb: 10mg/kg; Zn: 50mg/kg). In the same way, potassium, sodium and sulphur are highly leached (K = 100%; Na= 72% and S=14%), but do not exceed the reference limit values.

Both test results confirm that the wastes are susceptible to generating leachates with high concentrations of pollutants which could be harmful to human health and the environment.

Element	Detection Limit (mg/L)	C_{SWC} (mg/L)	η (%)	C_{CFD} (mg/L)	η (%)	Threshold Level (mg/L)
Ag	0.005	<LD	-	<LD	-	5.0
Al	0.1	<LD	-	<LD	0.02	-
As	0.03	0.43 ± 0.09	0.002 ± 0.001	3.9 ± 2.1	0.03 ± 0.02	5.0
Ba	0.02	<LD	-	<LD	-	100
Bi	0.02	<LD	-	<LD	-	-
Ca	0.1	148 ± 2	2.6 ± 0.5	1378 ± 256	0.59 ± 0.17	-
Cd	0.002	28 ± 4	1.15 ± 0.32	4.6 ± 1.9	0.31 ± 0.15	1.0
Co	0.002	0.17 ± 0.01	0.24 ± 0.03	0.03 ± 0.01	0.10 ± 0.04	-
Cr	0.02	<LD	-	<LD	-	5.0
Cu	0.002	20 ± 1	0.05 ± 0.01	18 ± 10	0.10 ± 0.07	-
Fe	0.01	0.35 ± 0.06	$(2.5 \pm 0.8)\cdot10^{-4}$	<LD	-	-
K	0.1	24 ± 5	2.4 ± 0.9	174 ± 61	3.6 ± 2.2	-
Mg	0.1	63 ± 4	2.2 ± 0.3	5.1 ± 1.6	0.32 ± 0.12	-
Mn	0.01	3.51 ± 0.12	0.54 ± 0.06	0.05 ± 0.02	0.06 ± 0.02	-
Mo	0.005	<LD	-	0.028 ± 0.16	0.03 ± 0.02	-
Na	0.1	173 ± 56	6.7 ± 2.4	39 ± 11	2.3 ± 0.8	-
Ni	0.005	<LD	-	LD	-	-
P	0.02	0.19 ± 0.07	0.008 ± 0.004	0.17 ± 0.08	0.03 ± 0.02	-
Pb	0.01	16 ± 1	0.02 ± 0.01	4.3 ± 0.80	0.01 ± 0.01	5.0
S	1	114 ± 3	2.7 ± 0.5	389 ± 34	0.79 ± 0.07	-
Sb	0.01	0.18 ± 0.03	0.003 ± 0.001	0.20 ± 0.07	0.01 ± 0.01	-
Se	0.02	<LD	-	<LD	-	1.0
Si	0.1	19.0 ± 1	0.08 ± 0.01	5.1 ± 2.1	0.05 ± 0.03	-
Sr	0.01	0.42 ± 0.04	0.66 ± 0.23	0.70 ± 0.23	0.62 ± 0.23	-
Te	0.01	0.09 ± 0.03	2.1 ± 1.0	<LD	-	-
Tl	0.01	0.29 ± 0.02	0.94 ± 0.17	0.52 ± 0.19	10.72 ± 0.31	-
U	0.05	<LD	-	LD	-	-
Zn	0.005	2340 ± 27	0.57 ± 0.01	553 ± 217	0.24 ± 0.15	-

Table 3.12. *Results of the TCLP tests on the samples (USEPA method 1311). C = element concentration in the leaching liquid;* ***η****= transfer coefficient = fraction of the problem element in the solid transferred into the extracting liquid*

Element	Detection Limit (mg/L)	C_{SWC} (mg/L)	η (%)	C_{CFD} (mg/L)	η (%)	Threshold Level (mg/L)
Al	0.1	<LD	-	<LD	-	-
As	0.03	3.9 ± 2.1	0.01 ± 0.01	2.0 ± 0.4	0.016 ± 0.003	2
Ba	0.02	0.40 ± 0.04	0.13 ± 0.02	<LD	-	100
Ca	0.1	1380 ± 500	24 ± 10	14700 ± 700	6.3 ± 0.7	-
Cd	0.002	1.04 ± 0.68	0.04 ± 0.02	1.35 ± 0.07	0.09 ± 0.01	1
Co	0.002	<LD	-	<LD	-	-
Cr	0.02	<LD	-	<LD	-	10
Cu	0.002	35 ± 22	0.10 ± 0.06	6.6 ± 0.3	0.037 ± 0.003	50
Fe	0.01	1.93 ± 1.89	0.001 ± 0.001	1.6 ± 0.3	0.006 ± 0.001	-
K	0.1	502 ± 146	50 ± 17	5450 ± 270	114 ± 29	-
Mg	0.1	560 ± 197	19 ± 7	<LD	-	-
Mn	0.01	0.35 ± 0.05	0.05 ± 0.01	<LD	-	-
Mo	0.005	2.7 ± 0.6	0.16 ± 0.04	18 ± 1	1.8 ± 0.2	10
Na	0.1	3382 ± 1300	130 ± 49	1220 ± 60	72 ± 6	-
Ni	0.005	3.3 ± 2.2	2.4 ± 1.6	<LD	-	10
P	0.02	1.7 ± 0.3	0.07 ± 0.01	0.6 ± 0.6	0.09 ± 0.09	-
Pb	0.01	1.8 ± 1.1	0.002 ± 0.001	68 ± 3	0.15 ± 0.04	10
S	1	3458 ± 1353	80 ± 34	6780 ± 339	14 ± 1	20000
Sb	0.01	0.40 ± 0.17	0.007 ± 0.003	<LD	-	0.7
Se	0.02	<LD	-	<LD	-	0.5
Si	0.1	22 ± 6	0.09 ± 0.03	<LD	-	-
Sr	0.01	3.7 ± 1.1	5.7 ± 2.1	2.9 ± 0.6	2.5 ± 0.5	-
Te	0.01	<LD	-	<LD	-	-
Tl	0.01	2.4 ± 0.7	7.8 ± 2.3	11.6 ± 5.8	16 ± 8	-
U	0.05	<LD	-	<LD	-	-
Zn	0.005	24 ± 16	0.006 ± 0.004	78 ± 4	0.04 ± 0.01	50

Table 3.13.*Results of the UNE tests on the samples (UNE-12457-4).* ***C*** *= element concentration in the leaching liquid;* ***η****= transfer coefficient = fraction of the problem element in the solid transferred into the extracting liquid.*

3.3.4. Diagnose for their valorisation

Considering the characterization of these wastes and the literature consulted, two possibilities could arises for the recovery of the Zn and Pb: pyrometallurgy, and hydrometallurgy.

The principle of pyrometallurgical processes is to recover Zn and Pb, based on carbothermic reduction at 1200 °C ($ZnO/PbO\ (s) + CO_{(g)} \rightarrow Zn_{(g)}/Pb_{(g)} + CO_{2(g)}$), and later reoxidation of the vapour produced ($Zn_{(g)}/Pb_{(g)} + ½\ O_{2(g)} \rightarrow ZnO_{(s)}/PbO_{(g)}$). The final products from this process are the so called Waelz Oxide (Morcali et al., 2012: Suetens et al., 2014), a zinc and lead rich product that can be sold, and an iron slag ($Fe_2O_{3(s)} + 3\ CO_{(g)} \rightarrow Fe_{(s)} + 3CO_{3(g)}$) called the Waelz slag, which can be used as in civil engineering (Quijorna et al., 2012, 2014).

The hydrometallurgical process consists on selective leaching of metals using chemical agents in certain conditions. In the process there is a significant influence of mineral species bearing Zn, zincite being the most favourable because ZnO is easily dissolved both at acidic (sulphuric acid) and basic solutions (ammoniacal solutions) (Kukurugya et al., 2015; Miki et al, 2016). At the same time the low particle size favours the Zn leaching. Hydrometallurgical process has the possibly to recover also Pb, mainly as sulphate, and consequently can generate an iron oxide residue having a lower content in metal contamination, which their application appears to have no limitations from environmental point of view (Skaf et al., 2017).

The wastes have good characteristics for a successful recovery of metals in both pyrometallurgy and hydrometallurgy. But certain conditions should be taking into account in order to select the most suitable method.

The pyrometallurgical process:

- It is required high energy consumption.
- It is needed a great investment and equipment maintenance.
- The mineral species in which metals are present is of not great importance.

The hydrometallurgical process:

- It is considered more environmentally suitable and economical to treat low zinc containing materials.
- It is significantly influenced by mineral species in which metals are bearing.
- The products contain high moisture that needs to be reduced.

3.3.5. CONCLUSIONS

The characterization of two wastes, SWD and CFD, generated in the reprocessed of slag cleaning furnace flue dust from copper smelting have been performed as an essential step towards finding applications or treatments for these wastes.

Both waste contain very fine particles size and are mainly enriched of Zn, Pb and Fe. Zincite (ZnO) is the major mineral phase in which Zn is presented in both wastes. Pb is found as carbonate ($PbCO_3$) in SWD while sulphate ($PbSO_4$) is detected in CFD. On the other hand, iron oxides and hydroxides (Fe_3O_4 and FeOOH) are existed in the two wastes. The CFD also contain high concentration of Ca that is in form of $Ca(OH)_2$, $CaCO_3$ and $CaSO_4$. They are considered hazardous materials because they are susceptible to generating leachates with high concentrations of metals.

Both wastes are an important secondary resource of Zn and Pb and their reprocessing has both remarkable economic and environmental benefits in contrast with their disposal or incorporation into other products. Pyrometallurgical and hydrometallurgical process appears to be attractive options for the management of these hazardous wastes. But, more future research is needed to establish the best method according to the requirements of the smelter.

Acknowledgments

This research has been supported by Atlantic Copper company project “Characterization of wastes from copper smelting and evaluation of potential applications”.

3.4. VALIDATION OF THE BCR SEQUENTIAL EXTRACTION PROCEDURE FOR NATURAL RADIONUCLIDES

S.M Pérez-Moreno[1], M.J. Gázquez[2], R. Pérez-López[3], J.P. Bolivar[1]

[1]Department of Integrated Science Physics, University of Huelva, Huelva, Spain.
[2]Department of Applied Physics, University of Cádiz, Cádiz, Spain.
[3]Department of Earth Sciences, University of Huelva, Huelva, Spain

Submitted to Chemosphere Journal (Under Review)

ABSTRACT

Determining the availability of natural radionuclides in environmental conditions is increasingly important in order to evaluate their toxicity. A validated procedure is necessary to ensure the comparability and accuracy of the results obtained by different laboratories. For that, an optimised BCR sequential extraction procedure has been applied to the certified reference material (CRM), coded as BCR-701, and their resulting liquid and solid fractions were subjected to an exhaustive chemical and radioactivity characterisation. In this sense, several material characterisation techniques were used for chemical, mineralogical, and radioactive characterisation, in order to gain basic information about the obtained fractions. In accordance with the results of this work, the BCR sequential extraction procedure has been validated for the most significant alpha-emitter natural radionuclides (^{210}Po, ^{234}U, ^{238}U, ^{230}Th, ^{232}Th, and ^{226}Ra). It has been demonstrated that their mobility is related to the speciation under environmental conditions and the type of radionuclide; we have even found differences between radionuclides of the same element, such as the cases of the pairs ^{234}U-^{238}U and ^{230}Th-^{232}Th, for the BCR-701. In addition, we found that radium was mainly bound to the reducible fraction (Fe- and Mn-oxyhydroxides), uranium to the oxidizable fraction (organic matter and sulphides), and that the polonium and thorium isotopes had a high affinity with the particulate phase (non-mobile fraction).

Keywords: *BCR Sequential extraction, BCR-701, mobility, speciation, natural radionuclides.*

3.4.1. INTRODUCTION

The mobility of trace metals and radionuclides, as well as their bioavailability and related eco-toxicity to the environment, depends strongly on their specific chemical form and methods of binding. In this sense, the potential danger from these materials relies directly on their ability to release contaminants into the environment. Therefore, the determination of the total contaminant content in a solid sample is not enough to evaluate its potential risk, since under normal environmental conditions only a proportion of the total content will be mobile and/or bioavailable.

Determination of mobile forms using operational extraction procedures can be a good compromise to give information on the environmental contamination risk. One of the first sequential extraction procedures to evaluate the mobility of heavy metals in fresh sediments (e.g., Cd, Co, Cu, Fe, Mn, Ni, Pb, and Zn) was developed by Tessier et al. (Tessier et al., 1979). It provides information on the different forms of the trace metals in the sediments, as well as physicochemical availability, mobilisation, and transportation. So, this technique would allow determination of the degree of mobility, and the fate of potentially toxic metals, in different leaching conditions. The sequential extraction techniques provide a good estimate of contaminant-bearing phases, although they are analytically very complex and sometimes hardly reproducible (López Julian and Mandado Collado, 2002; D'Amore et al., 2005).

Since the publication of the operating scheme designed by Tessier, many studies aimed at validating the results obtained by applying this protocol and other later procedures have been applied to different types of solid materials (Sahuquillo et al., 2003; Guevara-Riba et al., 2004; Pueyo et al., 2008; Sutherland, 2010). Despite this, the most significant advance in sequential extraction studies occurred in 1987 when the European Commission launched a program in the framework of the BCR (in French "Bureau Communautaire de Référence"; in English "Community Bureau of Reference"). This was aimed at harmonising the extraction procedures (Rubio and Lopez-Sanchez, 2008), and finally, in 1993 a standard sequential extraction procedure known as BCR was proposed (Thomas et al., 1994). This procedure was associated with the development of a certified reference material (CRM) in 1997, CRM 601, which was sediment from Lake Maggiore, Italy. Inconsistencies in trace element extraction using the BCR protocol (1993) lead to different investigations (Sahuquillo et al., 1999). The results of these investigation were

used in 1999 as recommendations for the development of an optimised BCR procedure, generating the production of a new CRM, BCR-701, which was sediment from Lake Orta Piemonte, Italy (Rauret et al., 1999). This material has certified the extractable contents of some trace elements (Cd, Cr, Cu, Ni, Pb, and Zn) in each step of the optimised BCR procedure.

The application of sequential extraction procedures in radioactivity studies is increasingly important (Pefia et al., 2003; Aguado et al., 2004; Blanco et al., 2004; Guo et al., 2007; Virtanen et al., 2013), because they allow for the provision of necessary information on the bioavailability of the considered isotopes, in the same way as for trace elements. In this sense, the usefulness of sequential extraction procedures is evident from the detailed information provided on the origin, mode of occurrence, biological and physicochemical availability, mobilisation, and transport of natural radionuclides in the environment. However, it is crucial to develop a validation of the sequential procedure for natural radionuclides to ensure the accuracy and reproducibility of the results, and in order to compare results obtained by different laboratories. Therefore, a certified reference material will be needed in the future to guarantee the measured concentrations of natural radionuclides at each extraction step.

Due to this fact, BCR-701 is proposed in this work as a potential certified reference material for determining the mobility of natural radionuclides (^{210}Po, U-isotopes, Th-isotopes, and Ra-isotopes) in different environmental conditions. This general objective was achieved through the following specific tasks: a) validation of improved BCR procedure according to the certified extractable content of trace elements (Cd, Cr, Cu, Ni, Pb, and Zn); and b) repeatability and reproducibility of the results for the natural radionuclides.

3.4.2. MATERIALS AND METHODS

3.4.2.1. Modified BCR Sequential Extraction Procedure

The BCR procedure is summarised below (Table 3.14) and its specific details can be found elsewhere (Sahuquillo et al., 1999; Rauret et al., 1999).

Step 1. Water/acid soluble and exchangeable fraction (F1)

For each solid sample, 40 mL of 0.11 M acetic acid was added to 1.0 g aliquot in a 60 mL centrifuge tube and shaken end-over-end (30 ± 10 rpm) for 16 h at 22.5 °C (overnight). The liquid extract was separated from the solid residue (SF1) by centrifugation for 20 min, and stored at 4 °C until analysis. The residue was washed with 20 mL of distilled water, shaken for 20 min, and centrifuged; finally, the washing was discarded. This extraction step (water/acid soluble and exchangeable fraction) is designed to extract exchangeable metals and those soluble in water or in slightly acidic conditions. This fraction is the most labile in environmental samples, and therefore, the most bioavailable and dangerous for the environment.

Step 2. Reducible fraction (F2)

40 mL of 0.5 M $NH_2OH{\cdot}HCl$ (adjusted to a pH of around 2 by adding HNO_3) was added to the solid obtained in Step 1 (SF1) in the centrifuge tube and was shaken for 16 h at 22.5 °C. The extract was separated as in Step 1. The solid wash procedure was also carried out (solid SF2 is obtained). Fraction 2 (reducible fraction) represents all metals bound to Fe and Mn oxi-hydroxides that can be released if conditions change from an oxic to an anoxic state.

Step 3. Oxidizable fraction (F3)

Small aliquots of 10 mL of H_2O_2 were added carefully to the Step 2 residue (SF2). The tubes were covered and digested for 1 h at room temperature with occasional manual shaking, and then heated to 85 ± 2 °C for 1 h in a water bath. The volume was reduced to < 3 mL (uncovered) by further heating of the uncovered tube. A further 10 mL of H_2O_2 was added and it was heated again to 85 ± 2 °C for 1 h (covered vessel). Later, the volume of liquid was reduced to about 1 mL. Finally, 50 mL of 1 M NH_4OAc (pH 2) was added and shaken for 16 h at 22 ± 5 °C. The extract was separated from the solid residue (SF3) by centrifugation as described in Step 1, and the procedure for washing the solid was followed. Fraction 3 (oxidizable fraction) is mainly composed of metals bound to organic compounds and sulphides that could be released under oxidising conditions.

The sum of the three steps of the sequential extraction corresponds to the total metal content associated with the mobile fraction (M = F1+F2+F3).

Step 4. Residual fraction (F4)

Additionally, as an internal check on the procedure, it is recommended that the residue from Step 3 (SF3) be digested in aqua regia and the total amount of metal extracted (i.e., S = sum of Step 1 + Step 2 + Step 3 + Residue) be compared with that obtained via "direct analysis" by aqua regia (D); the aim is that both amounts should be similar (S=D).

The residue SF3, from Step 3, was digested by adding 10 mL of aqua regia (a mixture of 12 M HCl and 15.8 M HNO_3 in the ratio 3:1) and allowed to stand for 16 h at room temperature. After that, samples were heated slowly under reflux conditions maintained for 2 h. The extract was separated as in Step 1. The non-mobile fraction, or fraction 4, corresponds to those metals that are strongly associated with crystalline structures of minerals and are therefore unlikely to be released from the samples unless they are exposed to extreme conditions.

Step	Fraction	Nominal target phases	Extractant (1 g of dry solid)	Conditions
F1	Water/acid soluble and exchangeable	Soluble species, carbonates and cation exchange sites	40 mL 0.11M CH_3COOH	Shaking during 16 h. at room temperature (RT).
F2	Reducible	Iron and manganese oxyhydroxides	40 mL 0.5M $NH_2OH{\cdot}HCl$ (pH 2)	Shaking during 16 h. at RT.
F3	Oxidizable	Organic matter and sulphides	10 mL 8.8 M H_2O_2 (pH 2) + 10 mL 8.8 M H_2O_2 (pH 2), then 50 mL 1M NH_4OAc (pH 2)	1h at RT, 1 h at 85 ºC; 1 h a 85 ºC; and shaking during 16 h. at RT.
F4	Residual	non-mobile fraction	10 mL aqua regia 3:1 (12M HCl + 15.8M HNO_3)	16 h at room temperature, and then to heat on hot plate during 2 h under reflux.

Table 3.14. *Modified BCR sequential extraction procedures.*

3.4.2.2. Materials

The certified reference material BCR-701, corresponds to a sediment sample collected from Lake Orta (Italy), which is known for a serious metal contamination because of industrial effluent discharge containing ammonia sulphate and copper from a rayon factory and heavy metals (Cu, Cr, Zn, and Ni) from several electroplating factories (Rossi

et al., 1992) . This material has been certified for six trace elements (Cd, Cr, Cu, Ni, Pb, and Zn) in all steps of a modified BCR sequential procedure (Rauret et al., 2001).

Three aliquots (1.0 g) were subjected to the modified BCR sequential procedure in order to validate the results and their repeatability, since it is an operationally defined method. In addition, blanks of the different extractants were also analysed.

3.4.2.3. Characterisation Techniques

Several analytical techniques have been used to characterise the liquid fractions and solid phases resulting from applying the modified BCR sequential extraction to the certified reference material BCR-701.

The major composition, mineral phases, and grain morphology were analysed at the General Research Services of the University of Seville (SGI-CITIUS, Seville), accredited under ISO 9001, by using the following techniques: X-ray fluorescence (XRF; Panalytical spectrometer AXIOS model), X-ray diffraction (XRD; Panalytical X'Pert Pro), and scanning electron microscope (SEM; QUANTA Fei-200) with energy dispersive spectroscopy (EDS). To verify the quality of results, several CRMs were used: a gold alloy (FISHER 603-683) for XRF and Corindon (SRM 1976a) for XRD.

The trace element concentrations were analysed at Activation Laboratories Ltd (ACTLABS, Ontario, Canada), accredited under ISO 9001 and 9002, and determined by either inductively coupled plasma mass spectrometry (ICP-MS) or inductively coupled plasma optical emission spectrometry (ICP-OES) (Perkin Elmer Sciex ELAN 9000/Varian 735ES). For the solid phases, they were previously digested with the mix of the four acids (hydrochloric, nitric, perchloric, and hydrofluoric) for a near total dissolution of the samples. Several CRMs (AC-E, GBW 07238 (NCS DC 70006), BIR-1a, and SX 18-04), blanks, and replica solutions were measured to ensure the quality of the results.

In order to determine the radionuclide activity concentrations (U, Th, Po, and Ra), each of the liquid fractions extracted in the BCR sequential extraction method and the solid phases (previously digested with the mix of four acids) was subjected to a sequential radiochemical procedure by using back-extraction with tributylphosphate (TBP), and purification/isolation with ion exchange resins. After isolation of the radioelements U-,

Th-, and Ra-isotopes (Oliveira and Carvalho, 2006), they were electrodeposited onto stainless steel discs (Martin and Hancock, 2004). In addition, Po was self-deposited onto silver disks by using the method of Flynn (Flynn, 1968). Then, the alfa sources were counted using an ion-implanted silicon (PIPS) detector (EG & G Ortec). For these determinations, the samples were spiked with the accurately known activities of ^{232}U, ^{229Th}, and ^{209}Po. It was not possible to measure the ^{228}Th because it exists in the ^{232}U solution used as a tracer. Several CRM (IAEA-434 and IAEA-327), blanks, and replica solutions were measured to guarantee the reproducibility of the data.

3.4.3. RESULTS AND DISCUSSION

3.4.3.1. Chemical Characterisation

The major element composition of BCR-701 measured by XRF is shown in Table 3.15. As can be observed, BCR-701 mostly contains Si (26 ± 2 %), Al (8.0 ± 0.4 %), Fe (4.1 ± 0.2 %), K (2.5 ± 0.2 %), Ca (2.1 ± 0.1 %), Mg (1.5 ± 0.1 %), and Na (1.0 ± 0.1 %), with concentrations are very similar to the estimated values for the composition of the continental crust (Rudnick R.L. and Gao, 2014). However, the P and S contents exceed these expected values. In addition, some trace elements exceed these stablished values (Table 3.15), such as Ag (9.0 ± 0.5 ppm), As (38 ± 2 ppm), Bi (2.3 ± 0.2), Cd (12 ± 1 ppm), Cr (249 ± 13 ppm), Cu (288 ± 15 ppm), Hg (0.89± 0.05 ppm), Mo (4.2 ± 0.2), Ni (114 ± 6 ppm), Pb (160 ± 8 ppm), Se (0.5 ± 0.5 ppm), and Zn (494 ± 25 ppm). The Cd and Ag concentrations stand out at 200 times higher than the concentration in the upper crust (Hu and Gao, 2008).

Elements	Al	Ca	Cl	F	Fe	K	Mg	Mn	Na	P	S	Si	Ti	C.L.*	Ag	As	Ba	Be	Bi
Unit	%	%	%	%	%	%	%	%	%	%	%	%	%	%	ppm	ppm	ppm	ppm	ppm
DL	0.01	0.01	0.01	0.01	0.01	0.01	0.01	0.01	0.01	0.01	0.01	0.01	0.01	0.01	0.05	0.1	1	0.1	0.02
BCR_701	8.0 ± 0.4	2.1 ± 0.1	0.02 ± 0.02	< DL	4.1 ± 0.2	2.5 ± 0.2	1.5 ± 0.1	0.08 ± 0.08	1.0 ± 0.1	0.39 ± 0.04	0.29 ± 0.03	26 ± 2	0.50 ± 0.05	11.47	9.0 ± 0.5	38 ± 2	540 ± 27	2.9 ± 0.6	2.3 ± 0.2
Upper Crust	8.2 ± 0.5	2.6 ± 0.2	0.37 ± 0.38	-	3.9 ± 0.4	2.3 ± 0.2	1.5 ± 0.2	0.08 ± 0.01	2.4 ± 0.4	0.07 ± 0.01	0.006 ± 0.003	31 ± 1	0.38 ± 0.05	-	0.05 ± 0.01	5.7 ± 1.2	628 ± 83	1.9 ± 0.2	0.23 ± 0.03
BCR-701/Crust ratio	0.98 ± 0.08	0.82 ± 0.06	0.05 ± 0.07	-	1.04 ± 0.12	1.08 ± 0.10	1.01 ± 0.15	1.03 ±1.03	0.42 ± 0.07	5.95 ± 0.99	49 ± 25	0.82 ± 0.04	1.32 ± 0.21	-	179 ± 37	6.7 ± 1.5	0.86 ± 0.12	1.5 ± 0.4	10 ± 2
Elements	Cd	Co	Cr	Cs	Cu	Hg	Li	Mo	Ni	Pb	Sb	Se	Sn	Sr	Th	U	V	Zn	Zr
Unit	ppm	ppm	ppm	ppm	ppm	ppm	ppm	ppm	ppm	ppm	ppm	ppm	ppm	ppm	ppm	ppm	ppm	ppm	ppm
DL	0.1	0.1	0.5	0.05	0.2	0.01	0.5	0.05	0.5	0.5	0.1	0.1	1	0.2	0.1	0.1	1	0.2	1
BCR-701	12 ± 1	17 ± 4	249 ± 13	6.1 ± 0.3	288 ± 15	0.89 ± 0.05	38 ± 2	4.2 ± 0.2	114 ± 6	160 ± 8	1.0 ± 0.2	0.5 ± 0.5	3.0 ± 1.0	171 ± 9	14 ± 1	5.8 ± 1.2	77 ± 4	494 ± 25	62 ± 3
Upper Crust	0.06 ± 0.02	15 ± 1	74 ± 8	4.9 ± 0.3	27 ± 2	0.05 ± 0.04	41 ± 6	0.6 ± 0.3	32 ± 4	17 ± 1	0.75 ± 0.11	0.09 ± 0.05	2.2 ± 0.2	320 ± 46	11 ± 1	2.6 ± 0.1	106 ± 7	75 ± 9	193 ± 28
BCR-701/Crust ratio	195 ± 67	1.1 ± 0.3	3.4 ± 0.4	1.2 ± 0.1	11 ± 1	18 ± 14	0.92 ± 0.14	7.1 ± 3.5	3.6 ± 0.5	9.4 ± 0.7	1.3 ± 0.3	5.6 ± 6.4	1.4 ±0.5	0.53 ± 0.08	1.3 ± 0.1	2.2 ± 0.5	0.7 ± 0.1	6.6 ± 0.9	0.32 ± 0.05

Table 3.15. *Major element (%) and trace element composition (ppm) of certified reference material BCR-701 and typical composition of the upper continental crust samples (Rudnick and Gao, 2014; Hu and Gao, 2008). The standard uncertainties are given according to the RSD value for measured elements and one standard deviation of the mean for upper crust elements. (*CL: calcination loss).*

The mineral phases of BCR-701 were analysed by XRD. The diffraction pattern (Figure 3.26) reveals that the mineralogical composition is in agreement with the chemical one obtained by XRF. BCR-701 is mainly composed of quartz (SiO_2), muscovite ($KAl_2(AlSi_3O_{10})(OH)_2$), feldspar ($CaAl_2Si_2O_8$), and clinochlore ($(Mg_5Al)(AlSi_3)O_{10}(OH)_8$). These mineral phases are typically found in both soils and sediment matrices (Osman, 2013).

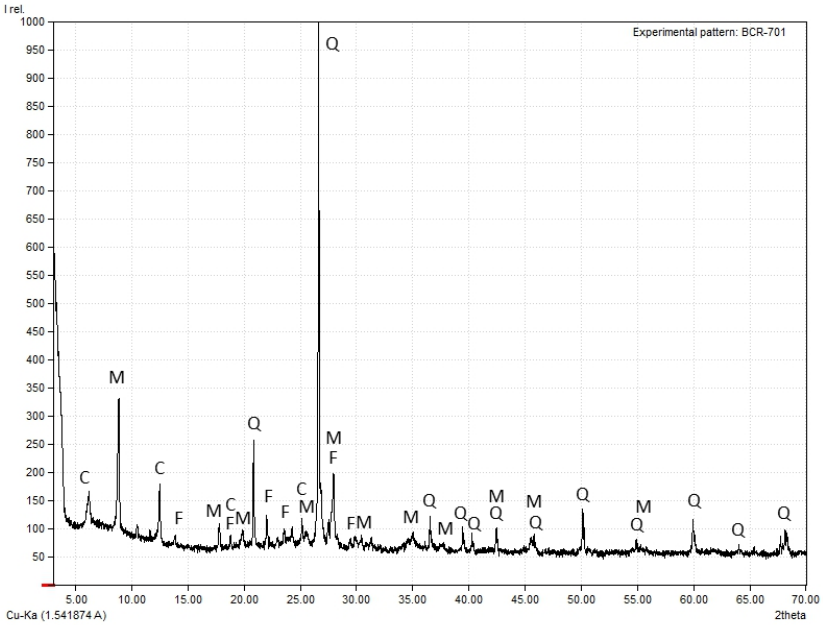

Figure 3.26. *Diffraction pattern of BCR-701. Mineral phases identified: quartz (Q), muscovite (M), clinochlore (C), and feldspar (F).*

The certified reference material BCR-701 was also studied with SEM-EDS (Figure 3.27). As it can be seen, the sample morphology is quite heterogeneous, as is the particle size distribution. The sample seems to constitute particles, whose sizes vary between 50 and 100 µm, which are surrounded by finer particles. So, they could be classified as silt particles (0.02–0.002 mm of effective diameter) (Osman, 2013). Most particles analysed contain the major elements detected by XRF and, according to their composition, several minerals have been identified such as biotite (point 1and point 4), muscovite (point 2), quartz (point 3), and albite (point 5).

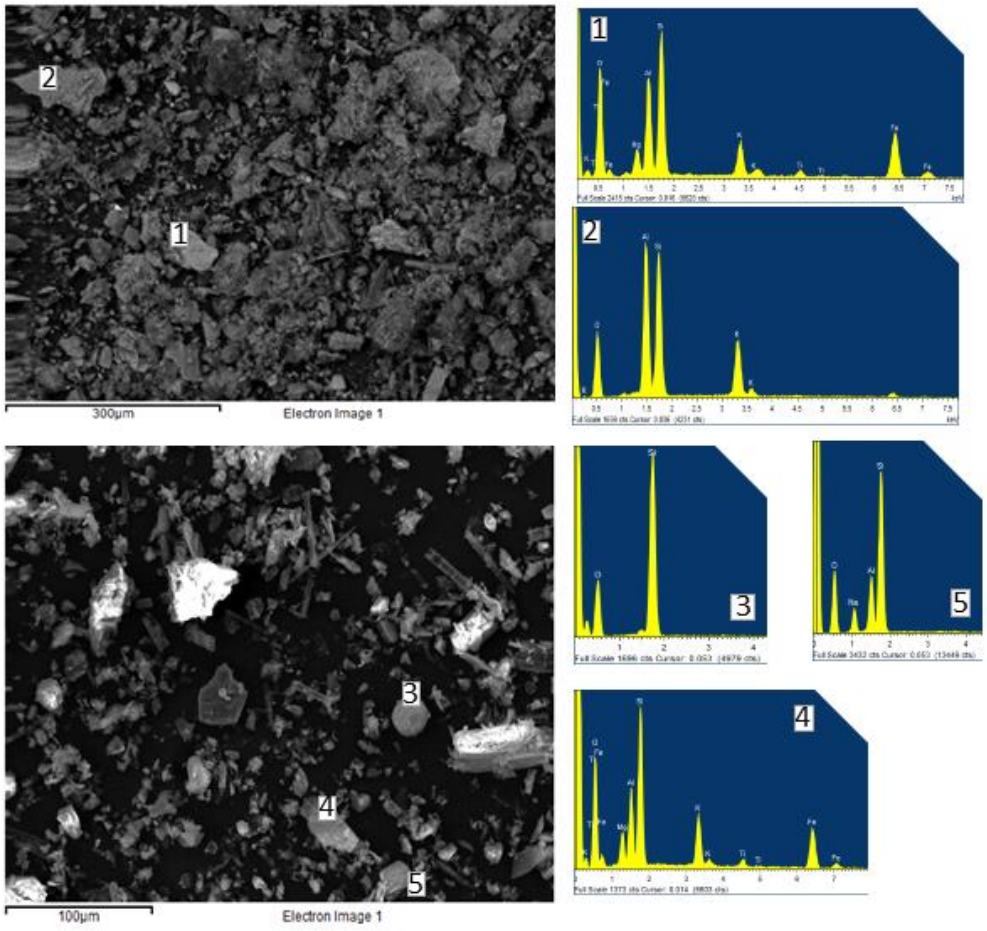

Figure 3.27. *Morphology of BCR-701 as well as its particle composition.*

3.4.3.2. Validation of the BCR Procedure in our laboratory by using BCR-701

3.4.3.2.1. Metals

3.4.3.2.1.1. Aqueous Phase

The first part of this work was to validate the operational procedure of the BCR speciation method applied in our laboratory. For that, the BCR-701 certified reference material was used. Table 3.16 presents both the measured and certified values of Cr, Ni, Cu, Zn, Cd, and Pb of the three extraction steps (F1, F2, F3), and the corresponding standard uncertainties. This table also shows the indicative concentrations (values not certificated) for the residual phase (F4), and the total contents obtained by direct analysis (dissolving the solid sample with aqua regia). Moreover, the sums for all fractions are also displayed (S = F1+F2+F3+F4) in Table 3.16.

The agreement between the two results (measurements of our laboratory and the CRM values) is proven by applying the Z-score methodology, if both variables follow Gaussian distributions. The Z-score is defined by the following equation:

$$Z = \frac{\underline{X}_{measured} - \underline{X}_{certified}}{\sqrt{(\sigma_{measured})^2 + (\sigma_{certified})^2}}, \quad \text{[Eq. 3.35]}$$

Where $\underline{X}_{measured}$ is the mean value measured in a given step for a particular element, $\underline{X}_{certified}$ is the certified value reported for BCR-701, and σ is the standard uncertainty.

The Z-score values are also presented in Table 3.16, with the null hypothesis being that there are not significant differences between measured and certified values. All Z-score values of fractions are lower than 2, reflecting the fact that is not possible to reject the null hypothesis with a confidence level of 95%. So, there are no statistically significant differences between the measured concentrations and the certified ones in the extractable fractions of BCR-701. Therefore, the application of the modified BCR operational procedure in our laboratory has been validated since the certified heavy metals concentrations (Cr, Ni, Cu, Zn, Cd, and Pb) in BCR-701 have been reproduced.

In order to quantify the percentage of metals in the different chemical species, the transfer coefficients (TC) have been calculated. The experimental transfer coefficient is defined as the proportion of metal that is transferred to the liquid phase in each step (F_i), in relation to the total concentration of the sample (sum of concentrations for all fractions S), found in the solid according to:

$$TC\ (\%) = \frac{Fi}{S} 100\ (\%). \quad \text{[Eq. 3.36]}$$

The transfer coefficients are shown in Figure 3.28, and the qualitative ranking for metals in BCR-701 in each fraction is indicated as follows:

F1: Cd > Zn > Cu > Ni > Pb ~ Cr

F2: Pb > Cu > Ni ~ Cd ~ Zn > Cr

F3: Cr > Cu ~ Ni > Zn > Pb > Cd

M (F1 + F2 + F3): Cd > Pb ~ Cu > Zn ~ Cr > Ni.

So, both Cd and Zn are mainly related to the most soluble fraction (soluble species, carbonates, and exchangeable cations). This fact is associated with the higher capacity of principal polarisation, resulting in strong adsorption of Cd and Zn onto colloids in the sediments (Ahdy et al., 2011; Saleem et al., 2015). On the other hand, lower proportions of these metals are also released in the second step (reducible fraction), which means that they are bound with iron and manganese oxyhydroxides. In addition, most of the Pb, Cu, and Ni content is associated with F2, since the Fe and Mn oxides are excellent scavengers for Pb, Cu, and Ni metals, and depend on the E_h changes in the sediment (Korfali and Jurdi, 2011; Nemati et al., 2011). Finally, Cr is mainly bound with the oxidizable fraction (organic matter and sulphides); this is expected if we consider that organic matter increases the solubility and mobility of Cr (III) and thus facilitates its oxidation (Chattopadhyay et al., 2010; Kennou et al., 2015). Taking into account all of these fractions (M), the most mobile metal is Cd, followed by Pb and Cu, Zn and Cr, and finally Ni.

	Cr (mg/kg)			Ni (mg/kg)			Cu (mg/kg)			Zn (mg/kg)			Cd (mg/kg)			Pb (mg/kg)		
	Obtained value	**Certified value**	**|Z| score**	**Obtained value**	**Certified value**	**|Z| score**	**Obtained value**	**Certified value**	**|Z| score**	**Obtained value**	**Certified value**	**|Z| score**	**Obtained value**	**Certified value**	**|Z| score**	**Obtained value**	**Certified value**	**|Z| score**
F1	2.9 ± 0.3	2.26 ± 0.08	2.0	13.1 ± 1.5	15.4 ± 0.5	1.5	52.9 ± 1.6	49.3 ± 0.9	2.0	185 ± 9	205 ± 3	2.0	6.7 ± 0.4	7.3 ± 0.2	1.2	2.6 ± 0.6	3.18 ± 0.1	1.0
F2	46.5 ± 2.0	45.7 ± 1.0	0.4	31.4 ± 3.8	26.6 ± 0.7	1.2	121 ± 2.4	124 ± 2	1.1	119 ± 6	114.0 ± 2.5	0.07	3.0 ± 0.9	3.8 ± 0.1	0.90	124 ± 5	126 ± 2	0.33
F3	137 ± 6	143 ± 4	0.8	17.8 ± 1.3	15.0 ± 1.0	1.8	56 ± 4	55 ± 2	0.20	48 ± 3	46 ± 2	0.50	0.28 ± 0.10	0.27 ± 0.03	0.06	9.9 ± 2.5	9.3 ± 1.0	0.24
F4[1]	56 ± 4	63 ± 4	1.2	33.2 ± 5.8	41.4 ± 2.0	1.3	34.9 ± 7.2	38.5 ± 5.6	0.40	86 ± 6	94.6 ± 6.1	1.1	0.2 ± 0.1	0.125 ± 0.038	0.10	12 ± 8	11 ± 3	0.13
Sum[2]	242 ± 7	254 ± 5	1.2	96 ± 7	99 ± 2.0	0.40	265 ± 9	267 ± 6	0.20	437 ± 13	460 ± 8	1.5	10.1 ± 1.0	11.5 ± 0.2	1.4	149 ± 9	149 ± 4	0.04
Total[3]	218 ± 12	272 ± 20	2.3	87 ± 6	103 ± 4	2.2	233 ± 15	275 ± 13	2.1	402 ± 14	454 ± 19	2.2	9.4 ± 0.6	11.7 ± 1.0	2.0	141 ± 6	143 ± 6	0.24

Table 3.16. *Obtained, certified, and Z score values in certified reference material BCR-701. [1]Indicative values: aqua regia extractable content (residue from sequential extraction); [2] Sum of fractions; [3] Indicative values: aqua regia extractable contents (direct analysis). Standard uncertainty calculated as the standard deviation of the mean of three counts. (Detection limit of measured value: 1 ppb).*

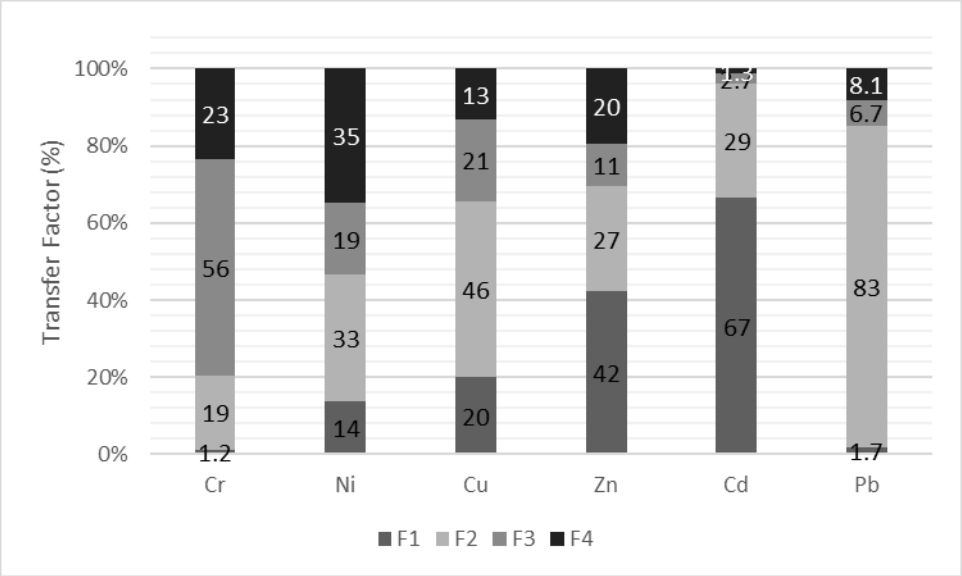

Figure 3.28. *Transfer coefficient (TF in %) for the certified metals in BCR-701.*

3.4.3.2.1.2. Solid Phase

In order to deepen our understanding of the fractionation mechanisms of the heavy metals considered, the solid phases resulting from each extraction step were also studied. This was done in an attempt to find mineral and micro-structural changes that could prove the differences in solubility of metals under the testing conditions.

For that, the following experiment was developed: (a) four aliquots of around 1.0 g of BCR-701 were taken and subjected to the first extraction step. The consequent solids were dried and homogenised (SF1: 0.94 ± 0.02 g per g of BCR-701); (b) five aliquots of about 1.0 g of BCR-701 were subjected sequentially to the first and second steps (F1+F2). The remaining solids obtained were dried and homogenised (SF2: 0.91 ± 0.01 g per gram of BCR-701); (c) five aliquots of about 1.0 g of BCR-701 were sequentially subjected to the three sequential steps (F1+F2+F3). The residual solid was dried and homogenised (SF3: 0.81 ± 0.01 g per gram of BCR-701). What stands out is that the SF1 and SF2 mass is practically constant, while that of SF3 is reduced. This possibly means that the extractants used in step 1 and 2 released the metals adhered on the surface of the solid, whereas part of the sample is considerably dissolved in step 3.

The concentrations of the certified trace elements in the solid fractions (SF1, SF2, and SF3) obtained by the BCR procedure, given as mass of the heavy metal per gram of initial dry solid sample, are given in Table 3.17. Figure 3.29 shows the fluxes (%) of each metal

that remain in the solid and liquid fractions in relation to the amount contained in the original solid sample.

It is observed that the metal concentration is reduced in each step according to the speciation of each metal, i.e., Zn and Cd are easily soluble in water/acid solution; in reducible conditions the release of Cu, Ni, and Pb is favoured; at the same time, Cr is more mobile in oxidizable conditions. This behaviour in in agreement with the calculated fluxes indicated in Figure 3.29. In general, it can be pointed out that the calculated fluxes are consistent, although in some cases they seem to be significantly lower than 100%. This suggests that some of the initial content in BCR-701 could be lost during the procedure (washing, adsorption on the walls, etc.). This problem will be evaluated in future studies.

	Cd (mg/kg)	Cr (mg/kg)	Cu (mg/kg)	Ni (mg/kg)	Pb (mg/kg)	Zn (mg/kg)
DL	0.1	0.5	0.2	0.5	0.5	0.2
BCR-701	12 ± 1	249 ± 13	288 ± 15	114 ± 6	160 ± 8	494 ± 25
SF-1	3.3 ± 0.7	207 ± 10	238 ± 12	90 ± 5	140 ± 7	291 ± 15
SF-2	0.5 ± 0.5	201 ± 10	132 ± 7	68 ± 3	39 ± 2	185 ± 9
SF-3	0.1 ± 0.1	96 ± 5	44 ± 2	50 ± 2	27 ± 1	121 ± 6

Table 3.17. *Concentration (mg/kg) of trace elements in solid fractions (digested with the mix of four acids). D.L.: detection limit.*

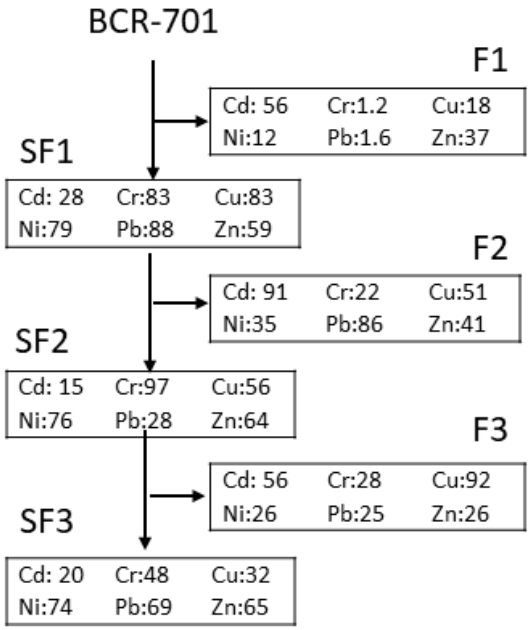

Figure 3.29. *Metal flux diagram (%) of BCR sequential extraction procedure applied to BCR-701 (solid samples digested with the mix of four acids). The uncertainty is around 10–25%.*

In addition, solid samples were analysed by XRD in order to determine if new major mineral phases were formed. The results show (Figure 3.30) that there are no significance differences between the diffraction pattern of BCR-701 and the others from solid phases resulting after applying the modified BCR sequential procedure. Thus, identical mineral phases are found in BCR-701, SF1, SF2, and SF3. Therefore, the silicate clays in BCR-701 do not exert any notable control on trace metal speciation (Cappuyns et al., 2007; Ryan et al., 2008).

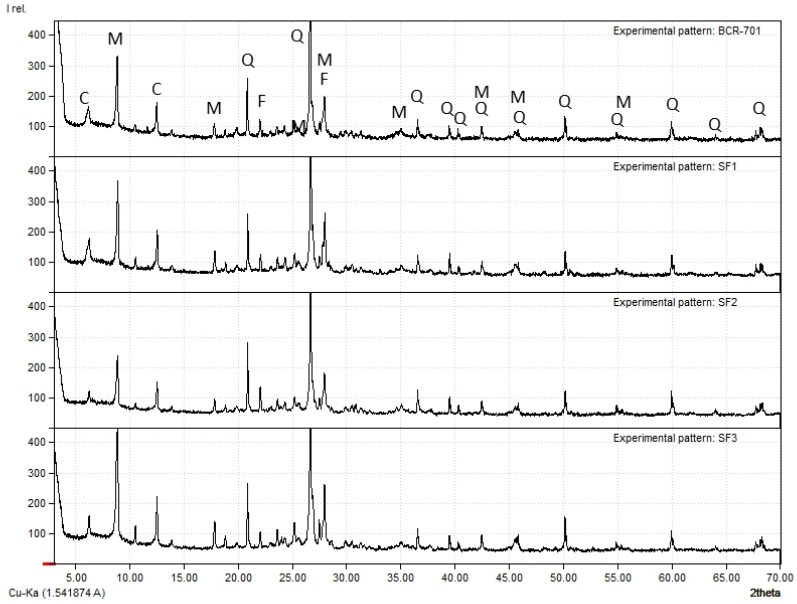

Figure 3.30. *Diffraction pattern of solid fraction (BCR-701, SF1, SF2, SF3). Mineral phases identified: quartz (Q), muscovite (M), feldspar (F), and clinochlore (C).*

3.4.3.3. BCR Validation for Natural Radionuclides using he CRM BCR-701

3.4.3.3.1. Aqueous Phase

The next step was to develop a preliminary validation of the BCR methodology for natural radionuclides, since there is no certified reference material that can be used to know the mobility of radionuclides in the environment. In the same way as for metals, the radio-toxicity and the bioavailability of radionuclides will depend strongly on their mobility in different aqueous environmental conditions.

The certified reference material BCR-701 was used to evaluate the mobility of long-life natural radionuclides such as ^{210}Po, ^{234}U, ^{238}U, ^{230}Th, ^{232}Th, and ^{226}Ra. Table 3.18 shows the activity concentrations measured for the different radionuclides and their transference coefficients in each fraction. The total activity concentration has been measured both by direct analysis (D) and through the sum (S) of the activity concentrations obtained in the different fractions (S = F1 + F2 + F3 + F4). The total activity concentrations measured directly for ^{238}U, ^{232}Th, and ^{226}Ra are typical of undisturbed soils (around 45 Bq kg^{-1} and 40 Bq kg^{-1} for U- and Th-series radionuclides, respectively) (UNSCEAR, 2000). They are also in agreement with the sum of fractions (S) of the corresponding radionuclides

(Table 3.18). Moreover, the measured concentrations by direct analysis for all radionuclides from the ^{238}U-series are in agreement with the secular equilibrium (^{238}U, ^{234}U, ^{230}Th, and ^{226}Ra). A similar comment can be made for the ^{232}Th-series progeny (^{232}Th, ^{228}Ra, and ^{228}Th) since the BCR701 sample was also measured by gamma spectrometry.

According to the results, the radionuclides are distributed in each fraction as follows:

F1: ^{226}Ra > ^{230}Th > ^{234}U > ^{238}U > ^{232}Th

F2: ^{226}Ra > ^{210}Po > ^{234}U > ^{230}Th > ^{238}U > ^{232}Th

F3: ^{238}U > ^{234}U > ^{226}Ra > ^{210}Po > ^{230}Th > ^{232}Th

M (F1+F2+F3): ^{226}Ra > ^{234}U ~ ^{238}U > ^{210}Po > ^{230}Th > ^{232}Th

A significant fraction of ^{226}Ra (11%) is bound with the most soluble species (soluble in water for typical environmental conditions) and reducible species (45%). These results are in agreement with other studies (IAEA, 2014) which indicate that Ra is readily adsorbed onto clays and mineral oxides present in soils, especially at near neutral and alkaline pH conditions. For the pH conditions of most natural waters, mobile Ra will be present primarily as the uncomplexed Ra^{2+} cation. Sorption studies generally confirm the adsorption behaviour expected for Ra^{2+} as a function of pH, with negligible adsorption at very acidic pH values and increasing adsorption with increasing pH (Szabo et al., 2012).

Uranium isotopes in this lacustrine sediment are mainly bound with the oxidizable fraction (around 25%), which is probably formed by organic matter since this is a more efficient sorbent for U than clay minerals and amorphous Fe and Mn-oxyhydroxides (Wang et al., 2014). Uranium is often found in a highly oxidised form (U (VI)) in oxic environments, whereas in sediments under reducing conditions the U is reduced and precipitates as U (IV). Uranium in sediments is precipitated under reducing conditions in underlying low-oxygen bottom water or in sediments receiving high fluxes of particulate organic carbon (Lee et al., 2017). Hexavalent uranium forms complexes such as uranyl carbonates (UO_2CO_3) and uranyl sulphates (UO_2SO_4), which tend to maintain the U in dissolution (UNSCEAR, 2016).

Polonium has a relative low mobility if it is compared to Ra and U, since only 20–30% is bound to mobile phases. Several studies (Ansoborlo et al., 2012) affirm that ^{210}Po is generally present in natural waters in the form of Po (IV), which is slightly soluble due to the hydrolysis of Po (IV) and the formation of colloids, and has a high affinity for the particulate phase. Polonium-210 is generally adsorbed on particles and colloids (mineral or organic). The major parameter controlling sorption/desorption is the redox state (E_h), with a strong decrease of ^{210}Po (in the particle form) when moving from oxic surface water to anoxic deep water. This can be explained by the fact that ^{210}Po is adsorbed onto manganese oxides and is released when Mn (IV) is dissolved by reducing it into Mn (II).

And finally, it must be pointed out that Th is very much bound to the immobile fraction, justified by its very high reactivity with the particulate matter; this radioelement is considered to be a "reactive element" (Guo et al., 2007). Nevertheless, it is very interesting to highlight the different behaviours of the two Th isotopes studied. While almost 100% of the ^{232}Th is found in the residual fraction, only 85% of the ^{230}Th is in F4, showing that ^{230}Th has preferentially leaching compared to ^{232}Th. This result is probably due to the fact that ^{230}Th comes from the ^{234}U decay, and therefore the crystalline structure that surrounds it will be activated with many defects, due to the alpha-particles emitted by its parents (^{238}U and ^{234}U). This case is very similar to the ^{234}U-^{238}U fractionation produced in the dissolution of U from solid media. Thorium has a very low mobility under most environmental conditions, mainly due to the high stability of the insoluble oxide ThO_2 and the strongly resistant nature of its carrier minerals such as monazite ((Ce, La, Th, U)PO_4) and zircon ($ZrSiO_4$) (Santschi et al., 2006). The mobility of Th in soil is governed by the formation of the hydrated cation Th^{4+}, which is responsible for its solubility over a wide range of soil pH. Organic acids increase the solubility of Th in soil, but its mobility may be limited due to the formation of slightly soluble precipitates (e.g., phosphates and oxides) and by adsorption on clay minerals and organic matter. Any Th released into solution will be rapidly sorbed by clay minerals and hydrolysed to the hydrous oxide $Th(OH)_4$, which will be intimately associated with the clay-mineral fraction.

The sum of all fractions (F1+F2+F3) will reflect the total mobile fraction (M); Ra and U are the radionuclides with greater amount in the environment, and Th is the most

immobile since more than 95% remains in F4. The ^{210}Po presents an intermediate behaviour between Ra-U and Th with a 75% residual fraction.

	^{238}U (Bq/kg)	TC (%)	^{234}U (Bq/kg)	TC (%)	^{230}Th (Bq/kg)	TC (%)	^{226}Ra (Bq/kg)	TC (%)	^{210}Po (Bq/kg)	TC (%)	^{232}Th (Bq/kg)	TC (%)
F1	0.69 ± 0.08	1.6 ± 0.2	1.84 ± 0.05	3.9 ± 0.2	2.75 ± 0.17	6.9 ± 0.5	3.9 ± 1.4	11 ± 1	<LD	-	0.22 ± 0.08	0.59 ± 0.21
F2	1.37 ± 0.05	3.2 ± 0.1	2.39 ± 0.06	5.1 ± 1.0	1.92 ± 0.05	4.8 ± 0.1	20.2 ± 1.4	45 ± 2	11.2 ± 0.4	23 ± 1	0.23 ± 0.08	0.61 ± 0.22
F3	24.2 ± 0.1	56 ± 1	24.8 ± 0.2	53 ± 1	1.58 ± 0.15	3.9 ± 0.4	5.0 ± 0.7	11 ± 2	2.98 ± 0.24	5.8 ± 0.4	0.71 ± 0.04	1.9 ± 0.1
F4	17.0 ± 0.8	39 ± 2	18.1 ± 0.7	39 ± 1	34.1 ± 0.5	85 ± 1	15.2 ± 0.9	33 ± 2	37 ± 1	74 ± 1	36 ± 1	97 ± 3
S[1]	43 ± 1	-	47 ± 1	-	40 ± 1	-	44.3 ± 2.3	-	51 ± 1	-	37± 1	-
D[2]	47 ± 3	-	47 ± 4	-	39 ± 4	-	50 ± 9	-	52 ± 3	-	38 ± 3	-
Soil[3]	42 ± 5		42± 5		42± 5		36 ± 2		36 ± 2		36 ± 3	

Table 3.18. *Activity concentration of radionuclides (Bq per kg of initial solid sample) in the liquid fractions by applying the BCR procedure to BCR-701. N = 3 aliquots. Uncertainties calculated as the standard deviation of the mean of the three measures; ([1]) Sum of fractions; ([2]) Direct measurement by using the same digestion protocol; (3) Activity concentration of typical soils (UNSCEAR, 2000).*

The relative mobility of each radionuclide can be also observed by analysing the activity ratios between the most significant radionuclides, which are shown in Table 3.19. The $^{234}U/^{238}U$ ratio is one in fractions 3 and 4. It increases slowly in fraction 2 (1.7 ± 0.1), and exhibits a significant enhancement in the fraction 1 (2.7 ± 0.3). This last result confirms that a significant preferential leaching of ^{234}U in comparison to ^{238}U takes place in fraction F1; this is to be expected if it is taken into account that most U is present in very old minerals, and therefore the preferential leaching of ^{234}U is favoured since it comes from the ^{238}U decay (Andersen et al., 2009; El-Aassy et al., 2015). In addition, a slightly ^{234}U preferential leaching in the reducible fraction (Fe/Mn oxides) is also observed, while both uranium isotopes are in secular equilibrium in both oxidizable and residual fractions (fractions 3 and 4).

	$^{234}U/^{238}U$	$^{230}Th/^{232}Th$	$^{234}U/^{230}Th$	$^{226}Ra/^{230}Th$
F1	2.7 ± 0.3	13 ± 3	0.67 ± 0.05	1.4 ± 0.5
F2	1.7 ± 0.1	8.3 ± 1.5	1.2 ± 0.1	11 ± 1
F3	1.0 ± 0.1	2.2 ± 0.3	16 ± 2	3.1 ± 0.5
F4	1.1 ± 0.1	0.95 ± 0.03	0.53 ± 0.02	0.45 ± 0.03

Table 3.19. *Activity ratios in liquid fraction in certified reference material BCR-701.*

On the contrary, the $^{230}Th/^{232}Th$ isotopic ratio values are much higher than 1 in most fractions, except for the residual fraction where is close to one. This behaviour can be explained by considering that ^{230}Th and ^{232}Th belong to different radioactive decay series. They could be bound to different mineral species since probably the majority of ^{230}Th will come from the decay of the ^{238}U contained in the minerals. Therefore, in this case preferential leaching of ^{230Th}, due to damage in the crystalline structure caused by the alpha emissions from U decays, it is to be expected, as was commented previously. The greatest disequilibrium between these isotopes was found in fraction 1 and 2, with $^{230}Th/^{232}Th$ activity ratios of around 10. This means that a little part of ^{230}Th is associated with soluble and reducible fractions (less than 15%), while ^{232}Th is strongly joined to the non-available fraction (residual fraction).

The $^{234}U/^{230}Th$ activity ratio shows the maximum disequilibrium in the oxidizable fraction ($^{234}U/^{230}Th = 16 \pm 2$), due to the uranium being strongly dissolved in the aqueous medium of F3. Nevertheless, the activity ratio is close to one in the reducible fraction (2), which means that ^{230}Th is as soluble as ^{234}U in these conditions.

With respect to $^{226}Ra/^{230}Th$, the highest activity ratio is found in the reducible fraction where radium is notably dissolved.

3.4.3.3.2. Solid Phase

The activity concentrations of solid phases have been also determined by alpha spectrometry. The results are given in Table 3.20. The obtained values have been corrected by taking into account the mass of solid recovered in each extraction. As can be observed, the mobility tendency is in accordance with the TCs calculated in the liquid fractions, as shown in the fluxes diagram (Figure 3.31). The major mobility of ^{210}Po and ^{226}Ra is found in step 2, which represents reducible conditions. Uranium isotopes are mainly released in oxidizable conditions (step 3). Nevertheless, practically all activity concentration of the Th isotopes is kept in the solid phase.

	^{238}U (Bq/kg)	^{234}U (Bq/kg)	^{230}Th (Bq/kg)	^{226}Ra (Bq/kg)	^{210}Po (Bq/Kg)	^{232}Th (Bq/kg)
BCR-701	45 ± 3	49 ± 3	50 ± 4	45 ± 8	80 ± 4	71 ± 4
SF1	43 ± 3	43 ± 3	53 ± 3	41 ± 6	80 ± 4	67 ± 3
SF2	40 ± 3	41 ± 3	56 ± 4	26 ± 5	48 ± 3	68 ± 4
SF3	20 ± 2	21 ± 2	58 ± 5	18 ± 3	36 ± 3	64 ± 5

Table 3.20. *Activity concentrations (Bq/kg) in solid fractions (digested with the mix of four acids).*

More details about the behaviour of radionuclides can be observed by looking at the activity concentration ratios, which are shown in Table 3.21. The results indicate that the $^{234}U/^{238}U$ ratio is one in all fractions, as well as in BCR-701. In this case, the preferential leaching of ^{234}U is not observed due to the low quantity dissolved in the remaining solid sample. The same applies to the $^{230}Th/^{232}Th$ ratio, which is practically constant in all fractions. However, more significant differences are found in $^{234}U/^{230}Th$ and $^{226}Ra/^{230}Th$, where the ratios strongly decrease in oxidizable and reducible conditions, respectively, due to selectivity for uranium and radium solubility in each fraction.

Table 3.21. *Activity ratios in solid fraction of certified reference material BCR-701.*

	$^{234}U/^{238}U$	$^{230}Th/^{232}Th$	$^{234}U/^{230}Th$	$^{226}Ra/^{230}Th$
BCR-701	1.1 ± 0.1	0.71 ± 0.07	0.98 ± 0.09	0.90 ± 0.17
SF1	1.0 ± 0.1	0.79 ± 0.06	0.81 ± 0.07	0.78 ± 0.13
SF2	1.0 ± 0.1	0.82 ± 0.07	0.73 ± 0.07	0.47 ± 0.09
SF3	1.1 ± 0.2	0.91 ± 0.11	0.36 ± 0.05	0.31 ± 0.06

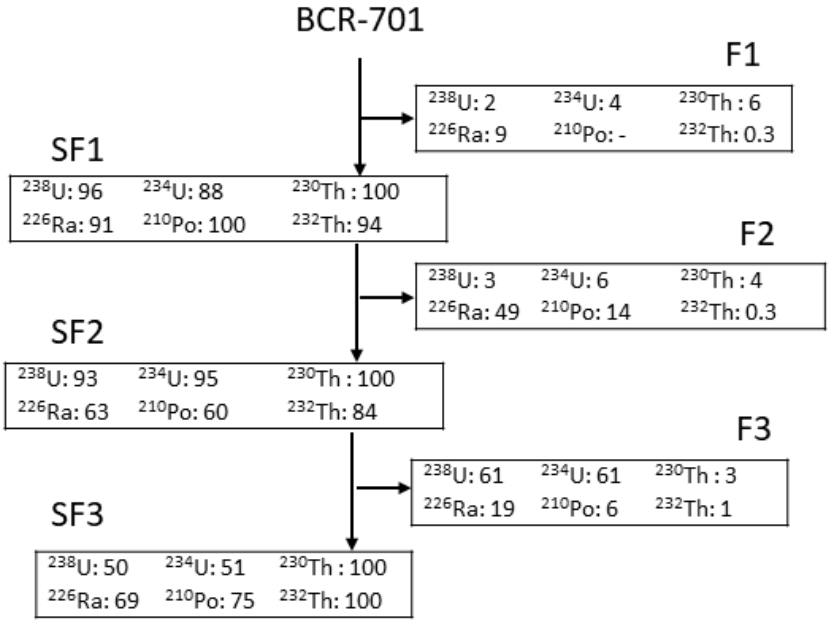

Figure 3.31. *Radionuclide flux diagram (%) of BCR sequential extraction procedure applied to BCR-701 (solid samples digested with the mix of four acids). The uncertainty is around 10–25%.*

3.4.4. CONCLUSIONS

The BCR sequential extraction procedure is the only one that has a certified reference material (code BCR-701) for determining the mobility of some heavy metals in different environmental conditions. There is no CRM for natural radionuclides. This study is the first time that mobility of natural radionuclides (U-isotopes, Th-isotopes, 226Ra, and 210Po) has been evaluated in BCR-701 by applying the BCR procedure, in an attempt to develop a preliminary validation of this CRM for natural radionuclides.

The main conclusions of this study can be summarised as follows:

- The application of BCR in our laboratory has been validated by the measurement of certified trace metals (Cd, Cr, Cu, Ni, Pb, and Zn) in BCR-701. We found that there were no significant differences (5% significant level) between our measurements and the certified ones.
- The mobility order for the heavy metals was as follows: F1 (Cd > Zn > Cu > Ni > Pb ~ Cr); F2 (Pb > Cu > Ni ~ Cd ~ Zn > Cr); and F3 (Cr > Cu ~ Ni > Zn > Pb > Cd). The total mobility (F1 + F2 + F3) was: (Cd > Pb ~ Cu > Zn ~ Cr > Ni).
- The modified BCR sequential procedure was applied to natural radionuclides. Good reproducibility was obtained for the different sequential extractions. We propose that BCR-701 could a candidate certified reference material for natural radionuclides when the BCR procedure is used. Nevertheless, it would be interesting to develop an international project, involving several expert laboratories, to measure radioactivity with the objective of obtaining a CRM (i.e. BCR-701) material to be used for validating the BCR procedure when this method is applied to natural radionuclides.
- The application of BCR allowed us to obtain the mobility order of the studied natural radionuclides: F1 (^{226}Ra > ^{230}Th > ^{234}U > ^{238}U > ^{232}Th ~ ^{210}Po); F2 (^{226}Ra > ^{210}Po > ^{234}U > ^{230}Th > ^{238}U > ^{232}Th); F3 (^{238}U > ^{234}U > ^{226}Ra > ^{210}Po > ^{230}Th > ^{232}Th), and (F1+F2+F3): (^{226}Ra > ^{234}U ~ ^{238}U > ^{210}Po > ^{230}Th > ^{232}Th).
- We highlight that in the F1 liquid fraction a high ^{234}U/^{238}U activity ratio was found (2.7). This result confirms preferential leaching of ^{234}U in relation to ^{238}U found for the majority of soils and sediments. On the other hand, the ^{230}Th/^{232}Th isotopic ratios value are much higher than 1 in most fractions, except for residual fraction where it is close to one.

3.5. ASSESMENT OF NATURAL RADIONUCLIDES MOBILITY IN A PHOSPHOGYPSUM DISPOSAL AREA

S. Pérez-Moreno[1], M.J. Gázquez[2], R. Pérez-López[3], I. Vioque[4], J.P. Bolivar[1]*

[1]Department of Integrated Science Physics, University of Huelva, Huelva, Spain
[2]Department of Applied Physics, University of Cádiz, Cádiz, Spain
[3]Department of Earth Sciences, University of Huelva, Huelva, Spain
[4]Department of Applied Physic, University of Seville, Seville, Spain

Abstract

The phosphogypsum (PG) stacks located at Huelva (SW Spain) store about 100 Mt of PG, and covers a surface of 1000 ha. It has been very well established that this waste contains significant U-series radionuclides concentrations, with average activity concentrations rounding the 650, 600, 400 and 100 Bq kg^{-1} for ^{226}Ra, ^{210}Pb, ^{230}Th and ^{238}U, respectively. However, the radionuclide emissions from this repository into the environment by the aquatic pathway will depend on the mobility of each radionuclide.

The mobility of the natural radionuclides (U-isotopes, Th-isotopes, ^{226}Ra, and ^{210}Po) contained in the PG piles were evaluated by using the optimized BCR sequential extraction procedure (BCR "Community Bureau of Reference"). The radionuclides were measured in the liquid fractions by alpha-particle spectrometry with semiconductor PIPS detectors. In addition, to validate the obtained results with the BCR methodology, waters from different locations of the PG piles (pore-water, perimeter channel and edge outflow leachates) were taken.

The results show that uranium isotopes present the same and highest mobility, being its total mobile fraction around 70%, while ^{210}Po and ^{226}Ra present a total mobility of about 50% and 30%, respectively. And finally, the Th-isotopes have very low mobility (mobile fraction < 5%), being fixed to the residual fraction. It is noteworthy that this behaviour has been also found in the water samples taken from the stacks, demonstrating that this sequential leaching operational methodology is a useful tool for assessing the release capacity of radionuclides by inorganic wastes.

3.5.1. INTRODUCTION

Phosphogypsum (PG) is a waste generated in the production of phosphoric acid, which widely comes from the chemical treatment of phosphate rock ($Ca_5(PO_4)_3F$) with sulphuric acid (H_2SO_4) [Eq. 1]. It is estimated that about 4.5-5 tons of PG per ton of phosphoric acid produced are generated. The phosphate ore contains impurities of major elements (Si, Al, Fe and Ti), trace elements (Sr, Cr, V, Zn, Y, Ni, Ba), and natural radionuclides coming from U and Th series, which are partially transferred into the PG during the industrial process (Bolivar et al., 1995 and 1996). This waste is currently considered a NORM (naturally occurring radioactive material).

$$Ca_5(PO_4)_3F + 5H_2SO_4 + 10H_2O \rightarrow 3H_3PO_4 + 5\ CaSO_4\cdot 2H_2O + HF \quad \text{[Eq. 3.37]}$$

PG is mainly composed by the gypsum mineralogical phase ($CaSO_4\cdot 2H_2O$). In addition, other minor phases, such as quartz (SiO_2), chukhrovite ($Ca_4AlSi(SO_4)F_{13}\cdot 12(H_2O)$ and fluorite (CaF_2), are also present (Rentería-Villalobosa et al., 2010; Azaroual et al., 2012; Khamar et al., 2014). The worldwide PG generation is estimated to be around 280 Mt per year. This waste is mostly disposed of without any treatment, usually by dumping in large stockpiles. These are generally located in coastal areas close to phosphoric acid plants, where they occupy large land areas and cause serious environmental damage (Tayibi et al., 2009).

In Spain, concretely in Huelva, the production of phosphoric acid, and hence the generation of PG, began in 1965 and remained active for 45 years until 31 December 2010. During this period about 100 Mt of PG were stored in piles that reach up to 30 m in height, covering a surface of approximately 1000 ha. These deposits are located at the confluence of the Tinto and Odiel rivers, an estuarine area of salt marshes with a high ecological value, declared as Biosphere Reserve by UNESCO in 1983, which is known as “Ría de Huelva”. In 1992, around 30% of the disposal area (zone 1) was restored, covering it with a 30 cm layer of natural soil and vegetation (Mas, et al., 2001), Figure 3.32. Subsequently, another area (zone 4) was restored (20% of the total area) with more complex cover that comprises the following layers (in ascending order): a 1 m layer of building wastes, a 2 m layer of theoretically inert industrial wastes and 30–50 cm layer

of topsoil (Mas et al., 2006; Directive 61/CE, 1996). However, nowadays about 50% of the disposal area is openly exposed to the environment weathering (unrestored areas; zones 2 and 3), see Figure 3.32. The piles have a series of perimeter channels for collecting leachates from the PG weathering, but there are numerous points and diffuse sources of edge outflows that discharge pollution to the estuary (Pérez-López et al., 2016).

The U-series radionuclides activity concentrations of the ore used in Huelva ranged from 1300 to 1700 Bq kg^{-1}, being them in secular equilibrium. During the industrial process of phosphoric acid manufacture the radioactive equilibrium is broken, and each radionuclide is independently distributed according to its chemical behaviour. It has been estimated that more than 95% of the total ^{226}Ra, ^{210}Pb, and ^{210}Po contained in the phosphate rock is transferred into the PG, whereas the uranium is transferred variably between 5% and 20% (Bolivar et al., 2009).

Several studies have tried to evaluate the environmental impact of the disposal areas, measuring the total activity concentration of PG (Rutherford et al., 1994 and 1995; Martin et al., 1995; Bolivar et al., 1996, 2000 and 2002; Dueñas et al., 2010). However, the total contaminant content in a waste is not a good measure of its potential risk, since under normal environmental conditions only a proportion of the total contaminant content will be mobile and/or bioavailable. The mobility and toxicity of elements in the environment depend on the chemical form to which they are bound to the solid phase (Pérez-López et al., 2007).

Sequential extraction methods have been widely applied to assess the chemical speciation of metals. The most significant advance in sequential extraction studies came in 1987 when the European Commission launched the BCR (Community Bureau of Reference) programme aimed at the harmonization of extraction procedures. In 1993 a standard sequential extraction procedure, known as BCR (Thomas et al., 1994), was proposed. Inconsistencies in trace element extraction using the BCR protocol led to different investigations (Sahuquillo et al., 1999; Rauret et al., 1999) that recommended the development of an optimized BCR procedure (1999). This procedure has been applied in previous studies to determine the dynamic and/or fate of the impurities contained in the PG (Pérez-López et al., 2010 and 2011), but this BCR procedure has not been applied until this date to evaluate the mobility of natural radionuclides. Nevertheless, a few works

have studied the mobility of natural radionuclides in PG samples applying only one extractant agent, such as distilled water, seawater or rainwater (Haridasan et al., 2002; Aguado et al., 2005; Santos et al., 2006; Ceballos et al., 2017). But, these extractants do not reproduce all local weathering conditions, which concretely in Huelva stacks are: (1) acid water leaching not only due to rainy periods but also to tidal cycles with the Tinto River estuarine water, which exhibit low pH values due to abandoned mining activity (Hierro et al., 2014), (2) oxidising conditions in the non-saturated zone of the PG stack, and (3) reducing conditions imposed by the organic matter-rich marshland contacting with the stack in the saturated zone (Pérez-López et al., 2015).

Taking into account these previous facts, the main objective of this work was to assess the mobility of natural radionuclides contained in the PG stored in Huelva (SW Spain), ^{210}Po, U-isotopes, Th-isotopes, and ^{226}Ra, applying the optimized BCR sequential extraction procedure. In addition, the potential application of BCR sequential extraction will be validated by comparison with the activity concentrations found in pore-waters, edge outflow leachates reaching the Estuary of Huelva and process water of perimeter channel. In the same way, this BCR procedure could be used to analyse the mobility of natural radionuclides from others world PG stacks.

3.5.2. MATERIALS AND METHODS

3.5.2.1. Samplings

PG samples were collected at different depths from two bore-holes (U and D cores) carried out using a soil-sampling auger at the unrestored zone 3 of the stack in May 2013 (Figure 3.32). Seven samples were collected from the U core; whereas six samples were taken from the D core, which was performed inside an inactive perimeter channel to easily access the deepest part of the stack. The samples were taken approximately at intervals of 50 cm, being the thickness of each sample around 5 cm. In the laboratory the pore-water was extracted from solid samples using suction cup lysimeters and hollow-fibre tube sampler devices (Rhizon samplers; Eijkelkamp Agrisearch Equipment, Netherlands). Subsequently, solid samples were frozen and then lyophilized using a freeze-dryer.

In addition, PG wastewaters in zone 3 of PG stack were sampled, corresponding to edge outflow leachates reaching the Estuary of Huelva (from E1 to E12), and process water samples were taken at the perimeter channel (from P1 to P3), in order to confirm the mobility of radionuclides in the PG disposal area conditions.

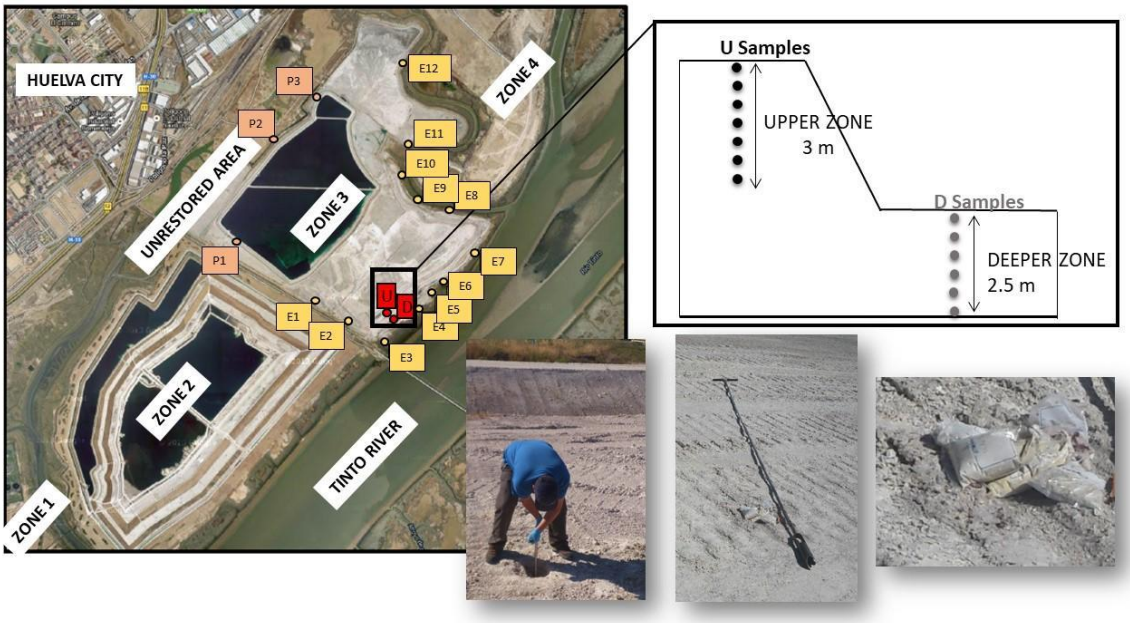

Figure 3.32. *Location of sampling points and sampling profile in the pile.*

3.5.2.2. Physico-Chemical Characterization Techniques

The pH, redox potential (Eh) and electrical conductivity (EC) of the solutions were measured in the field, except for the pore-waters that were measured immediately in the laboratory after extraction, using a portable Multiparametric Crison Mm 40+ meter, which was calibrated prior to the experiments. Measured redox potential was referenced to standard hydrogen electrode (Eh) as proposed by Nordstrom and Wilde (1998).

3.5.2.3. Optimised BCR Sequential Extraction Procedure

In order to study in detail the partitioning of radionuclides in the PG, the following BCR sequential extraction procedure was applied to the solids using around 1 g of each dried and homogenized sample. A summary of the sequential extraction procedure in Table 3.22 is shown, and more detailed information can be found elsewhere (Sahuquillo et al., 1999; Rauret et al., 1999). This procedure was already tested and validated for mobility

of natural radionuclides (^{210}Po, ^{234}U, ^{238}U, ^{230}Th, ^{232}Th and ^{226}Ra) by using the BCR-701 certified reference material, being these results published in a previous work (Pérez-Moreno et al., 2018).

Step	Fraction	Nominal target phases	Extractant (1 g of dry solid)	Conditions
F1	Water/acid soluble and exchangeable	Soluble species, carbonates and cation exchange sites	40 mL 0.11M CH_3COOH	Shaking during 16 h. at room temperature (RT).
F2	Reducible	Iron and manganese oxyhydroxides	40 mL 0.5M $NH_2OH{\cdot}HCl$ (pH 2)	Shaking during 16 h. at RT.
F3	Oxidizable	Organic matter and sulphides	10 mL 8.8 M H_2O_2 (pH 2) + 10 mL 8.8 M H_2O_2 (pH 2), then 50 mL 1M NH_4OAc (pH 2)	1h at RT, 1 h at 85 ºC; 1 h a 85 ºC; and shaking during 16 h. at RT.
F4	Residual	Non-mobile fraction	10 mL aqua regia 3:1 (12M HCl + 15.8M HNO_3)	16 h at room temperature, and then to heat on hot plate during 2 h under reflux.

Table 3.22. *Modified BCR sequential extraction procedure.*

The total recovery (R) of a specific radionuclide along the application of the BCR is defined as the sum of the activity concentrations recovered for all fractions (F_i) in relation to the total activity (T) of the PG sample directly measured, and will be given by the Eq. 3.38:

$$R\ (\%) = \frac{\sum_{i=1}^{i=4} Fi}{T} \cdot 100 \qquad \text{[Eq. 3.38]}$$

In addition, the transfer factors (TF) were also determined. The transfer factor (%) is defined as the amount of element that is transferred to the liquid phase in each step (*Fi*), in relation to the total concentration found in the solid sample (sum of concentrations for all fractions, *S*), so it is calculated by the next equation (Eq. 3.39):

$$TF\ (\%) = \frac{Fi}{S} 100 \qquad \text{[Eq. 3.39]}$$

3.5.2.4. Alpha Spectrometry

The activity concentrations of the radionuclides in the samples were measured by alpha-particle spectrometry by using a sequential radiochemical procedure based on the tributylphosphate (TBP), and ion exchange resins for the radioelements purification, where the Po, U, Th and Ra isotopes were isolated (Holm and Fukai, 1977). After the isolation, the different radioelements were electrodeposited onto stainless steel discs (cases of U, Th and Ra), while the Po was self-deposited onto silver discs (Flynn, 1968). Then, the activity concentrations of the different isotopes were measured using ion implantation Si (PIPS) semiconductor detectors, EG & G Ortec. For these determinations, the samples were spiked with accurately known activities of ^{232}U, ^{229}Th and ^{209}Po. For every 5 samples a blank was measured, obtaining detection limits for the measured radionuclides around 0.4-1.2 mBq.

3.5.3. RESULTS AND DISCUSSION

3.5.3.1. Physical-Chemical parameters

The physico-chemical parameters analysed in the pore-water show significant variations along the profiles (Table 3.23). The pH decreases with depth from 3.5 to 2.8 along the U core, and the pH is practically constant in D core, and around 2.0. The EC values are of around 3.5 mS cm^{-1} in the shallowest part but increases one order of magnitude (36 - 60 mS cm^{-1}) in the deeper zone. On the contrary, there is not significant differences in the redox potential (Eh) of both cores samples. These results are in concordance with previous hydrogeochemical studies (Aguado et al., 2005), where low pH values are related to content of phosphoric acid and high EC associated with the presence of chlorides.

	Code	Depth (m)	pH	EC (mS/cm)	Eh (mV)
U core	**U1**	0	-	-	-
	U2	0.5	-	-	-
	U3	1	-	-	-
	U4	1.5	3.55	3.38	419
	U5	2	2.89	3.41	448
	U6	2.5	3.03	3.40	471
	U7	3	2.82	3.83	464
	Average*		3.07 ± 0.17	3.51 ± 0.11	451 ± 12
D core	**D1**	0	-	-	-
	D2	0.5	2.05	44.0	480
	D3	1	2.03	39.8	445
	D4	1.3	1.97	36.7	432
	D5	2	2.02	35.5	415
	D6	2.5	2.05	59.7	385
	Average*		2.02 ± 0.02	43.1 ± 4.4	432 ± 16

Table 3.23. *Physico-chemical parameters of pore-water solutions.*

The main physico-chemical characteristics of the edge outflow leachates (E1-E12) and the process waters collected in perimeter channels (P1-P3) are their extreme acidity (pH < 2), especially in the perimeter channel (pH = 1.42 ± 0.14), and high EC values ($\bar{E}$: 40.3 ± 2.9 mS cm^{-1}; $\bar{P}$: 59.4 ± 2.5 mS cm^{-1}) (Table 3.24). The values observed for the edge outflows are very similar to those found in the pore-water of the deeper zone, which is expectable since the excess of groundwater leads to the formation of these acid leakages at the toe of the stack. On the other hand, the Eh values are slightly higher in perimeter channel (583 ± 36) than edge outflow leachate (483 ± 15).

	pH	EC (mScm^{-1})	Eh (mV)
Edge outflow leachate			
E1	1.83	61.8	579
E2	1.98	27.0	527
E3	2.10	31.4	452
E4	2.17	31.4	460
E5	2.06	38.6	451
E6	2.03	46.9	432
E7	2.04	34.4	450
E8	2.13	38.8	447
E9	1.93	47.7	453
E10	2.17	34.3	451
E11	1.93	50.4	561
E12	2.02	40.4	532
Average ($\bar{E}$)*	2.03 ± 0.03	40.3 ± 2.9	483 ± 15
Perimeter channel			
P1	1.32	54.4	511
P2	1.24	62.3	629
P3	1.69	61.4	606
Average ($\bar{P}$)*	1.42 ± 0.14	59.4 ± 2.5	582 ± 36

Table 3.24. *Physico-chemical parameters of edge outflow leachates and perimeter channel process waters.* Standard uncertainty (1 σ) of the average has been calculated as the standard deviation of the mean, σ = Sx/(n)1/2.*

3.5.3.2. Characterization of phosphogypsum in depth

Total activity concentrations (Bq kg^{-1}) of radionuclides in PG versus depth are shown in Figures 3.33-3.36. The concentrations of ^{210}Po, ^{226}Ra and ^{230}Th range from 500 to 1000 Bq kg^{-1} in both cores samples (U and D samples). Both ^{234}U and ^{238}U activity concentrations are similar (secular equilibrium), and range from 70 to 500 Bq kg^{-1}. In contrast, the concentrations of ^{232}Th are very low, ranging from 5 to 40 Bq kg^{-1}. These results are in agreement with previous studies developed in this zone (Bolivar et al., 2000 and 2002; Dueñas et al., 2010). In addition, these radionuclides levels are in accordance with measurements made previously in the production process of phosphoric acid (Bolivar et al., 2009). It is worth highlighting that there are no significant differences between the average concentrations of both cores (Z score < 2 for all radionuclides). The high dispersion of concentrations is probably due to differences in the used ore or changes in the phosphoric acid production process.

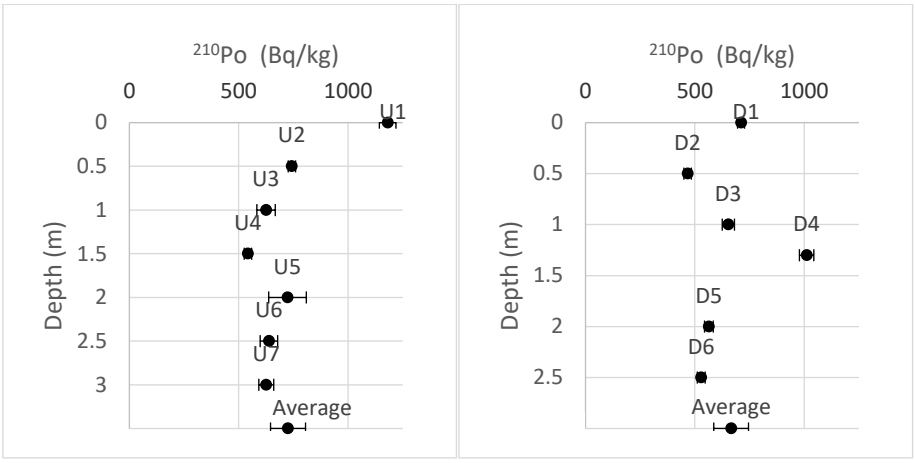

Figure 3.33. *Total activity concentrations (Bq kg^{-1}) of ^{210}Po in depth.*

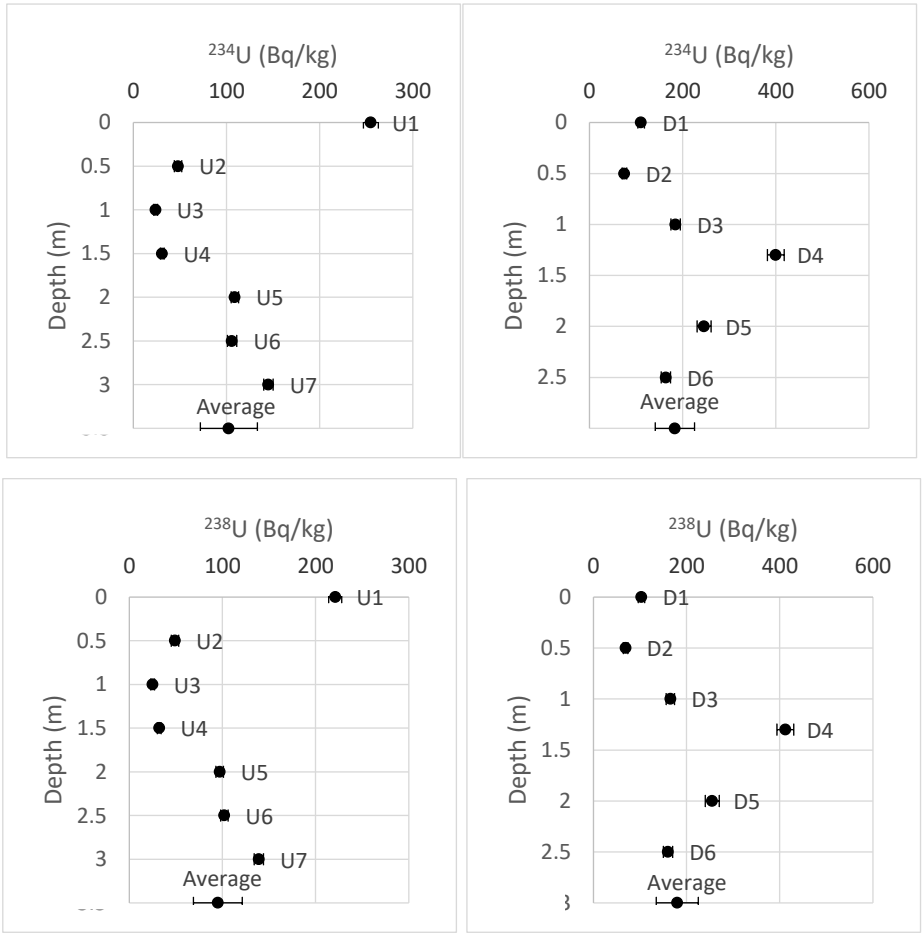

Figure 3.34. *Total activity concentrations (Bq kg^{-1}) of U-isotopes in depth.*

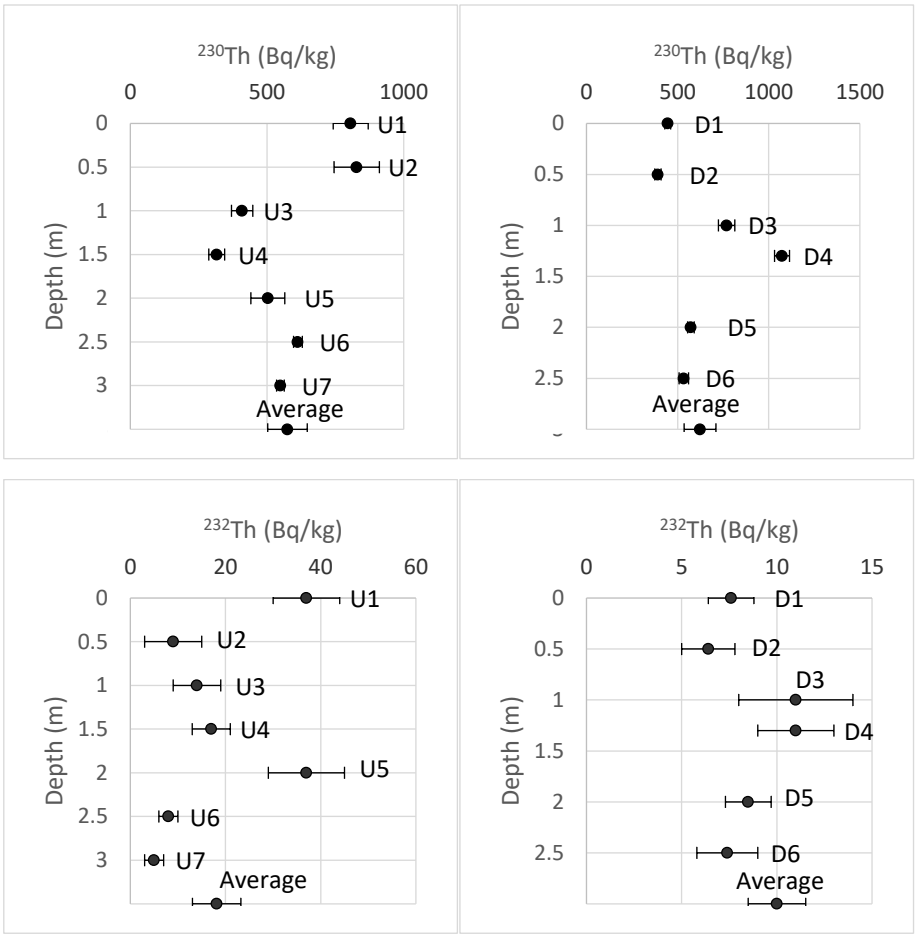

Figure 3.35. *Total activity concentrations (Bq kg^{-1}) of Th-isotopes in depth.*

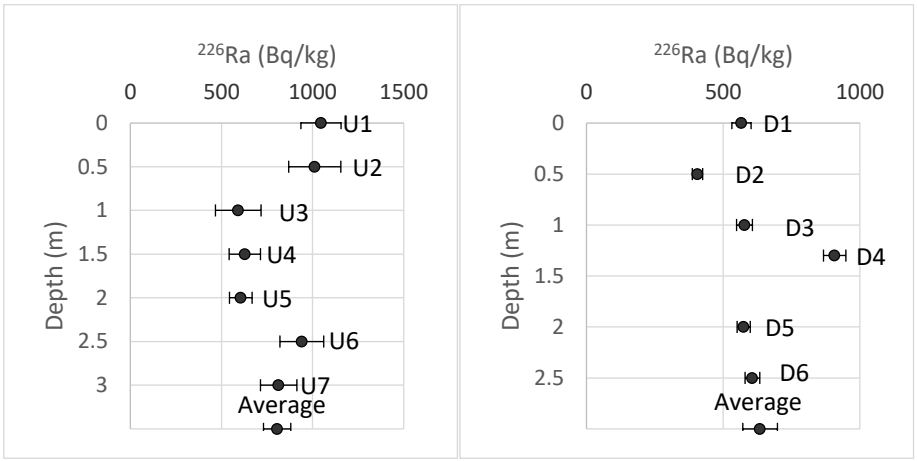

Figure 3.36. *Total activity concentrations (Bq kg^{-1}) of ^{226}Ra in depth.*

The most significant activity ratios for both cores are compiled in Table 3.25. It can be observed that ^{234}U/^{238}U value is the unity by considering the experimental uncertainties, as well as the ^{210}Po/^{226}Ra ratios. At the same time, the ^{230}Th/^{232}Th values are very high, being more than 50 the relation between ^{230}Th and ^{232}Th in almost all samples, which is

the value found in the raw material used in the industrial process (Bolivar et al., 2009). In contrast, the $^{234}U/^{230}Th$ activity ratios are about 0.14 and 0.3 in U and D samples, respectively. These values are also reported by other authors (Rentería-Villalobosa et al., 2010).

	$^{234}U/^{238}U$	$^{230}Th/^{232}Th$	$^{234}U/^{230}Th$	$^{210}Po/^{226}Ra$
U1	1.15 ± 0.05	22 ± 4	0.32 ± 0.03	1.13 ± 0.12
U2	0.98 ± 0.11	92 ± 62	0.06 ± 0.01	0.73 ± 0.11
U3	0.96 ± 0.11	29 ± 11	0.06 ± 0.01	1.06 ± 0.23
U4	0.97 ± 0.09	19 ± 5	0.10 ± 0.01	0.86 ± 0.12
U5	1.12 ± 0.06	14 ± 3	0.22 ± 0.03	1.19 ± 0.19
U6	1.04 ± 0.06	77 ± 19	0.17 ± 0.01	0.68 ± 0.10
U7	1.04 ± 0.05	110 ± 44	0.26 ± 0.01	0.77 ± 0.10
Average*	**1.02 ± 0.03**	**57 ± 17**	**0.14 ± 0.04**	**0.88 ± 0.08**
D1	1.08 ± 0.10	59 ± 10	0.25 ± 0.02	1.25 ± 0.08
D2	1.09 ± 0.11	61 ± 14	0.19 ± 0.02	1.15 ± 0.07
D3	1.12 ± 0.09	70 ± 20	0.24 ± 0.02	1.13 ± 0.07
D4	0.97 ± 0.06	98 ± 18	0.37 ± 0.02	1.11 ± 0.06
D5	0.96 ± 0.08	67 ± 10	0.43 ± 0.03	0.98 ± 0.05
D6	1.03 ± 0.09	72 ± 16	0.31 ± 0.02	0.87 ± 0.05
Average*	**1.04 ± 0.03**	**71 ± 6**	**0.30 ± 0.04**	**1.08 ± 0.06**

Table 3.25. *Activity ratios of $^{234}U/^{238}U$, $^{230}Th/^{232}Th$, $^{234}U/^{230}Th$ and $^{210}Po/^{226}Ra$ in both cores samples.*Standard uncertainty (1 σ) has been calculated as the standard deviation of the mean, σ = Sx/(n)1/2.*

3.5.3.3. Mobility of Natural Radionuclides in Phosphogypsum

POLONIUM

The activity concentrations (expressed in Bq kg^{-1} of PG) of ^{210}Po found in each liquid fraction of the BCR sequential extraction are shown in Table 3.26. The highest activity concentrations of polonium are found in the residual (non-mobile) fraction of both cores. At the same time, an important proportion of ^{210}Po (F1+F2+F3) could be mobilized to the environment depending on the weathering conditions. The water/acid soluble and

exchangeable fraction (F1) shows the minimum activity concentration, especially in D core. On the other hand, polonium does not show a clear tendency for the reducible (F2) or oxidizable fraction (F3), due to the activity concentration do not differ between both fractions. It is noteworthy that there are no significant differences between the average concentrations of each fractions of both cores. The average of ^{210}Po recovery is around of 70 %.

Samples	F1 (Bq kg^{-1})	F2 (Bq kg^{-1})	F3 (Bq kg^{-1})	F4 (Bq kg^{-1})
U1	19 ± 1	335 ± 18	6 ± 2	494 ± 18
U2	43 ± 2	97 ± 5	38 ± 3	391 ± 14
U3	106 ± 5	79 ± 6	82 ± 4	170 ± 12
U4	23 ± 2	73 ± 7	74 ± 4	130 ± 24
U5	33 ± 2	77 ± 8	103 ± 5	130 ± 9
U6	27 ± 2	94 ± 9	106 ± 6	180 ± 9
U7	38 ± 2	112 ± 28	177 ± 8	121 ± 11
Average*	**41 ± 11**	**124 ± 36**	**84 ± 21**	**231 ± 56**
D1	6.1 ± 1.1	111 ± 3	121 ± 5	368 ± 14
D2	7.8 ± 1.3	47 ± 2	89 ± 3	130 ± 7
D3	3.1 ± 0.5	51 ± 2	142 ± 4	208 ± 4
D4	2.4 ± 0.4	40 ± 2	178 ± 5	601 ± 12
D5	15 ± 1	66 ± 3	104 ± 3	249 ± 6
D6	11 ± 1	45 ± 2	124 ± 4	258 ± 6
Average*	**7.6 ± 2.0**	**60 ± 11**	**126 ± 13**	**302 ± 68**

Table 3.26. *Activity concentration (Bq kg $^{-1}$) of ^{210}Po in each fraction of both cores samples. *Standard uncertainty (1 σ) has been calculated as the standard deviation of the mean, σ = Sx/(n)1/2.*

The transfer factor TF (%) were plotted in Figure 3.37. The ^{210}Po is portioned between fractions in both cores as follows: F4 > F3 ~ F2 > F1. It is of standing out that the TF in F1 fraction is slightly higher in U core than in D core. This fact is probably related to the pH conditions, being D samples subjected to lower pH, and part of this polonium has been already released. So, the speciation of ^{210}Po seems to follow the same tendency in both cores with a certain dispersion, independently of the sampling point and the depth.

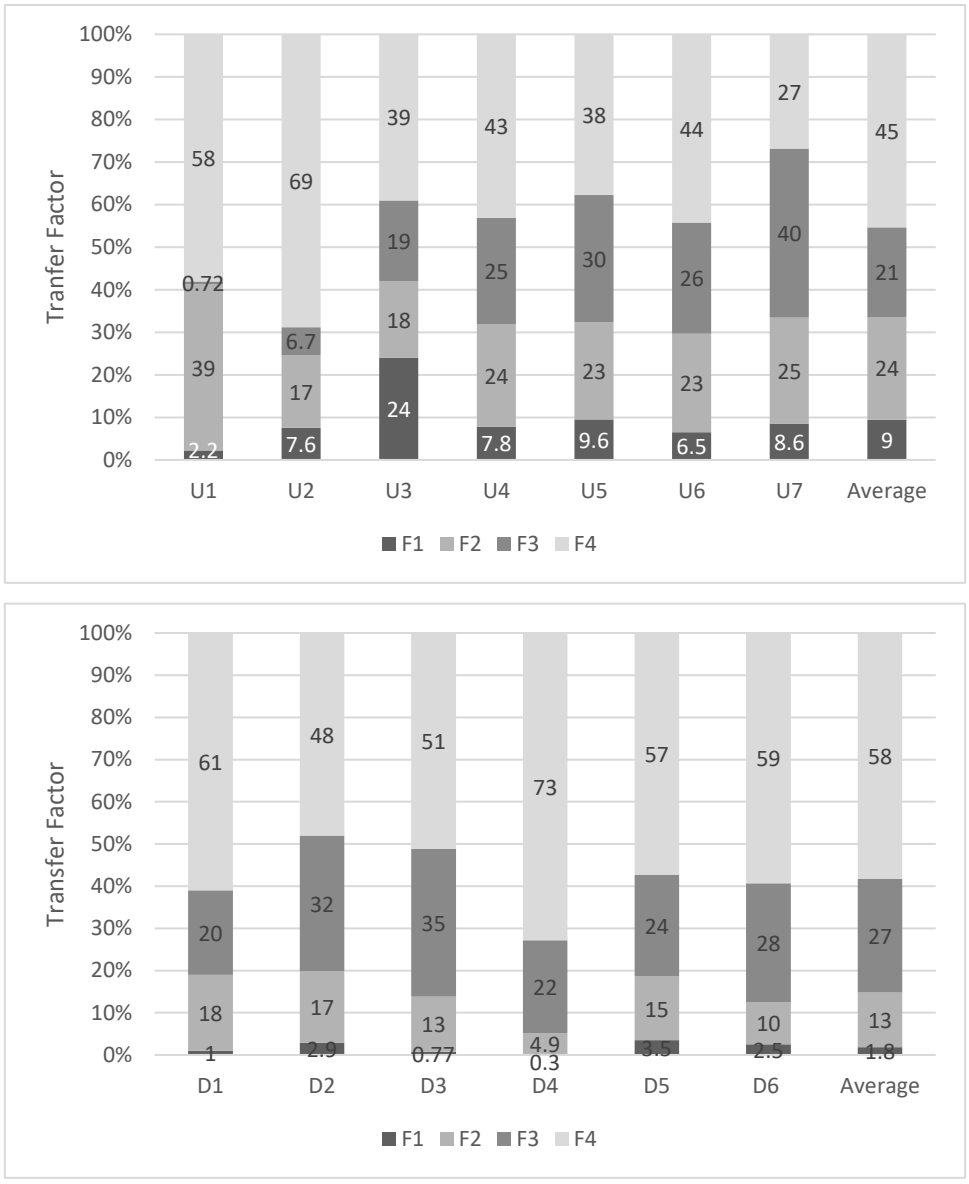

Figure 3.37*. TF (%) of ^{210}Po in each BCR fraction for PG samples of both cores.*

URANIUM

Table 3.27 shows the activity concentrations (Bq kg^{-1}) measured for uranium isotopes (^{234}U and ^{238}U) in each fraction from BCR procedure for the two sampling points. The total recovery (%) of U-isotopes varies between 70-100%. Similar activity concentrations of ^{234}U and ^{238}U are found in each fraction of both cores. In residual and oxidizable fractions are found the higher activity concentrations and the lowest activity is presents in reducible fraction. It is stand out that the activity concentration of these fraction are not statistically different in both cores. On the other hand, F1 contain major activity concentration in D core than U core, that possibly is related to the pH condition under

these samples are subjected, in which U-isotopes are more easily released into the environment.

	F1 (Bq kg^{-1})	F2 (Bq kg^{-1})	F3 (Bq kg^{-1})	F4 (Bq kg^{-1})
		^{234}U		
U1	37±3	31±2	46±4	67±5
U2	19±2	5.0±1.4	27±3	<LD
U3	4.1±1.0	0.14±1.23	2.1±2.5	8.6±1.5
U4	6.5±1.6	1.7±1.5	6±2	2.6±1.7
U5	5.1±1.6	14±2	40±4	7.6±1.9
U6	5.1±1.6	5.6±1.5	31±3	30±6
U7	5.9±1.7	16±2	63±4	17±3
Average*	**12±5**	**10±4**	**31±8**	**22±10**
D1	33±1	10±1	47±2	30±2
D2	26±1	9.9±1.0	30±2	9.2±0.9
D3	35±1	11±1	99±5	43±2
D4	56±2	9.4±1.2	176±13	195±6
D5	51±2	18±1	137±7	50±6
D6	20±1	7.7±0.7	77±3	38±2
Average*	**37±6**	**11±1**	**94±23**	**52±27**
		^{238}U		
U1	34±2	32±2	41±2	64±4
U2	22±2	6.3±1.3	22±2	<LD
U3	4.3±0.8	0.36±1.09	4.5±1.6	8.3±2.5
U4	8.3±1.4	3.7±1.5	6.1±1.1	2.7±1.1
U5	6.6±1.2	15±2	32±2	7.7±1.4
U6	8.3±1.4	8.4±1.5	32±3	25±2
U7	7.3±1.4	18±2	56±3	16±2
Average*	**13±4**	**12±4**	**28±7**	**21±9**
D1	33±1	11±1	46±2	29±1
D2	25±1	10±1	28±2	8.4±0.7
D3	36±2	10±1	99±5	42±1
D4	57±2	8.5±3.2	189±7	191±5
D5	48±2	16±1	133±7	49±2
D6	20±1	7.2±1.2	77±3	37±1
Average*	**37±6**	**10±1**	**95±24**	**59±27**

Table 3.27. *Activity concentration (Bq kg $^{-1}$) of ^{234}U and ^{238}U in each fraction of both cores samples. *Standard uncertainty (1 σ) has been calculated as the standard deviation of the mean, σ = Sx/(n)1/2.*

According to the TF (Fig. 3.38), uranium isotopes present high mobility since about 70-75% of the total concentration found in PG could be released depending on the

environmental conditions, where soluble (F1: 21-26%) and oxidizable fractions (F3: 41-47%) are the most relevant. These data means that un important fraction of U contained in PG samples is in form of U(IV), that can be oxidized to U(VI), when the conditions change from anoxic to oxic. That specie constitute the most mobile form of uranium (Lee et al., 2017; UNSCEAR, 2016). On the other hand, only 25-30% of the total is bound to the residual fraction.

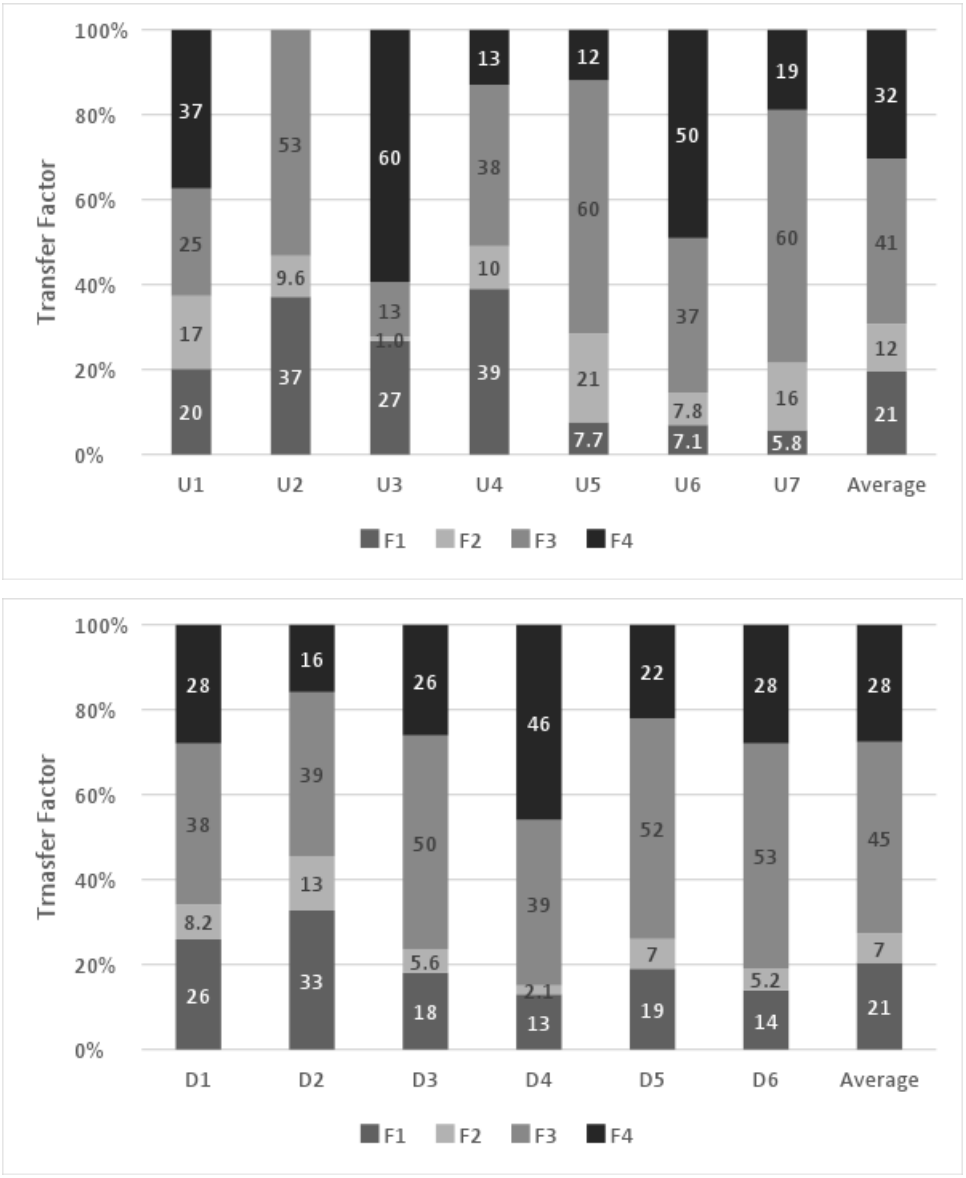

***Figure 3.38**. TF (%) of ^{234}U in each BCR fraction for PG samples for PG samples of both cores.*

The potential fractionation of uranium isotopes can be also tested by analysing the activity ratios. These activity ratios are one in all fractions taking into account the experimental

uncertainties. This fact reveals that both uranium isotopes are transferred in the same way to the liquid fraction, and that the material has been formed recently from dissolution since the preferential leaching mechanisms are not manifested. Previous studies (Pérez-Moreno et al., 2018) have found a high $^{234}U/^{238}U$ disequilibria in fraction F1 when BCR is applied to soil samples.

THORIUM

The activity concentrations (Bq kg^{-1}) of thorium isotopes (^{230}Th and ^{232}Th) for each BCR step are compiled in Table 3.28. The thorium isotopes are practically only detected in the residual fraction (F4) in both core samples, around 98% according the TF (Figure 3.39). These results are independent of the pH, CE or Eh conditions in depth. This fact is reported by other studies (Santschi ET AL., 2006), which indicate that thorium has a very low mobility under most of environmental conditions mainly due to the high stability of the insoluble oxide ThO_2 and the strongly resistant nature of its carrier minerals such as monazite ((Ce, La, Th, U)PO_4) and zircon ($ZrSiO_4$). The results also indicate that nearly total thorium isotopes are recovered (85-100%).

	F1 (Bq kg^{-1})	F2 (Bq kg^{-1})	F3 (Bq kg^{-1})	F4 (Bq kg^{-1})
		^{230}Th		
U1	< DL	< DL	18±9	927±27
U2	< DL	1.5±1.2	<DL	785±30
U3	<DL	< DL	1.3±1.2	348±18
U4	<DL	6.0±1.7	4.2±1.3	251±10
U5	<DL	6.2±4.0	4.5±1.4	365±15
U6	<DL	5.1±1.5	<DL	386±17
U7	<DL	3.7±1.2	<DL	371±35
Average*	**< DL**	**3.9±0.8**	**7.0±2.8**	**490±97**
D1	<DL	< DL	6.2±1.0	273±10
D2	< DL	< DL	9.3±1.6	416±15
D3	<DL	< DL	10±1	828±36
D4	<DL	<DL	6.8±0.8	1166±58
D5	<DL	< DL	18±1	510±14
D6	< DL	< DL	8.2±0.8	430±12
Average*	**< DL**	**< DL**	**9.8±1.8**	**604±135**
		^{232}Th		
U1	< DL	<DL	<DL	29±2
U2	< DL	<DL	<DL	7.2±1.5
U3	<DL	<DL	<DL	11±2
U4	<DL	<DL	<DL	10±2
U5	<DL	<DL	<DL	36±3
U6	<DL	<DL	<DL	6.3±1.4
U7	<DL	<DL	<DL	3.8±2.7
Average*	**< DL**	**< DL**	**<DL**	**15±5**
D1	<DL	<DL	<DL	2.8±0.4
D2	<DL	<DL	<DL	4.1±0.5
D3	<DL	<DL	<DL	8.9±1.0
D4	<DL	<DL	<DL	11±2
D5	<DL	<DL	<DL	9.4±0.6
D6	< DL	<DL	<DL	6.5±0.5
Average*	**< DL**	**< DL**	**<DL**	**7.1±1.3**

Table 3.28. *Activity concentration of ^{230}Th (Bq kg $^{-1}$), and recovery (%) in each fraction of both cores samples. *Standard uncertainty (1 σ) has been calculated as the standard deviation of the mean, σ = Sx/(n)1/2. DL = 1 Bq kg^{-1}*

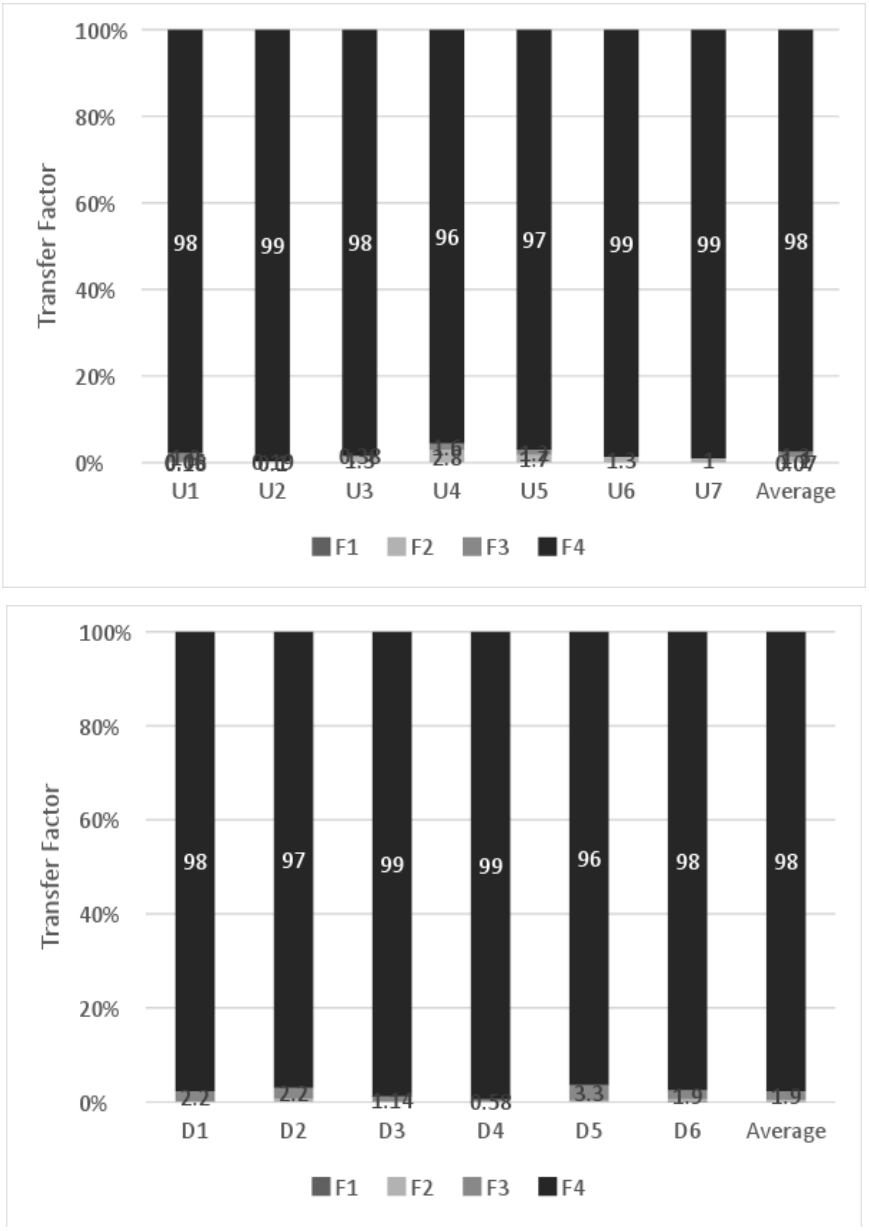

Figure 3.39. *TF (%) of ^{230}Th in each BCR fraction for PG samples with depth.*

RADIUM

Table 3.29 displays the ^{226}Ra activity concentration in each fraction from BCR procedure for the two sampling cores. The results show a high activity concentration in F4 for most PG samples. On the contrary the minimum activity concentration is detected in F1, being no different the value found in both cores. On the other hand, F3 contains a higher activity concentration of radium when is compared with F2, indistinctly in all the samples. The total recovery of radium is around 80%.

Concerning the TF (Fig. 3.40), both cores follow the same tendency, but the J core displays more homogeneity in the fraction distribution. All samples are characterised by a high percentage in the non-mobile fraction, being the mobile fraction around 30-50% of total radium contained in the PG.

	F1 (Bq kg^{-1})	**F2 (Bq kg^{-1})**	**F3 (Bq kg^{-1})**	**F4 (Bq kg^{-1})**
U1	14±2	44±10	59±8	291±55
U2	6.5±1.1	24±5	71±4	383±64
U3	3.5±0.7	19±4	69±8	304±37
U4	5.1±1.2	7.1±4.6	39±6	298±30
U5	6.7±2.1	22±3	73±9	167±22
U6	8.9±1.8	4.6±2.8	57±14	188±15
U7	11±5	17±3	138±19	207±10
Average*	**8.0 ± 1.4**	**20 ± 5**	**72 ± 12**	**263 ± 29**
D1	13±2	45±4	257±20	135±13
D2	7.2±0.8	32±2	224±17	79±10
D3	4.8±0.8	46±6	68±6	481±26
D4	2.9±0.7	33±3	80±11	679±38
D5	13±2	56±4	212±33	179±8
D6	11±1	62±7	192±51	175±8
Average*	**8.7 ± 1.8**	**46 ± 5**	**172 ± 32**	**288 ± 97**

Table 3.29. *^{226}Ra activity concentration (Bq/kg) and recovery (%) in of both cores samples. *Standard uncertainty (1 σ) has been calculated as the standard deviation of the mean, σ = Sx/(n)1/2.*

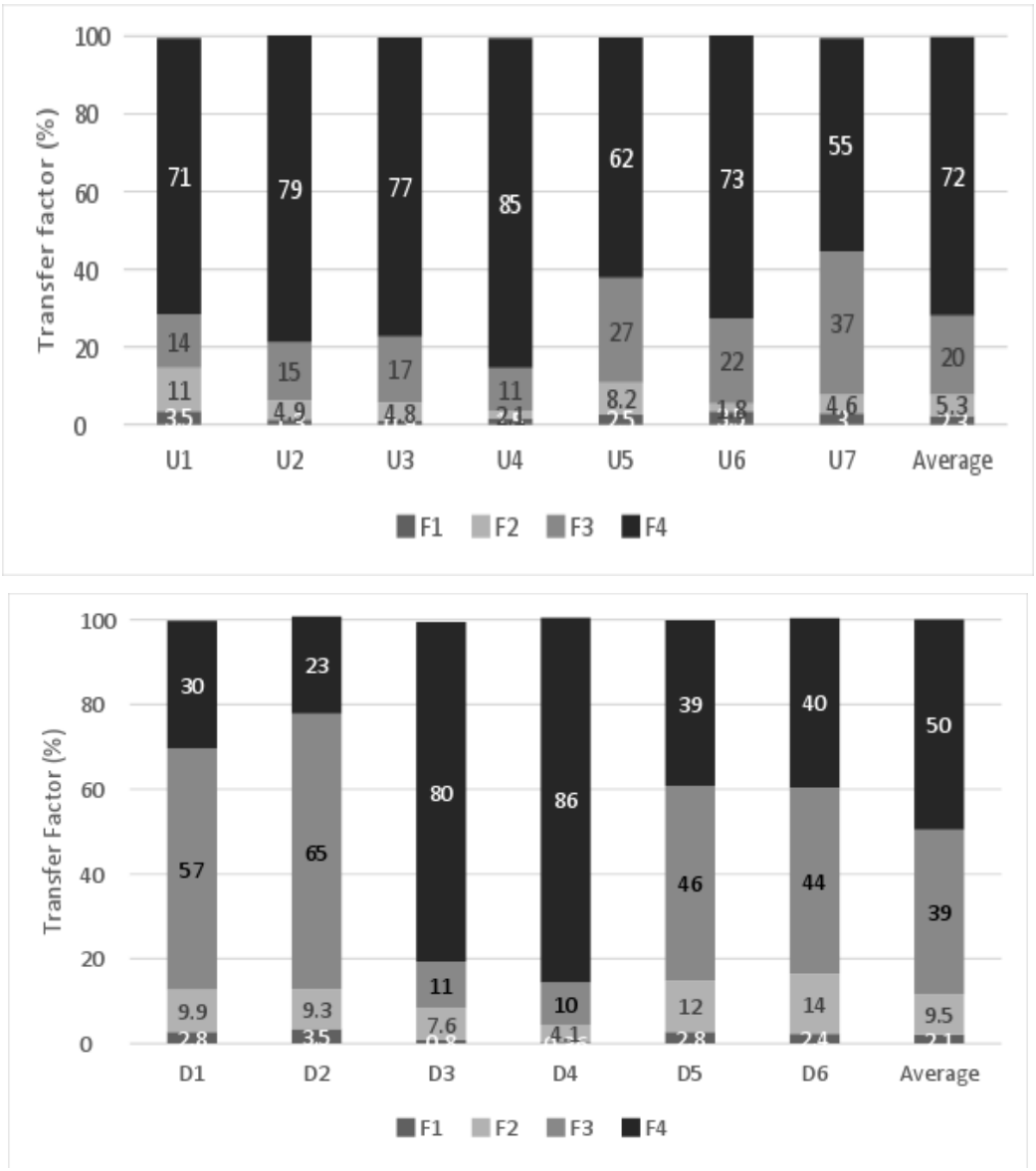

Figure 3.40. *TF (%) of ^{226}Ra in each BCR fraction for PG samples with depth.*

3.5.3.4. Waters of Disposal Area

The activity concentrations of ^{210}Po, U-isotopes (^{234}U and ^{238}U), Th-isotopes (^{230}Th and ^{232}Th) and ^{226}Ra measured in pore-water solutions of both core samples are shown in Table 3.30. The results show higher activity concentration of ^{210}Po and U-isotopes in the D core, where pH values are lower, than in the U core. Concretely, the activity concentration detected in D core exceed in one order of magnitude to the U core. On the other hand, Th- isotopes and ^{226}Ra activity concentrations are much lower compared with the other radionuclides in both zones. These results are in concordance with the

information provided by BCR procedure and, even, with other earlier studies (Haridasan et al., 2002; Santos et al., 2006; Ceballos et al., 2017), which affirm that thorium isotopes and ^{226}Ra tend to be associated with crystalline forms of the PG and their release is limited in environmental weathering conditions.

	Depth (m)	^{210}Po (BqL^{-1})	^{234}U (BqL^{-1})	^{238}U (BqL^{-1})	^{230}Th (BqL^{-1})	^{232}Th (BqL^{-1})	^{226}Ra (BqL^{-1})
U samples	2.0	4.8±0.2	2.1±0.2	2.1±0.2	0.81±0.09	0.13±0.04	0.33±0.05
	2.5	3.44±0.09	1.7±0.1	1.8±0.1	0.18±0.02	0.05±0.01	0.18±0.02
	3.0	5.8±0.2	3.4±0.2	3.5±0.2	0.23±0.02	0.06±0.01	0.26±0.03
	Average *	**4.7±0.7**	**2.4±0.5**	**2.5±0.5**	**0.4±0.2**	**0.08±0.03**	**0.26±0.04**
D samples	3.5	47±1	39±5	38±5	1.1±0.1	0.05±0.03	0.85±0.13
	4.3	45±1	35±3	36±3	0.89±0.05	0.03±0.01	0.84±0.06
	5.0	44±1	12±4	13±4	0.39±0.04	0.03±0.01	0.42±0.05
	5.5	53±2	7.3±1.6	7.0±1.6	0.10±0.02	0.02±0.01	0.36±0.03
	Average *	**47 ± 2**	**23 ± 8**	**24 ± 8**	**0.62 ± 0.23**	**0.03 ± 0.01**	**0.62 ± 0.13**

Table 3.30. *Activity concentration (Bq L^{-1}) of pore-water from PG samples.*Standard uncertainty (1 σ) has been calculated as the standard deviation of the mean, σ = Sx/(n)1/2*

Table 3.31 presents the activity ratios of ^{234}U/^{238}U, ^{230}Th/^{232}Th, ^{234}U/^{230}Th and ^{210}Po/^{226}Ra in the pore-water samples. The ^{234}U/^{238}U values are similar in both core samples, being practically close to unit. This confirms that independently of the PG pile conditions both uranium isotopes have the same behaviour, as it was deduced by BCR procedure. Slight differences are found in ratios of ^{230}Th/^{232}Th of both cores, having somewhat higher values in D samples. At the same time, ^{234}U is also preferentially concentrated in pore-water conditions in relation to ^{230}Th. In addition, ^{210}Po is subjected to a preferential leaching in low pH conditions against the ^{226}Ra leaching. However, behaviour of ^{226}Ra and ^{230}Th do not seem to be different in both cores.

		$^{234}U/^{238}U$	$^{230}Th/^{232}Th$	$^{234}U/^{230}Th$	$^{210}Po/^{226}Ra$	$^{226}Ra/^{230}Th$
U samples	**U5**	1.0 ± 0.1	6.2 ± 2.0	2.6 ± 0.3	55 ± 9	0.77 ± 0.14
	U6	0.94 ± 0.08	3.6 ± 0.82	9.4 ± 1.0	54 ± 4	0.94 ± 0.09
	U7	1.0 ± 0.1	3.8 ± 0.72	15 ± 8	105 ± 13	1.08 ± 0.17
	Average	**1.0 ± 0.1**	**4.6 ± 0.7**	**8.9 ± 3.1**	**147 ± 13**	**0.85** ± 0.19
D samples	**D2**	1.0 ± 0.1	24 ± 1	35 ± 6	90 ± 22	0.77 ± 0.14
	D4	0.97 ± 0.02	31 ± 1	39 ± 4	15 ± 2	0.94 ± 0.09
	D5	0.93 ± 0.11	16 ± 1	31 ± 11	19 ± 2	1.08 ± 0.17
	D6	1.1 ± 0.1	4.5 ± 0.4	73 ± 22	22 ± 3	3.6 ± 0.8
	Average	**0.99 ± 0.03**	**19 ± 6**	**45 ± 10**	**19 ± 2**	**1.6 ± 0.7**

***Table 3.31**. Activity ratio of $^{234}U/^{238}U$, $^{230}Th/^{232}Th$, $^{234}U/^{230}Th$ and $^{210}Po/^{226}Ra$ in pore-water samples.*Standard uncertainty (1 σ) has been calculated as the standard deviation of the mean, σ = Sx/(n)1/2.*

The activity concentrations of ^{210}Po, ^{234}U, ^{238}U, ^{230}Th, ^{232}Th and ^{226}Ra found in process water of perimeter channel and edge outflow samples are shown in Table 3.32. The activity concentrations of ^{210}Po vary from 5 to 67 Bq L^{-1} in the edge outflow leachates and between 29 and 54 Bq L^{-1} in process water. On the other hand, U-isotopes activity concentrations range from 24 to 73 Bq L^{-1} in the edge outflows and reach up to 557 Bq L^{-1} in process water samples. The values of edge outflow samples are very similar to those observed in the pore-water of the deepest zone (D samples), and also reported by others authors (Bolivar et al., 2000), where the activity concentrations exceed the typical range 0.005 - 0.5 Bq L^{-1} for continental waters (Mas et al., 2006). It is noteworthy the low activity concentration of Th-isotopes and ^{226}Ra found with respect to the other radionuclides. Concomitantly with pore-water, these results are in agreement with the data provided by BCR procedure.

		^{210}Po	^{234}U	^{238}U	^{230}Th	^{232}Th	^{226}Ra
Edge outflow leachate	**E1**	67.4 ± 1.4	39.6 ± 1.5	39.5 ±1.5	<DL	<DL	0.04 ± 0.01
	E2	37.1 ± 0.9	74.4 ± 2.0	74.3 ± 2.0	<DL	<DL	0.10 ± 0.01
	E3	5.3 ± 0.1	31.3 ± 0.8	31.4 ± 0.8	<DL	<DL	0.11 ± 0.01
	E4	5.4 ± 0.1	28.4 ± 0.9	28.1 ± 0.8	< DL	<DL	N.M
	E5	13.1 ± 0.4	41.9 ±1.3	42 ± 1.3	< DL	<DL	0.03 ± 0.01
	E6	21.0 ± 0.7	30.3 ±0.9	30.2 ± 0.9	< DL	<DL	0.01 ± 0.01
	E7	6.3 ± 0.2	29.7 ± 1.0	30.2 ± 1.0	< DL	<DL	0.03 ± 0.01
	E8	10.6 ± 0.3	24.3 ± 0.8	24.4 ± 0.8	< DL	<DL	0.05 ±0.01
	E9	14.2 ± 0.5	72.7 ± 2.2	72.3 ± 2.1	< DL	<DL	0.04 ±0.01
	E10	6.6 ± 0.3	40.8 ± 1.5	40.9 ± 1.5	< DL	<DL	N.M
	E11	16.0 ± 0.6	70.5 ±3.6	71.3 ± 3.6	0.59 ± 0.06	0.04 ± 0.01	0.01 ± 0.01
	E12	16.1 ± 0.6	53.4 ± 1.8	53.8 ± 1.8	<DL	< DL	0.14 ± 0.03
	Average	18.3 ± 5.2	44.8 ± 5.3	44.9 ± 5.3	0.59 ± 0.06	0.04 ± 0.01	0.06 ± 0.01
Process water of perimeter channel	**P1**	30.3 ± 0.7	44.7 ± 1.3	44.0 ± 1.3	0.34 ± 0.08	0.19 ± 0.04	0.28 ± 0.02
	P2	29.2 ± 1.0	557 ± 27	561 ± 27	NM	N.M	0.39 ± 0.15
	P3	53.6 ± 1.6	464 ± 25	469 ± 25	NM	N.M	1.53 ± 0.22
	Average	37.7 ± 4.0	355 ± 79	358 ± 80	0.34 ± 0.08	0.19 ± 0.04	0.73 ± 0.20

Table 3.32. *Activity concentration (Bq L^{-1}) of edge outflow leachate and perimeter channel water. (DL: detection limit of thorium isotopes 0.01 Bq L^{-1}; N.M: no measured)*

3.5.4. CONCLUSIONS

This work has been carried out to evaluate the mobility of natural radionuclides (^{210}Po, ^{234}U, ^{238}U, ^{230}Th, ^{232}Th and ^{226}Ra) in PG disposal area from Huelva. For this purpose, two cores were subjected to the optimized BCR sequential extraction procedure. In addition, the mobility of natural radionuclides were assessed in pore-water, edge outflow leachates reaching the Estuary of Huelva and in process water of perimeter channel.

The BCR results indicate an important proportion of Polonium-210 can be released depending of the environmental conditions. Concretely, it is observed that can be release around 45% of the total polonium contained in PG, being the most susceptible the acid soluble (~10%) and oxidizable fraction (~25%). But, U- isotopes present the maximum mobility, which can mean the release of approximately 70% of the uranium contained in PG (~20 % in acid soluble fraction and ~43 % oxidizable fraction). In contrast Th-isotopes show the lowest mobility because of their tendency to being bound to the crystalline forms of the PG, while about 30 % of the ^{226}Ra content in PG can be released to the environment in oxidizable condition.

These results are in agreement with the behaviour of radionuclides found in pore-water, process water of perimeter channel and edge outflow leachates. This work confirms that the BCR procedure is a useful tool for assessing the speciation of different radionuclides under PG stack conditions.

Chapter 4. General Conclusions

In this chapter, the general conclusions obtained in this doctoral thesis work are summarised, being the main objective the characterisation and valorisation of the different industrial wastes: red gypsum, ilmenite mud, slag cleaning furnace flue dust and phosphogypsum.

The results obtained in this work has allowed to draw the following main conclusions:

Red Gypsum (RG) and Ilmenite Mud (Tionite)

- RG is composed mainly of gypsum (calcium sulphate dehydrate, $CaSO_4 \cdot 2H_2O$), iron and titanium oxides.

- Tionite is formed of ilmenite ($FeTiO_3$) and rutile (TiO_2) as main components, and being minerals such as zircon ($ZrSiO_4$), quartz (SiO_2) and Fe and Ti oxides ($Fe_3Ti_3O_{10}$) in minor proportion. In addition, it is considered as NORM waste due to their natural radionuclides content.

- It has been demonstrated that the plates manufactured (75% RG + 25% tionite; 80% RG, 15% tionite and 5% vermiculite) perform better than some materials used in construction such as Pladur® against fire. The tested materials also present acceptable mechanical properties that showed no noticeable distortion or breakage during the test. So, they could be used as potential building materials for fire wall insulation or as fire-resistant panels.

- In addition, it has been proven that the plates manufactured are agree with EU radioactivity requirements, since the use of these wastes as building materials not exceeded the radioactive thresholds.

- Furthermore, RG could be used as capture agent for carbon dioxide sequestration. It has been demonstrate that a high carbonation efficiency is reached using NaOH as Ca extracting agent, as well as a reduction of the resulted solid.

- However, the natural radionuclides are concentrated in calcite ($CaCO_3$), the main product of the carbonation process, which implies its consideration as a NORM material, which requires radiological studies in their commercial applications.

Slag Cleaning Furnace Flue Dust (SWC and CFD)

- SWD contains Zincite (ZnO), lead carbonate ($PbCO_3$) and iron oxides and hydroxides (Fe_3O_4 and FeOOH).

- CFD is composed of portlandite ($Ca(OH)_2$), zincite (ZnO), anglesite ($PbSO_4$), calcite ($CaCO_3$) and calcium sulphate ($CaSO_4$).

- It has been demonstrated that both wastes are an important secondary resource of Zn and Pb and their reprocessing has both remarkable economic and environmental benefits in contrast with their disposal or incorporation into other products. Pyrometallurgical and hydrometallurgical process appears to be attractive options for the management of these hazardous wastes

Phosphogypsum (PG)

- Calcium sulphate dihydrate is the main component of PG, and is considered as NORM waste due to their natural radionuclides content.

- It has been demonstrated that the total contaminant content in a waste is not a good measure of its potential risk, since only a proportion of the total contaminant content will be mobile depending on their specific chemical forms or ways of binding.

- The BCR sequential extraction procedure has showed to be a useful tool for assessing the speciation of different radionuclides.

- U-isotopes contained in PG show the same and highest mobility, being its total mobile fraction around 70%, while ^{210}Po and ^{226}Ra present a total mobility of about 50% and 30%, respectively. And the Th-isotopes have very low mobility (mobile fraction < 5%), being fixed to the crystalline forms of the PG.

- The same behaviour of natural radionuclides has been also found in the water samples taken from the stacks.

-

Chapter 5. References

- Acevedo-Sandoval O., Ortiz-Hernández E., Cruz-Sánchez M., Cruz-Chávez E. Role of iron oxides in soils, Terra Latinoamericana 22 (2004) 485–497.

- ACTLABS. Activation Laboratories Ltd.(2013), http://www.actlabs.com (accessed June 2013)

- Addison J. Vermiculite: a review of the mineralogy and health effects of vermiculite exploitation. Regulatory Toxicology and Pharmacology. 21, 1995, pp. 397.

- Agency for Toxic Substances and Disease Registry (ATSDR), Toxicological Profile For Ammonia U.S. Department Of Health And Human Services, September 2004.

- Aguado Casas J. L., 2003. Tesis: Aplicaciones de la espectrometría alfa en la caracterización de isótopos de Ra y U en residuos industriales y matrices ambientales. Universidad de Sevilla.

- Aguado J. L., Bolívar J. P., García-Tenorio R., 2004. Sequential extraction of ^{226}Ra in sediments from an estuary affected historically by anthropogenic inputs of natural radionuclides. Journal of Environmental Radioactivity 74, 117–126.

- Aguado J.L., Bolívar J.P., San Miguel E.G., García-Tenorio R. Ra and U isotopes determination in phosphogypsum leachates by alpha-particle spectrometry. Radioactivity in the Environment (2005), VOLUME 7 (ISSN 1569-4860/DOI 10.1016/S1569-4860(04)07018-4)

- Ahdy, A.E., Rifaat and S.E.O Draz, 2011. The Speciation and Potential Mobility of Pb, Cd, Cu and Zn in Lake Qarun Bottom Sediments, Fayioum, Egypt. Journal of King Abdulaziz University: Marine Science. Vol. 22, No. 2, pp: 111-133.

- Al-Homoud M. S. Performance characteristics and practical applications of common building thermal insulation materials. Building and Environment 40, 2005, pp. 353–366.

- Alkaç D., Atalay Ü. Kinetics of thermal decomposition of Hekimhan–Deveci siderite ore samples. Elsevier International Journal of Mineral Processing 87, 2008, pp. 120–128.

- Andersen M. B., Erel Y., Bourdon B., 2009. Experimental evidence for 234U–238U fractionation during granite weathering with implications for 234U/238U in natural waters. Geochimica et Cosmochimica Acta, 73, 4124–4141.

- Andersson L, Jansson B. Analytical Fire Design with Gypsum - A Theoretical and Experimental Study. Institute of Fire Safety Design: Lund. 1987.

- Ang C.N., Wang Y.C. The effect of water movement on specific heat of gypsum plasterboard in heat transfer analysis under natural fire exposure. Construction and Building Materials 18, 2004, pp. 505–515.

- Ansoborlo E., Berard P., Auwer C. D., Leggett R., Menetrier F., Younes A., Montavon G., and Moisy P., 2012. Review of Chemical and Radiotoxicological Properties of Polonium for Internal Contamination Purposes. Chemical research in toxicity 25(8), 1551-1564

- Armarego W.L.F., Chai C.L.L. Chapter 5 – Purification of inorganic and metal-organic chemicals: (including organic compounds of B, Bi, P, Se, Si, and ammonium and metal salts of organic acids), Purification of Laboratory Chemicals (Sixth Edition), 2009, 445–576.

- Azaroual M., Kervevan C., Lassin A., André L., Amalhay M., Khamar L., EL Guendouzi M. Thermo-kinetic and Physico-Chemical Modeling of Processes Generating Scaling Problems in Phosphoric Acid and Fertilizers Production Industries. Procedia Engineering 46 (2012) 68 – 75.

- Balladares E., Kelm U., Helle S., Parra R. and Araneda E. Chemical-mineralogical characterization of copper smelting flue dust. DYNA, Volumen 81, Número 186 (2014) p. 11-18,

- Blanco P., Vera Tome F., Lozano J.C., 2004. Sequential extraction for radionuclide fractionation in soil samples: a comparative study. Applied Radiation and Isotopes 61, 345–350.

- Bolívar J. P., García-Tenorio R. and García-León M.. Radioactive Impact of some Phosphogypsum Piles in Soils and Salt Marshes Evaluated by y-Ray Spectrometry. Appl. Radiat. Isot. Vol. 47, No. 9/10, pp. 1069-1075, 1996.

- Bolivar J.P., García-Tenorio R. and García-León. Fluxes and distribution of natural radionuclides in the production and use of fertilizers. Appl. Radiat. Isot. Vol. 46, No. 6/7, pp. 717-718, 1995.

- Bolivar J.P., Garcia-Tenorio R. and Vaca F. Radioecological study of an estuarine system located in the south of Spain. Wat. Res. Vol. 34, No. 11, pp. 2941-2950, 2000.

- Bolivar J.P., García-Tenorio R., Garcia-Leon M. Fluxes and distribution of natural radionuclides in the production and use of fertilizers. Appl. Radiat. Isot. 46 (1995) 717–718.

- Bolívar J.P., García-Tenorio R., García-Leon M. On the fractionation of natural radioactivity in the production of phosphoric acid by the wet acid method. J. Radioanal. Nucl. Chem. (1996) 214, 77-88.

- Bolıvar J.P., Garcıa-Tenorio R., Mas J.L., Vaca F. Radioactive impact in sediments from an estuarine system affected by industrial wastes releases. Environment International 27 (2002) 639– 645.

- Bolıvar J.P., Martın J.E., Garcıa-Tenorio R., Perez-Moreno J.P., Mas J.L. Behaviour and fluxes of natural radionuclides in the production process of a phosphoric acid plant. Applied Radiation and Isotopes 67 (2009) 345–356.

- Braz de Abreu G., Marques Costa S. M., Guerra Gumieri A., Fonseca Calixto J. M., França F. C., Silva C., Delgado Quinõnes A. Mechanical properties and microstructure of high performance concrete containing stabilized nano-silica. Matéria, v.22, n.2, (2017).

- Cappuyns V., Swennen R., Niclaes M., 2007. Application of the BCR Sequential Extraction Scheme to Dredged Pond Sediments Contaminated by Pb-Zn Mining: A combined geochemical and mineralogical approach. Journal of Geochemical Exploration 93, 78–90.

- Cárdenas-Escudero C., Morales-Flórez V., Pérez-López R., Santos A., Esquivas L. Procedure to use phosphogypsum industrial waste for mineral CO_2 sequestration, J. Hazard. Mater. 196 (2011) 431–435.

- Ceballos M. R., Borràs A., García-Tenorio R., Rodríguez R., Estela J.M., Cerdà V., Ferrer L. 226Ra dynamic lixiviation from phosphogypsum samples by an automatic flow-through system with integrated renewable solid-phase extraction. Talanta 167 (2017) 398–403.

- Chang J., Tian H., Jiang J., Zhang C., Guo Q. Simulation and experimental study on the desulfurization for smelter off-gas using a recycling Ca-based desulfurizer, Chem. Eng. J. 291 (2016) 225–237.

- Chattopadhyay B., Roy U. S., Mukhopadhyay S. K., 2010. Mobility and Bioavailability of Chromium in the Environment: Physico-Chemical and Microbial Oxidation of Cr (III) to Cr (VI). Journal of Applied Sciences and Environmental Management, Vol. 14 (2) 97 – 101.

- Chernet T. Applied mineralogical studies on Australian sand ilmenite concentrate with special reference to its behavior in the sulphate process. Mineral Engineering Vol. 12. Nº 5, 1999, pp. 485-495.

- Colombo P., Grusatin G., Bernardo E., Scarinci G. Inertization and reuse of waste materials by vitrification and fabrication of glass-based products. Current Opinion in Solid State & Materials Science 7, 2003, pp. 225-239.

- Commission Decision of 18 December 2014 amending Decision 2000/532/EC on the list of waste pursuant to Directive 2008/98/EC of the European Parliament and of the Council.

- Commission Regulation (EU) No 1357/2014 of 18 December 2014 replacing Annex III to Directive 2008/98/EC of the European Parliament and of the Council on waste and repealing certain Directives.

- Consejería De Medio Ambiente De La Junta De Andalucía (CMAJA). “Los criterios y estándares para declarar un suelo contaminado en Andalucía y la

metodología y técnicas de toma de muestra y análisis para su investigación", Enero 1999.

- Council Decision 2002/358/EC of 25 April 2002 concerning the approval, on behalf of the European Community, of the Kyoto Protocol to the United Nations Framework Convention on Climate Change and the joint fulfilment of commitments thereunder.

- Council Directive 2013/59/EURATOM of 5 December 2013 laying down basic safety standards for protection against the dangers arising from exposure to ionising radiation, and repealing Directives 89/618/Euratom, 90/641/Euratom, 96/29/Euratom, 97/43/Euratom and 2003/122/Euratom.

- Council Directive 96/61/EC of 24 September 1996 concerning Integrated Pollution Prevention and Control (IPPC).

- Csavina J., Taylor M. P., Félix O., Rine K. P., Sáez A. E., Betterton E. A. Size-resolved dust and aerosol contaminants associated with copper and lead smelting emissions: Implications for emission management and human health, Sci. Total Environ 493 (2014) 750–756.

- Currie, L.A. Limits for qualitative detection and quantitative determination. Anal. Chem. 40 (1968) 586-593.

- D'Amore J.J., Al-Abed S.R., Scheckel K.G., Ryan J.A, 2005. Methods for speciation of metals in soils: a review. Journal of Environmental Quality 8; 34 (5):1707-45.

- Decision No 1600/2002/EC of the European Parliament and of the Council of 22 July 2002 laying down the Sixth Community Environment Action Programme.

- Demir F., Donmez B., Okur H. y Sevim F. Calcination kinetic of magnesite from Thermogravimetric data. Institution of Chemical Engineers. Trans IChemE, Vol 81, 2003, Part A.

- Directiva 96/61/CE DEL CONSEJO de 24 de septiembre de 1996 relativa a la prevención y al control integrado de la contaminación.

- Directive 2008/98/EC OF THE EUROPEAN PARLIAMENT AND OF THE COUNCIL of 19 November 2008 on waste and repealing certain Directives.
- Directive 2008/98/EC of the European Parliament and of the Council of 19 November 2008 on waste (Waste Framework Directive).
- Directive 2010/75/EU of the European Parliament and of the Council of 24 November 2010 on industrial emissions (integrated pollution prevention and control).
- Doebrich J., 2009, Copper–A Metal for the Ages: U.S. Geological Survey Fact Sheet 2009-3031, 4 p.
- Dudka S. and Adriano D. C. Environmental Impacts of Metal Ore Mining and Processing: A Review. Published in J. Environ. Qual. 26 (1997) 590-602.
- Dueñas C., Fernández M.C., Cañete S., Pérez M.. Radiological impacts of natural radioactivity from phosphogypsum piles in Huelva (Spain). Radiation Measurements 45 (2010) 242–246.
- El Mouzdahir Y., Elmchaouri A., Mahboub R., Gil A., Korili S.A. Synthesis of nano-layered vermiculite of low density by thermal treatment. Elsevier Powder Technology 189, 2009, pp. 2–5.
- El-Aassy I. E., El-Feky M. G., Issa F. A., Ibrahim N. M., Desouky O. A., Khattab M. R., 2015. Uranium and 234U/238U isotopic ratios in some groundwater wells at Southwestern Sinai, Egypt. Journal of Radioanalytical and Nuclear Chemistry.
- Environmental Protection Agency (EPA), 1992. SW-846 Test Method 1311: Toxicity Characteristic Leaching Procedure.
- Environmental Protection Agency (EPA), 1996. METHOD 3052.-Microwave Assisted Acid Digestion of Siliceous and Organically Based Matrices.
- Environmental Protection Agency (EPA), 40 CFR 261.24:2011: Toxicity characteristic.

- Erin R.B., Qingxia L., Zhenghe X., Hongbo Z. Carbon capture and storage using alkaline industrial wastes. Prog. Energ. Combust. 38 (2012) 302–320.
- European Environment Agency. EEA Report No 35/2016. Prevention of hazardous waste in Europe — the status in 2015.
- Fan Y., Shibata E., Iizuka A. and Nakamura T. Crystallization Behaviors of Copper Smelter Slag Studied Using Time-Temperature-Transformation Diagram, Mater. T., 55 (2014) 958-963.
- Fauziah I., Zauyah S., Jamal T. Characterization and land application of RG: a waste product from the titanium dioxide industry, Sci. Total Environ. 188 (1996) 243–251.
- Fernández Bertos M., Simons S.J.R., Hills C.D., Carey P.J. A review of accelerated carbonation technology in the treatment of cement-based materials and sequestration of CO_2, J. Hazard. Mater. B112 (2004) 193–205.
- Fernández I., Garea A. and Irabien A. SO2 reaction with Ca(OH)2 at medium temperatures (300-425°C):Kinetic behavior, Chem. Eng. Sci., 53 (1998) 1869-1881.
- Flynn W.W. The determination of low levels of Polonium-210 in environmental materials. Analytica Chimica Acta, 43 (1968), pp. 221-227.
- Földvári M. Handbook of thermogravimetric system of minerals and its use in geological practice, Geological Institute of Hungary (Magyar ÁllamiFöldtaniIntézet), (2011) 213.
- Gabrovšek R., Vuk T., Kaučič V. Evaluation of the Hydration of Portland Cement Containing Various Carbonates. Acta Chim. Slov. 53 (2006) 159–165.
- García Arenas C., Marrero M., Leiva C., Solís-Guzmán J., Vilches Arenas L. F. High fire resistances in blocks containing coal combustion fly ashes and bottom ash. Waste Management 31, 2011, pp. 1783–1789.

- Gázquez M. J., Mantero J., Bolívar J.P., García-Tenorio R., Vaca F., Lozano R.L. Physico-chemical and radioactive characterization of TiO_2 undissolved mud for its valoration. Journal of Hazardous Materials 191, 2011, pp. 269-276.

- Gázquez M.J., Bolívar J.P., Garcia-Tenorio R., Vaca F. A review of the production cycle of titanium dioxide pigment, Materials Sciences and Applications, 5 (2014) 441–458.

- Gázquez M.J., Bolívar J.P., García-Tenorio R., Vaca F. Physicochemical characterization of raw materials and co-products from the titanium dioxide industry. Journal of Hazardous Materials 166, 2009, pp. 1429–1440.

- Gazquez M.J., Bolivar J.P., Vaca F., García-Tenorio R., Caparros A. Evaluation of the use of TiO_2 industry RG waste in cement production, Cement Concrete Comp. 37 (2013) 76–81.

- Gázquez M.J., Mantero J., Bolívar J.P., García-Tenorio R., Vaca F., Lozano R.L. Physico-chemical and radioactive characterization of TiO_2 undissolved mud for its valorization, J. Hazard. Mater. 191 (2011) 269–276.

- Groves AW. Gypsum and Anhydrite. Overseas Geological Surveys, Mineral Resources Division. Her Majesty's Stationery Office: London. 1958.

- Guevara-Riba A., Sahuquillo A., Rubio R., Rauret G., 2004. Assessment of metal mobility in dredged harbour sediments from Barcelona, Spain. Science of the Total Environment 32, 241–255.

- Guézennec A., Huber J., Patisson F., Sessiecq P., Birat J., Ablitzer D., Dust formation in Electric Arc Furnace: Birth of the particles, Powder Technol. 157 (2005) 2 – 11.

- Guo P., Duan T., Song X., Chen H., 2007. Evaluation of a sequential extraction for the speciation of thorium in soils from Baotou area, Inner Mongolia. Talanta 71, 778–783.

- Haridasan P.P., Maniyan C.G., Pillai P.M.B., Khan A.H. Dissolution characteristics of 226Ra from Phosphogypsum. Journal of Environmental Radioactivity 62 (2002) 287–294.

- Hawthorne C., Dieter H., Bidwe A., Schuster A., Scheffknecht G., Unterberger S., Käß M. CO_2 capture with CaO in a 200 kWth dual fluidized bed pilot plant, Energy Procedia 4 (2011) 441–448.

- Hierro A., Olías M., Cánovas C.R., Martín J.E., Bolivar J.P. Trace metal partitioning over a tidal cycle in an estuary affected by acid mine drainage (Tinto estuary, SW Spain). Science of The Total Environment Volumes 497–498, 1 November 2014, Pages 18-28.

- Holm E. and Fukai R. Method for multi-element alpha-spectrometry of actinides and its application to environmental radioactivity studies. Talanta, Volume 24, Issue 11, November 1977, Pages 659-664.

- Hu Z. and Gao S. Upper crustal abundances of trace elements: A revision and update, Chem. Geol. 253 (2008) 205–221.

- Hudson-Lamb D.L., Strydom C.A., Potgieter J.H. Thermal dehydration of natural gypsum and pure calcium sulphate dihydrate (gypsum). Elsevier Science Thermochimica Acta 282/283, 1996, pp. 483-492.

- Huijgen W. J. J., Witkamp G., and Comans R. N. J. Mineral CO2 Sequestration by Steel Slag Carbonation. Environ. Sci. Technol. 2005, 39, 9676-9682.

- Huijgen W.J.J., Comans R.N.J. Carbon dioxide sequestration by mineral carbonation, Petten, NL: Energy Research Centre of the Netherlands, 2003.

- Hwanju J., Young-Nam J., Young J. H., Influence of NaCl on mineral carbonation of CO_2 using cement material in aqueous solutions, Chem. Eng. Sci. 80 (2012) 232–241.

- IAEA (International Atomic Energy Agency), Safety standards series, Application of the Concepts of Exclusion Exemption and Clearance, Safety Guide No. RS-G 17, 2004, STI/PUB/1202.

- International Atomic Energy Agency (IAEA), 2012. Safety Reports Series No.76Radiation. Radiation Protection and Norm Residue Management in the Titanium Dioxide and Related Industries.

- International atomic energy agency (IAEA), 2014. The Environmental Behaviour of Radium: Revised Edition. Technical Reports Series No. 476.

- International Atomic Energy Agency IAEA. Safety Reports Series No. 78. Radiation Protection and Management of NORM Residues in the Phosphate Industry. 2013.

- ISO 13320:2009. Particle size analysis - Laser diffraction methods.

- Issa H., Korać M., Kamberović Ž., Gavrilovski M., Kovačević T. A Two-Stage Metal Valorisation Process from Electric Arc Furnace Dust (EAFD). Metalurgija 55 (2016) 2, 149-152.

- Jha M.K., Kumar V., Singh R.J. Review of hydrometallurgical recovery of zinc from industrial wastes. Resour Conserv Recycl 33 (2001) 1–22.

- Kaithwas A., Murari P., Ankita K., Sanjay V. Industrial wastes derived solid adsorbents for CO2 capture: A mini review, Chem. Eng. Res. Des. 90 (2012) 1632–1641.

- Kennou B., Meray M. E., Romane A., Arjouni Y., 2015. Assessment of heavy metal availability (Pb, Cu, Cr, Cd, Zn) and speciation in contaminated soils and sediment of discharge by sequential extraction. Environmental Earth Sciences, 74:5849–5858.

- Khamar L., EL Guendouzi M., Amalhay M., Aboufaris El alaoui M., Rifai A., Faridi J., Azaroual M. Evolution of soluble impurities concentrations in industrial phosphoric acid during the operations of desupersaturation. Procedia Engineering 83 (2014) 243 – 249.

- Kontogeorgos D.A., Founti M.A.. Gypsum board reaction kinetics at elevated temperatures. Thermochim. Acta 529 (2012) 6–13.

- Korfali S. I., Jurdi M. S., 2011. Speciation of metals in bed sediments and water of Qaraaoun Reservoir, Lebanon. Environmental Monitoring and Assessment, 178:563–579.

- Kovler K. Radiological constraints of using building materials and industrial by-products. Constr. Build. Mater. 23 (2009) 246–253.

- Kukurugya F., Vindt T., Havlík T. Behavior of zinc, iron and calcium from electric arc furnace (EAF) dust in hydrometallurgical processing in sulfuric acid solutions: Thermodynamic and kinetic aspects. Hydrometallurgy. Volume 154, (2015) 20-32.

- Kuryatnyk T., Angulski da Luz C., Ambroise J. Valorization of phosphogypsum as hydraulic binder, J. Hazard. Mater. 160 (2008) 681–687.

- L'vov B. V. Mechanism and kinetics of thermal decomposition of carbonates, Thermochim. Acta, 386 (2002) 1–16.

- L'vov B. V., Leonid K. Polzik, Valery L. Ugolkov. Decomposition kinetics of calcite: a new approach to the old problem. Thermochimica Acta 390, 2002, pp. 5–19.

- Ledesma E.F., Jiménez J.R., Ayuso J., Fernández J.M., de Brito J.. Experimental study of the mechanical stabilization of electric arc furnace dust using fluid cement mortars. J Hazard Mater 326 (2017) 26–35.

- Lee S., Povinec P. P., Chisholm J. R.M., Levy I., Miquel J., Jung-Suk Oh. Distribution of natural and anthropogenic radionuclides in northwest Mediterranean coastal sediments. Journal of Environmental Radioactivity 172 (2017) 145-159.

- Leiva C., Garcia Arenas C., Vilches L.F., Vale J., Giménez A., Ballesteros J.C., Fernandez-Pereira C. Use of FGD gypsum in fire resistant panels. Waste Management 30, 2010, pp. 1123–1129.

- Leiva C., Vilches L. F., Vale J., Fernández-Pereira C. Fire resistance of biomass ash panels used for internal partitions in buildings. Fire Safety Journal 44, 2009, pp. 622–628.

- Leiva C., Vilches L. F., Vale J., Fernández-Pereira C. Influence of type of ash on the fire resistance characteristics of ash-enriched mortars. Fuel 84, 2005, pp. 1433-1439.

- Leiva C., Vilches L. F., Vale J., Olivares J., Fernández-Pereira C. Effect of carbonaceous matter contents on the fire resistance and mechanical properties of coal fly ash enriched mortars. Fuel 87, 2008, pp. 2977–2982.

- Li G. G., Keener T. C., Stein A. W., Khang S. J. CO2 reaction with Ca(OH)2 during SO2 removal with convective pass sorbent injection and high temperature filtration. Environ. Eng. Policy 2 (2000) 47–56.

- Lin X., Peng Z., Yan J., Li Z., Hwang J.Y., Zhang Y., Li G., Jiang T.. Review Pyrometallurgical recycling of electric arc furnace dust. J Clean Prod 149 (2017) 1079-1100.

- Liu Y., Lin C., Wu Y. Characterization of red mud derived from a combined Bayer Process and bauxite calcination method. Journal of Hazardous Materials 146, 2007, pp. 255-261.

- Lochamy, J.C. The Minimum Detectable Activity concept. Systems and applications Studies.PSD No. 17, EG&G Ortec, Oak Ridge, U.S.A, 1981.

- López Julián P. L. y Mandado Collado J. M., 2002. Extracciones Químicas Secuenciales de Metales Pesados. Aplicacion en Ciencias Geologicas. Estudios Geologicos, 58: 133-144.

- López-Periago A.M., Fraile J., López-Aranguren P., Vega L.F., Domingo C. CO2 capture efficiency and carbonation/calcination kinetics of micro and nanosized particles of supercritically precipitated calcium carbonate, Chem. Eng. J. 226 (2013) 357–366.

- Lutandula M. S., Kashala G. N. Zinc oxide production through reprocessing of the electric arc furnace flue dusts. J Environ Chem Eng 1 (2013) 600–603.

- Machado J. G.M.S., Brehm F. A., Mendes Moraes C. A., Dos Santos C. A., Faria Vilela A. C., Marimon da Cunha J. B. Chemical, physical, structural and morphological characterization of the electric arc furnace dust, J. Hazard. Mater. B136 (2006) 953–960.

- Maciejewski M. Computational aspects of kinetic analysis. Part B: The ICTAC kinetic project – the decomposition kinetics of calcium carbonate revisited, or some tips on survival in the kinetic minefield, Thermochim. Acta 355 (2000) 145–154.

- Mai U., Mati U., Rein K. CO2 mineral sequestration in oil-shale wastes from Estonian power production, J. Environ. Manage. 90 (2009) 1253–1260.

- Mantero J., Gazquez M.J., Bolivar J.P., Garcia-Tenorio R., Vaca F. Radioactive characterization of the main materials involved in the titanium dioxide production process and their environmental radiological impact, J. Environ. Radioactiv. 120 (2013) 26–32.

- Martin J.E., Bolivar J.P., Respaldiza M.A., Garcia-Tenorio R., da Silva M.F. Environmental impact of fertilizer industries evaluated by PIXE. Nuclear Instruments and Methods in Physics Research B 103 (1995) 477-481.

- Martin P. and Hancock G.J., 2004. Routine analysis of naturally occurring radionuclides in environmental samples by alpha-particle spectrometry. Supervising Scientist Report 180, Supervising Scientist, Darwin NT.

- Mas J. L., Bolıvar J. P., GarcÍa-Tenorio R., Aguado J. L., San Miguel E. G., and Gonzalez-Labajo J.. A dosimetric model for determining the effectiveness of soil covers for phosphogypsum waste piles. Health Physics January 2001, Volume 80, Number 1.

- Mas J.L., San Miguel E.G., Bolívar J.P., Vaca F., Pérez-Moreno J.P.. An assay on the effect of preliminary restoration tasks applied to a large TENORM wastes

disposal in the south-west of Spain. Science of the Total Environment 364 (2006) 55–66.

- Mas, J.L., García-León, M., García-Tenorio, R., Bolívar, J.P. (2006). Radionuclide concentrations in water. In: Nollet, E. (Ed.), Radionuclide Concentrations in Food and the Environment, pp. 59-113.

- Maslehuddin M., Awan F.R., Shameem M., Ibrahim M., Ali M.R. Effect of electric arc furnace dust on the properties of OPC and blended cement concretes. Constr Build Mater 25 (2011) 308–312.

- Masset P., Poinso J.-Y. and Poignet J.-C. TG/DTA/MS study of the thermal decomposition of FeSO4·6H2O. Journal of Thermal Analysis and Calorimetry, Vol. 83, 2, 2006, pp. 457–462.

- Matschei T., Lothenbach B., Glasser F.P. The role of calcium carbonate in cement hydration, Cement Concrete Res. 37 (2007) 551–558.

- McGee M. (2017). CO2 Earth. Are we stabilizing yet? Retrieved from https://www.co2.earth/

- McNulty G.S. Production of titanium dioxide, in: Proceedings of NORM V International. Conference, Seville, Spain, 2007, pp. 169–189.

- Mehdi G., Muhammad R.H., Ishwar K.P. Influence of natural and anthropogenic carbon dioxide sequestration on global warming, Ecol. Model. 235–236 (2012) 1–7.

- Miki T., Chairaksa-Fujimoto R., Maruyama K., Nagasaka T. Hydrometallurgical extraction of zinc from CaO treated EAF dust in ammonium chloride solution. J Hazard Mater Volume 302, 25 (2016) 90-96.

- Mineralogy Database, http://www.webmineral.com/, 2016 (accessed Sept 2016).

- Minhee L., In Sung P., Insu K., Hyunmin K., Sanghoon L. Remediation of heavy metal contaminated groundwater originated from abandoned mine using lime and calcium carbonate, J. Hazard. Mater. 144 (2007) 208–214.

- Morcali M.H., Yucel O., Aydin A., Derin, Min J. Carbothermic reduction of electric arcfurnace dust and calcination of waelz oxide by semi-Pilotscale rotary furnace. Metall. Sect. B-Metall. 48 (2) B (2012) 173 – 184.

- Multi-Agency Radiological Laboratory Analytical Protocols Manual (MARLAP) EPA 402-B-04-001C Volume III, 2004.

- Muriithi G.N., Gitari W.M., Petrik L.F., Ndungu P.G. Carbonation of brine impacted fractionated coal fly ash: Implications for CO2 sequestration, J. Environ. Manage. 92 (2011) 655–664.

- Myung Gyu L., Young Nam J., Kyung Won R., Wonbeak K., Jun-Hwan B. Mineral carbonation of flue gas desulfurization gypsum for CO2 sequestration, Energy 47 (2012) 370–377.

- Nemati K., Abu Bakar N. K., Radzi Abas Mhd., Sobhanzadeh E., 2011. Speciation of heavy metals by modified BCR sequential extraction procedure in different depths of sediments from Sungai Buloh, Selangor, Malaysia. Journal of Hazardous Materials 192, 402– 410.

- Newhook R., Hirtle H., Byrne K., Meek M. E. Releases from copper smelters and refineries and zinc plants in Canada: human health exposure and risk characterization. Sci. Total Environ. 301 (2003).

- Nia Y., Garnier M., Rigaud S., Hanna K., Ciffroy P. Mobility of Cd and Cu in formulated sediments coated with iron hydroxides and/or humic acids: A DGT and DGT-PROFS modeling approach, Chemosphere 85 (2011) 1496–1504.

- NOAA/ESRL (2013) Ed. Dlugokencky and Pieter Tans, http://www.esrl.noaa.gov/gmd/ccgg/trends (accessed April 2013).

- Nordstrom, D.K., Wilde, F.D., 1998. Reduction-oxidation potential (electrode method), in: National field manual for the collection of water quality data, U.S. Geological Survey Techniques of Water-Resources Investigations, Book 9, chapter 6.5.

- Oliveira J. M. and Carvalho F.P., 2006. Sequencial extraction procedure for determination of uranium, thorium, radium, lead and polonium radionuclides by alpha spectrometry in environmental samples. Czechoslovak Journal of Physics, Vol. 56.

- Osman K. T., 2013. Soils Principles, Properties and Management.DOI 10.1007/978-94-007-5663-2.

- Paulik F., Paulik J. y Arnold M. Thermal decomposition of gypsum. Elsevier Science Thermochimica Acta, 200, 1992, pp. 195-204.

- Pefia V., Nalda J.C., Cazurro C. and Pardo R., 2003. Study of Two Sequential Extraction Methods and its Application to Environmental Radioactivity Measures. Applied Physics (APHYS) A. Méndez-Vilas (Ed.).

- Perez-Lopez R., Alvarez-Valero A. M., Nieto J. M. Changes in mobility of toxic elements during the production of phosphoric acid in the fertilizer industry of Huelva (SW Spain) and environmental impact of phosphogypsum wastes. Journal of Hazardous Materials 148 (2007) 745–750.

- Pérez-López R., Castillo J., Sarmiento A. M., Nieto J. M. Assessment of phosphogypsum impact on the salt-marshes of the Tinto River (SW Spain): Role of natural attenuation processes. Marine Pollution Bulletin 62 (2011) 2787–2796.

- Pérez-López R., Macías F., Cánovas C. R., Sarmiento A. M., Pérez-Moreno S. M. Pollutant flows from a phosphogypsum disposal area to an estuarine environment: An insight from geochemical signatures Science of the Total Environment 553 (2016) 42–51.

- Pérez-López R., Nieto J. M., de la Rosa J. D., Bolívar J.P. Environmental tracers for elucidating the weathering process in a phosphogypsum disposal site: Implications for restoration. Journal of Hydrology Volume 529, Part 3, October 2015, Pages 1313-1323.

- Perez-Lopez R., Nieto J. M., Lopez-Coto I., Aguado J.L., Bolivar J.P., Santisteban M.. Dynamics of contaminants in phosphogypsum of the fertilizer industry of

Huelva (SW Spain): From phosphate rock ore to the environment. Applied Geochemistry 25 (2010) 705–715.

- Pérez-Maqueda L. A., Balek V., Poyato J., Pérez-Rodríquez J. L., Šubrt J. , Bountsewa I. M., Beckman I. N. y Málek Z. Study of natural and ion exchanged vermiculite by emanation thermal analysis, TG, DTA AND XRD. Journal of Thermal Analysis and Calorimetry, Vol. 71, 2003, pp. 715–726.

- Pérez-Moreno S.M, Gázquez M.J., Pérez-López R., Bolivar J.P. Validation of the BCR Sequential Extraction Procedure for Natural Radionuclides. Chemosphere Journal (current status: under review).

- Pérez-Moreno S.M, Gázquez M.J., Ríos G., Ruiz-Oria I. and Bolívar J.P. Diagnose for Valorisation of Reprocessed Slag Cleaning Furnace Flue Dust from Copper Smelting. Journal of Cleaner Production (current status: under review).

- Pérez-Moreno S.M., Gázquez M.J., Barneto A.G., Bolívar J.P. Thermal characterization of new fire-insulating materials from industrial inorganic TiO2 wastes. Thermochimica Acta 552 (2013) 114– 122.

- Pérez-Moreno S.M., Gázquez M.J., Bolívar J.P. CO2 sequestration by indirect carbonation of artificial gypsum generated in the manufacture of titanium dioxide pigments. Chemical Engineering Journal 262 (2015) 737–746.

- Pérez-Moreno, J. P.; San Miguel, E. G.; Bolívar, J. P.; Aguado, J. L. A comprehensive calibration method of Ge detectors for low level gamma-spectrometry measurements. Nuclear Instruments and Methods in Physics Research Section A, Volume 491, Issue 1-2, p. 152-162, 2002.

- Pistorius P.C. and Coetzee C. Physicochemical aspects of titanium slag production and solidification. Metallurgical and Materials Transactions B 34B, 2003, pp. 581-588.

- Potysz A., Kierczak J., Fuchs Y., Grybos M., Guibaud G., Lens P.N.L., Van Hullebusch E. D. Characterization and pH-dependent leaching behavior of historical and modern copper slags. J. Geochem. Explor. 160 (2016) 1–15.

- Poyato J., Pérez-Maqueda L. A., Jiménez de Haro M. C., Pérez-Rodríguez J. L., Subrt J. y Balek V. Effect of Na+ and NH+ 4 Cations on Microstructure Changes of Natural Vermiculite During Heat Treatment. Journal of Thermal Analysis and Calorimetry 67, 2002, pp. 73.

- Praetorius B., Schumacher K. Greenhouse gas mitigation in a carbon constrained world: The role of carbon capture and storage, Energ. Policy 37 (2009) 5081–5093.

- Prasad P.S., Ramana G.V. Feasibility study of copper slag as a structural fill in reinforced soil structures, Geotext. Geomembranes 44(2016) 623–640.

- PRTR. Registro Estatal de Emisiones y Fuentes Contaminantes. Ministerio de Agricultura, Alimentación y Medio Ambiente. Gobierno de España, http://www.prtr-es.es/informes/fichacomplejo.aspx?id_complejo=2882 (accessed April 2013).

- Pueyo M., Mateu J., Rigol A., Vidal M., López-Sánchez J.F., Rauret G., 2008. Use of the modified BCR three-step sequential extraction procedure for the study of trace element dynamics in contaminated soils. Environmental Pollution 152, 330-341.

- Quijorna N., Coza A., Andres A., Cheeseman C. Recycling of Waelz slag and waste foundry sand in red clay bricks. Resour Conserv Recycl Volume 65 (2012) 1-10.

- Quijorna N., de Pedro M., Romero M., Andrés A. Characterisation of the sintering behaviour of Waelz slag from electric arc furnace (EAF) dust recycling for use in the clay ceramics industry. J Environ Manage 132 (2014) 278-286.

- Randall S.R., Sherman D.M., Ragnarsdottir K.V., Collins C.R. The mechanism of cadmium surface complexation on iron oxyhydroxide minerals, Geochim. Cosmochim. Acta 63 (1999) 2971–2987.

- Raposeiras A.C., Vargas-Cerón A., Movilla-Quesada D., Castro-Fresno D. Effect of copper slag addition on mechanical behavior of asphalt mixes containing reclaimed asphalt pavement, Constr. Build. Mater. 119 (2016) 268–276.

- Rauret G., Lopez-Sanchez J. F., Sahuquillo A., Rubio R., Davidson C., Ure A. and Quevauviller Ph., 1999. Improvement of the BCR three step sequential extraction procedure prior to the certification of new sediment and soil reference materials. Journal of Environmental Monitoring 1, 57–6.

- Rauret G., López-Sánchez J.F., Luck D., Yli-Halia M., Muntau H. and Quevauviller Ph., 2001. BCR information Reference materials. The certification of the extractable contents (mass fractions) of Cd, Cr, Cu, Ni, Pb and Zn in freshwater sediment following a sequencial extraction procedure. BCR 701. European Commission.

- Raza N., Raza W., Iqbal Z., Zafar, and Kumar R. V. Beneficiation of Zinc from Electric Arc Furnace Dust Using Hydrometallurgical Approach. Russ J Appl Chem, 2016, Vol. 89, No. 5, pp. 836-845.

- Real Decreto 110/2008, de 1 de febrero, por el que se modifica el Real Decreto 312/2005, de 18 de marzo, por el que se aprueba la clasificación de los productos de construcción y de los elementos constructivos en función de sus propiedades de reacción y de resistencia frente al fuego.

- Real Decreto 1481/2001 de 27 de diciembre, por el que se regula la eliminación de residuos mediante depósito en vertedero.

- Regulation (EC) No 1272/2008 of the European Parliament and of the Council of 16 December 2008 on classification, labelling and packaging of substances and mixtures, amending and repealing Directives 67/548/EEC and 1999/45/EC, and amending Regulation (EC) No 1907/2006.

- Rentería-Villalobosa M., Vioquea I., Manteroa J., Manjóna G. Radiological, chemical and morphological characterizations of phosphate rock and phosphogypsum from phosphoric acid factories in SW Spain. Journal of Hazardous Materials 181 (2010) 193–203.

- Rios G., Arbizu C., Sunyer A. and Viñals Joan. New process for treating Slag Cleaning Furnace (SCF) flue dust at Atlantic Copper. T.T. Chen Honorary Symposium on Hydrometallurgy, Electrometall and Mater Charact (2012).

- Rossi G.E., Muntau H. and Tartari G., 1992. The evolution of copper concentrations in Lake Orta, Italy. Ecological Modelling, 64, 23-45.

- Rubio R., Lopez-Sanchez J.F., 2008. Assessment of inorganic priority pollutants in contaminated soils: Harmonization of analytical protocols for heavy metal extractions: Analytical speciation, in: L. Simeonov, V. Sargsyan (Eds.), Soil Chemical Pollution, Risk Assessment, Remediation and Security, Springer, Dordrecht.

- Rudnick R.L. and Gao S., 2014. Composition of the Continental Crust. Treatise on geochemistry.

- Rutherford M., Dudas M. J. and Arocena J. M. Radioactivity and elemental composition of phosphogypsum produced from three phosphate rock sources. Waste Management & Research (1995) 13, 407-423.

- Rutherford P.M., Dudas M.J., Samek R.A. Review article Environmental impacts of phosphogypsum. The Science of the Total Environment 149 (1994) 1-38.

- Ryan P.C., Hillier S., Wall A.J., 2008. Stepwise effects of the BCR sequential chemical extraction procedure on dissolution and metal release from common ferromagnesian clay minerals: A combined solution chemistry and X-ray powder diffraction study. Science of the total environment 407, 603–614.

- Sahoo P.K, Galgali R.K., Singh S.K., Bhattacharyee S., Mishra P.K., Mahanty B.C. Preparation of titania-rich slag by plasma smelting of ilmenite. Scad. J. Metall. 28, 1999, pp. 243-248.

- Sahuquillo A., Lopez-Sanchez J.F., Rubio R., Rauret G., Thomas R.P., Davidson C.M., Ure A.M., 1999. Use of a certified reference material for extractable trace metals to assess sources of uncertainty in the BCR three-stage sequential extraction procedure. Analytica Chimica Acta 382, 317-327.

- Sahuquillo A., Rigol A., Rauret G., 2003. Overview of the use of leaching/extraction tests for risk assessment of trace metals in contaminated soils and sediments. Trends in Analytical Chemistry, Vol. 22, No. 3.

- Said A. A., Abd El-Salaam K. M., Hassan E. A., El-Awad A. M. y M. M. Mohamed. A study on the thermal decomposition of iron-cobalt mixed hydroxides. Journal of Thermal Analysis, Vol. 39, 1993, pp. 309-321.

- Saleem M., Iqbal J., Shah M.H., 2015. Geochemical speciation, anthropogenic contamination, risk assessment and source identification of selected metals in freshwater sediments— A case study from Mangla Lake, Pakistan. Environmental Nanotechnology, Monitoring & Management Volume 4, Pages 27-36.

- Sanders J.P., Gallagher P.K. Kinetic analyses using simultaneous TG/DSC measurements. Part I. Decomposition of calcium carbonate in argon, Thermochim. Acta 388 (2002) 115–128.

- Santos A.J.G., Mazzilli B.P., Favaro D.I.T., Silva P.S.C. Partitioning of radionuclides and trace elements in phosphogypsum and its source materials based on sequential extraction methods. Journal of Environmental Radioactivity 87 (2006) 52-61.

- Santschi P.H., Murray J.W., Baskaran M., Benitez-Nelson C.R., Guo L.D., Hung C. C., Lamborg C., Moran S.B., Passow U., Roy-Barman M., 2006. Thorium speciation in seawater. Marine Chemistry 100, 250–268.

- Schlesinger, M. E., King, M. J., Sole, K. C., & Davenport, W. G. Extractive metallurgy of copper. Elsevier (2011).

- Seetharaman S., McLean A., Guthri R. Chapter 2.1 – Copper Production, Treatise Process Metall (2014) 534-624.

- Siriwardane R. V., Poston J. A., Fisher E. P., Shen M-S., Miltz A. L. Decomposition of the sulfates of copper, iron _II/, iron _III/, nickel, and zinc: XPS, SEM, DRIFTS, XRD, and TGA study. Elsevier Science Applied Surface Science 152, 1999, pp. 219–236.

- Skaf M., Manso J. M., Aragón Á., Fuente-Alonso J. A., Ortega-López V. Review. EAF slag in asphalt mixes: A brief review of its possible re-use. Resour Conserv Recycl 120 (2017) 176–185.

- Song K., Young-Nam J., Wonbaek K., Myung Gyu L., Dongbok S., Jun-Hwan B., Chi Wan J., Soo Chun C. Precipitation of calcium carbonate during direct aqueous carbonation of flue gas desulfurization gypsum, Chem. Eng. J. 213 (2012) 251–258.

- Stathopoulos V.N., Papandreou A., Kanellopoulou D., Stournaras C.J. Structural ceramics containing electric arc furnace dust. J Hazard Mater 262 (2013) 91– 99.

- Suetens T., Klaasen B., Van Acker K., Blanpain B. Comparison of electric arc furnace dust treatment technologies using exergy efficiency. J Clean Prod 65 (2014) 152-167.

- Sultan M. A., A Model for Predicting Heat Transfer Through Noninsulated Unloa ed Steel-Stud Gypsum Board Wall Assemblies Exposed to Fire. Fire Technology journal. Third Quarter, 1996, pp. 239-259.

- Sutherland R. A., 2010. Review BCR®-701: A review of 10-years of sequential extraction analyses. Analytica Chimica Acta 680, 10–20.

- Szabo Z., Paul V. T., Fischer J. M., Kraemer T. F., Jacobsen E., 2012. Occurrence and geochemistry of radium in water from principal drinking-water aquifer systems of the United States. Applied Geochemistry 27, 729–752.

- Tayibi H., Choura M., López F.A., Alguacil F.J., López-Delgado A.. Review Environmental impact and management of phosphogypsum. Journal of Environmental Management 90 (2009) 2377–2386.

- Tessier A., Campbell P. G. C., and Bisson M., 1979. Sequential Extraction Procedure for the Speciation of Particulate Trace Metals. Analytical Chemistry, Vol. 51, No. 7.

- The International Copper Study Group (ICSG). The World Copper Factbook (2016).
- Thomas G. Thermal Properties of Gypsum Plasterboard at High Temperatures. Fire and Materials 26, 2002, pp 37–45.
- Thomas P. S., Hirschausen D., White R. E., Guerbois J. P y Ray A. S. Characterization of the oxidation products of pyrite by thermogravimetric and evolved gas analysis. Journal of Thermal Analysis and Calorimetry, Vol. 72, 2003, pp. 769–776.
- Thomas R.P., Ure A.M., Davidson C.M. and Littlejohn D., 1994. Three-stage sequential extraction procedure for the determination of metals in river sediments. AnaIytica Chimica Acta, 286, 423-429.
- U.S. Congress. Office of Technology Assessment. Copper: Technology and Competitiveness. Chapter 8: Environmental Aspects of Copper Production, OTA-E-367, Washington. DC: U.S. Government Printing Office (1988).
- UNE-EN 12457-4:2003 Caracterización de residuos. Lixiviación, Ensayo de conformidad para la lixiviación de residuos granulares y lodos (2003).
- UNE-EN 12457-4:2003. Characterization of waste. Leaching. Compliance test for leaching of granular waste materials and sludges. Part 4: One stage batch test at a liquid to solid ratio of 10 l/kg for materials with particle size below 10 mm (without or with size reduction).
- UNE-EN 13501-1: 2007 + A1: 2010 Fire classification of construction products and building elements - Part 1: Classification using data from reaction to fire tests.
- UNE-EN 1363-1:2000. Fire Resistance Tests. Part 1: General Requirements.
- United Nations Scientific Committee on the Effects of Atomic Radiation (UNSCEAR), 2000. United Nations Scientific Committee on the Effects of Atomic Radiation. SOURCES AND EFFECTS OF IONIZING RADIATION. Report to the General Assembly.

- United Nations Scientific Committee on the Effects of Atomic Radiation. SOURCES, EFFECTS AND RISKS OF IONIZING RADIATION.UNSCEAR 2016 Report.

- United Nations Scientific Committee on the effects of Atomis Radiation (UNSCEAR), Report of the United Nations Scientific Committee on the effects of Atomis Radiation, United Nations 2000, New York.

- UNSCEAR, 2000. United Nations Scientific Committee on the Effects of Atomic Radiation. SOURCES AND EFFECTS OF IONIZING RADIATION. Report to the General Assembly.

- UNSCEAR, 2016. United Nations Scientific Committee on the Effects of Atomic Radiation. SOURCES, EFFECTS AND RISKS OF IONIZING RADIATION. Report.

- US Environmental Protection Agency, 1992. SW-846 Test Method 1311: Toxicity Characteristic Leaching Procedure.

- Vilches L. F., Fernández-Pereira C., Olivares del Valle J., Vale J. Recycling potencial of coal fly ash and titanium waste as new fireproof products. Chemical Engineering Journal 95, 2003, pp. 155-161.

- Vilches L. F., Leiva C., Vale J., Fernández-Pereira C. Insulating capacity of fly ash pastes used for passive protection against fire. Cement & Concrete Composites 27, 2005, pp. 776-781.

- Virtanen S., Vaaramaa K., Lehto J., 2013. Fractionation of U, Th, Ra and Pb from boreal forest soils by sequential extractions. Applied Geochemistry Volume 38, Pages 1-9.

- Walburga Keglevich de Buzin P. J., Heck N. C., Faria Vilela A. C. Review Article EAF dust: An overview on the influences of physical, chemical and mineral features in its recycling and waste incorporation routes. J. Mater. Res. Technol. 6(2) (2017) 194–202.

- Wang W., Ramkumar S., Liang-Shih F. Energy penalty of CO2 capture for the carbonation–calcination reaction (CCR) process: Parametric effects and comparisons with alternative processes, Fuel 104 (2013) 561–574.

- Wang X., Ni S., Shi Z., 2014. Uranium distribution in the sediment of the Mianyuan River near a phosphate mining region in China and the related uranium speciation in water. Chemie der Erde Geochemistry. Volume 74, Issue 4, Pages 661-669.

- Young J. H., Jin Ha K., Young Jae L., Meehye L., Suk-Joo C., Evaluation of factors affecting mineral carbonation of CO2 using coal fly ash in aqueous solutions under ambient conditions, Chem. Eng. J. 183 (2012) 77–87.

- Zhao H., Xiao Q., Huang D., and Zhang S. Influence of Pore Structure on Compressive Strength of Cement Mortar. Sci World J. (2014) 247058.